ORNL-1896 (Del.)

Contract No. W-7405-eng-26

AIRCRAFT NUCLEAR PROPULSION PROJECT

QUARTERLY PROGRESS REPORT

For Period Ending June 10, 1955

W. H. Jordan, Director
S. J. Cromer, Co-Director
R. I. Strough, Associate Director
A. J. Miller, Assistant Director
A. W. Savolainen, Editor

DATA RECEIVED BY INFORMATION AND REPORTS DIVISION
(JUNE 28, 1955)

DATE ISSUED

JUL 28 1955

Declassified with deletions November 13, 1959

OAK RIDGE NATIONAL LABORATORY
Operated by
CARBIDE AND CARBON CHEMICALS COMPANY
A Division of Union Carbide and Carbon Corporation
Post Office Box P
Oak Ridge, Tennessee

617

ASSIFIED

Reports previously issued in this series are as follows:

ORNL-528	Period Ending November 30, 1949
ORNL-629	Period Ending February 28, 1950
ORNL-768	Period Ending May 31, 1950
ORNL-858	Period Ending August 31, 1950
ORNL-919	Period Ending December 10, 1950
ANP-60	Period Ending March 10, 1951
ANP-65	Period Ending June 10, 1951
ORNL-1154	Period Ending September 10, 1951
ORNL-1170	Period Ending December 10, 1951
ORNL-1227	Period Ending March 10, 1952
ORNL-1294	Period Ending June 10, 1952
ORNL-1375	Period Ending September 10, 1952
ORNL-1439	Period Ending December 10, 1952
ORNL-1515	Period Ending March 10, 1953
ORNL-1556	Period Ending June 10, 1953
ORNL-1609	Period Ending September 10, 1953
ORNL-1649	Period Ending December 10, 1953
ORNL-1692	Period Ending March 10, 1954
ORNL-1729	Period Ending June 10, 1954
ORNL-1771	Period Ending September 10, 1954
ORNL-1816	Period Ending December 10, 1954
ORNL-1864	Period Ending March 10, 1955

FOREWORD

This quarterly progress report of the Aircraft Nuclear Propulsion Project at ORNL records the technical progress of the research on circulating-fuel reactors and all other ANP research at the Laboratory under its Contract W-7405-eng-26. The report is divided into three major parts: I. Reactor Theory, Component Development, and Construction, II. Materials Research, and III. Shielding Research.

The ANP Project is comprised of about 475 technical and scientific personnel engaged in many phases of research directed toward the achievement of nuclear propulsion of aircraft. A considerable portion of this research is performed in support of the work of other organizations participating in the national ANP effort. However, the bulk of the ANP research at ORNL is directed toward the development of a circulating-fuel type of reactor.

The design, construction, and operation of the Aircraft Reactor Test (ART), with the cooperation of the Pratt & Whitney Aircraft Division, are the specific objectives of the project. The ART is to be a power plant system that will include a 60-Mw circulating-fuel reflector-moderated reactor and adequate means for heat disposal. Operation of the system will be for the purpose of determining the feasibility, and the problems associated with the design, construction, and operation, of a high-power, circulating-fuel, reflector-moderated aircraft reactor system.

CONTENTS

PART I. REACTOR THEORY, COMPONENT DEVELOPMENT, AND CONSTRUCTION

PART II. MATERIALS RESEARCH

PART IV. APPENDIX

ANP PROJECT QUARTERLY PROGRESS REPORT

SUMMARY

PART I. REACTOR THEORY, COMPONENT DEVELOPMENT, AND CONSTRUCTION

1. Reflector-Moderated Reactor

The development of the reactor layout is continuing. New features that have been incorporated because of stress, fluid flow, or fabricability considerations include an elliptical fuel expansion tank, a rounded dome to enclose the top of the reactor, a newly designed sodium pump impeller, and other related items. Recently completed heat exchanger tests yielded consistent data from which a series of heat exchangers is being designed. The most promising of these will be chosen for the ART.

The preliminary layout of the interior of the ART test cell which shows the major items of equipment and the recommended provisions for support was completed. A similar layout for the NaK piping and radiators was also completed so that drawings for the building and concrete work could proceed. More detailed drawings of the cell that will show the disposition of the small items and the instrumentation are being prepared.

Information block diagrams showing the basic-control actions desired for the ART have been prepared and will be used as a basis for selection of the hardware types and the control techniques to be used and for determination of areas of control that will require new component development.

Calculations were made of the temperature coefficients of the ART that check well with previous multigroup calculations. The results support the postulated negative over-all temperature coefficient. It has also been found that, if as much as 5 wt % lithium were added to the NaK in the secondary coolant circuit, the reactivity of the ART would be a fairly sensitive indication of a NaK leak into the fuel circuit. Burnup and gamma-ray heating of rare-earth oxides being considered as control rod materials are being studied.

2. Experimental Reactor Engineering

A series of design changes have been made in the nose, or heater, section of the in-pile loop as more information concerning the neutron flux in the MTR beam hole and the flux depression of the materials of loop construction has become available. The present nose section consists of a $2\frac{1}{2}$-turn coil (an increase of 1 turn) with its axis parallel to the beam hole center line. The flux seen by the fuel in the in-pile loop is now expected to be 30% of the unperturbed value, and the average power density in the nose section will be 0.7 kw/cm^3.

A working mockup of the in-pile loop has been completed and is being operated with the fuel mixture NaF-ZrF$_4$-UF$_4$ (53.5-40-6.5 mole %) at a Reynolds number of about 5000, a temperature differential of 175°F, and a maximum fuel temperature of 1500°F. Resistance heating is employed. The experience gained will aid in operation of the in-pile loop at the MTR.

The fission gas holdup system for the loop is being tested with flow rates of 0.15 and 0.03 scfh of helium with about 0.13% krypton. After 15 days of operation, no significant amounts of krypton were getting through the liquid-nitrogen-cooled charcoal-adsorption traps. Assembly of the first loop for the MTR in-pile experiment is under way, with operation scheduled for the next quarter.

Three additional test stands were installed for the operation of resistance-heated high-velocity forced-circulation loops with large temperature differentials for investigating corrosion and mass transfer of Inconel by fluoride fuel mixtures. Also, three more gas furnaces were placed in service as heat sources for these loops, bringing the total number of test stands to ten. Operation of 16 loops was terminated during the quarter. The majority of these loops operated for 1000 hr in the Reynolds number range of 1,000 to 15,000 and with temperature differentials of 100 to 300°F. The excessive high wall temperature in the bends of electric-resistance-heated loops was corrected by relocation of the heating elements so that heat is applied in only straight sections of tubing.

Four test stands are now in operation for studying corrosion and mass transfer of sodium-Inconel and sodium–Inconel–stainless steel systems. Operation of six such loops was terminated this quarter at the conclusion of periods of either 500 or 1000 hr with maximum sodium temperatures of up to 1500°F. Appreciable deposits of mass-transferred material were found in the cold legs of these loops, and therefore a controlled series of experiments was started. The loops will provide information on the effects of the oxygen content of the sodium, the use of a cold trap, the use of a lower temperature, and the use of an all-stainless-steel system.

The ART fuel pump (model MF-2) was operated in water performance tests. Some cavitation noises were present in all tests, but no serious effect of the apparent cavitation on performance could be found. It is estimated that the efficiency of the pump at design point, exclusive of seal and bearing losses, is 70%. New inlet volute configurations are currently being designed and tested. The bearing and seal, cold mechanical shakedown, and high-temperature test stands are being fabricated and assembled.

An extensive program of heat exchanger testing is under way for obtaining reliable heat transfer data on fuel-to-NaK heat exchangers of the general type and configuration for ART application. Considerable information will be obtained on the effect of corrosion and mass transfer on materials of fabrication in high-temperature, high-heat-flux, NaK and fluoride systems. An opportunity will also be provided for ascertaining the structural integrity and reliability of fabrication of heat exchangers and radiators supplied by outside vendors.

The program involves the operation of three intermediate heat exchanger (IHE) test stands and two small heat exchanger (SHE) test stands, such as the SHE stand now in operation. The IHE stands will be used to test large tube bundles (about 100 tubes) of the general size and configuration of ART heat exchangers (arranged for regenerative operation), while the SHE stands will be used to test smaller, more easily fabricated, tube bundles (20 to 50 tubes). The SHE stand now in operation will be modified for use as a general test loop following termination of the current test.

Design of all IHE test stands is complete, and procurement and assembly are well under way. Design of the SHE test stands and procurement of equipment are under way.

Water tests with a full-scale aluminum model of the 21-in. ART core and the entrance header region were initiated. Without inlet guide vanes, the fluid was observed to enter the core at an angle of about 70 deg from the vertical. Flow reversal at the island was observed. Data from these tests are being used in the design of turning vanes and vortex generators to correct this unacceptable flow condition.

A second thermal-cycling test of a sodium-Inconel-beryllium system was completed. Over 100 thermal cycles were applied to the beryllium piece between the range of the high power level, 61 w/cm^3 to the beryllium, and the low power level, 2.5 w/cm^3. The sodium temperature from inlet to outlet at the high power level ranged from 1050 to 1200°F. Inspection of the beryllium piece after the test (total operating time, 1030 hr) revealed three axial cracks on the outer surface of the hot end of the beryllium.

The 100-kw gas-fired heater was tested and was found to perform very satisfactorily. Minor modifications can be made to this heater that will increase the capacity.

3. Critical Experiments

The critical assembly of the reflector-moderated reactor consisting of the beryllium island and reflector enclosing the fuel region and having axial extrusions simulating the exit and entrance flow channels was loaded with sufficient uranium to give several per cent excess reactivity. This overloading was used to evaluate some of the materials of interest in the design of the ART prior to dilution of the fuel to the critical uranium density.

Measurements were made with samples of a mixture of the oxides of the rare-earth elements being considered for the absorber material of the control rod of the ART. A cylinder of the mixture

0.79 in. in diameter and 21 in. long decreased the reactivity nearly 2%; measurements with shorter lengths of the material indicated that the total value of the rod could be increased by 60% if the diameter were increased to 1⅜ in. Tests made on tubes of several different dimensions gave data for the design of the control rod guide thimble.

A high-temperature critical experiment embodying the nuclear characteristic of the ART has been designed which will operate at zero nuclear power at about 1200°F. The purposes of the experiment are to measure the critical uranium concentration, the temperature coefficient of reactivity, and the effectiveness of control rods.

PART II. MATERIALS RESEARCH

4. Chemistry of Reactor Materials

Interest in obtaining fuel mixtures more suitable for use in a circulating-fuel reactor than those available in the NaF-ZrF_4-UF_4 system has led to evaluation of the NaF-LiF-ZrF_4 ternary and the NaF-LiF-ZrF_4-UF_4 quaternary systems. The NaF-LiF-ZrF_4 system has been reasonably well defined, but much work remains to be done on the quaternary system. Phase-equilibrium data show that quite low melting points are available in the ternary system and that adequately low melting points are available at ZrF_4 concentrations as low as 21 mole %; however, no composition with physical properties better than those available in the NaF-ZrF_4-UF_4 system has been found.

Study of the analogous NaF-LiF-BeF_2 system has shown that adequately low melting points are available over wide areas. Physical property data have not yet been obtained in sufficient detail for comparison with available fuel material. Preliminary data on the solubility of UF_3 in BeF_2-bearing compositions were obtained. The scattered data show a trend of increasing UF_3 solubility with increasing temperature and decreasing BeF_2 content, but in no case does it appear that the solubility of UF_3 at 600°C is sufficiently high to provide more than a fraction of the concentration needed for an ART fuel.

Previous measurements of the partial pressure of HF at equilibrium during the reduction of FeF_2 by hydrogen in $NaZrF_5$ showed higher values than would be predicted from thermochemical data and ideal solution behavior, and it was postulated that the higher values were due to a lowered activity of the metallic iron because of alloying with the nickel apparatus. The postulated alloying has been confirmed by low values for final FeF_2 content of the melt and by chemical analyses of portions of the nickel apparatus.

Additional data were obtained on the reduction of UF_4 by structural metals. Data on the reduction of UF_4 by metallic chromium with NaF-ZrF_4-UF_4 (51-45-4 mole %) showed that, in comparison with the data obtained with NaF-ZrF_4-UF_4 (48-48-4 mole %) as the solvent, an increase in the final mole fraction of NaF from 0.48 to 0.51 in the melt containing uranium causes a significant decrease in the equilibrium CrF_2 concentration. Data for the reaction of UF_4 with metallic iron in these mixtures and in NaF-KF-LiF (11.5-42-46.5 mole %) agreed very closely and were somewhat higher at 600°C than at 800°C. Some, as yet inconclusive, data were obtained on the reaction of UF_4 plus UF_3 with chromium metal and Inconel in NaF-KF-LiF (11.5-42-46.5 mole %) at 600 and 800°C. Additional data were obtained that confirmed previous findings that FeF_2 is relatively stable in the NaF-KF-LiF eutectic at 600 and 800°C and that CrF_2 is not stable.

Previous evidence that UF_3 was more stable at elevated temperatures than free energy estimates had indicated was substantiated by vapor pressure measurements on UF_3 in the temperature range 1270 to 1390°C. The disproportionation pressure curve that was obtained shows that the disproportionation of UF_3 is far from complete under the conditions prevailing in the vapor pressure cell and that UF_3 is thermodynamically stable with respect to pure UF_4 and uranium metal at temperatures below 1400°C.

In the investigation of variables affecting the reduction of UF_4 with uranium in alkali fluorides, the effects of the surface area of nickel or copper exposed to the melt and of adding excess uranium metal were studied. It has become apparent that alloying of nickel and uranium can occur at temperatures far below the minimum nickel-uranium liquidus temperature (732°C) and, consequently, that disproportionation of UF_3 can be expected to occur at the temperatures of interest at nickel surfaces or at any metallic surface with which uranium can alloy. Preliminary evidence was obtained which indicated that UF_3 dissolved in an alkali fluoride mixture is more stable in copper than in nickel.

Investigations of methods for rapid purification of fuel mixtures included attempts to use electrolysis under a hydrogen atmosphere to remove oxides in order to avoid the container corrosion that results when HF is used and to use metallic zirconium to replace most of the hydrogen in the stripping operation. The use of zirconium metal was demonstrated on a 5- and a 50-lb test scale and was found to be a quite rapid and effective method for purification if small quantities of UF_3 in the product are tolerable or desirable. In electrolysis experiments, the ZrF_4-bearing mixtures could be electrolyzed smoothly, but the alkali fluoride mixtures gave variable results. Attempts to prepare mixtures containing UF_3 and no UF_4 were unsuccessful, the largest UF_3 content attained being 85% in an NaF-ZrF_4 base.

Fifty-six pilot-scale preparations totaling 630 lb of material were produced in various compositions for small-scale corrosion studies, for physical property determinations, or, in many cases, for use as purified intermediates in phase-equilibrium studies. Uranium trifluoride was a component of nearly 25% of the materials requested. Production operations were resumed on March 1, 1955, on a three-shift, five-day-week basis to provide test material for the greatly accelerated ANP engineering program. A total of 4800 lb of purified material was prepared during the quarter. Attempts to find a commercial source of ZrF_4 are under way. If a commercial source is not found, it will be necessary to expand the Y-12 production facilities immediately. Two batches of enriched fuel were prepared for use in an in-pile loop, and preparations are being made for the production of the materials for the proposed high-temperature critical experiment.

Potential measurements were made with combinations of several half cells consisting of metal electrodes bathed in solutions of the corresponding metal ion in the molten salts. The temperature range studied was, in general, 550 to 700°C. Cells consisting of zirconium rods immersed in various NaF-ZrF_4 melts and cells consisting of metallic nickel electrodes immersed in solutions of NiF_2 in molten NaF-ZrF_4 melts were studied.

Vapor pressure measurements of mixtures in the LiF-ZrF_4 system were started. The data showed the vapor pressures of the LiF-ZrF_4 mixtures to be considerably higher than those of the corresponding NaF-ZrF_4 mixtures.

An x-ray diffractometer for studying the structure of liquids has been constructed and is undergoing final testing. A high-temperature attachment for an x-ray spectrometer has been used for studies of compositions in the systems NaF-ZrF_4, LiF-ZrF_4, and NaF-BeF_2.

5. Corrosion Research

Several Inconel forced-circulation loops that were operated with fluoride mixtures and with sodium as the circulated fluids were examined. The fluoride mixtures included ZrF_4-base mixtures with UF_4 and with combinations of UF_3 and UF_4 and an alkali-metal base mixture containing UF_4. Favorable results were obtained with the ZrF_4-base materials in that the depths of attack were no deeper than have been found previously in thermal-convection loops. Attacks as low as 5 mils in 1000 hr appear to be obtainable. The conversion of some of the UF_4 to UF_3 decreases the attack. The most important variables appear to be maximum wall temperature and the hot-zone surface-to-loop volume ratio, whereas large variations in velocity and Reynolds number have very little effect on the depth of attack. The alkali-metal base mixture containing UF_4 caused excessive mass transfer and a very heavy intergranular concentration of subsurface voids to a depth of 35 mils. The mass-transferred deposit in the cold zone was up to 65 mils thick.

Mass transfer of large amounts of nickel metal was found in the Inconel forced-circulation loop that circulated molten sodium at 1500°F. Layers of dendritic metal crystals up to 26 mils thick were found to have formed in 1000 hr. The use of type 316 stainless steel in the cold portions was found to reduce the mass transfer slightly, but further study of the variables in the process is needed to confirm this finding.

Alkali-metal base mixtures containing combinations of UF_3 and UF_4 were circulated in Inconel thermal-convection loops, and, when about 2 wt %

uranium was present as U^{3+}, low depths of attacks and no deposits were found. Higher U^{3+} concentrations resulted in decreased attack, but hot-leg layers were found.

Inconel thermal-convection loops in which ZrF_4-base fuels containing about 2 wt % uranium as U^{3+} were circulated did not show so large a reduction in attack as was found in the loops that circulated alkali fluoride fuels also containing 2 wt % uranium as U^{3+}. However, some reduction in depth of attack and a fair reduction in amount were found. The effect of the hot-leg temperature (1200 to 1600°F) on mass transfer was investigated in several Inconel thermal-convection loops operated for 1500 hr. A definite increase in depth of attack with an increase in hot-leg temperature was noted that may be attributed to mass transfer, inasmuch as loops operated previously for 500 hr did not show the effect of temperature on depth of attack. The mass transfer effect is masked by the effect of impurities and nonequilibrium conditions during the first 500 hr.

Considerable work is being done in an effort to find the cause of the increases in depth of attack and the nonuniformity of results now being obtained in Inconel thermal-convection loops operated as control loops under standard conditions. Contamination during filling or operation does not appear to be the cause of the difficulty.

Corrosion tests of brazed type 310 stainless steel T-joints in static sodium and in static NaF-ZrF_4-UF_4 (53.5-40-6.5 mole %) showed the brazing alloy 9% Si–2.5% P–88.5% Ni to be satisfactory in both mediums. Similar tests of brazed "A" nickel T-joints showed the following brazing alloys to be satisfactory in both mediums: 90% Ni–10% P, 80% Ni–10% Cr–10% P, and Nicrobraz. Seesaw corrosion tests in both mediums on brazed Inconel T-joints showed the Coast Metals alloy No. 52 to have the best resistance in sodium and in the fluoride mixture.

Since the structural metal alloys that have been proposed for use in the fabrication of reactor fuel and coolant lines have a tendency to form solid-phase bonds at elevated temperatures in liquid metals and in fused salts, they are unsuitable for use in valves, bearings, and seals. Therefore cermets and ceramics that do not bond to each other but that can be bonded to the structural metal alloys are being investigated. The cermets (metal-bonded ceramics) appear to be the more promising because of their high corrosion resistance and other satisfactory chemical and physical properties. Several Kentanium cermets tested in NaF-ZrF_4-UF_4 (53.5-40-6.5 mole %) at 1500°F for 100 hr were found to have good resistance to solid-phase bonding if the contact pressure between the specimens did not exceed 50,000 psi. The compositions of the cermets tested were:

80 wt % TiC–10 wt % $NbTaTiC_2$–10 wt % Ni
70 wt % TiC–10 wt % $NbTaTiC_3$–20 wt % Ni
64 wt % TiC–6 wt % $NbTaTiC_3$–30 wt % Ni
64 wt % TiC–6 wt % $NbTaTiC_3$–
25 wt % Ni–5 wt % Mo

Lithium was circulated in two stainless steel thermal-convection loops for periods of 1000 and 3000 hr, respectively. The hot- and cold-leg temperatures were 1000 and 550°F, respectively. Operation was satisfactory throughout the test periods, and macroscopic examination revealed no mass-transferred crystals in the loops or in the lithium drained from the loops. Metallographic examination revealed subsurface voids and a ferritic surface layer 0.3 to 1.0 mil thick in the loop operated for 1000 hr and 1.0 to 1.5 mils thick in the loop operated for 3000 hr. Lithium metal had penetrated to the depth of the subsurface voids. The weld zone of the pipe was attacked to a depth of 3 mils in the 1000-hr test and 4 to 5 mils in the 3000-hr test. A few small (0.2-mil) carbide particles were found attached to the wall in the cold-leg sections of both loops.

Determinations of the oxidation rate of sodium have been made at −79, −20, 25, 35, and 48°C. The experimental results indicate that, contrary to current oxidation theory, the oxide films formed on sodium are highly protective in the absence of water vapor. The rate curves do not conform to any of the "standard" rate equations reported in the literature, but they are qualitatively comparable to low-temperature curves for copper. It is hoped to clarify the oxidation mechanism associated with a linear rate law through a careful study of the structure and composition of the oxide films formed on columbium in the neighborhood of 400°C.

Studies of corrosion and mass transfer by fused hydroxides indicate that both nickel and Inconel may possibly be compatible with hydroxides at temperatures of about 600°C. Hastelloy B is unsatisfactory because of its poor corrosion resistance. In the temperature range 600 to 700°C, there is evidence of an accelerated rate of mass transfer with both nickel and Inconel, as well as corrosion of Inconel.

The BeF_2-bearing mixtures $LiF\text{-}BeF_2$ (69-31 mole %) and $LiF\text{-}BeF_2\text{-}UF_4$ (67.3-30.2-2.5 mole %) were tested in Inconel capsules in 100-hr tilting furnace tests. No evidence of attack by either mixture was found. A study of the effect on corrosion of the ratio of UF_3 to UF_4 in various solvents revealed that increasing the UF_3 content up to 50% was beneficial and that any further increase had little effect.

6. Metallurgy and Ceramics

Investigations were continued in the study of the properties of nickel-base alloys containing 15 to 32% molybdenum, ternary alloys with a nickel-molybdenum base, and Hastelloy B. Attempts are being made to improve Hastelloy B with regard to fabricability, oxidation resistance, and mechanical properties. Additional evidence has been obtained which indicates that the poor high-temperature fabricability of the commercial material is related to the impurity content; however, it is felt that the superior strength of commercial Hastelloy B may be derived from the impurities. Therefore mechanical property tests are under way on an alloy with the nominal Hastelloy B composition, 4% Fe–28% Mo–68% Ni, but without the tramp elements vanadium, silicon, manganese, cobalt, chromium, tungsten, and aluminum.

A tube blank extruded from a vacuum-melted cast billet of commercial Hastelloy B fractured during the first step of a reduction operation; however, a blank made from a wrought billet was successfully reduced from 1.5-in.-OD, 0.250-in.-wall to 0.187-in.-OD, 0.017-in.-wall seamless tubing. Two impact extrusions of as-cast vacuum-melted commercial Hastelloy B were made at 2000°F with good recovery of sound rod. Attempts to roll the rod at 2000°F were, however, unsuccessful; the material cracked severely.

Design curves were prepared from the results of creep-rupture tests of Hastelloy B sheet in the solution-annealed condition in an argon atmosphere at 1500 and 1650°F. A comparison of these data with preliminary data from tests in fused salts shows that properties of the alloy in the fused salts are actually superior to the properties in an argon atmosphere. Creep tests in air, in argon, and in hydrogen at 12,000 psi showed the effects of argon and hydrogen to be similar, but the effects of air followed closely the pattern observed for Inconel and "A" nickel in air, insofar as reduced creep rate and longer rupture life are concerned. However, the final elongations of Hastelloy B in air are equivalent to or lower than those in argon, whereas the elongations of other nickel-molybdenum alloys are markedly greater in air than in argon.

A program has been initiated to determine whether aging treatment results in serious embrittlement at service temperatures. Typical microstructures have been obtained from specimens heat-treated at temperatures from 1100 to 1600°F for times from 100 to 1000 hr, and a correlation is to be made between physical properties and the microstructures. The relative merits of various preaging heat treatments of Hastelloy B are also being studied, and it is hoped that, as a result of this work, a procedure can be developed that will stabilize the microstructure sufficiently to reduce the sensitivity to high-temperature aging.

The binary nickel-molybdenum alloys that have been studied have included 15 to 32% molybdenum, and the ternary alloys contained 20% molybdenum plus nickel and one of the following: 3 to 10% chromium, 2 to 10% columbium, 2% aluminum, 1% titanium, 2% vanadium, or 1% zirconium. The results of stress-rupture tests have shown low strengths and ductilities for most of these alloys and indicate that vacuum melting alone is not sufficient to obtain optimum properties. The possibility of increasing the strength and ductility through cerium additions appears to be promising, since the addition of cerium has been shown to improve the physical properties of the alloy. It has become apparent that improved deoxidation practices are necessary in melting these alloys, and efforts are being directed toward the production of sounder ingots.

Oxidation tests of nickel-molybdenum alloys containing 3 to 10% chromium have shown that about 10% chromium is necessary to form a nonspalling protective oxide on the alloy. However, the oxidation rate under static conditions can be reduced 50% by the addition of 3% chromium.

Cyclic tests consisting of 190 air cools from 1500°F in 500 hr have now been completed for brazing alloys previously evaluated in static oxidation resistance tests at 1500 and 1700°F. Most of the alloys tested showed good resistance to oxidation under both static and cyclic conditions. Cyclic tests at 1700°F are now under way on these brazing alloys, which include commercial alloys, experimental nickel-base alloys, and experimental precious-metal base alloys. Physical property tests showed that the physical properties of Inconel are not impaired by the brazing process.

The fabrication of several major experimental heat transfer test components was completed. The items fabricated included a 20-tube fuel-to-NaK Inconel heat exchanger, a full-scale 200-tube fuel-to-NaK heat exchanger (intermediate heat exchanger No. 2), two 500-kw NaK-to-air radiators, and a full-scale integral-fin liquid metal-to-air radiator designed by the Cornell Aeronautical Laboratory. The combination welding and brazing procedures used in the fabrication of these units are described.

Three billets of vanadium were extruded at 2000°F. Tubing prepared from these blanks is to be clad on the outside with stainless steel, and the clad tubing will be used in corrosion studies. Four high-purity molybdenum billets containing 0.7% titanium were extruded into rod to be used in welding studies. Flow pattern studies of the extrusion of duplex and three-ply composites were continued. The three-ply materials are to be used in the production of stainless-steel-clad seamless tubular fuel elements.

Ceramics composed of rare-earth oxides, which combine the property of high absorption cross section for thermal neutrons and the usual ceramic properties of high density, strength, corrosion resistance, and high melting temperature, were prepared in the shapes required for testing in critical assemblies to determine their possibilities as control rod materials. The possibility of coating UO_2 particles with ZrO_2 to protect the UO_2 from reaction with molten silicon in an SiC-Si fuel element is being investigated. Also, graphite-hydrogen reactions are being studied.

7. Heat Transfer and Physical Properties

The friction factor as a function of Reynolds modulus was determined experimentally for the case of turbulently flowing NaF-ZrF_4-UF_4 (53.5-40-6.5 mole %) in Inconel tubes; the results are in agreement with conventional friction data. A full-scale ART fuel-to-NaK heat exchanger was studied as a water-to-water heat exchanger. Preliminary measurements indicate that the heat transfer coefficients on the fuel side of the exchanger, which has the controlling thermal resistances in the system, are about 1.6 times lower than would be obtained by the conventional relation for turbulent flow in circular-pipe systems; also, the corresponding pressure drops were two times as high as those for flow in smooth pipes. Some velocity profile data were obtained for the 18-in. ART core for the case where the fluid enters the core with a rotational velocity component; the influence of turbulence-promoting screens at the core inlet on the flow was also studied. A study was made of the temperature and corresponding tensile stress fluctuations in the Inconel walls of the ART core for momentary periods of flow stagnation near the wall. The results of a theoretical and an experimental study of a free-convection system containing a volume heat source are given.

The enthalpies and heat capacities of five materials were determined: namely, NaF-ZrF_4-UF_4 (50-46-4 mole %), NaF-ZrF_4 (50-50 mole %), NaF-ZrF_4-UF_4 (56-39-5 mole %), NaF-LiF-ZrF_4-UF_4 (20-55-21-4 mole %), and lithium hydride. The heat capacities in the liquid state of the 17 fluoride mixtures that have been studied to date are represented by the simple equation

$$c_p = 9.0 \frac{\overline{N}}{\overline{M}} ,$$

where $\overline{N}$ is the average number of ions and $\overline{M}$ the average molecular weight. The viscosities of seven fluoride mixtures were determined: namely, NaF-LiF-ZrF_4-UF_4-UF_3 (20.9-38.4-35.7-4-1 mole %), NaF-ZrF_4-UF_4 (50-46-4 mole %), NaF-UF_4 (66.7-33.3 mole %), NaF-KF-UF_4 (46.5-26.0-27.5 mole %), NaF-LiF-ZrF_4-UF_4-UF_3 (20-55-21-3.6-0.4 mole %), NaF-LiF-ZrF_4 (22-55-23 mole %), and NaF-LiF-BeF_2 (56-16-28 mole %). From the viscosity measurements that are now available for BeF_2-bearing fluoride mixtures, a relationship between BeF_2 concentration and viscosity was investigated. In general, the viscosity decreased as the BeF_2 concentration decreased. Some preliminary thermal-conductivity data of a ZrF_4-bearing fluoride mixture in the liquid state were obtained with a new conductivity cell and are in agreement with previous data obtained with a different type of cell.

8. Radiation Damage

The program of MTR irradiations of Inconel capsules designed for comparing UF_3- and UF_4-base fluoride fuels has continued. The results of examinations made thus far have shown no evidence of radiation damage in that there is no corrosion, no significant segregation of uranium, and no changes in the impurity content of the fluoride mixtures.

The fluoride-fuel loop that was operated in the LITR horizontal beam-hole has been disassembled, and parts of it have been examined metallographically. Subsurface void attack of the Inconel tubing used for the fuel loop was limited to less than 1 mil in depth. The fission products Ru^{103} and Nb^{95} were found to have plated out in two sections of the loop, and thus partial substantiation of a similar occurrence in the ARE was obtained.

The small loop intended for operation in a vertical hole in the LITR has been charged with fuel and is now in the final stages of assembly for the in-pile test. Data which were obtained for three different sizes of charcoal traps to delay fission gases from the small loop in the event of rupture were positively correlated. Two charcoal traps have been incorporated in the cooling-air off-gas line.

A tube-burst stress-corrosion apparatus has been assembled and awaits filling prior to irradiation in the LITR, and an LITR-irradiated stress-corrosion rig is ready to be examined in the hot cells. The creep apparatus installed in the MTR has just completed six weeks of irradiation and is ready to be returned to ORNL for postirradiation measurements.

An equation describing the behavior of the xenon poisoning in a fluid-fueled reactor was derived and was applied to the ART design. The calculations indicate that the removal of xenon by sparging with helium will be a satisfactory means of controlling xenon poisoning in the ART. Also, no difficulties appear to exist in connection with shutdown poisoning at the sparging rates selected for ART operation.

9. Analytical Chemistry of Reactor Materials

Apparatus was calibrated for the determination of uranium metal in fluoride salts by the method in which the metal is converted to UH_3 and subsequently ignited in oxygen at 400°C to form water and UO_2. Samples of UF_3 and KF-UF_3 were then analyzed. The coefficient of variation was 7% for the range 6 to 60 mg of uranium. No interference from the presence of either fluoride salts or trivalent uranium was encountered, and therefore the procedure should be applicable to all types of fluoride fuels.

A comparison of the methylene-blue and hydrogen-evolution methods for the determination of trivalent uranium in LiF-BeF_2-, NaF-LiF, and NaF-BeF_2 base fuels was made. Satisfactory agreement of the methods was observed for these materials; however, the results for trivalent uranium in a KF base obtained by the methylene-blue method showed *negative* bias when compared with those from the hydrogen-evolution method. Methylene-blue solutions which were 1.5 to 6 *M* with respect to HCl were shown to be reduced to methylene white at room temperature by finely divided metallic chromium, iron, nickel, and uranium-nickel alloy.

Studies were continued on the simultaneous determination of trivalent uranium and total uranium in fluoride salts. The postulation of an interaction species of pentavalent uranium and methylene white was investigated.

By using an anion-exchange resin in the hydroxide form to retain zirconium, beryllium, uranium, and sulfate ions, the quantitative separation of alkali metal ions was rapidly effected. Determination of the alkali metal concentration was made by titration of the free base which results from the anion resin exchange. When more than one alkali metal was present, the 2-ethyl-1-hexanol procedure was applied to the determination of lithium, and the tetraphenyl boron method was applied to the determination of potassium. Sodium was determined by difference methods.

A rapid volumetric method for the determination of zirconium in fluoride salts was proposed. In this method, which is a modification of the method of Fritz and Johnson, a standard solution of disodium dihydrogen ethylenediaminetetraacetate is used to complex zirconium, and the excess reagent is back-titrated with iron(III), with disodium-1,2-dihydroxybenzene-3,5-disulfonate as the indicator.

The bromination method for the determination of oxygen as oxide was applied to samples of CrF_3 and Na_2ZrF_6. Further tests were made on the electrolysis method for this determination. A modification of the Winkler method for the determination of oxygen in water was applied to determine the oxygen in the off-gases from the electrolysis. The oxygen is absorbed in a solution of $Mn(OH)_2$ and KI, which, upon acidification, liberates a quantity of iodine equivalent to that of oxygen. The iodine is determined spectrophotometrically by extracting it with orthoxylene.

An investigation was made of the determination of trace quantities of nickel in fluoride by the use of the reagent sodium diethyldithiocarbamate. The present experiments were not successful because of the interference of uranium and iron. Absorbance spectra of the carbon tetrachloride extracts were determined for aqueous solutions containing sodium diethyldithiocarbamate and such cations as nickel, iron, chromium, zirconium, and uranium.

10. Recovery and Reprocessing of Reactor Fuel

The feasibility of repeated use of a nickel reaction vessel in the fluoride volatility–fused salt process for recovery of ARE-type fuel was demonstrated in 20 laboratory-scale runs. Nickel test coupons held in the nickel reaction vessel during the 20 fluorination runs showed corrosion of the solution type that was even over all surfaces, including welds, in contact with the molten salt. Severe local pitting was noted that varied in depth up to 19 mils on the fluorine gas inlet tube in the vapor zone above the molten salt. The attack on this tube in the liquid zone was more uniform, and varied from 4 to 7.5 mils in depth. The reaction vessel showed nonuniform attack of the solution type that varied from 5 to 9 mils in both the liquid and gas zones.

At either 200 or 650°C, CaF_2 was much less efficient than NaF at 650°C in removing volatilized ruthenium from the UF_6-F_2 gas. However, results of runs made under various conditions indicated that the temperature, size, and conditioning of the NaF bed are very important.

The engineering flowsheet for the ARE fuel recovery pilot plant is 85% complete. Design of 10 of the anticipated 29 process equipment pieces is complete, and the pieces have been ordered.

Part I

REACTOR THEORY, COMPONENT DEVELOPMENT, AND CONSTRUCTION

1. REFLECTOR-MODERATED REACTOR

E. S. Bettis A. P. Fraas
W. K. Ergen A. M. Perry
Aircraft Reactor Engineering Division

AIRCRAFT REACTOR TEST DESIGN

A. P. Fraas
Aircraft Reactor Engineering Division

The preliminary layout of the interior of the reactor cell for the Aircraft Reactor Test (ART) which shows the major items of equipment and the recommended provisions for support was completed. A similar layout for the NaK piping and radiators was also completed. It has been established that five bulkheads will be required in the tank and cell walls for instrument and control wiring, piping, and miscellaneous service lines. Consideration has been given to the design of the addition to Building 7503 required for the ART, the layout of the blower house, and the electrical power system, distribution, and auxiliary equipment. Mounting arrangements have been described for the radiators, for the fill and drain tanks, for the inner and outer reactor cells, and for structurally attaching the reactor assembly to the cell, dump lines, NaK piping, and other service and instrumentation lines. The type of equipment by which oxygen will be removed from the inner cell has been specified.

The basic requirements of the heat dump system and the instrumentation and control thereof have been specified. The ART heat dump system is to provide heat dissipation capacity of 60 Mw of heat with a mean temperature level of 1300°F in the NaK system. The most convenient, inexpensive, and compact heat dump has been found to be a round-tube, plate-fin radiator core. This basic type of heat transfer surface has been found to be sufficiently reliable in heat exchanger test rigs. Five separate systems will be used; four will constitute the main heat dump system, while the fifth will be the moderator heat dump system. Layouts have been prepared of the air duct and stack associated with the heat dump radiators, and air flow rates and pressure drop have been calculated.

Design considerations have been tentatively established for the prevention of failure of the Inconel core and reflector shells during operation of the ART. The core shells are to be $\frac{1}{8}$-in.-thick Inconel. They are to be cooled on one side with flowing sodium in order to maintain the shells everywhere below 1500°F. The reflector shell is to be maintained below 1300°F by surrounding it with a layer of boron-bearing material, a gas space to serve as a heat dam, and an Inconel cladding layer to separate it from the hot fuel in the heat exchanger. To prevent buckling of the outer core shell because of external radial pressure differences and to prevent excessive deformation of the reflector shell because of excessive pressure differences, the pressures in the sodium coolant system and in the fuel are to be adjusted to be approximately equal at a point halfway through the primary heat exchanger. In order to limit cyclic thermal stresses, the temperature difference across the shells is not to exceed 300°F. Stress and heat transfer analyses are far from complete, but tentative pressures have been established for the fluid circuits.

In case of a failure of a part of the reactor system, for instance a fuel pump, during operation, it may be necessary to maintain emergency conditions for short periods in which the pressure differences across the shells will be much greater than those existing during normal operation. Calculations indicate that these conditions can be maintained without sudden failure of the shells by buckling or rupture. However, the total life of the reactor for normal operation will be disproportionately shortened.

Details of the basic design of the reflector-moderator cooling system have been set forth. Final design awaits confirmation of the values used in the design by critical experiments, heat exchanger optimization, core hydrodynamic tests, and beryllium thermal stress and corrosion tests now in progress (cf. Secs. 2, 3, and 7).

The xenon-removal system has been designed, as described previously,[1] and the fuel and sodium pumps are being tested (cf. Sec. 2, "Experimental Reactor Engineering"). New features that have been incorporated because of stress, fluid flow, or fabricability considerations include an elliptical

---

[1] G. Samuels and W. Lowen, *ANP Quar. Prog. Rep. Dec. 10, 1954*, ORNL-1816, p 21.

fuel expansion tank, a rounded dome to enclose the top of the reactor, a newly designed sodium pump impeller, and other related items.

A number of fuel-to-NaK heat exchanger designs have been calculated by utilizing the heat transfer data obtained experimentally (cf. Sec. 2, "Experimental Reactor Engineering," and Sec. 7, "Heat Transfer and Physical Properties"). The most promising of these designs are described in Table 1.1. The values given in the table are intended to facilitate comparison of typical heat exchangers. The values listed for heat exchanger thickness and shield weight are only relative and were based on a minimum-thickness tube array suited to the present design layouts. Final selection of the heat exchanger must be contingent on a composite evaluation of stress limitations, geometry, mass transfer and corrosion effects, and heat transfer requirements.

Conservative calculations were made of the neutron and gamma-ray dose rates at various locations in the ART facility. It was determined that radiation levels in the building during power operation would everywhere be below laboratory tolerance. Further, with the exception of a few locations, the initial dose rate from a reactor catastrophe would not be more than a few roentgens per hour. These low dose rates are the result of the reactor being located 16 ft underground and shielded (in addition to the lead-water reactor shield) by 3 ft of water in the cell annulus and substantial thicknesses of concrete and dirt. The radiators are to be shielded so that, in the event that 10% of the fuel entered the radiators, the radiation dose would not exceed 1 r/hr at any point outside the main air duct or reactor cell.

Research is under way that will provide much of the information needed as a basis for final design. In the experiments that are now being made with room-temperature critical assemblies of the reflector-moderated reactor, materials of interest in the design of the ART, such as beryllium, Inconel, and rare-earth oxides, are being evaluated. The information being obtained will be of benefit in making final decisions on reflector-moderator and island dimensions, configuration, and cooling requirements. Data on power distributions in the core will be used in determining the final configuration and size of the core and the end ducts, as well as the thickness of the Inconel shells and the cooling required. Measurements being made on rare-earth oxides are expected to provide data needed for design of the control rod for the ART.

Intensive experimentation is in progress in attempts to find fuels superior to the ZrF_4-bearing fuel used in the ARE. As yet, no positively superior fuel mixtures have been obtained, but the physical properties of the ZrF_4-bearing mixture have been improved to some extent by varying the

TABLE 1.1. ART HEAT EXCHANGER DESIGNS

Tube diameter, in.	$\frac{3}{16}$	$\frac{3}{16}$	$\frac{1}{4}$	$\frac{1}{4}$
Number of tubes per bundle	143	143	130	130
Tube spacing, in.	0.030	0.030	0.020	0.020
Tube wall thickness, in.	0.025	0.035	0.025	0.035
Fuel temperature range, °F	1250 to 1600	1250 to 1600	1250 to 1600	1250 to 1600
NaK temperature range, °F	1070 to 1500	1070 to 1500	1070 to 1500	1070 to 1500
Tube length, ft	6.0	6.3	5.45	5.81
Fuel ΔP, psi	41	45	28.4	30.1
NaK ΔP, psi	39.6	95	5.5	9.6
Heat exchanger thickness, in.	2.62	2.62	2.78	2.78
Reactor shield weight, water plus lead, lb	72,800	72,800	74,100	74,100
Total number of welds	6864	6864	6240	6240
Power, Mw	55	55	55	55
Relative NaK activation	1	1	2	2

composition, and the corrosiveness has been lowered by the addition of even small amounts of trivalent uranium.

The operation of forced-circulation, high-temperature-differential, Inconel loops with fuel mixtures of interest has demonstrated that the velocity of the circulated fluid has little effect on corrosion and mass transfer and that the results of the numerous thermal-convection loop tests are applicable to the dynamic ART system.

One in-pile forced-circulation Inconel loop that circulated a fuel mixture in the LITR has been examined, and radiation was found not to have a detrimental effect on corrosion and mass transfer; a second loop will be operated in the LITR during the next quarter. An in-pile loop that will more closely simulate the ART conditions is to be operated soon in the MTR.

Experiments with sodium in Inconel loops have thus far indicated unsatisfactorily high mass transfer, but it is thought that better purification and handling of the sodium will greatly decrease the mass transfer; also, the use of stainless steel in the cold portions of the system is being investigated.

Cermets for use as valves, bearings, and seals are undergoing intensive self-bonding and corrosion resistance tests, and procedures for brazing cermets to Inconel have been developed.

Studies of experimental nickel-molybdenum base alloys and commercial Hastelloy B, in particular, have indicated possibilities of finding a structural material with properties superior to those of Inconel for circulating-fuel reactor application, but some of the problems involved are of such a magnitude that it is not thought that such materials can be made available in time for use in the ART. The welding and brazing materials and techniques needed for fabrication of the ART have been developed and thoroughly tested in the construction of test components, such as heat exchangers and radiators.

A study of the behavior of xenon poisoning in a fluid-fueled reactor has indicated that the removal of xenon by sparging with helium will be a satisfactory means for controlling xenon poisoning in the ART. The study also indicated that no difficulty would exist in connection with shutdown poisoning at the sparging rates selected for ART operation.

Experiments now under way at the Lid Tank Shielding Facility will provide much of the data needed for final design of the reactor and, in particular, the shielding. A mockup of the reactor and shield is being used to determine activations within the heat exchanger and the effect on dose rates at various locations of varying materials and thicknesses of materials. The activation of the NaK within the heat exchanger is of particular importance because of the effect it will have on dose rates at the NaK-to-air radiators, which are outside the reactor shield.

Design of the engineering flow sheet of a fuel recovery pilot plant is 85% complete. It is hoped that the rapid reprocessing and recovery of fuel that would be required under service conditions can be demonstrated with this pilot plant.

The many calibration and performance tests scheduled for the ART are summarized in Table 1.2. Some of the tests can be run in the course of the endurance tests, which should consist first of 25 simulated flight cycles (16 hr at full power and 8 hr at from 1 to 10% power) and then of 100 hr of continuous operation at full power. This will give a total of 500 hr at full power and 200 hr at low power during the endurance test period. It is expected that the preliminary calibration and performance tests can be carried out during the first 400 hr of operation, with allowances for servicing and maintenance. In reviewing the design requirements and the tests planned for the ART, it is evident that many modifications could be made in the test conditions to vary the severity of the test. The key variables, together with the desired values for the test, are given in Table 1.3.

ART CONTROL

J. M. Eastman
Bendix Products Division

E. R. Mann
Instrumentation and Controls Division

Information block diagrams showing the basic control actions desired (without reference to hardware or techniques) have been prepared for the ART. They will be used as a basis for selection of the hardware types and the control techniques to be used and for determination of areas of control that will require new component development. Information for reactor simulation has been supplied to Pratt & Whitney, and they have built a simulator. It will be used to check the adequacy of the basic

TABLE 1.2. NUCLEAR EXPERIMENTS ON THE ART

Zero-Power Experiments

Criticality
  Demonstrate procedure for going critical
  Determine critical mass
Reactivity Experiments
  Determine fuel temperature coefficient
  Determine reflector and island temperature coefficient
  Determine mass reactivity coefficient
  Measure reactivity as a function of flow rate
  Determine delayed neutron loss to xenon purge system
Shielding
  Survey surface of shield for radiation
  Determine NaK activation in heat exchanger

High-Power Experiments

Demonstrate That the Reactor Is a Slave to the Load Demand
  Simulate sudden demand for increased power by turbojets
  Simulate failure of one turbojet
Determine Reactivity Effects of Other Transients
  Results of sudden flow stoppage
  Results of NaK flow stoppage
Determine Effectiveness of Xenon Removal System
Determine Compensation Required for Fission-Product Poisoning and Burnup
Demonstrate Afterheat Removal upon Shutdown
Obtain Heat Balances at Various Powers to Determine Extracted Power vs Nuclear Power for the Core, Heat Exchanger, Island, Reflector, Pressure Shell, Gamma Shield, and Neutron Shield

control actions and to determine control component design data. Additional simulator work will also be done at ORNL.

Control Principles

The control system is to provide automatic corrective action for emergencies requiring action too rapid to permit operator deliberation. Automatic interlocks will prevent inadvertent dangerous operation, with minimum operator limitation. Operation in the design power range will be independent of nuclear instrumentation and will have only limited dependence (for safety) on other instrumentation during power transients. Three classes of emergencies will be provided for:

1. those requiring automatic rod insertion, load removal, and fuel dump,
2. those requiring only automatic rod insertion and load removal (followed by manual dump at operator's discretion),
3. those requiring only operator warning and manual action.

One-half the wind tunnel blowers and one-half the pumps (of each type) will be powered by commercial supply. The remaining blowers and pumps will be powered by a deisel system. Duplicate fuel and sodium pumps have been provided for safety, but if any one of these four pumps failed, the output of each of the remaining three pumps would have to be decreased to prevent pump cavitation or pressure overstressing of the Inconel core shells in the current design. The basic control actions provide for this depression of output, but it is questionable whether pump speeds can be decreased fast enough to prevent adverse transient conditions. For example, the Inconel may be over-

TABLE 1.3. KEY ART PERFORMANCE VARIABLES

Variable	Desired Performance
Time at full power	500 hr
Total time critical	1100 hr
Total time thermally hot	1500 hr
Power level	60 Mw
Peak fuel temperature	1600°F
Peak metal temperature	1540°F
Peak NaK temperature	1500°F
Temperature difference between fuel and NaK	100°F
Number of power cycles	30
Rate of change of mean fuel temperature	7°F/sec
Number of dump cycles	5

stressed momentarily, with a consequent increase in creep rate. To prove at least that the reactor can be safely scrammed after such a pump failure, it is planned to include cutting off the commercial power (or diesel) at design point (60 Mw) as a part of the test procedure. This will constitute a class 1 emergency, as defined above.

The control rod cannot be abruptly inserted in the case of an emergency, because to do so and yet prevent the fuel from freezing or getting too hot would require accurate transient matching of absorbed power and flux power, which would be impractical to accomplish. Therefore a scram (class 1 or class 2 emergency) will abruptly insert the rod only enough to reduce $\Delta k/k$ by 1%. This will be followed by automatic insertion at the rate of 1% $\Delta k/k$ in 30 sec. This speed will be the "fast" normal rate of rod movement. The operator may also choose "slow" rod movement of 1% $\Delta k/k$ in 5 min. Below 10-Mw power operation, the operator will be automatically limited to the slower rate.

The 1% scram will automatically cut off one-half the blowers to reduce the load. The load will then be further reduced by automatic closing of the radiator shutter in response to a 1050°F low limit signal for the NaK-to-air radiator outlet temperature.

Since the design point occurs at the high temperature limit (1600°F) for the fuel, accurate limiting will be required. In addition to thermocouples in the fuel, the maximum fuel temperature will be indicated by continuous computing from NaK thermocouple signals by using heat exchanger calibration data. The dependability of fuel-temperature-sensing thermocouples is questionable because of the poor conductivity of the fuel and the high gamma-ray heating.

Operating Procedure

The reactor is to be initially filled with barren (without uranium) fuel carrier to check out the system. This will be done with the system isothermal at 1200°F and all NaK and sodium pumps operating. Electric heaters will supply the heat needed beyond that produced by pump work dissipating. After the checkout of the system, part of the barren carrier will be removed and replaced with fuel-enriched material to provide 80% of the calculated critical amount of U^{235}. Criticality will be checked, and the fuel will be further enriched in steps until criticality is obtained. The control rod will be calibrated in the process. A flux servo will then be available for holding the reactor at very low power levels (under 10 kw) during low-power experimentation. At these levels the temperature coefficient will be inadequate for good control because of the high thermal capacity of the system.

The minimum power level for control by the temperature coefficient is expected to be about 300 kw – the estimated heat removal by the radiators with the heat barrier doors open and no air flow. To take the reactor to the 300-kw level, it will manually be put on not less than a 20-sec positive period, and the barrier doors will be opened when the flux level reaches a set value equivalent to something less than 300 kw. If the doors were opened too soon or too late, excessive power surges might occur before the flux stabilized and there might possibly be damaging thermal shocks. After stabilization at 300 kw, the control rod will be slowly adjusted to bring the mean fuel temperature to 1200°F (it will have gone somewhat above this).

To increase the power above 300 kw, the blowers will be turned on and the shutters opened as desired. The control rod will be used to adjust the mean fuel temperature. Automatic limiters will close the shutters if the minimum NaK temperature drops below about 1050°F (to prevent fuel freezing) and will open them if the minimum NaK temperature goes above 1300°F (to dissipate afterheat and prevent loss of ZrF_4). To take out more than 20 Mw will require that the mean fuel temperature be set above 1200°F (it must be set at 1425°F to take out 60 Mw). Below about 6 to 10 Mw, the heat dump will have to be adjusted slowly to avoid high flux and temperature surges. Above this power the temperature coefficient is expected to permit reasonably fast (for jet engines) load changes without excessive transient surges.

REACTOR PHYSICS

ART Temperature Coefficient

L. T. Anderson

Aircraft Reactor Engineering Division

A calculation of the ART temperature coefficient showed a positive contribution resulting from the decrease of the absorption cross section of the Inconel core shells[3] with increasing neutron energy. The smaller Inconel cross section allows more neutrons to enter the fuel annulus and thus increase the reactivity. It seems justified to assume a $1/v$ cross section for the Inconel on the basis of the experimentally measured value of the resonance integral, and therefore, if an increase, ΔT, of the beryllium temperature causes a neutron energy increase proportional to ΔT, the fractional cross-section decrease of the shells is $\frac{1}{2}\,\Delta T/T$, and the number of fissions is increased by the factor

$$\tfrac{1}{2}(\Delta T/T)\Sigma_{th} \times \text{shell thickness} \times \text{cadmium fraction}$$

if only the subcadmium neutrons are affected and the neutrons are incident normal to the shell. Actually, the thickness of the Inconel that the neutrons go through is somewhat greater than that of the shell, on the average, but this is at least partially offset by the cross section of

Inconel having a less-than-thermal value for some of the subcadmium neutrons. The value of $\Delta k/k$ calculated in this way is $+1.7 \times 10^{-5}\ \Delta T$ (°F) for ⅛-in. Inconel shells. As pointed out by Mills and Reece[3] and Ergen (above), core shells of materials of lower absorption cross section would reduce this positive coefficient contribution. If $\frac{1}{16}$ in. of the ⅛-in. Inconel shell were replaced by columbium, the $\Delta k/k$ value would be reduced to

$$1.7 \times 10^{-5}\,\frac{f(\text{Inc.} + \text{Cb})}{f(\text{Inc.})}$$

$$= 1.7 \times 10^{-5}\,\frac{0.035}{0.060} = 1.0 \times 10^{-5}/{}^{\circ}\text{F} ,$$

where f is the fraction of thermal neutrons incident on the shells that are absorbed (cf. preceding paper by W. K. Ergen, this report).

The effect of beryllium expansion is considered by using, as a model for the reactor, a sphere (radius, R_2) of noncapturing beryllium with a high energy neutron shell source at R_1. The source neutrons slow down according to age theory, and the slowing down density at thermal age is used as a source for the thermal diffusion equation. It is assumed that at thermal energy every neutron striking the shell at R_1 is absorbed and causes a fission. By using this model, $\Delta k/k$ turns out to be[5]

$$\frac{-2KR_2\sqrt{\tau}\,\Delta T}{\sqrt{\tau}\,R_1(R_2 - R_1) - R_2\sqrt{\tau}} ,$$

where K is the coefficient of linear thermal expansion for the beryllium and τ is the thermal age. By using $K = 9.3 \times 10^{-6}/{}^{\circ}\text{F}$, $\tau = 90\ \text{cm}^2$, $R_1 = 25$ cm, and $R^2 = 56$ cm, it is found that $\Delta k/k = -1.2 \times 10^{-5}\ \Delta T$.

The net of these two contributions is then $0.5 \times 10^{-5}/{}^{\circ}\text{F}$ for ⅛-in. Inconel core shells and -0.2×10^{-5} for core shells of $\frac{1}{16}$-in. Inconel and $\frac{1}{16}$-in. columbium. A fuel coefficient of $-1.7 \times 10^{-5}/{}^{\circ}\text{F}$, which is based on a conservative value of 0.1 for $(\Delta k/k)/(\Delta M/M)$, gives over-all coefficients of $-1.2 \times 10^{-5}/{}^{\circ}\text{F}$ and $-1.9 \times 10^{-5}/{}^{\circ}\text{F}$ for the two cases. It should be noted, however, that the calculation is of a *marginal* type, and hence there might be a sizable error in the results. Nevertheless, the results support the postulated negative over-all temperature coefficient of the ART.

Reactivity Effect of a Heat Exchanger Leak

A. M. Perry
Electronuclear Research Division

If the pressure in the NaK coolant circuit exceeds that in the fuel circuit, a leak in the intermediate heat exchanger may first become apparent through its effect on the reactivity of the ART. The effect will be due to dilution of the fuel and to increased parasitic absorption. It has been suggested by the Advisory Committee on Reactor Safeguards that the reactivity effect can be greatly enhanced by adding lithium or Li^6 to the NaK. Preliminary experiments[6] indicate that perhaps 5 wt % lithium can be added to the NaK eutectic without raising the melting point above 25°C. The loss of reactivity due to parasitic absorption is calculated on the assumption that

$$\frac{\Delta k}{k} = \frac{\Delta f}{f} = \frac{\Delta\Sigma_p}{\Sigma_F} ,$$

where f equals (neutrons absorbed in fuel)/(neutrons absorbed in core), $\Delta\Sigma_p$ is the change in poison cross section, and Σ_F is the fuel cross section.

The loss of reactivity due to fuel dilution is calculated on the assumption that

$$\frac{\Delta k}{k} = \frac{1}{10}\,\frac{\Delta\Sigma_F}{\Sigma_F} = \frac{1}{10}\,\frac{\Delta V}{V} ,$$

where V is the initial fuel volume, and ΔV the volume of NaK leaked into the fuel circuit. The factor $\frac{1}{10}$ is a conservative estimate based on critical experiment results.

The over-all reactivity loss, if ΔV is in cubic feet of coolant leak into the fuel circuit, is given by

$$\frac{\Delta k}{k} = -2.4\,\Delta V(\%) ,$$

if the coolant is NaK; by

$$\frac{\Delta k}{k} = -(2.4 + 2.2\,W)\,\Delta V(\%) ,$$

if the coolant is NaK plus W wt % lithium; and by

$$\frac{\Delta k}{k} = -(2.4 + 29.6\,W)\,\Delta V(\%) ,$$

---

[5] L. Anderson, *Calculation of the Beryllium Contribution to the ART Temperature Coefficient of Reactivity*, ORNL CF-55-5-76 (May 11, 1955).

[6] W. D. Manly, private communication.

if the coolant is NaK plus W wt % Li^6. (Of course, the approximations made are valid only for small changes in reactivity and for small percentage additions of lithium to the NaK.)

The maximum volume available before an overflow would occur will be 0.37 ft^3. This volume of NaK in the fuel circuit would produce a reactivity change of 0.9%. The same volume of NaK plus 5 wt % lithium would produce a reactivity change of 5%. A leak of 0.007 ft^3 of NaK plus 5 wt % Li^6 would produce a reactivity loss of 1%.

Burnup and Gamma-Ray Heating of Control Rod

W. Fader

Pratt & Whitney Aircraft

Burnup of Poison. The equations of burnup in a slab of neutron absorber with thermal neutrons incident on one face are, for the case of an absorber with n isotopes with high thermal capture cross sections σ_i,

$$\frac{\partial J}{\partial x} + \Sigma\phi = 0 \ ,$$

$$\frac{\partial \Sigma_i}{\partial t} + \sigma_i \Sigma_i \phi = 0 \ ,$$

where

J = net neutron current normal to slab face,

x = linear coordinate normal to the slab,

$\Sigma = \Sigma_1 + \Sigma_2 + \ldots + \Sigma_n$ = macroscopic thermal neutron absorption cross section,

ϕ = flux,

t = exposure time.

By making use of the relationship $J = \bar{\mu}\phi$, where $\bar{\mu}$ is the average value of the cosine for the angular distribution of the neutron flux, the equations become

$$\bar{\mu}\frac{\partial J}{\partial x} + \Sigma J = 0 \ , \tag{1}$$

$$\bar{\mu}\frac{\partial \Sigma_i}{\partial t} + \sigma_i \Sigma_i J = 0 \ . \tag{2}$$

In the region where most of the burnup takes place, $\bar{\mu}$ is constant if the macroscopic absorption cross section is much greater than the macroscopic scattering cross section. Its value may be expected to range between unity at points deep in the slab to 0.5 at the surface, the latter value being the diffusion theory approximation to the boundary condition at the plane interface of a scattering medium and a strong absorber.

Solutions for $J(x,t)$ and $\Sigma(x,t)$ were found for the case of a single absorber and the results have been plotted in Fig. 1.1 for a slab of Sm$_2$O$_3$. For large values of $\sigma J_0 t/\bar{\mu}$, where $J_0 = J(0,t)$, the curves of $J(x,t)$ and $\Sigma(x,t)$ assume rigid shapes that are propagated in the direction of increasing x with apparent velocity

$$v = \frac{\sigma J_0}{\Sigma_0} \ ,$$

which, for the case of the curves in Fig. 1.1, was $v = 2.9 \times 10^{-8}$ cm/sec. This suggests the use of the linear formula

$$X(t) \cong 0.012 + (2.9 \times 10^{-22} J_0 t) \text{ cm} \tag{3}$$

for the thickness of a slab of Sm$_2$O$_3$ that will transmit 10% of J_0 neutrons/cm^2·sec incident on its front surface after an exposure time of t sec.

Equations 1 and 2 were integrated numerically for the case of gadolinium with two isotopes with high thermal absorption cross sections, and the results are shown in Fig. 1.2 for Gd$_2$O$_3$. The linear relation between X and t for large $\sigma J_0 t/\bar{\mu}$ for Gd$_2$O$_3$ is

$$X(t) = 0.0025 + (1.4 \times 10^{-22} J_0 t) \text{ cm} \ . \tag{4}$$

Formulas 3 and 4 may also be used as an approximation of the burnup of a cylindrical shell of absorber, provided that the inner radius of the shell is much larger than the thermal neutron mean free path of the absorber; for, in this case, Eq. 2 remains unchanged, while Eq. 1 becomes

$$\bar{\mu}\frac{\partial J}{\partial r} = \Sigma J - \bar{\mu}\frac{J}{r} \tag{5}$$

for neutrons incident on the outer surface. For a shell of this kind, the term $\bar{\mu}J/r$ in Eq. 5 is always negligible compared with ΣJ in the region of burnup. In the ART, a 20-in. control rod with a 1$\frac{3}{8}$-in. outside diameter must absorb an average of at least 2 × 10^{14} neutrons/cm^2·sec in order to be 5% effective in reactivity. Thus, if a cylindrical shell of Sm$_2$O$_3$ absorbs 2 × 10^{14} neutrons/cm^2·sec for 1000 hr, the neutrons will penetrate a distance

$$X(t) = 0.012 + (2.9 \times 10^{-8})(7.2 \times 10^{6}) \sim 0.22 \text{ cm} .$$

A shell of Sm$_2$O$_3$ must have at least this thickness

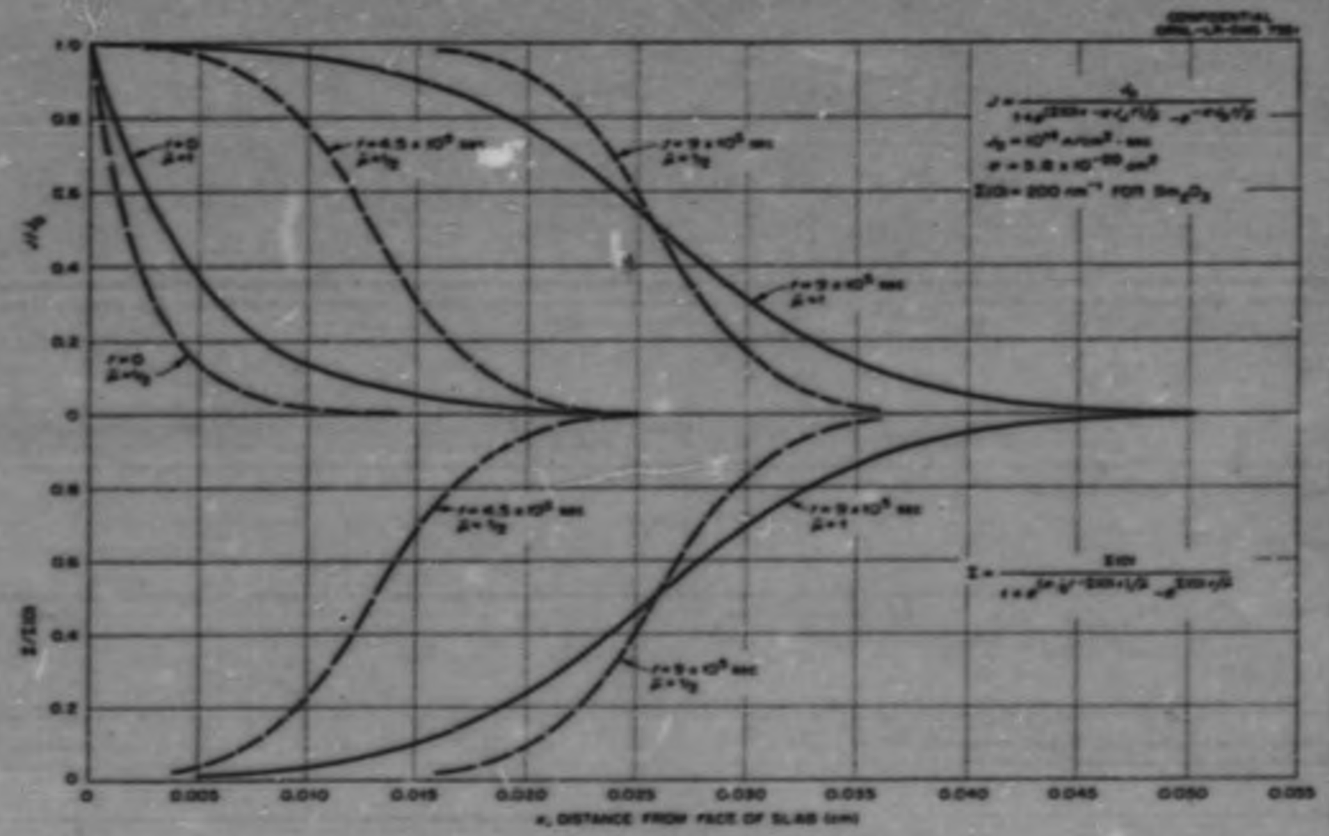

Fig. 1.1. Burnup of a Samarium Oxide Slab.

to remain black to neutrons after 1000 hr with $J_0 = 2 \times 10^{14}$. For Gd_2O_3,

$$X(t) = 0.0025 + 1.4 \times 10^{-8}(7.2 \times 10^6) = 0.10 \text{ cm} .$$

To obtain an estimate of the error of the approximation, note that for a shell with an outside diameter of $1\frac{3}{8}$ in. = 1.76 cm and a length of 20 in. = 50.8 cm, an absorption rate of 2×10^{14} neutrons/cm²-sec at the outer surface will burn up 4.05×10^{23} atoms or 100 g of Sm^{149}. This corresponds to 868 g of Sm_2O_3; the volume of burned up material would be 116 cm³. A shell with an outside diameter of 1.76 cm, a length of 50.8 cm, and a volume of 116 cm³ has a wall thickness of 0.22 cm. The burnup of Eu_2O_3 slabs has also been calculated, and the results are presented in Fig. 1.3.

Gamma-Ray Heating. Two effects are expected to contribute to the internal heating of control rods of rare-earth oxides: absorption of gamma radiation emitted immediately after capture of neutrons in the rod and absorption of gamma rays from the reactor fuel.

Preliminary calculations of the gamma-ray heating in the control rod indicate that the average energy absorption will be at least 100 w/cm³. More detailed calculations made by Pratt & Whitney Aircraft indicate that the gamma energy absorption may be as high as 170 w/cm³. For the higher value the maximum interior temperature rise above the surface temperature is 460°C for a $1\frac{3}{8}$-in.-OD hollow rod of rare-earth oxide with a $\frac{1}{4}$-in. wall, if the thermal conductivity is assumed to be 0.0048 cal/sec·°C·cm. If a cermet of rare-earth oxide and iron is used in place of the oxide, the maximum temperature rise is about 45°C, if a thermal conductivity of one-third that of iron, or 0.050 cal/sec·°C·cm, is assumed.

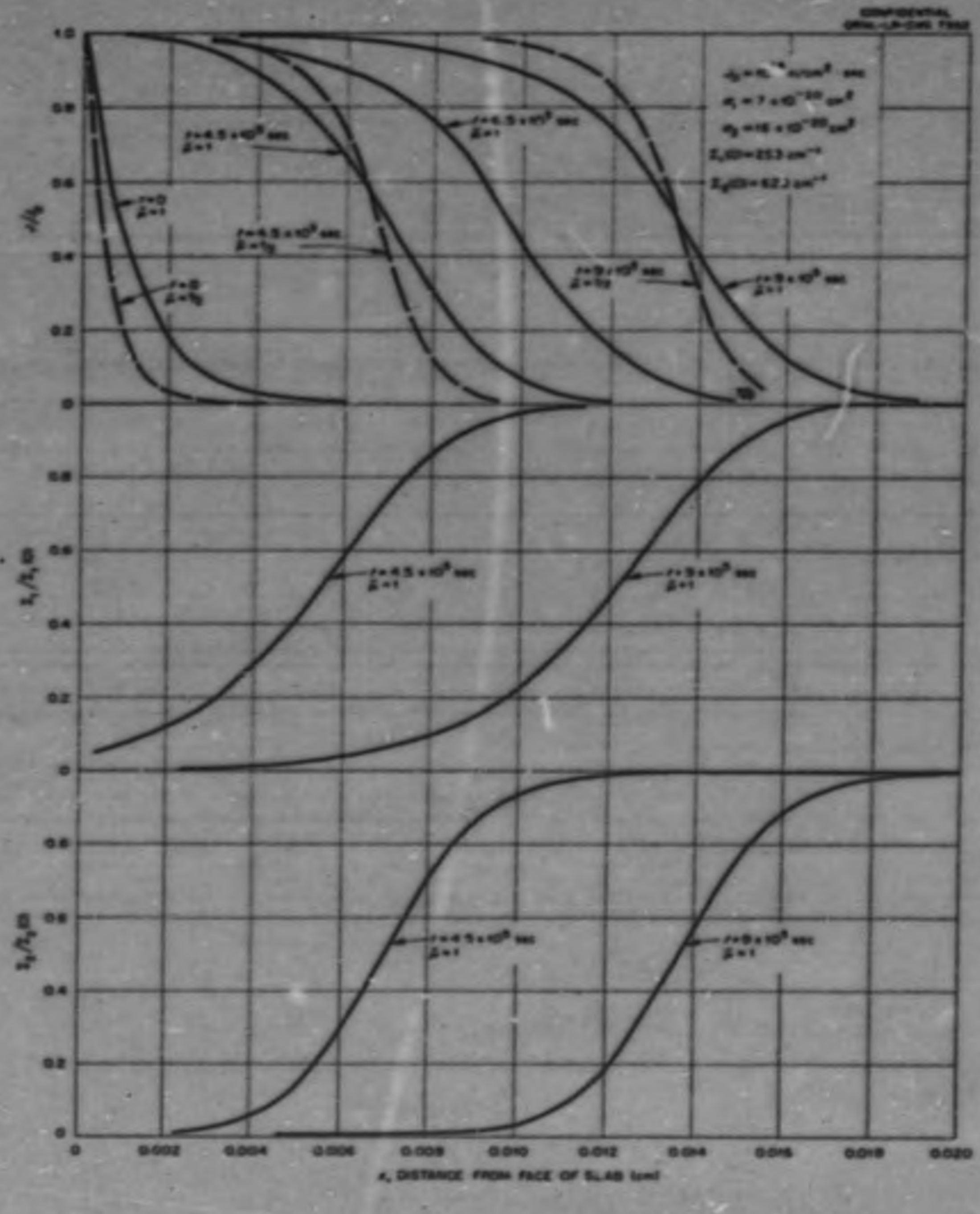

Fig. 1.2. Burnup of a Gadolinium Oxide Slab.

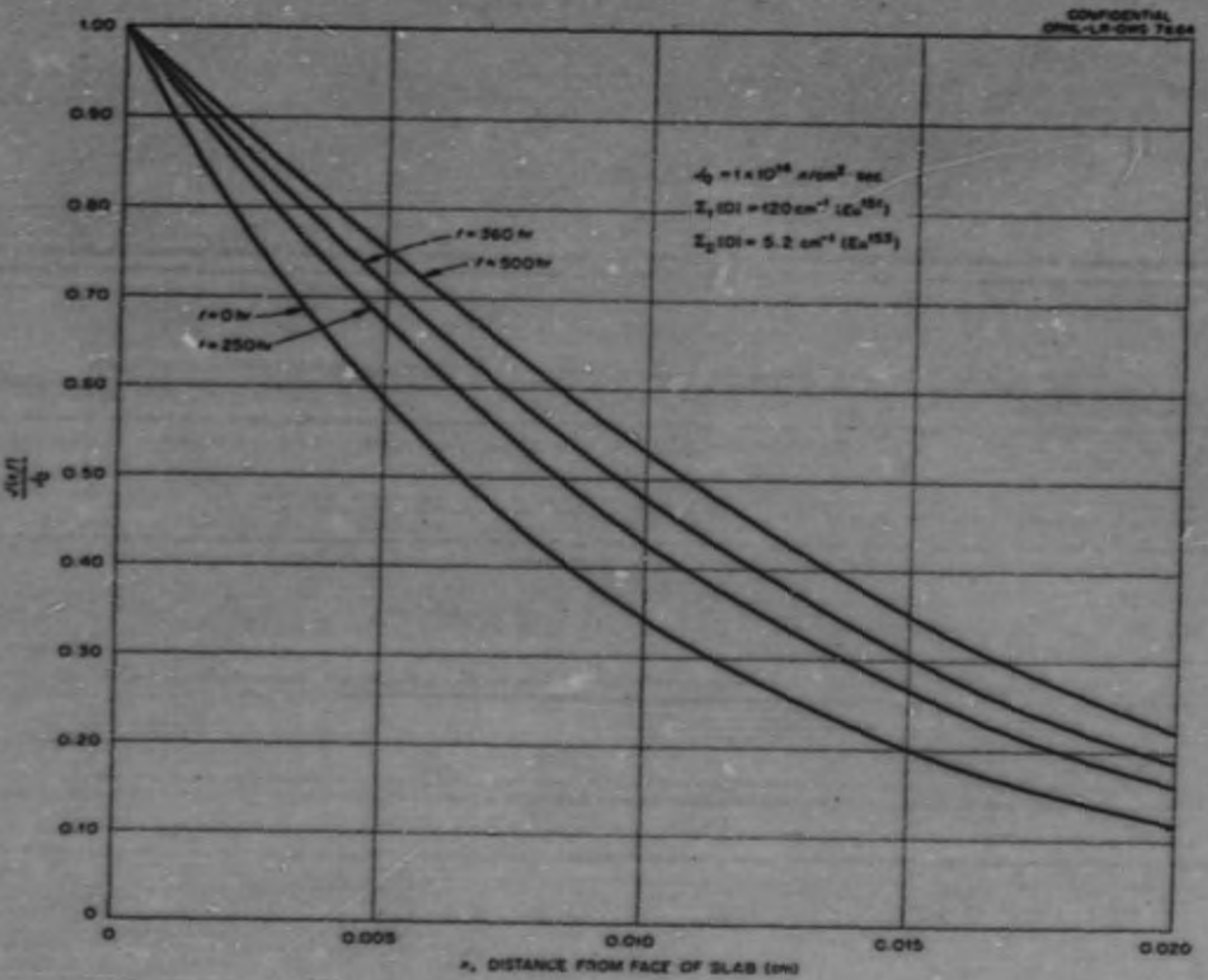

Fig. 1.3. Burnup of a Europium Oxide Slab.

2. EXPERIMENTAL REACTOR ENGINEERING

H. W. Savage E. S. Bettis
Aircraft Reactor Engineering Division

Design work on the in-pile loop for operation in the MTR has been completed, and the final loop is being fabricated and assembled. A bench test of a working mockup is under way. Twenty-two high-velocity forced-circulation large-temperature-differential loops were operated for investigating the corrosion and mass transfer of Inconel by fluoride fuel mixtures under dynamic conditions. Six similar loops were operated to test mass transfer in Inconel and stainless steel loops in which sodium is circulated.

A full-scale model of the ART fuel pump was tested with water, and performance characteristics were obtained. A test stand for high-temperature tests has been designed. A test stand for intermediate heat exchangers (100-tube bundle) is being assembled, and tests are under way with a stand designed for testing small-scale (20-tube bundle) heat exchangers.

Flow patterns are being studied in a full-scale model of the proposed 21-in. reactor core and entrance header. Several modifications are to be tried in an attempt to prevent flow separation in the core.

A thermal-cycling test was made on a sodium-Inconel-beryllium system, and apparatus for a third test is being assembled. A small-scale gas-fired heat source was operated successfully at a power output of 100 kw, and minor modifications were planned that will increase the capacity.

IN-PILE LOOP COMPONENT DEVELOPMENT

D. B. Trauger
Aircraft Reactor Engineering Division

Flux Measurements

D. M. Haines
Pratt & Whitney Aircraft

Flux measurements, as previously described,[1] were carried out in the HB-3 beam hole of the MTR. Cobalt foils installed in various assemblies that simulated the loop were irradiated for 3 hr at about 5 Mw. Plans to make measurements at full power were abandoned because an excessively long irradiation was required to override the effects of the minimum period in which the reactor could be brought to full power. Gold foils irradiated at the low power and again at full power in a vertical hole adjacent to HB-3 provided a means for extrapolating the data to full power.

This measurement made it possible to evaluate the effect of materials and geometry of the in-pile loop on the flux. Values obtained from foils inside the fuel tube were consistent with other data taken from foils irradiated in Inconel tubes by using a rabbit facility for irradiation in hole HB-3. Other data on the depression of flux in Inconel tubes with a fuel mockup present were also used to estimate the flux for the MTR in-pile loop.

The flux seen by the fuel in the in-pile loop is now expected to be 30% of the unperturbed value. The heater loop, or nose section, originally designed for a depression of 50%, has been modified to obtain more power. The present nose section consists of a $2\frac{1}{2}$-turn helical coil shaped, in outline, somewhat as a truncated cone. It is mounted with its axis parallel to the beam hole center line and with the small end forward. This will permit the nose to be placed in the most forward position possible by utilizing the conical end of the water jacket. The developed length of the coil is slightly over 3 ft. A total power generation of 24 kw is required for the design conditions: Reynolds number, 5,000; temperature differential, 200°F. The average power density in the nose section, on this basis, will be 0.7 kw/cm^3; however, this value may be conservative. Provision is being made to change the loop position in the beam hole during operation and thus utilize the flux gradient to adjust the power. A higher power density may be feasible for later loops.

Fission-Gas Holdup

D. W. Magnuson
Aircraft Reactor Engineering Division

The adsorption of krypton from helium by activated carbon at liquid-nitrogen temperature is being tested in adsorption traps designed for use with the MTR in-pile loop. The traps contain 280 g of Columbia ACA activated carbon. A helium cylinder

---

[1] D. M. Haines, *ANP Quar. Prog. Rep. Mar. 10, 1955*, ORNL-1864, p 32.

containing 0.13% krypton is being used to supply five times the design flow rate through one trap. The same supply furnishes the design flow of 0.03 scfh to a second system containing two carbon traps in series. The second trap will be isolated at the conclusion of the experiment, and the adsorbed gas will be analyzed for total krypton. After 15 days of operation, the krypton concentration in the effluent stream was approximately 1 ppm in both systems, or the fractional breakthrough was less than 0.001. A temperature-sensing element filled with oxygen, with an automatic fill device, is being used to keep a constant liquid level in the metal Dewar which contains the traps.

Bench Test

L. P. Carpenter
Aircraft Reactor Engineering Division

A bench test for the in-pile loop has been operated for more than 666 hr. The purpose of this bench test is to determine the feasibility of construction techniques, to test the suitability of the various materials of construction, to aid in establishing control and operational procedures and in training operators for the in-pile test, and to determine the endurance of supporting equipment.

The design conditions as set forth for the in-pile loop were adhered to as closely as possible in the bench apparatus. Modifications were limited to incorporating a resistance-heater coil for power generation. The loop is enclosed in a plug that differs from the actual in-pile loop plug only in that the forward end is open to accommodate connections with the resistance heater. All service lines to the loop run through the plug in the same manner as they will in the in-pile test.

The instrumentation and the control panel for the bench test are identical to those to be used at the MTR, except for the absence of radiation-detection instruments. Thus operator training can be accomplished under closely simulated conditions.

Fabrication and assembly of the bench apparatus served to point up certain difficulties in building this type of system. One basic requirement for an in-pile loop is concentricity of less than $\frac{1}{16}$ in. in 14 ft of length. Some difficulty was experienced because of warping at thermocouple wells and poor fits. Fixtures are being fabricated for use in aligning parts during construction, and the drawings have been revised in some instances.

The commercial Kovar-glass seals used to bring power and thermocouple wires through bulkheads and to form leaktight closures have proved troublesome by not being adequately leaktight. A seal has been developed at the Gaseous Diffusion Plant, K-25, which is quite satisfactory, except that it is vulnerable to breakage during loop assembly. Fourteen thermocouple leads or eight power leads can be brought through a $1\frac{1}{8}$-in.-dia glass cup seal.

Bench test experience showed that the use of a poured barytes concrete shield in the rear section of the shield plug required that the lead wires be protected from moisture condensation and the concrete. Glass-braid insulation was applied to individual wires, which were then bunched and encased in plastic tubing. After the concrete was poured, the wires were found to be shorted. Heating and pumping on the concrete made the connections usable, but other steps are being taken to prevent recurrence of this trouble for the in-pile loop.

The operating conditions for the bench test are: temperature differential, 175°F; Reynolds number, 5100; power input, 21 kw; temperature differential for air, 250°F at 250 scfm. Control is achieved by regulation of the air flow through the heat exchanger by an automatic controller that maintains a nearly constant temperature, ±10°F, on the fuel tube at the pump. The electrical power input is manually controlled.

Operation of the loop is proceeding satisfactorily. Cavitation of the hydraulic power unit has caused momentary fluctuations in the pump speed that trip the alarm system. A leak in the drive pump suction line has been found to be the cause of cavitation and has been corrected. The in-pile power unit is also being operated and checked prior to shipment to NRTS.

Horizontal-Shaft Sump Pump

J. A. Conlin
Aircraft Reactor Engineering Division

The regenerative turbine-type in-pile pump, previously described,[2] was disassembled and inspected after completing 1300 hr of operation. As can be seen in Fig. 2.1, there was no erosion and only a slight indication of rubbing between the pump

---

[2] J. Conlin, *ANP Quar. Prog. Rep. Mar. 10, 1955*, ORNL-1864, p 32.

Fig. 2.1. Horizontal-Shaft Sump Pump for In-Pile Loop After 1000 hr of Operation Circulating NaF-ZrF_4-UF_4 (53.5-40-6.5 mole %) at 1400°F and 1 gpm in an Isothermal Loop.

shaft extension and the pump housing. This rubbing is known to have occurred during preheating of the pump and to have been caused by thermal stresses induced by an unduly rigid pump mounting. There was no evidence of zirconium fluoride vapor in the rear pump housing beyond a point $\frac{3}{4}$ in. from the pump sump proper, and no salts were found in the vent line after the test. A continuous helium purge of this area of about 0.3 cfh was used. There was no evidence of oil in the fuel portion of the pump, the measured oil seal leakage being 0.15 cm^3 for the 1000 hr. However, the pump sump gas pressure was higher than the bearing housing pressure, which would tend to cause seal leakage to be toward the bearing housing. The shaft seal facos were in good condition and apparently could have operated for an additional 1000 hr, or more.

The pump impeller that will be used in the in-pile experiment is identical with the one used in the test described above. The bearing housing and seal designs are different, however, in order to overcome the problems of radiation damage to the oil and to prevent leakage of fission gases. Instead of the oil cooling, the shaft is cooled by a copper spool on the shaft that operates in a helium atmosphere with a close clearance to the water-cooled housing. The pump bearings and seals are drop-lubricated. To seal fission gases from the oil in the hydraulic drive motor, two shaft seals are employed, one between the pump sump and the bearing housing and one between the bearing housing and the hydraulic motor. These are face-type seals with metallic bellows for the flexible member. The gas volumes in both the sump and the bearing housing are purged with helium to further reduce the possibility of oil contamination. The pump housing also serves as a leaktight bulkhead in the water jacket to seal the loop end from the bearing housing and motor section of the water jacket. This section between the pump bulkhead and the intermediate bulkhead will be used to accumulate the waste bearing- and seal-lubricating oil. An exploded view of this pump is shown in Fig. 2.2.

Difficulty is still being experienced with failure of the rotating seals. This trouble is principally associated with the bellows and with breakage of the carbon rings. Replacement of the brass bellows with stainless steel bellows and the exercise of greater care in assembly seem to have improved the situation. The sliding surfaces have given little, or no, trouble.

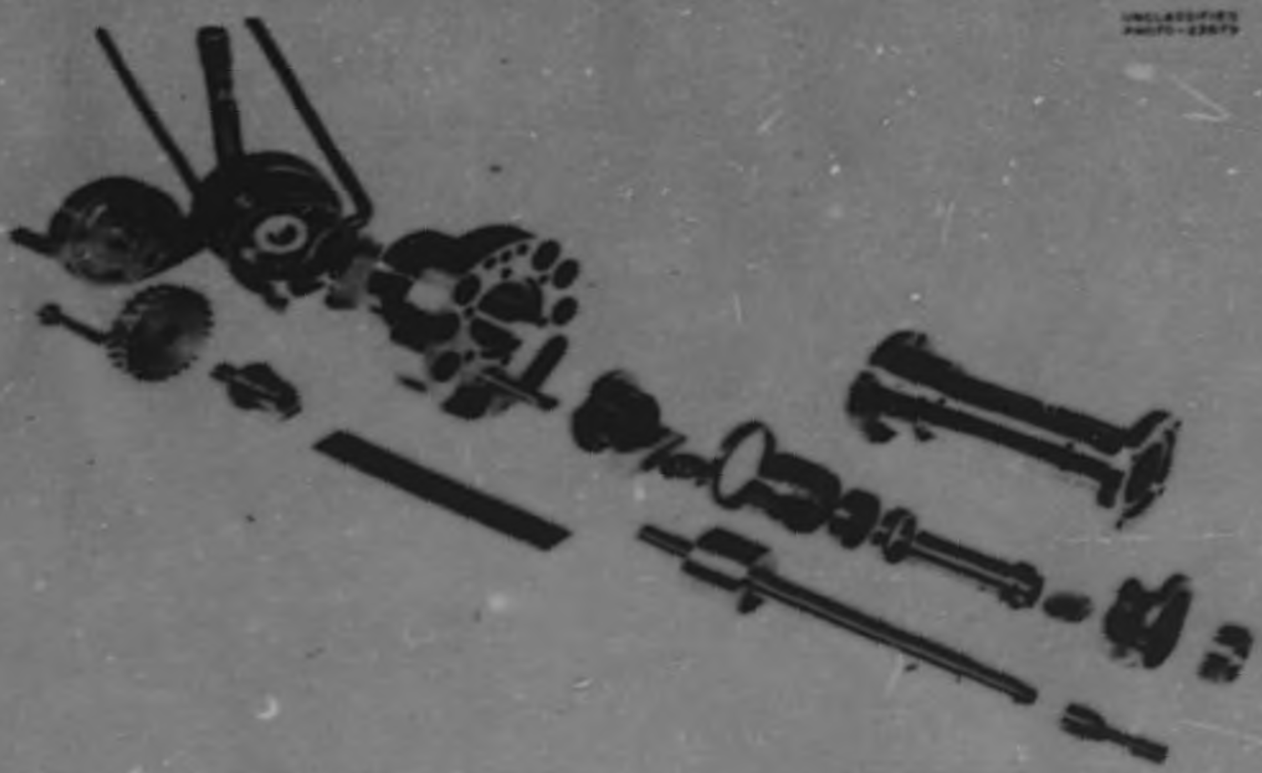

Fig. 2.2. Exploded View of Pump to Be Used for MTR In-Pile Loop No. 1.

Instrumentation

R. G. Affel P. A. Gnadt
Aircraft Reactor Engineering Division

Instrumentation design has been completed, and the panel for MTR operation is nearly assembled. Operating experience with the bench test panel has demonstrated smooth and dependable operation of most of the instruments. Some difficulty has been encountered with the pump rpm meter, where false signals have been generated. Shielding of lines and further isolation of components are expected to correct this condition. Since the bench test panel is identical with that for MTP operation, except for the ommision of radiation-detecting equipment, it has provided a good test of the recording and control systems.

Assembly of MTR In-Pile Loop No. 1

C. W. Cunningham
Aircraft Reactor Engineering Division

Most parts for the first in-pile loop have been fabricated, and assembly is under way. A wooden model of the cubicle space has been fabricated as an aid in the installation of lines to the loop and its auxiliaries. The parts, including a cut-off device for the various lines, will be installed on the model first, and then removed for shipment to NRTS. This, it is hoped, will ensure a proper fit and minimize on-the-site installation time.

DEVELOPMENT AND OPERATION OF FORCED-CIRCULATION CORROSION AND MASS TRANSFER TESTS

Operation of Fused-Salt-Inconel Loops

W. B. McDonald
C. P. Coughlen P. G. Smith
Aircraft Reactor Engineering Division
J. J. Milich R. A. Dreisbach
Pratt & Whitney Aircraft

The operation of high-velocity forced-circulation large-temperature-differential loops for investigating the corrosion of Inconel by fluoride fuel mixtures under dynamic conditions has become so routine that operation can be scheduled, and the schedules can be maintained for long periods without serious interruption. Twelve loops have been terminated following scheduled operation; five loops were terminated short of scheduled operating time because of various failures; and five loops were started and are continuing in operation. A summary of the typical operating conditions is given in Table 2.1.

During the early part of the quarter, loop failures were encountered because heater lugs were welded

TABLE 2.1. SUMMARY OF OPERATING CONDITIONS FOR 22 FUSED-SALT-INCONEL FORCED-CIRCULATION CORROSION AND MASS TRANSFER TESTS

Maximum Fused Salt Temperature: 1500°F

Loop No.	Method of Heating	Type of Heated Section	Reynolds Number	Temperature Differential (°F)	Maximum Recorded Tube Wall Temperature (°F)	Fused Salt Circulated	Operating Time (hr)	Reason for Termination
4950-1	Direct resistance	Straight	5,000	200	1650	$NaF-ZrF_4-UF_4$[a]	1000	Scheduled
4950-2	Direct resistance	Straight	5,000	200	1565	$NaF-ZrF_4-UF_4$[a]	1000	Scheduled
4950-3	Direct resistance	Straight	10,000	200	1690	$NaF-ZrF_4-UF_4$[b]	1000	Scheduled
4950-4	Direct resistance	Straight	10,000	100	1600	$NaF-ZrF_4-UF_4$[a]	1000	Scheduled
4950-5	Direct resistance	Straight	10,000	200	1575	$NaF-ZrF_4-UF_4$[a]	1500	Scheduled
4950-6	Direct resistance	Straight	8,000	300	1620	$NaF-ZrF_4-UF_4$[a]	1000	Scheduled
4930-A	Direct resistance	Coiled	1,000	300	1695	$NaF-ZrF_4-UF_4$[c]	1000	Scheduled
4895-1	Direct resistance	Coiled	10,000	300	1720	$NaF-ZrF_4-UF_4$[b]	385	Leak
4895-2	Direct resistance	Straight	15,000	200	1670	$NaF-ZrF_4-UF_4$[b]	887	Pump-bearing failure
4895-3	Direct resistance	Straight	10,000	300	1640	NaF-KF-LiF[d]	620	Leak
4895-4A	Direct resistance	Straight	10,000	200		$NaF-ZrF_4-UF_4$[a]	0	Terminated after cleaning operation as first of a series for determination of effect of time
4895-5A	Direct resistance	Straight	10,000	200		$NaF-ZrF_4-UF_4$[a]	10	Scheduled
4895-4B	Direct resistance	Straight	10,000	200		$NaF-ZrF_4-UF_4$[a]	50	Scheduled
4895-4C	Direct resistance	Straight	10,000	200		$NaF-ZrF_4-UF_4$[a]	100	Scheduled
4895-5B	Direct resistance	Straight	10,000	200		$NaF-ZrF_4-UF_4$[a]	241	Leak
4895-5C	Direct resistance	Straight	10,000	200		$NaF-ZrF_4-UF_4$[a]	500	Scheduled
4935-1	Gas-fired heater	Coiled	1,000	300	1670	$NaF-ZrF_4-UF_4$[c]	1000	Scheduled
4935-2	Gas-fired heater	Coiled	5,000	200	1675	$NaF-ZrF_4-UF_4$[a]	1000	Scheduled
4935-3	Gas-fired heater	Coiled	10,000	100	1540	$NaF-ZrF_4-UF_4$[a]	1000	Scheduled
4935-4	Gas-fired heater	Coiled	10,000	100	1690	$NaF-ZrF_4-UF_4$[a]	486	Leak
4935-5	Gas-fired heater	Coiled	10,000	200	1645	$NaF-ZrF_4-UF_4$[a]	1000	Scheduled
4935-6	Gas-fired heater	Coiled	8,000	200	1550	$NaF-ZrF_4-UF_4$[a]	1000	Scheduled

[a] Composition: 50-46-4 mole %.

[b] Composition: 50-46-4 mole % with 2 wt % of total uranium converted to U^{3+}.

[c] Composition: 53.5-40-6.5 mole %.

[d] Composition: 11.7-59.1-29.2 mole %.

to the tube wall in such a manner as to cause high thermal stress concentrations and high electrical current density in the lugs. Three identical failures resulted before butt welds were substituted for axial bead welds to alleviate the condition that caused the failures.

Two bearing failures resulted in an investigation of the thrust bearings used in the pumps (model LFB). This study indicated that the fits were too tight, and new bearings with looser fits between balls and races were obtained. No further bearing failures have occurred.

Metallurgical examination of early direct-resistance-heated loops in which the heated sections were coiled revealed excessive attack on the compression side of the bends. Temperature measurements showed the compression side of the wall to be approximately 100°F hotter than the tension side. Since the wall of the tubing on the tension side of the bend would have become thinner during bending and the wall on the compression side thicker, it was thought that the greater current density of the thicker wall on the compression side could have caused the overheating and the resultant excessive corrosion. An investigation[3] of flow revealed that poor fused-salt flow distribution at and past the bends resulted in poor heat transfer and thus also caused overheating. A new heated section was therefore designed that eliminated bends from the sections that carried high current and provided approximately 40 diameters of straight section following each bend. In addition, the length of the heated section in the resistance-heated loops was increased from 12 ft to approximately 17 ft in order to reduce the maximum tube wall temperature to a more tolerable level. These modifications appear to have corrected the overheating and resultant excessive corrosion.

The gas-heated loops are being run to evaluate the effect of the heating method and the effect of tube wall temperature on corrosion and mass transfer. Loops 4935-5 and 4935-6 are the first two of a series of three loops to be run with wall temperatures of 1550°F, 1650°F, and 1800°F.

Sodium in Multimetal Loops

C. P. Coughlen D. R. Ward
Aircraft Reactor Engineering Division

R. A. Dreisbach
Pratt & Whitney Aircraft

Four loops with sodium in Inconel and two loops with sodium in Inconel and type 316 stainless steel were operated and terminated. The important operating conditions for these loops are given in Table 2.2. Since appreciable deposits of mass-transferred material were found in the cold legs of these loops, a controlled series of experiments was initiated. The operating conditions for these loops, which are now operating, are given in Table 2.3. These loops will provide information on the effects of the oxygen content of the sodium, the use of a cold trap, the use of a lower maximum sodium temperature, and the use of an all-stainless-steel system.

TABLE 2.2. SUMMARY OF OPERATING CONDITIONS FOR LOOPS THAT CIRCULATED SODIUM

Maximum sodium temperature: 1500°F

Loop No.	Loop Materials	Reynolds Number	Temperature Differential (°F)	Operating Time (hr)
4689-4	Inconel	~62,000	300	1000
4689-5	Inconel with type 316 stainless steel cold leg	~62,000	200	1000
4689-6	Inconel with type 316 stainless steel cold leg	~62,000	300	1000
4951-1	Inconel	>15,000	200	480
4951-2	Inconel	>15,000	300	500
4951-3	Inconel	>15,000	150	500

---

[3] H. W. Hoffman, L. D. Palmer, and N. D. Greene, *Electrical Heating and Flow in Tube Bends*, ORNL CF-55-2-148 (Feb. 22, 1955).

TABLE 2.3. SUMMARY OF OPERATING CONDITIONS FOR LOOPS NOW CIRCULATING SODIUM

Reynolds number: 15,000
Temperature differential: 300°F
Scheduled operating time: 1000 hr

Loop No.	Loop Material	Maximum Sodium Temperature (°F)	Controlled Variation
4951-4	Inconel	1300	Maximum fluid temperature
4951-5	Inconel	1500	0.15% O_2 added
4951-6	Inconel	1500	Special high-purity sodium cold trap used
4951-7	Type 316 stainless steel	1500	Loop metal

PUMP DEVELOPMENT

E. R. Dytko
Pratt & Whitney Aircraft

A. G. Grindell G. D. Whitman
Aircraft Reactor Engineering Division

Water Performance Tests

G. D. Whitman
R. L. Brewster M. E. Lackey
Aircraft Reactor Engineering Division

A full-scale model of the ART fuel pump design designated MF-2 was built, and water performance data were obtained for several impeller designs and pump suction conditions for a given discharge-volute design. The discharge volute and the test impellers were fabricated from brass, and a bearing housing used for the model MF-1 tests[4] was adapted for use in the rotary assembly. The unit was driven by a direct-coupled, 15-hp, variable-speed, d-c motor. The pump was installed in a test-loop built of 6-in. pipe with head and flow measuring instrumentation and a throttling valve.

The first experiment was performed by using a pump-suction configuration that simulated the reactor design. A box containing a flat plate 1 in. below and parallel to the pump-suction flange was used. For the second test, the flat plate was removed and an 8-in. pipe was connected directly to the pump suction. Since pump performance was about the same in both tests, the remainder of the experiments were conducted with the 8-in. suction line.

A series of ten experiments has been performed, to date, and the test conditions and results are given in Table 2.4. The performance data from experiment No. 3 are plotted in Fig. 2.3. These data are representative of the best operation obtained during the tests. The pump efficiencies are not considered to be accurate on an absolute basis, because the motor was not calibrated and the motor efficiencies were obtained from the manufacturer's computed data. It is estimated that the efficiency of the pump, exclusive of seal and bearing losses, is approximately 70% at the design point.

Data obtained by varying the running clearance between the lower impeller shroud and the volute indicated that the clearance could be in excess of 0.040 in. without loss in performance at design point. At low-flow high-head conditions, there was approximately a 10% loss in head because of recirculation in the pump.

A cavitation problem persisted throughout the experiments. At flows of over 400 gpm and speeds in excess of 2000 rpm, a slight noise was detected in the pump, and the intensity of this disturbance increased with increased flow or speed above the threshold values. However, no cavitation damage has been detected in the pump, and the data do not indicate a decrease in performance in the cavitation region. The performance of the pump was not altered by varying the suction pressure over a range of –5 to +15 psig; however, the intensity of the noise could be suppressed by increasing the system pressure. The suction conditions were altered by changing the radius of the inlet eye from ½ to 1 in., and the impeller nut was redesigned to give better fluid guidance. Neither of

---

[4] A. G. Grindell and W. C. Smeps, *ANP Quar. Prog. Rep. Mar. 10, 1955*, ORNL-1864, p 34.

TABLE 2.4. CONDITIONS AND RESULTS OF WATER PERFORMANCE TESTS OF ART FUEL PUMP MODEL MF-2

Design point: 620 gpm, 35-ft head

Experiment Number	Impeller Design	Suction Conditions	Remarks and Results
1	Five vanes; blade tip angle, 22 deg	Suction box simulating reactor; $\frac{1}{2}$-in. radius on suction eye	Design point met at approximately 2800 rpm
2	Same as above	8-in. pipe with four antiswirl vanes; $\frac{1}{2}$-in. radius on suction eye	No appreciable change in performance
3	Five vanes; blade tip angle, 26.5 deg	Same as above	Design point met at approximately 2600 rpm; approximately a 10% increase in efficiency with respect to experiment 1, with the peak efficiency shifted toward higher flows
4	[illegible]ve vanes; blade tip angle, 22 deg; leading edges cut back on an 80-deg cone angle	Same as above	Decrease in pump performance with respect to experiment
5	Five vanes; blade tip angle, 26.5 deg; increased lower shroud clearance from 0.010 to 0.025 in.	Same as above	No appreciable change in pump performance at design point
6	Same as above with radial clearance increased to 0.040 in.	Same as above	No appreciable change in pump performance at design point; 10% less in head with respect to experiment at flows below 300 gpm and speeds above 2000 rpm
7	Six vanes; blade tip angle, 22 deg	Same as above	Similar to experiment 1
7A	Same as above	8-in. pipe with four antiswirl vanes; 1-in. radius on suction eye	Similar to experiments 1 and 7
8	Five vanes; blade tip angle, 26.5 deg	Same as above	Tongue cut back on volute; performance similar to that in experiment 3
9	Same as above	Same as above	Tongue cut back on volute; modified impeller nut; performance similar to that in experiment 8

these changes had any detectable effect on the cavitation problem. It is believed, at present, that the cavitation may be a result of poor fluid guidance at the leading edges of the impeller vanes. A new vane design has been completed and will be tested soon.

Bearing and Seal Tests

D. R. Ward

W. C. Tunnell J. W. Kingsley

Aircraft Reactor Engineering Division

A test has been designed for studying the function of the interference fit between the journal

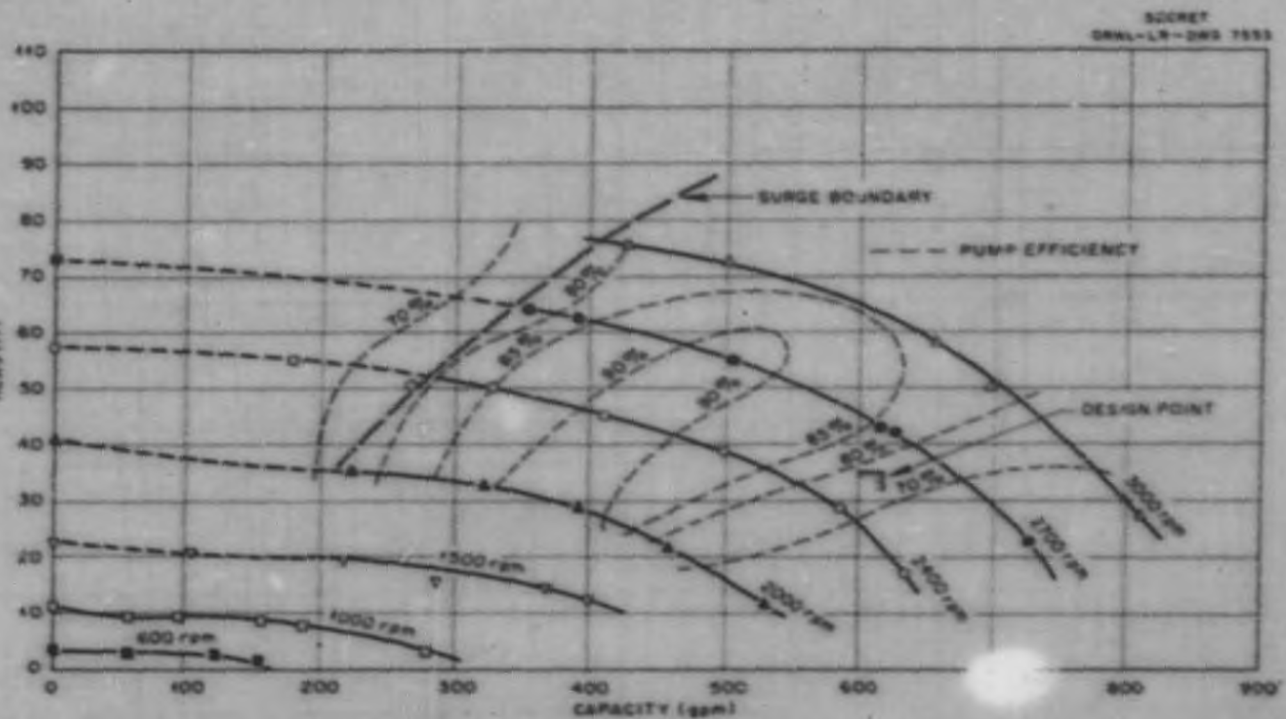

Fig. 2.3. Performance Characteristics of ART Fuel Pump Model MF-2 in Water Tests. For test conditions see Table 2.4.

bearing and the face seal in the model MF-2 pump at elevated shaft temperatures and under simulated bearing loadings. The test apparatus consists of an MF-2 rotary element to which a loading device is attached at the impeller location. The pump shaft rotates freely within the side-loading device. Heat is applied at the lower region of the pump to simulate gamma heating under actual operating conditions. One phase of the test will consist in an endurance run under simulated pump design conditions, and the other phase, for which a duplicate test assembly is to be used, will consist in short tests for studying the following variables: bearing loading, pump speed, lower shaft temperature, rate of coolant flow, and time.

Mechanical Shakedown Test

W. L. Snapp J. J. W. Simon
Pratt & Whitney Aircraft

A few additional mechanical shakedown tests were performed on the model MF-1 ART fuel pump. The rotary element was operated continuously for a period of 300 hr at 3800 rpm without achieving a successful seal at the lower journal-bearing region. It was found that the oil leakage rate was nearly constant at 1.8 in.^{3} per day. Although this rate is not excessive, the goal of zero leakage was not achieved, probably because the face of the journal was not flat. No further testing of this model is planned.

As part of the renovation of ARE-type sump pumps for use in heat exchanger and other tests, 100-hr cold mechanical shakedown tests of the rotary elements were conducted on five units. To assist in the development of the metal-to-metal seal for the model MF-2 pump, the floating Graphitar ring at the lower seal assembly was removed and replaced, on two units, by a modified upper seal bellows assembly. This modification made a metal-to-metal lower seal assembly. One element failed in the cold shakedown test because of a faulty bellows convolution, but the other element was found to be very satisfactory in that no leakage was detected. The latter element was then placed in operation at high temperature on a heat exchanger test stand. After about 200 hr of hot operation, a bearing hum developed and the unit was replaced; however, up to that time, there had been no oil leakage detected at this lower metal-to-metal seal. Upon disassembly of the unit, the seal surfaces were found to be in excellent condition. As a result of this test, all additional ARE-type pumps will have metal-to-metal seals at the lower journal.

Design work has been completed, and fabrication and assembly have been started on two mechanical shakedown test stands for testing model MF-2 rotary assemblies.

Short-Circuit Pump-Test Stand

S. M. DeCamp
Aircraft Reactor Engineering Division

The study and design of a short-circuit loop for testing model MF-2 pumps were completed, and fabrication was started. Tests are to be made with this loop at operating temperatures in the range 1100 to 1500°F. The tests have been designed for determining the following:

1. proper operation of the lubricating and coolant system at operating temperatures,
2. leakage rates of the upper and lower seals during actual pump operation at elevated temperatures,
3. temperature gradients along the pump support cylinder and in the rotary element,
4. proper clearances between the test impeller and pump casing at operating temperatures,
5. proper fitting of parts at operating temperatures and loads,
6. life of the pump assembly.

It was decided to build a short-circuit loop totally contained in a tank to eliminate the problem of differential thermal expansion. The loop contains two fixed area orifices to simulate ART fuel circuit head loss, and it has been designed so that the pump may be operated at flow rates of up to 600 gpm and a head of approximately 50 ft.

Since the design of the xenon-removal feature of the pump has not yet been settled, it was decided to use a conventional by-pass flow and pressure-breakdown labyrinth for leakage around the pump impeller. This labyrinth was designed to simulate pump-suction and discharge-volute conditions as presently envisioned for the ART fuel pumps.

The removal of pumping power, approximately 40 hp at the isothermal steady-state condition, is to be obtained by constructing a water wall around the pump tank. A movable furnace will be installed between the pump tank and the water wall. It should be possible to dissipate the pumping power at an isothermal operating condition by lowering the movable furnace and exposing a portion of the hot tank wall to the water wall. The fluid flow in this very short loop will be observed through ports during operation with water.

HEAT EXCHANGER TESTS

E. R. Dytko
Pratt & Whitney Aircraft

R. E. MacPherson
Aircraft Reactor Engineering Division

Heat Exchanger Tube-Spacer Pressure-Drop Tests

R. D. Peak
Pratt & Whitney Aircraft

J. W. Kingsley
Aircraft Reactor Engineering Division

In order to select the best spacer configuration for the ART heat exchanger tube bundle, a series of tests on various spacer arrangements has been conducted. The test apparatus consisted of a representative ART type of tube bundle composed of 25 aluminum rods 0.191 in. in diameter and 6 ft long contained in a square aluminum duct 1.12 in. inside. The tube spacers were formed from flattened copper wire 0.028 by 0.046 in. Tube-to-tube spacing was 0.028 in., and tube-to-wall spacing was 0.025 to 0.028 in. The spacer rods were soldered on opposite sides of the bundle into 0.020-in.-thick copper plate $\frac{1}{4}$ in. wide. Water was metered through the apparatus by a Rotameter, and total pressure drops were taken across the tube bundle by means of a manometer.

Six configurations were tested, and the results of each test are shown in Fig. 2.4. The results indicate that the pressure drop is least when the spacers are inclined at 45 deg to the direction of flow. Vertical, in-line spacers, of course, gave the highest pressure drop. Staggering the spacers at 45 and 60 deg lowered the pressure drop, but inclining these staggered spacers provided no improvement, as would be expected.

SECRET
ORNL–LR–DWG 7554

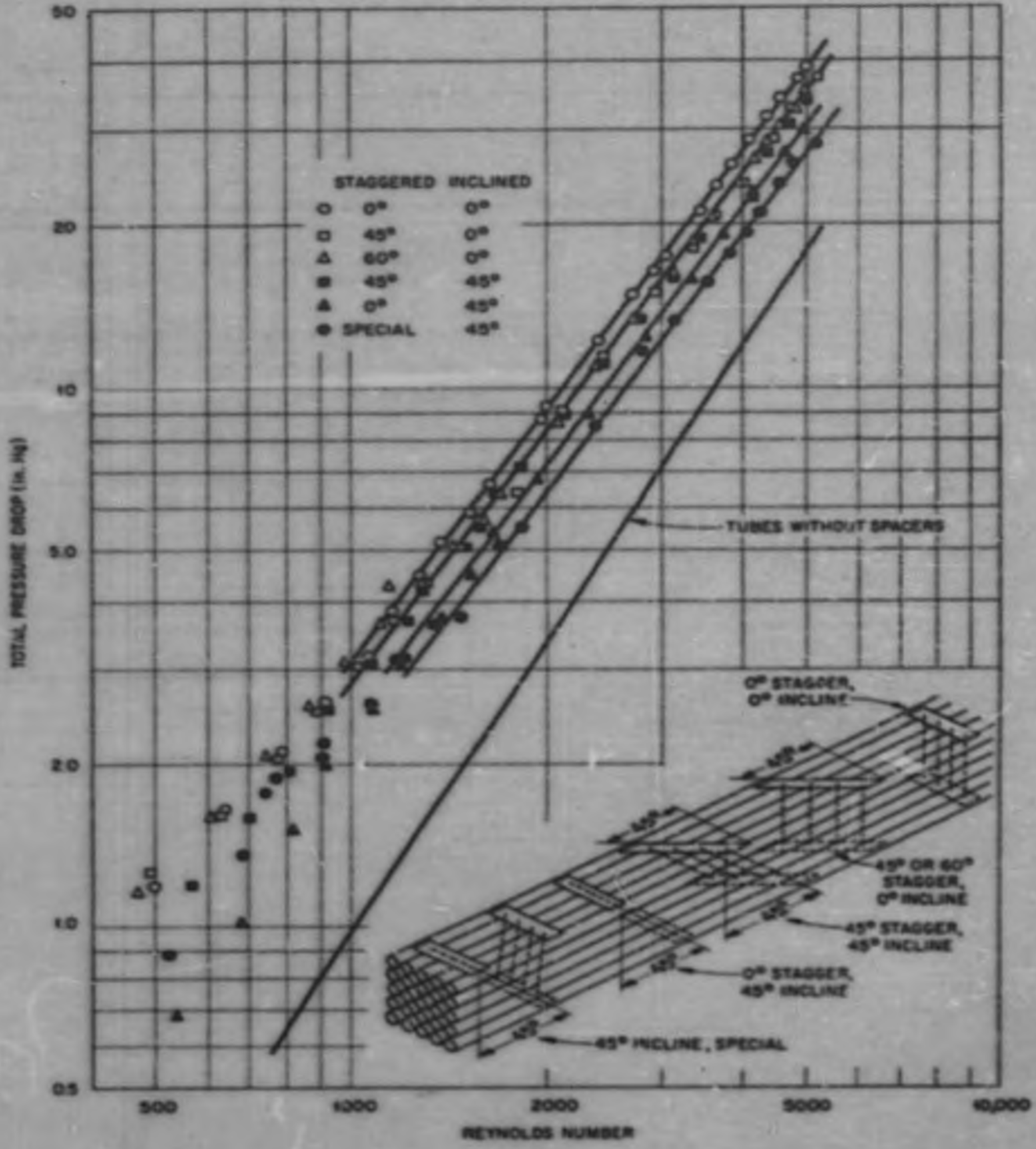

Fig. 2.4. Results of Pressure Drop Tests of Various Tube-Spacer Arrangements for an ART Heat Exchanger Tube Bundle.

Intermediate Heat Exchanger Tests

R. D. Peak
Pratt & Whitney Aircraft

Construction is about 70% completed on the test stand described previously[5] and shown here in Fig. 2.5. The two 1.3-Mw 100-tube heat exchanger bundles have been completed,[6] as well as the two 500-kw high-conductivity-fin radiators. The NaK pump (DANA), fuel pump (DAC), and the radiator blower are salvaged equipment from the ARE. The 1-Mw gas-fired heater for this test loop is now being fabricated by the Struthers Wells Corp.

Small Heat Exchanger Tests

J. C. Amos M. M. Yarosh
Aircraft Reactor Engineering Division
R. I. Gray
Pratt & Whitney Aircraft

A test of a small fuel-to-NaK heat exchanger was started April 10, 1955. Pressure drop and heat transfer data have been taken through the fluoride mixture Reynolds number range 500 to 6300. Preliminary analyses of the data indicate that the heat exchanger pressure drops are in good agreement with pressure-drop and friction-factor information obtained from recent water-pressure-drop tests carried out on tube bundles with similar geometry.

Basic heat transfer data are presented in Fig. 2.6, which compares the recent results with the theoretical relationship $Nu/Pr^{0.4} = 0.23\ Re^{0.8}$. The equivalent diameter used in calculating the Reynolds numbers was based on the total wetted perimeter of the tubes plus the side-wall area, while the equivalent diameter used in computing the Nusselt number utilized only the tube perimeter. The heat transfer area was based on the tube length between header-region center lines.

The heat exchanger being tested consists of 20 Inconel tubes $\frac{3}{16}$ in. in outside diameter, with 0.017-in.-thick walls. The tubes, which are approximately 6 ft long, are arranged in a 4 by 5 matrix and contained in a rectangular channel on 0.22-in. centers, with a 0.032-in. tube-to-wall clearance. The fluoride mixture NaF-ZrF$_4$-UF$_4$ (50-46-4 mole %) is circulated outside the tubes, and NaK (56% Na–44% K) is circulated in the tubes.

The assembly is now operating on an endurance run at a fluoride mixture Reynolds number of approximately 3000. It is planned to take data over the Reynolds number range 500 to 6000 after 500 hr of operation and again after 1000 hr.

CORE FLOW TEST

G. D. Whitman R. L. Brewster
Aircraft Reactor Engineering Division

A full-scale model of the proposed 21-in. reactor core and an entrance header have been fabricated and checked for fluid flow reversal and/or stagnation. The model was installed in a loop containing a 1000-gpm water pump, and two entrance lines were provided at the header to simulate the reactor design. Data were taken at flows that provided a Reynolds number correlation of 1:1 between water flow rates and design fuel flow.

The core model was machined from aluminum castings and was instrumented at 72 static pressure and 18 probe points at nine elevations along the vertical axis of the core. Direction-finding impact tubes were used to traverse the core-shell region at the probe points. There were two probe locations at each of the nine elevations and in the entrance header. A traverse was made from the inner to the outer wall of the fluid passage to obtain the direction of flow and a total pressure profile. Static pressure measurements were taken at the walls at each elevation, and the fluid velocity was computed from the total and static pressure data.

The data were taken in the upper half of the core, and a region of flow reversal was encountered around the inner core shell. This reversal extended approximately one quarter of the distance between the inner and outer shell surfaces and was not sensitive to flows down to one-half the design Reynolds number. Data were not taken at flows below this value.

The entrance geometry produced a large rotational component of velocity in the fluid entering the core, and turning vanes are to be inserted to direct the flow axially through the core volume. If intolerable flow separation is encountered at the outer core shell surface above the equator, turbulators will be attached to the surface in an attempt to reduce this trouble.

---

[5] R. E. MacPherson, *ANP Quar. Prog. Rep. Mar. 10, 1955*, ORNL-1864, p 76.

[6] P. Patriarca *et al.*, *ANP Quar. Prog. Rep. Mar. 10, 1955*, ORNL-1864, p 131.

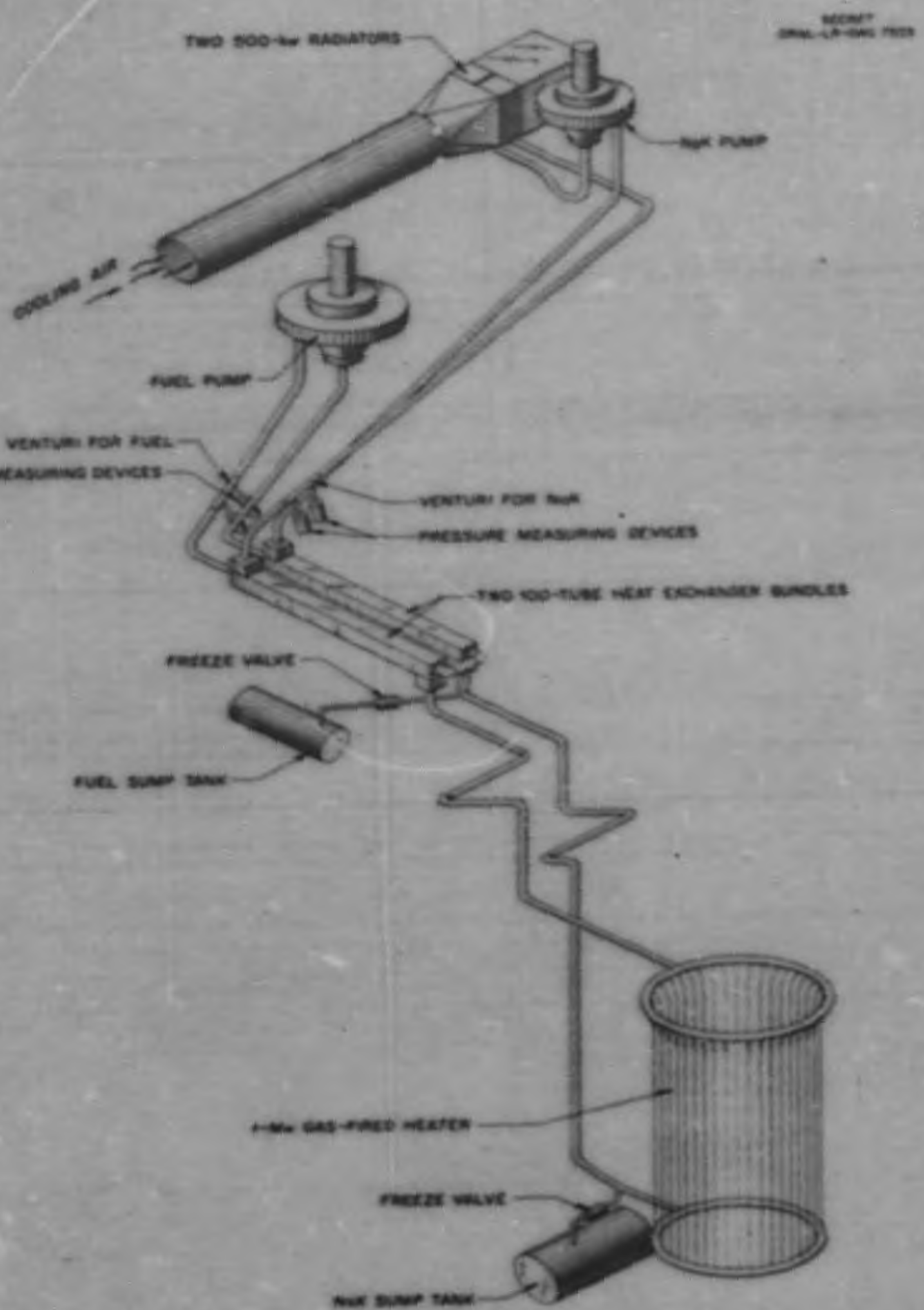

Fig. 2.5. Isometric Drawing of Intermediate Heat Exchanger Test Stand.

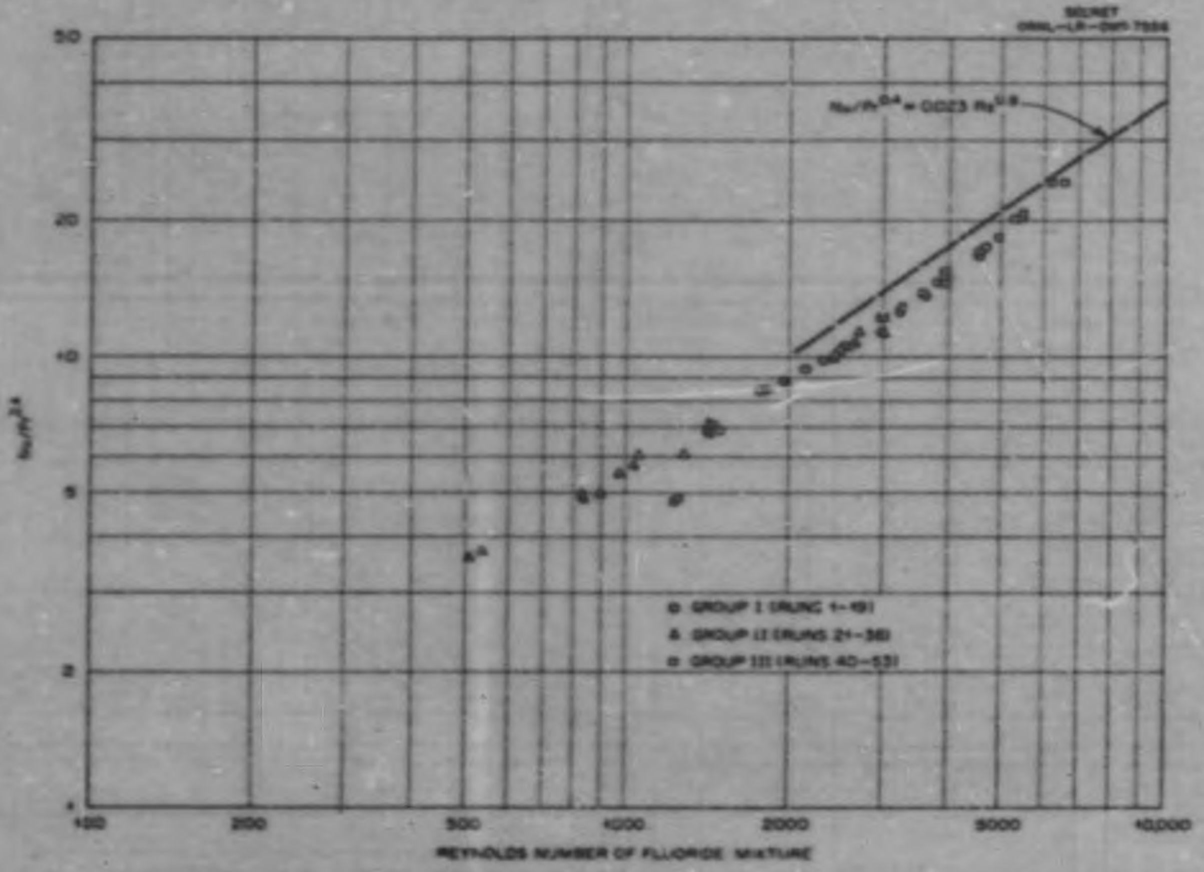

Fig. 2.6. Heat Transfer Data for 20-Tube Fuel-to-NaK Heat Exchanger.

THERMAL-CYCLING TEST OF SODIUM-INCONEL-BERYLLIUM SYSTEM

R. D. Peak   M. H. Cooper
Pratt & Whitney Aircraft

Operation of the second sodium-beryllium-Inconel compatibility testing apparatus, previously described,[7] has been completed. The test stand is shown in the isometric drawing Fig. 2.7. The cylindrical beryllium test piece was mounted between the secondary connections of a 250-kw transformer and directly heated by passing electrical current through it. Hot sodium was pumped through the beryllium test piece and then to a radiator. The pertinent operating conditions of the tests are tabulated in Table 2.5.

The beryllium piece was cycled 104 times between full power and low power, with 20 cycles having a cycle period of 20 min and 80 cycles having a cycle period of 4 hr; four cycles were required for instrument checks, power failures, and startup. The time required for a change from full power to low power or back was 2 min. Upon completion of the required cycles, the apparatus was run at full power to achieve a total operating time of 1030 hr. The beryllium test piece is shown in Fig. 2.8 after the unit was disassembled. The beryllium was found to have grown from 0.0003 to 0.0041 in. on an average outside diameter of 1.125 in. There were three axial cracks approximately $\frac{1}{16}$ in. long on the outer surface at the hot end of the beryllium. Inspection by the Dychek method revealed no other cracks on the outer surface.

---

[7] *Ibid.*, p 134.

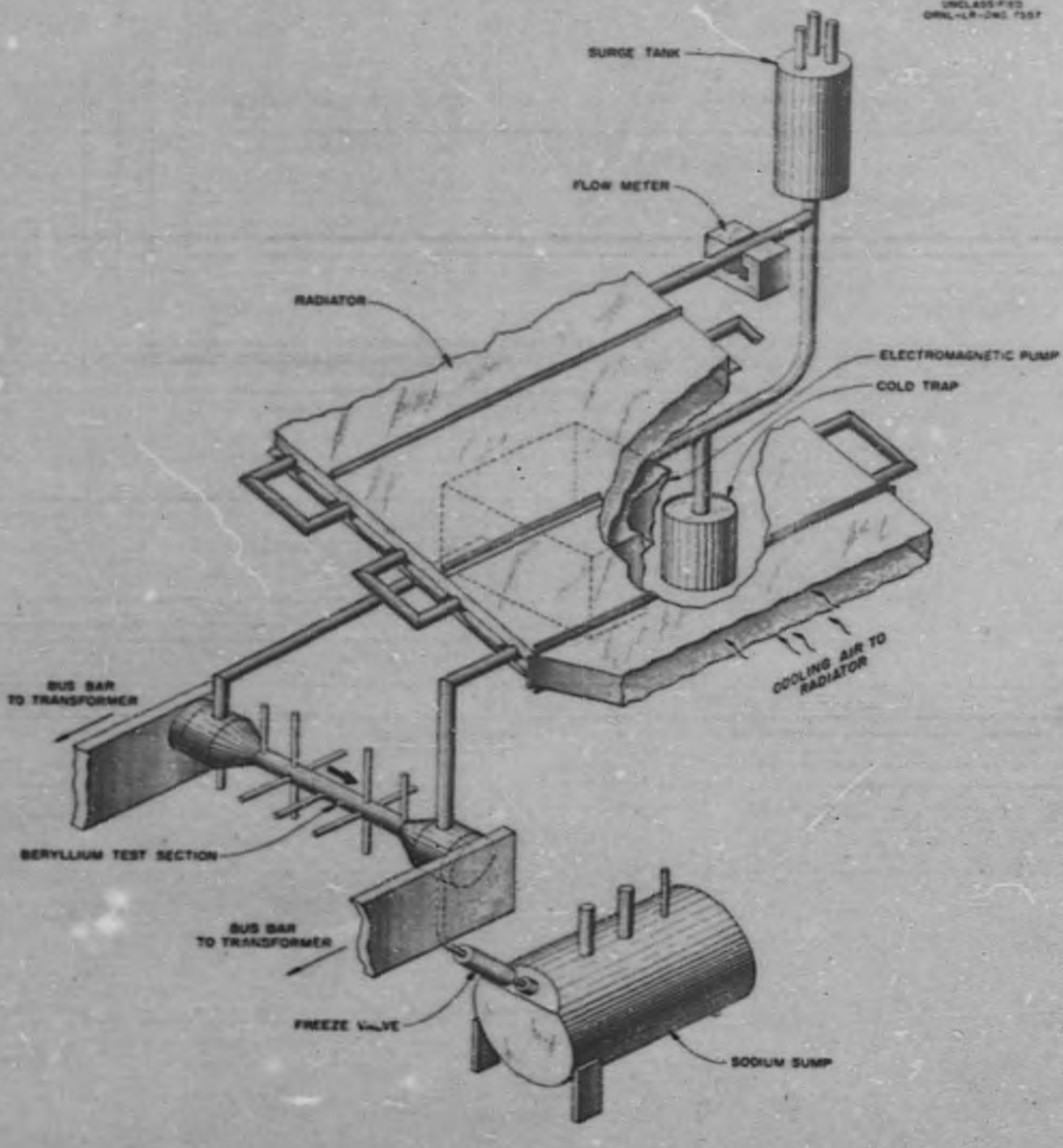

Fig. 2.7. Isometric Drawing of Loop for Thermal-Cycling Tests of a Sodium-Inconel-Beryllium System.

TABLE 2.5. SUMMARY OF OPERATING CONDITIONS FOR THERMAL-CYCLING TEST OF SODIUM-INCONEL-BERYLLIUM SYSTEM

	High Power Level	Low Power Level
Beryllium power, w/cm^3	61	2.5
Current through test piece, amp	11,100	1,900
Sodium flow, gpm	4.0	4.0
Sodium inlet temperature, °F	1050	1050
Beryllium-sodium interface temperature at sodium inlet, °F	1095	
Beryllium outside-diameter temperature at sodium inlet, °F	1225	
Sodium outlet temperature, °F	1200	1050
Beryllium-sodium interface temperature at sodium outlet, °F	1245	
Beryllium outside-diameter temperature at sodium outlet, °F	1375	

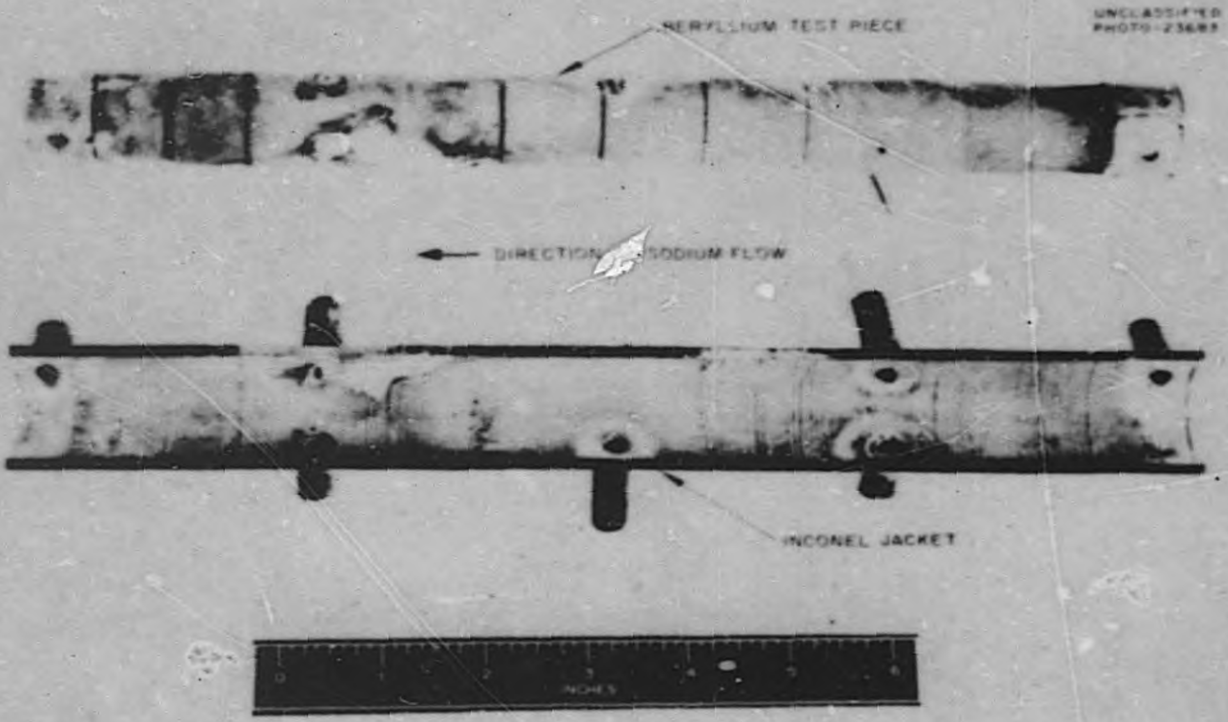

Fig. 2.8. Beryllium Test Piece from Thermal-Cycling Test of Sodium-Inconel-Beryllium System.

The beryllium pieces and sections of the loop are undergoing extensive metallographic examination.

Apparatus is being assembled for a third test. The test stand and test program will be similar to those used for the test described above. The same full-power density, 61 w/cm^3, will be employed, but the average sodium temperature will be increased from 1125 to 1225°F. The test is to be completed during the next quarter.

GAS-FIRED HEAT SOURCE

R. E. MacPherson
Aircraft Reactor Engineering Division

R. Curry
Pratt & Whitney Aircraft

The small-scale gas-fired source, described previously,[8] has been tested at a power output level of 100 kw. The operating conditions for a power output of 100 kw are given below.

Sodium flow rate, gpm	7.9
Sodium temperature differential through heater, °F	380
Furnace output, kw	103
Gas flow rate, scfm at 14.7 psia and 70°F	20.5
Chemical heat input rate (based on 980 Btu/scfm), kw	354
Furnace efficiency (furnace output vs chemical heat input), %	29

Testing was not attempted at higher outputs because a modification of the gas injection ports to reduce the pressure drop would have been necessary. Preheating of the heat exchanger section prior to sodium filling was accomplished by operating the burner at low power output and adding cooling air downstream of the combustion chamber. It was possible to maintain heat exchanger tube temperatures in the 800 to 1200°F range by this means.

No difficulties were encountered except for the failure of the spark-plug igniter and several plastic thermocouple connectors because of the high radiant heat emission from the combustion chamber barrel. The gas flow to the burner was momentarily interrupted several times in the course of the test of reliability of relighting. No problems arose prior to failure of the igniter mechanism, mentioned above.

With a few minor repairs, the furnace can be put into operation as a utility heat source. By enlarging the gas injection ports (a minor modification), the capacity of the furnace may be increased considerably for any future application.

---

[8] R. E. MacPherson and R. Curry, *ANP Quar. Prog. Rep. Mar. 10, 1955*, ORNL-1864, p 37.

3. CRITICAL EXPERIMENTS

A. D. Callihan, Physics Division

D. Scott W. C. Tunnell
Aircraft Reactor Engineering Division

R. M. Spencer, United States Air Force

J. J. Lynn, Physics Division

J. S. Crudele E. V. Sandin
J. W. Noaks S. Snyder
Pratt & Whitney Aircraft

ROOM-TEMPERATURE REFLECTOR-MODERATED-REACTOR CRITICAL EXPERIMENTS

A series of experiments have been done on several critical assemblies of the circulating-fuel reflector-moderated reactor. These experiments embodied a number of different configurations of fuel and reflector, which were described in detail previously.[1] The latest of these modifications consisted of a beryllium region surrounded by a fuel layer, which, in turn, was enclosed by the beryllium reflector. This configuration was extended, with reduced dimensions, on opposite sides of the central reactor region to form "end ducts" which simulate the entrance and exit fuel channels. Some results of a variety of experiments which were done with this assembly are presented here.

Reactivity Measurements

The fuel loading of the critical assembly was such that it contained about 3% excess reactivity, which was utilized for the evaluation of reactivity changes incurred by altering the structure and by adding samples of materials of interest in the design of the ART. It was feasible to make these measurements prior to the reduction of the fuel concentration to that required to determine the critical fuel loading. The evaluations were based on the critical positions of control rods.

Reflector. In one experiment the thickness of the beryllium reflector around the central region of the assembly was reduced from $11\frac{1}{2}$ to $8\frac{5}{8}$ in. by removing the outer (essentially cylindrical) annulus, which was $2\frac{7}{8}$ in. wide and $18\frac{3}{4}$ in. long. This annulus was coaxial with the fuel region. The decrease in reactivity was 165 cents.

ART Control Rod Materials. To provide bases for the design of the control rod for the ART, measurements were made on samples of several possible components. A test volume was formed by removing beryllium from a region $1\frac{7}{16}$ by $1\frac{7}{16}$ in. in cross section that extended 21.5 in. along the axis of the assembly from one end to a point 0.72 in. beyond the equatorial plane. A loss in reactivity of 19.1 cents resulted.

Consideration was also given to the thimble in which the control rod would operate. Tubes of different dimensions and materials were placed within the test volume, and the concomitant depressions in reactivity were determined. The results are given in Table 3.1. It is indicated that, in the range of the measurements, the change in reactivity depends more upon the quantity of material present than upon its shape. A plot of the loss in reactivity incurred by a sample as a function of its linear density, that is, its mass per unit length, is given in Fig. 3.1.

An evaluation was then made of the neutron absorption properties of a mixture of some of the oxides of the rare-earth elements being considered for use as the poison in the control rod. Tests on solid cylinders and on a cylindrical annulus were made along the axis of the critical assembly in the test volume described above.

The composition of the mixture of rare-earth oxides tested was the following:

Oxides in Mixture	Amount in Mixture (wt %)
Sm_2O_3	63.8
Gd_2O_3	26.3
Dy_2O_3	4.8
Nd_2O_3	0.9
Yt_2O_3 (and others)	4.2

---

[1] A. D. Callihan *et al.*, *ANP Quar. Prog. Rep. Mar. 10, 1955*, ORNL-1864, p 41.

TABLE 3.1. REACTIVITY EFFECT OF CONTROL ROD THIMBLE MATERIALS

Material	Dimensions (in.)		Linear Density (in.)	Reactivity Loss (cents)
	Outside Diameter	Wall Thickness		
Inconel	0.871	0.035	12.27	25.5
	1.255	0.045	20.72	41.7
	1.243	0.062	32.68	64.7
	1.255	0.045	32.99	63.3
	0.871	0.035		
	1.250	0.085	41.75	80.7
	1.250	0.085	54.02	97.5
	0.871	0.035		
Type 304 stainless steel	1.253	0.028	14.10	22.9
Type 302 stainless steel	1.240	0.060	27.91	41.7

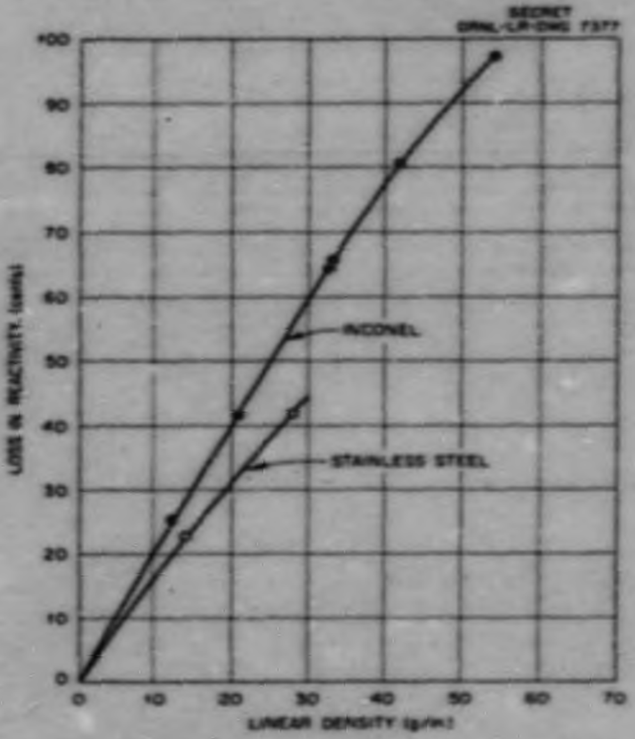

Fig. 3.1. Reactivity Effects of Thimble Materials.

The mixture was pressed into solid cylinders 0.450 and 1.375 in. in diameter and into annuli 0.790 in. in outside diameter and 0.140 in. in width. Each piece was about $\frac{3}{4}$ in. in height, and the pieces were combined to give various-length samples.

In the first set of experiments with the small-sized cylinders and the annuli, the Inconel thimble, which was 1.250 in. in outside diameter and 0.085 in. in wall thickness and which decreased the reactivity 80.7 cents, was in place in the axial void. The absorber samples were contained in an Inconel carrier tube which could be inserted into the thimble. The outside diameter of the carrier tube was 0.871 in., the wall thickness was 0.035 in., and the end was closed by a $\frac{3}{32}$-in.-thick plug. The small cylinders were centered in this carrier tube by a third Inconel sleeve, with an outside diameter of 0.500 in. and a wall thickness of 0.020 in., which, in turn, was centered by aluminum spacers. The effects of the carrier tube and of assemblies of cylinders and annuli, both separately and together, are summarized in Table 3.2. The reference zero for the reactivity changes is taken with the thimble alone. In all cases the test rod was inserted 21.5 in. into the thimble; that is, the end extended 0.72 in. beyond the equatorial plane of the assembly.

In a second series of experiments a comparison

TABLE 3.2. EFFECT OF SAMPLE CONTROL RODS ON REACTIVITY

Sample	Length (in.)	Diameter (in.)	Reactivity Loss (cents)
Carrier tube only			16.8 ± 0.5
Cylinders*	22.0	0.450	155.0 ± 15.0**
Annuli	21.0	0.790 (outside) 0.510 (inside)	230.0 ± 20.0**
Cylinders and annuli together	21.0	0.790	250.0 ± 20.0**

*The innermost centering tube alone decreased the reactivity about 5 cents.

**Obtained by extrapolation of a series of measurements with shorter samples; effect of carrier tube included.

was made of the effect on reactivity of the diameter of the samples of oxide mixture. The diameters of the samples were 0.450, 0.790, and 1.375 in., the one of intermediate size being formed by placing the small cylinders in the annuli described above. The samples were about 5.5 in. long, and each was tested at the same position in the assembly. The distance from the end of the sample to the midplane of the assembly was 2.0 in. It was necessary to remove the 1.25-in.-dia thimble for these measurements, and the absorbers had to be wrapped in aluminum foil. The changes in reactivity measured, referred to the array with the test section void (without the thimble), are given in Table 3.3.

TABLE 3.3. EFFECT OF ABSORBER DIAMETER ON REACTIVITY

Sample Diameter (in.)	Length (in.)	Reactivity Loss (cents)
0.450	5.6	95.0 ± 5.0
0.790	5.6	158.0 ± 5.0
1.375	5.4	256.0 ± 5.0

An estimate of the spectral distribution of the neutron absorption by the rare-earth elements was also made. The change in reactivity produced by a 3-in.-long cylindrical sample, 0.450 in. in diameter, was measured at a point where the cadmium fraction measured by gold-foil activation was about 0.5. The measurement was then repeated with the sample covered by cadmium 0.02 in. thick. The values were 55.9 and 61.7 cents, respectively. The cadmium alone reduced the reduced the reactivity 37.7 cents. From these data it appears that about 43% of the reactivity decrease is due to neutrons which penetrate the cadmium.

Inconel. A measurement, similar to that just described, was made with an Inconel sample in order to estimate the dependence of the reduction in reactivity upon neutron energy. The sample was $1\frac{1}{2} \times 4\frac{3}{8} \times \frac{3}{32}$ in.; it weighed 84.14 g; and it could be provided with a 0.02-in.-thick cadmium cover. The effects, as poisons, of the Inconel and the cadmium were measured singly and together at the center of the beryllium island and in the fuel region adjacent to the fuel reflector interface. (The $\frac{1}{8}$-in. Inconel core shell was reduced to $\frac{1}{16}$ in. in thickness in the region of this measurement.) The gold-activation cadmium fractions at the two positions were 0.57 and 0.33, respectively. The reactivity changes are given in Table 3.4. The fractions of the total change that are caused by neutrons penetrating the cadmium are also tabulated.

TABLE 3.4. REACTIVITY CHANGES FROM BARE AND CADMIUM-COVERED INCONEL

	In Island	At Fuel-Reflector Interface
Reactivity loss (cents)		
Inconel	18.0	4.0
Inconel, cadmium covered	117.4	26.8
Cadmium cover	115.2	26.5
Fractional change in reactivity caused by epicadmium neutrons (F)	12.2 ± 0.6	7.5 ± 2.6
Gold-activation cadmium fraction	0.57	0.33

Beryllium in the Fuel Region. Since the presence of beryllium in the circulating fuel stream would be another possible way of reducing the critical uranium concentration, an experiment was devised for evaluating the effect of beryllium in the fuel region of the critical assembly. One of the central fuel subassemblies that consisted of 27 uranium metal sheets (each 0.004 in. thick) and 55 Teflon sheets (each $\frac{1}{16}$ in. thick) was modified in the following manner. Seven uranium sheets and 16 Teflon sheets were removed from the center to effect a decrease in reactivity of 22.7 cents. The substitution of a sample of beryllium, $7\frac{3}{16} \times 2\frac{7}{8} \times 1$ in., for this uranium and Teflon resulted in a net reactivity gain of 8.5 cents over the unperturbed value. The addition of a $\frac{1}{16}$-in.-thick layer of Inconel completely around the beryllium reduced this net gain to 4.0 cents. An estimate of the effect of the Inconel-clad beryllium on the concentration is given by the observation that the removal of two of the remaining 20 uranium sheets further reduced the reactivity by 4.5 cents, that is, to a value slightly below that of the original array. The two sheets removed last were adjacent to the beryllium sample and were of greater than average importance.

Fuel in the End Ducts. One of the safety features of the high-temperature critical experiment presently being designed, which is described below, is that the liquid fuel can be removed by draining under gravity. The degree of safety depends upon the rate of removal and the sensitivity of the reactor to the fuel level, particularly the level in the upper end duct. A measure of this sensitivity was obtained in the room-temperature experiment to establish the basis for the design of the hot-fuel drain system.

Three annular rings of fuel were successively removed in $2\frac{7}{8}$-in. increments from one end duct, and the resulting decreases in reactivity were noted. Each ring contained 825 g of U^{235}, and thus a total of 2.475 kg of U^{235} was removed. The losses in reactivity accompanying the removal of the three rings are shown in Fig. 3.2, which also gives the loss in reactivity per unit displacement, or fuel sensitivity, averaged over each of the fuel annuli removed.

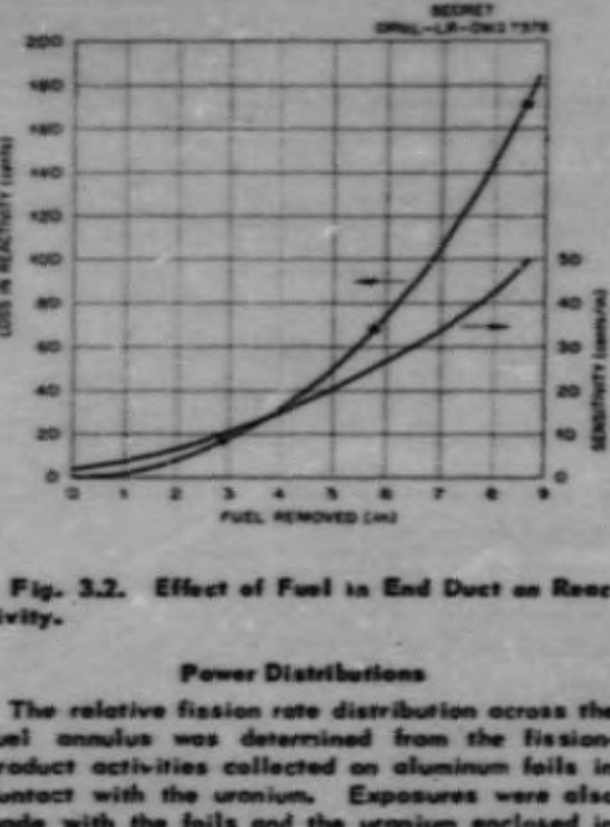

Fig. 3.2. Effect of Fuel in End Duct on Reactivity.

Power Distributions

The relative fission rate distribution across the fuel annulus was determined from the fission-product activities collected on aluminum foils in contact with the uranium. Exposures were also made with the foils and the uranium enclosed in 0.02-in.-thick cadmium in order to obtain a measure of the energy distribution of the neutrons causing fission. The locations of foil traverses within the fuel section of the assembly are shown at the top of Fig. 3.3. As may be recalled, the fuel consists of laminae of uranium (0.004 in. thick) and Teflon (0.142 in. thick); the measurements were made at selected positions on lines perpendicular to these laminae. The fission rate distribution across each traverse is plotted in the lower part of Fig. 3.3 as a function of the number of uranium sheets between

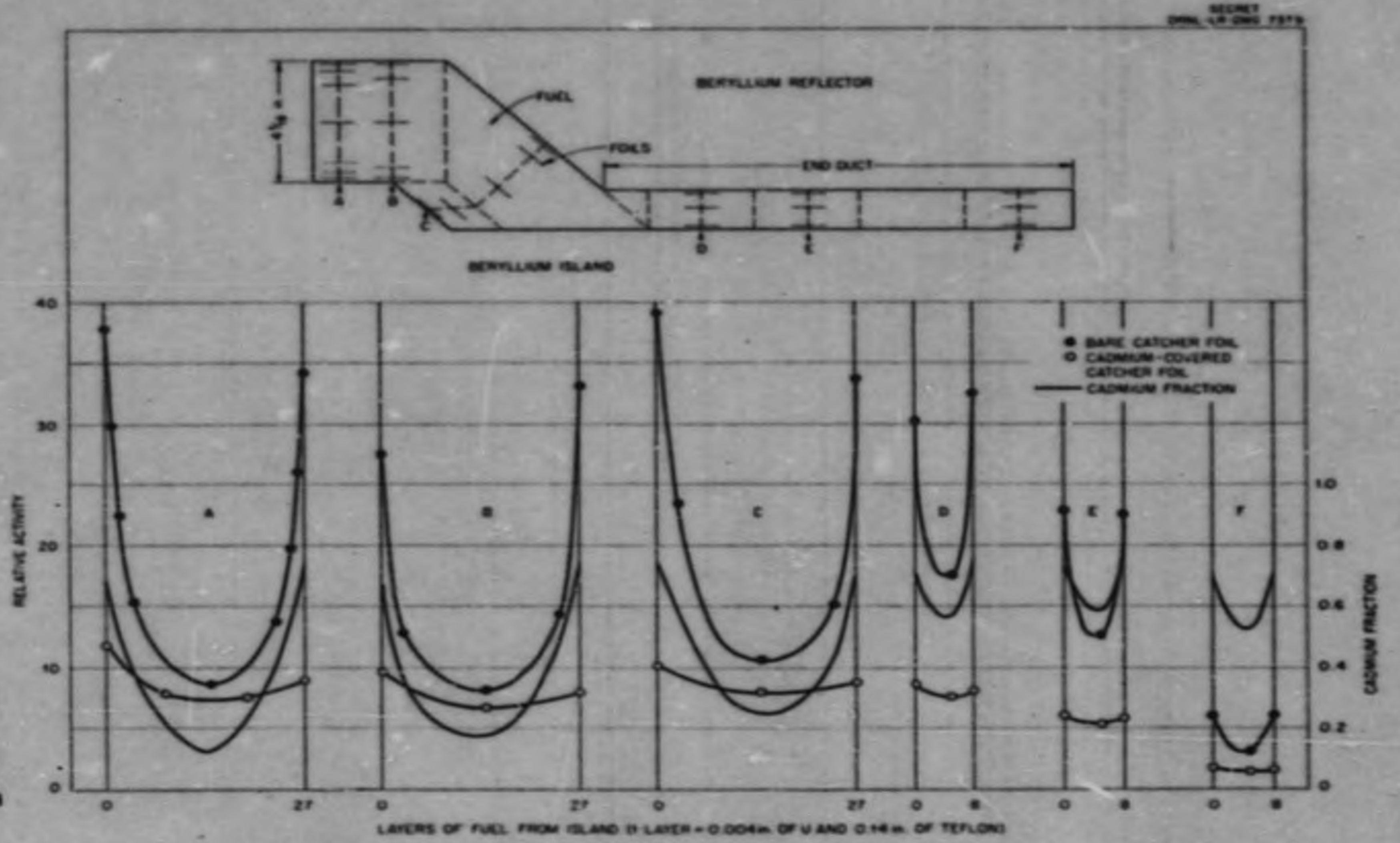

Fig. 3.3. Power Distribution Across Fuel Annulus.

the datum point and the island of the assembly. Values of the cadmium fraction (the fraction of all fissions produced by neutrons having energies less than ~0.5 ev) are also plotted. At the time these measurements were made, the reflector around the center section of the assembly was only $8\frac{5}{8}$ in. thick.

ASSEMBLY FOR HIGH-TEMPERATURE CRITICAL EXPERIMENT

Operation at high temperature of a critical assembly mockup of the ART is scheduled for late summer, 1955. In addition to a determination of the critical uranium concentration at the elevated temperature, the purposes of the experiment are to evaluate the temperature coefficient of reactivity, to investigate the effectiveness of control rod materials, and to measure the contribution of the fuel in the upper end duct to the over-all reactivity.

The experiment will be performed at zero nuclear power and at about 1200°F. Heat will be supplied by electrical heaters external to the reflector. The assembly is to include a beryllium island and a beryllium reflector, essentially 12 in. thick, which will be in a helium or argon atmosphere and will contain no sodium.

The ART core configuration, as presently envisioned, will be exactly mocked up in the experiment between points 18 in. above and below the equatorial plane of the core. Some minor deviations from the ART design are being made beyond these points to simplify filling and draining. The fuel will not be circulated. The core will be filled with molten fuel from a sump tank by using helium to force the molten salt into the assembly. The system will be filled initially for cleaning and testing with a 50-50 mole % mixture of NaF and ZrF_4. Increments of Na_2UF_6 (with the uranium enriched with 93% U^{235}) will subsequently be added to the NaF-ZrF_4 mixture in the sump tank. After each addition of Na_2UF_6, the mixture will be pressurized into the core and then drained until the critical uranium concentration is determined.

A single rod will be located within a 1.50-in.-ID Inconel thimble along the vertical axis of the beryllium island. It will extend from the top of the reactor tank to 10 in. below the equatorial plane of the core. The control rod will be a cylindrical annulus of the mixture of rare-earth elements described above, enclosed in an Inconel shell. Annuli of two widths, $\frac{1}{8}$ and $\frac{1}{4}$ in., will be provided for comparison.

The system is being designed to operate isothermally at 1200°F normally, with provision made for short periods of operation at temperatures up to 1300°F to enable reactivity temperature coefficient measurements to be made. An attempt will also be made to measure the fuel temperature coefficient by inserting the fuel into the reactor assembly at a temperature different from that of the beryllium.

Part II

MATERIALS RESEARCH

DECLASSIFIED

4. CHEMISTRY OF REACTOR MATERIALS

W. R. Grimes
Materials Chemistry Division

Phase equilibrium studies were made of the systems LiF-ZrF_4, NaF-LiF-ZrF_4, and NaF-LiF-ZrF_4-UF_4. Two BeF_2-bearing systems – NaF-LiF-BeF_2 and NaF-LiF-BeF_2-UF_4 – were studied, and the solubility of UF_3 in BeF_2-bearing systems was investigated. A method for zone melting of fused salts was devised as an aid in phase equilibrium studies. Additional work was done in investigating the equilibrium reduction of FeF_2 by hydrogen in $NaZrF_5$, the reduction of UF_4 by structural metals, and the stability of chromium and iron fluorides in molten fluorides. Vapor pressure measurements were made on UF_3 in the temperature range 1270 to 1390°C.

The investigation of the variables affecting the reduction with metallic uranium of UF_4 dissolved in alkali fluorides was continued. A study of the effect of the nickel filters used in experiments for determining the stability of UF_3 in the NaF-KF-LiF system showed that disproportionation of the UF_3 occurred because of the filter.

Fuel purification and preparation research included experimental use of electrolysis under a hydrogen atmosphere to remove oxides and the use of metallic zirconium to replace most of the hydrogen in the stripping operation. In addition, attempts were made to prepare mixtures containing very high UF_3/UF_4 ratios. A study of the conditions for the preparation of BeF_2-bearing melts was continued, and production operations were resumed to provide test material for the greatly accelerated engineering test program.

Potential measurements were made with combinations of several half cells consisting of metal electrodes bathed in solutions of the corresponding metal ion in the molten salt mixture NaF-ZrF_4. Also, vapor pressure measurements were made of mixtures in the LiF-ZrF_4 system. An x-ray diffractometer designed specifically for studies of the structure of liquids is described. Final testing of the diffractometer is under way. A high-temperature attachment for an x-ray spectrometer is also being used to help clarify phase relationships in fuel systems of interest.

PHASE EQUILIBRIUM STUDIES

C. J. Barton F. F. Blankenship
Materials Chemistry Division
H. Insley, Consultant

The very considerable interest in obtaining fuel mixtures with physical properties more favorable than those available in the NaF-ZrF_4-UF_4 system has led to evaluation of the NaF-LiF-ZrF_4 ternary and the NaF-LiF-ZrF_4-UF_4 quaternary systems. Largely as a consequence of studies pursued during the past quarter, the former system has been reasonably well defined; the latter requires considerably more effort. While phase equilibrium data show that quite low melting points are available in this system and that adequate melting points are available at ZrF_4 concentrations as low as 21 mole %, no composition with physical properties better than those available in the NaF-ZrF_4-UF_4 system has been demonstrated.

Study of the analogous NaF-LiF-BeF_2 system has been continued. Adequate melting points are available over wide areas in this system. Whether the physical properties of proper compositions in this system can show significant advantages over those in the NaF-ZrF_4-UF_4 system cannot yet be answered with certainty.

The Binary System LiF-ZrF_4

R. E. Moore R. E. Thoma
Materials Chemistry Division
D. L. Stockton, Merck & Company

A tentative diagram of the LiF-ZrF_4 binary system, based primarily on thermal analysis data, was published previously.[1] A re-examination of this system by petrographic and x-ray diffraction studies of quenched and slowly cooled samples and by differential thermal analysis was started during the past quarter because of current interest in the NaF-LiF-ZrF_4 system.

Although quenching of LiF-ZrF_4 mixtures is not completely satisfactory because of rapid crystallization of many mixtures in the system, some conclusions may be drawn from the results. A eutectic between LiF and Li_3ZrF_7 at about

---

[1] L. M. Bratcher, V. S. Coleman, and C. J. Barton, *ANP Quar. Prog. Rep. June 10, 1953*, ORNL-1556, p. 44.

21 mole % ZrF_4 was confirmed by quenching experiments on both sides of this composition. The eutectic temperature found by quenching is about 600°C instead of the 590°C indicated by thermal analysis. The melting point of Li_3ZrF_7 (645°C according to thermal analysis) could not be checked by quenching because of too rapid crystallization. Decomposition of Li_3ZrF_7 into Li_2ZrF_6 and LiF occurs somewhere below 480°C. This decomposition explains a series of cooling breaks at about 465°C and the apparent discrepancy between thermal analysis data and the results of solid-phase studies (reported earlier[1]). The melting point of Li_2ZrF_6 (585°C according to recent thermal analysis data[2]) was found to be approximately 590°C by quenching. The primary phase was found to be Li_2ZrF_6, and thus the belief that this compound melts congruently was confirmed.

The only other binary compound in the system, as yet unidentified, was found by examination of both quenched and slowly cooled samples containing more than 50 mole % ZrF_4. No evidence was found for the existence of $LiZrF_5$. A careful study of samples of compositions with 57.1, 60, 62.5, and 66.7 mole % ZrF_4 which were held both above and below the solidus temperature for about 12 hr before quenching indicates that the unidentified compound is probably $Li_2Zr_3F_{14}$ (60%) or $Li_3Zr_4F_{19}$ (57.1%) and that it melts incongruently to ZrF_4 and liquid at about 515°C. The optical properties of this compound are almost identical to those of Li_2ZrF_6, so it was necessary to rely almost entirely on x-ray diffraction to differentiate between them. Work on questionable aspects of the compositions with more than 50 mole % ZrF_4 is continuing.

The differential thermal analysis technique and the equipment previously used in the study of the NaF-ZrF_4 system[3] were also employed to obtain more precise thermal data for LiF-ZrF_4 mixtures. Ten-gram samples were prepared by mixing purified Li_2ZrF_6 with the required amount of ZrF_4 or Li_3ZrF_7 in welded nickel capsules fitted with thin-walled center thermocouple wells. Manual control of a Variac transformer was found to give a reasonably uniform rate of heating, about 90°C/hr, and of cooling, about 75°C/hr. The base line obtained on the automatic plot of sample temperature vs differential temperature (difference between sample and Al_2O_3 reference amplified by a d-c amplifier) seemed to be less erratic when the transformer was controlled manually than when the automatic temperature controller was used. The compositions studied to date cover the range from 31.9 to 66.7 mole % ZrF_4. These studies are incomplete, but the data obtained indicate a melting point of 493 ± 5°C for the eutectic at about 50 mole % ZrF_4 and a value of 520 ± 5°C for the incongruent melting point of the unidentified compound containing more than 50 mole % ZrF_4. The thermal effect at 462°C was apparent on the heating curves of all compositions, presumably because a small amount of LiF present in the Li_2ZrF_6 combined with Li_2ZrF_6 to give Li_3ZrF_7. This effect was noted only upon cooling of the mixture with 31.9 mole % ZrF_4, in which it would be expected that Li_3ZrF_7 would be present. The existence of only one thermal effect, at 565°C, for this composition, in addition to the 462°C solidus transition, appears to verify the existence of the Li_3ZrF_7-Li_2ZrF_6 eutectic near this composition. These studies are continuing, and it is expected that a revised diagram will be completed for this system in the near future.

The Ternary System NaF-LiF-ZrF_4

C. M. Blood H. A. Friedman
F. P. Boody F. W. Miles
R. E. Thoma
Materials Chemistry Division

Fuel mixtures based on the NaF-ZrF_4 system have suitable melting points only if the composition lies close to the compound $Na_7Zr_6F_{31}$, which is characterized on the phase diagram by a flat maximum at 520°C with 500°C eutectics on either side. The typical NaF-ZrF_4-UF_4 fuel mixture therefore contains about 45 mole % ZrF_4. It is unfortunate that several of the physical properties values of this class of fuels are somewhat unsatisfactory because of the high ZrF_4 content. The physical properties that are troublesome are vapor pressure, kinematic viscosity, and heat capacity per unit volume. In the LiF-ZrF_4 system, the low-melting region occurs at 50% ZrF_4 and 500°C, and therefore there is little promise of improved physical properties here.

---

[2] H. A. Friedman and F. F. Blankenship, unpublished data.

[3] R. A. Bolomey, *ANP Quar. Prog. Rep. Dec. 10, 1953*, ORNL-1649, p 54.

However, there was a possibility that low-melting regions with much lower ZrF_4 content would be found in the NaF-LiF-ZrF_4 ternary system. The substitution of LiF for NaF was expected to result in lower melting points, because Li_3ZrF_7 (mp, 645°C) melts at a much lower temperature than does Na_3ZrF_7 (mp, 850°C), and Li_2ZrF_6 (mp, 585°C) melts at a much lower temperature than does Na_2ZrF_6 (incongruent, liquidus at 700°C). The use of LiF would be expected to result in higher heat capacities. In order to find low-melting regions that would have as little ZrF_4 and as much LiF as possible, the ternary system NaF-LiF-ZrF_4 was explored. The results are summarized in Fig. 4.1. No ternary compounds were encountered.

The liquidus contours were obtained from cooling curves on melts of at least 500 g contained in 4-in. graphite liners which were enclosed in nickel pots in a 5-in. pot furnace. The melts were stirred by belt-driven nickel stirrers; temperatures were measured by thermocouples in the hollow shafts of the stirrers. A flowing atmosphere of helium was maintained over the melts. The important features of the ternary system were determined on mixtures blended from eutectic or compound compositions which had been purified

CONFIDENTIAL
ORNL–LR–DWG 7380

Fig. 4.1. Phase Diagram of NaF-LiF-ZrF_4 System.

by a high-temperature HF treatment. All the solidified samples were examined petrographically to determine the phases present, and representative samples were examined by x-ray diffraction whenever questions arose which could be studied by this technique.

The first objective of the investigation was to find quasi binaries which would serve to define the compatibility triangles in the ternary system. Beginning at the low ZrF_4 concentrations, the join between LiF and Na_3ZrF_7 was found to be a quasi binary with a simple eutectic at 625°C and 38 mole % LiF. The compatibility triangle formed with this join and NaF as an apex contains a ternary eutectic at NaF-LiF-ZrF_4 (51-38-11 mole %), which melts at 600°C and contains NaF, LiF, and Na_3ZrF_7.

The next quasi binary is the Na_3ZrF_7-Li_3ZrF_7 join. Here extensive solid solutions occur, as shown in Fig. 4.2. Cooling curves gave uncertain indications of the solidus, and therefore the limits of miscibility at the eutectic are not known. However, the limit of miscibility of Na_3ZrF_7 in Li_3ZrF_7 mixtures at 350°C is clearly defined. This is due to the existence of a lower limit of stability of Li_3ZrF_7 at 490°C, coupled with the lowering of the limit of stability by increasing amounts of solid solution with Na_3ZrF_7 and the large thermal effect associated with the decomposition. At the composition NaF-LiF-ZrF_4 (26-49-25 mole %) the lower limit of stability of the Li_3ZrF_7-rich solid solution has decreased to 350°C, and the saturation limit has been reached. The x-ray diffraction lines for the Na_3ZrF_7-rich solid solutions are puzzling in that they show the expected shifts up to about 30% LiF and unexpected, decreased shifts at higher LiF concentrations. The eutectic occurs at 50% and 590°C.

The compatibility triangle lying between the Na_3ZrF_7-LiF join and the Na_3ZrF_7-Li_3ZrF_7 join is characterized by three two-phase crystallization paths with a relatively small temperature gradient; the paths join to form a eutectic at NaF-LiF-ZrF_4 (22-55-23 mole %) that melts at 575°C.

Superficially, the join between Na_2ZrF_6 and Li_2ZrF_6 appears to be a quasi binary, since only the end members are readily identifiable in solidified melts lying on this join, and a eutectic-type break in the cooling curves is found at 445°C and 31% LiF. However, Na_2ZrF_6 melts incongruently at 630°C, and on the Na_2ZrF_6 limb of the eutectic, Na_3ZrF_7-rich solid solutions are the primary phase. The eutectic type of halt at 445°C is observable only on the Li_2ZrF_6 limb, and it corresponds to the appearance of an Na_3ZrF_7-rich phase, which must subsequently react with liquid to give the Na_2ZrF_6 found as a final product. The true eutectic between Na_2ZrF_6 and Li_2ZrF_6 appears to occur at about 435°C. The thermal effects accompanying this behavior are shown in Fig. 4.3.

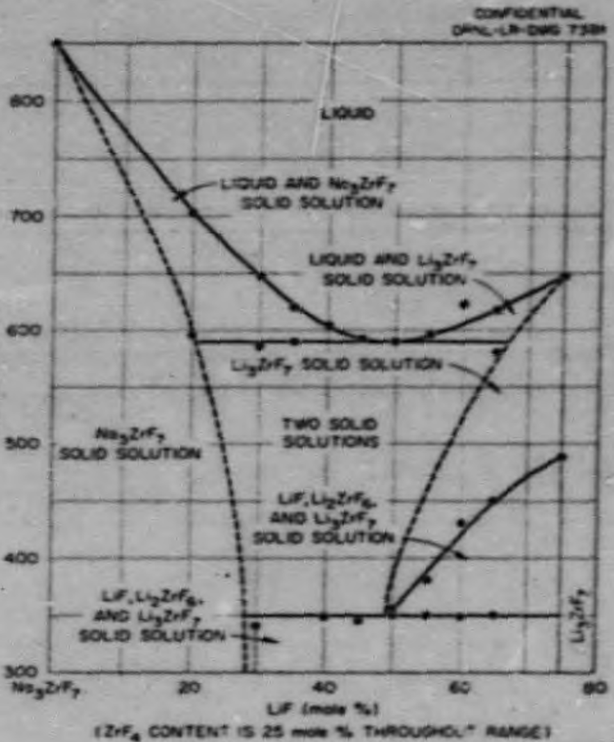

Fig. 4.2. Phase Diagram of the Quasi-Binary System Na_3ZrF_7-Li_3ZrF_7.

These complications have prevented the establishment of meaningful compatibility triangles between 25 and 33.3 mole % ZrF_4. In this region at 455°C and the composition NaF-LiF-ZrF_4 (34-35-31 mole %), there is an intersection of the two-phase crystallization paths involving Li_2ZrF_6-

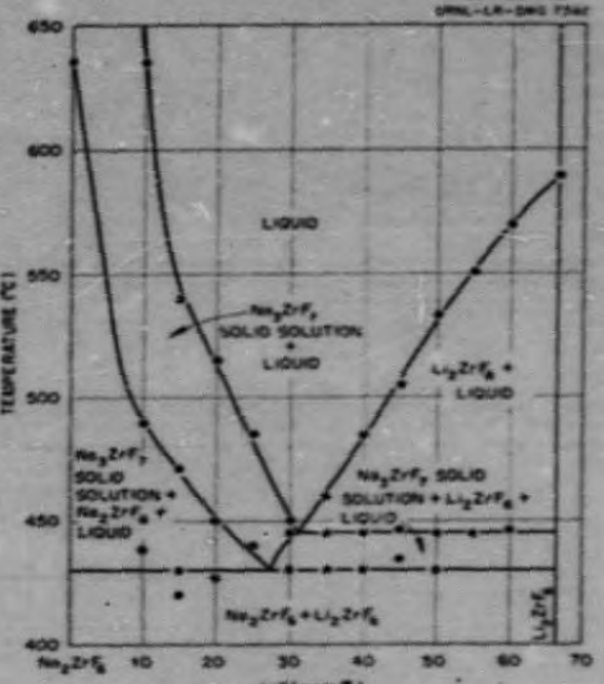

Fig. 4.3. Thermal Effects in the Na_2ZrF_6-Li_2ZrF_6 System.

and Li_3ZrF_7-rich solid solutions on the one hand, and Na_3ZrF_7- and Li_3ZrF_7-rich solid solutions on the other. From this junction a crystallization path crosses the Na_2ZrF_6-Li_2ZrF_6 join before reaching a eutectic.

The join between $Na_7Zr_6F_{31}$ and Li_2ZrF_6 is a quasi binary with a simple eutectic at 28% LiF that melts at 455°C. Between this join and the Li_2ZrF_6-Na_2ZrF_6 join there is a eutectic region of peculiar behavior which has not been explained. The system behaves as though a metastable ternary eutectic between $Na_7Zr_6F_{31}$, Li_2ZrF_6, and Na_2ZrF_6 forms at 425°C, but, before complete solidification can occur, a binary eutectic between $Na_3Zr_2F_{11}$ and Li_2ZrF_6 makes its appearance. The melting point of the stable eutectic is 435°C; the composition is NaF-LiF-ZrF_4 (38-25-37 mole %). The metastable eutectic at 425°C is more strongly evidenced at a slightly higher LiF concentration.

Attempts to define the crystallization path between Na_3ZrF_7 and Na_2ZrF_6 have been rather sketchy and unfruitful; cooling curves contributed relatively little toward the definition. Similarly, essentially nothing is known about the primary phase field of $Na_3Zr_2F_{11}$. The region above 45% ZrF_4 is of little interest from the standpoint of fuel composition, and has been investigated only sparingly. There was no evidence of melting points below 450°C when the join between $Na_7Zr_6F_{31}$ and LiF-ZrF_4 (50-50 mole %) was investigated. The composition of the LiF-ZrF_4 incongruent compound containing about 60% ZrF_4 has not been established, and attempts to find a quasi-binary join between this compound and $Na_7Zr_6F_{31}$ or between $Na_3Zr_4F_{19}$ and Li_2ZrF_6 were unsuccessful.

The Quaternary System NaF-LiF-ZrF_4-UF_4

C. M. Blood H. A. Friedman
F. P. Boody F. W. Miles
R. E. Thoma
Materials Chemistry Division

The quaternary system NaF-LiF-ZrF_4-UF_4 has been studied as a quasi-ternary system by considering only compositions containing 4 mole % UF_4 and by considering the UF_4 as a substitution for 4 mole % ZrF_4. When UF_4 is added to the NaF-LiF-ZrF_4 ternary system, the uranium is found in only four phases: $Na_3Zr(U)F_7$, $Li_3Zr(U)F_7$, $Na_7[Zr(U)]_6F_{31}$, and $Zr(U)F_4$. In each case the uranium forms a solid solution. No $Zr(U)F_4$ has appeared in compositions of interest as fuel.

The quasi binary between LiF and $Na_3Zr(U)F_7$ dropped 10°C, to 615°C, as a result of the lowering of the melting point of Na_3ZrF_7 by including enough uranium to give an over-all composition of 4 mole % U. On the NaF side of this join, the quasi-ternary eutectic was found at 590°C, and the composition was shifted to NaF-LiF-ZrF_4-UF_4 (53-35-8-4 mole %).

The saddle between $Na_3Zr(U)F_7$ and $Li_3Zr(U)F_7$ was depressed so strongly that the minimum in the join was overlaid by the LiF-phase field. The lowest melting composition along this join started freezing at 545°C and had the composition NaF-LiF-ZrF_4-UF_4 (20-55-21-4 mole %). The viscosity of a similar mixture has been measured (cf., Sec. 7, "Heat Transfer and Physical Properties"). Contrary to expectations, the reduction of the

ZrF_4 content resulted in an increase in the viscosity.

When this unexpected turn of events became apparent, attention was shifted to compositions containing more ZrF_4. The composition NaF-LiF-ZrF_4-UF_4 (32-35-29-4 mole %) melts at 445°C and resembles a eutectic containing $Na_3Zr(U)F_7$ and $Li_3Zr(U)F_7$ solid solutions and $Na_7[Zr(U)]_6F_{31}$. Most of the uranium is in the $Na_7[Zr(U)]_6F_{31}$ phase. It is interesting to note that the melt corresponds stoichiometrically to an approximately 50:50 mixture of $Na_2Zr(U)F_6$ and $Li_2Zr(U)F_6$.

The quasi binary between $Na_7Zr_6F_{31}$ and Li_2ZrF_6 was not changed much by the inclusion of 4 mole % UF_4. The eutectic rose only about 2°C (to 457°C), with an almost imperceptible shift in the direction of more Li_2ZrF_6. The composition of this quasi-binary eutectic is NaF-LiF-ZrF_4-UF_4 (31-28-37-4 mole %). Since this eutectic appears to be a saddle point, a quasi-ternary eutectic might be expected at somewhat lower ZrF_4 concentrations. A rather extensive search has not revealed any lower temperatures in this region. The important compositions established in the phase studies described above are summarized in Table 4.1.

BeF_2-Bearing Systems

L. M. Bratcher **R. J. Sheil**
B. H. Clampitt **R. E. Thoma**
Materials Chemistry Division

T. N. McVay, Consultant

The Ternary System NaF-LiF-BeF_2. A considerable amount of thermal data has been obtained by means of cooling curves with mixtures in the NaF-LiF-BeF_2 system containing 10 to 50 mole % BeF_2. The LiF-Li_2BeF_4-Na_2BeF_4-NaF section of the system has been investigated most thoroughly because it is expected that melts containing less than 33 mole % BeF_2 will have low viscosity, high heat capacity, and other favorable physical properties. The thermal analysis investigation of the system has been hampered by undercooling, most troublesome with melts containing more than 33 mole % BeF_2, and by difficulty in obtaining reproducible data. The filtration technique was used to determine liquidus temperatures with two compositions. Mixtures prepared for thermal analysis were studied by x-ray diffraction and petrographic techniques. Although some progress was made in understanding the phase relationships in this system, which are complicated by the existence of ternary components, they are far from being completely elucidated. It appears that

TABLE 4.1. LOW-MELTING MIXTURES IN THE NaF-LiF-ZrF_4 AND THE NaF-LiF-ZrF_4-UF_4 SYSTEMS

Composition (mole %)				Melting Point (°C)	Nature of Mixture
NaF	LiF	ZrF_4	UF_4		
51	38	11		600	Ternary eutectic: NaF-LiF-Na_3ZrF_7
53	35	8	4	590	Quasi-ternary eutectic: NaF-LiF-$Na_3Zr(U)F_7$
47	38	15		625	Saddle eutectic: LiF-Na_3ZrF_7
47	38	11	4	615	Saddle eutectic: LiF-$Na_3Zr(U)F_7$
22	55	23		575	Ternary eutectic: LiF-$[Na(Li)]_3ZrF_7$-$[Li(Na)]_3ZrF_7$
25	50	25		590	Saddle eutectic: $[Na(Li)]_3ZrF_7$-$[Li(Na)]_3ZrF_7$
20	55	21	4	545	Segregates: LiF (primary)—solid solutions—$Na_7[Zr(U)]_6F_{31}$
32	35	29	4	445	Quasi-ternary eutectic(?): solid solutions—$Na_7[Zr(U)]_6F_{31}$
38	25	37		430	Quasi-binary eutectic(?), $Na_3Zr_2F_{11}$-Li_2ZrF_6
31	28	41		455	Saddle eutectic: $Na_7Zr_6F_{31}$-Li_2ZrF_6
31	28	37	4	457	Saddle eutectic(?): $Na_7[Zr(U)]_6F_{31}$-Li_2ZrF_6
25	27	48		450(?)	High ZrF_4; not well established

equilibrium data are difficult to obtain in this system. It is expected that the quenching and differential thermal analysis techniques will be applied to the study of this system in the near future.

Thermal data for the LiF-Na_2BeF_4 join are shown in Fig. 4.4. Solid-phase studies of the slowly cooled melts showed that only the two components were present. The minimum-melting mixture on the join has the composition NaF-LiF-BeF_2 (56-16-28 mole %), and the melting point of 480 ± 5°C is the lowest thus far observed with BeF_2 mixtures containing significantly less than 33 mole % BeF_2. Consequently, this mixture is potentially important as a fuel carrier. The solid-phase studies have also shown that mixtures within the LiF-Na_2BeF_4-NaF triangle contain only these three components. Other compatibility triangles that have been tentatively postulated on the basis of incomplete, and sometimes conflicting, data are LiF-$Na_2LiBe_2F_7$-Li_2BeF_4 and LiF-Na_2BeF_4-$Na_2LiBe_2F_7$. The latter compound is the only ternary compound that has been definitely identified in the present studies, but other phases, as yet unidentified, have been observed.

The cooling-curve data suggest the existence of a ternary eutectic that melts at 325 ± 10°C. The composition of this low-melting eutectic is not definitely known, but it may be near the composition NaF-LiF-BeF_2 (27-35-38 mole %). If confirmed, this would be one of the lowest melting fluoride mixtures known that has favorable nuclear properties and, possibly, other good physical properties.

The Quaternary System NaF-LiF-BeF_2-UF_4. Only one composition in the NaF-LiF-BeF_2-UF_4 system was investigated. The addition of 2.5 mole % UF_4 to the LiF-Na_2BeF_4 eutectic lowered the apparent liquidus temperature, determined by visual observation, to 465 ± 5°C. The liquidus temperature will be checked by filtration because of the observation of poorly reproducible thermal effects on cooling curves at 570 ± 15°C. The uranium in this mixture was combined as Na_2UF_6,

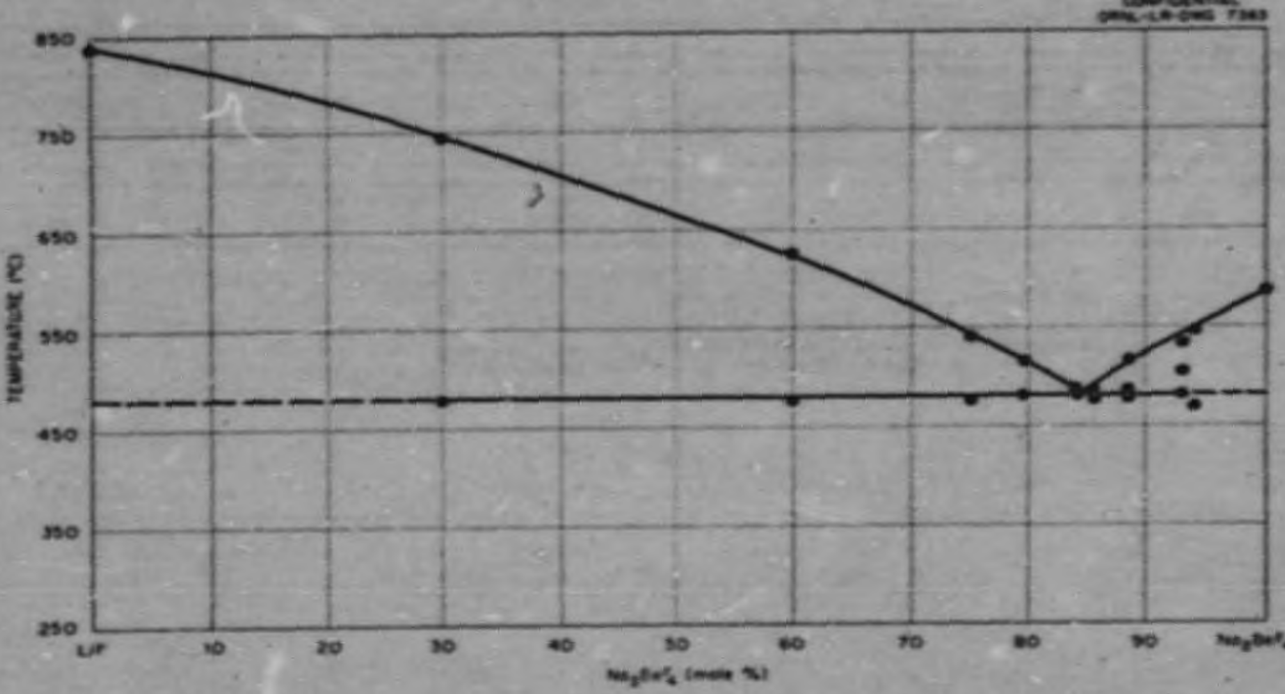

Fig. 4.4. Thermal Data for the System LiF-Na_2BeF_4.

and the remaining compounds were so poorly crystallized that they were almost unidentifiable in the preparations examined to date.

Solubility of UF_3 in BeF_2-Bearing Compositions. The solubility of UF_3 in BeF_2-bearing compositions was determined with six different alkali fluoride–BeF_2 mixtures, some of them at different temperatures. All the determinations were carried out in nickel filtration apparatus; the melt was filtered through nickel filters after an equilibration period of 2 hr. Some solubility data obtained with BeF_2-containing melts and reported earlier were obtained in the same type of equipment.[4] The poor reproducibility of the data, shown in Table 4.2, indicates that equilibrium was not attained in these experiments, probably because of alloying of the uranium with the nickel container and filter with consequent lack of control of the activity of the uranium.

The scattered data in Table 4.2 show a trend of increasing UF_3 solubility with increasing temperature and decreasing BeF_2 content, but in no case does it appear that the solubility of UF_3 at 600°C is sufficiently high to provide more than a fraction of the concentration needed for an ART fuel. The data reported by Mound Laboratory[5]

TABLE 4.2. SOLUBILITY OF UF_3 IN BeF_2-BEARING COMPOSITIONS

Composition (mole %)			Temperature (°C)	Uranium Added	Analysis of Filtrate (wt %)	
NaF	LiF	BeF_2			U^{3+}	Total U
57		43	600	UF_3	0.10	0.59
70		30	600	UF_3 + U	0.54	2.48
			600	UF_4 + U	0.52	4.38
			700	UF_3 + U	1.09	5.47
			700	UF_4 + U	1.54	8.79
			800	UF_3 + U	3.95	11.7
			800	UF_4 + U	4.74	16.0
			800	UF_3 + U	4.46	16.2
75		25	615	UF_4 + U	5.04*	16.8
			700	UF_4 + U	6.32*	17.5
			800	UF_4 + U	5.49	19.7
77		23	600	UF_3 + U	4.62	10.1
			600	UF_4 + U	3.52	7.6
			800	UF_4 + U	8.15	21.1
69		31	600	UF_3 + U	3.37	7.30
			600	UF_3 + U	1.83	3.68
			600	UF_4 + U	2.83	4.39
			600	UF_4 + U	2.61	5.82
56	16	28	600	UF_3 + U	1.77	3.49
			600	UF_4 + U	2.97	5.46
			600	UF_3 + U	1.54	4.09
			700	UF_3 + U	3.92	8.13
			700	UF_3 + U	4.76	15.4
			700	UF_4 + U	5.63	9.81
			800	UF_3 + U	8.95	18.6
			800	UF_3 + U	10.2	17.3

*Sample contained metal, result probably high.

---

[4] L. M. Bratcher *et al.*, *ANP Quar. Prog. Rep. Mar. 10, 1955*, ORNL-1864, p 51.

[5] Private communication, J. F. Eichelberger to W. R. Grimes, Feb. 1955.

for the solubility of UF_3 in $NaF-BeF_2$ mixtures were based upon the assumption that all uranium dissolved in the melt was in the trivalent form. This assumption was erroneous, as the data in Table 4.2 clearly demonstrate. The data in Table 4.2 are now supported by recent Mound data.[6]

The low concentration of uranium dissolved in the $NaF-BeF_2$ (57-43 mole %) mixture at 600°C, which is in line with results reported by Mound Laboratory,[6] suggests that a large part of the tetravalent uranium present in BeF_2 melts to which UF_3 and uranium metal were added was due to disproportionation rather than to oxidation by impurities in the melt. The $NaF-BeF_2$ (77-23 mole % and 75-25 mole %) mixtures and also the ternary mixture $NaF-LiF-BeF_2$ (56-16-28 mole %) shown in Table 4.2 were not purified, and it is quite possible that a part of the tetravalent uranium present was due to oxidizing impurities.

Reaction of Uranium Metal with BeF_2-Bearing Compositions. Uranium metal was added to all except one of the mixtures used for UF_3 solubility determinations, but only a few experiments were performed in which uranium metal was the only form of uranium added. The analyses of material filtered through nickel filters after equilibrating 20 g of a purified alkali fluoride–BeF_2 mixture with 4 g of uranium metal for 2 hr are shown in Table 4.3. The data in Table 4.3 are insufficient to determine whether the dissolved uranium was due to oxidation of uranium metal by BeF_2 or by oxidizing impurities in the melts, and further experimentation is planned to clarify this point.

Visual Observation of Fluoride Melts

R. J. Sheil
Materials Chemistry Division

A plastic, inert-atmosphere box similar to one previously described[7] was used for observation of a number of fluoride melts. Some of the results of these observations are given below.

All the alkali fluoride–BeF_2 mixtures prepared to date showed a scum when first melted. The unpurified mixtures were worse than the purified mixtures in this respect, as might be expected. The small amount of scum that appeared on melts of purified mixtures was dissolved when the melt was heated to about 750 or 800°C, and, in some instances, a water-clear melt was obtained. When the mixtures contained UF_4, the scum had a reddish-brown color suggestive of UO_2, but this scum likewise dissolved when the melt was heated to higher temperatures.

It was found that a melted mixture having the nominal composition $NaF-LiF-ZrF_4-UF_4$ (20-55-21-4 mole %) was reddish-brown when only 15% of the uranium was in the trivalent form. When all the uranium was in the tetravalent form, melts of this composition had the normal green coloration.

Alkali fluoride–BeF_2 melts appear to have a rather high surface tension, and they do not wet a clean nickel surface. These effects could possibly be ascribed to small amounts of impurities in the melts being concentrated in the liquid surface, but this is not considered to be likely.

Phase Separation by Zone Melting

F. Kertesz H. J. Buttram
N. V. Smith
Materials Chemistry Division

Apparatus has been assembled recently to determine whether zone melting of fused salts can

TABLE 4.3. ANALYSES OF FILTERED ALKALI FLUORIDE–BeF_2–URANIUM METAL MIXTURES

Alkali Fluoride–BeF_2 Mixture	Temperature (°C)	Analysis of Filtrate (wt %)	
		U^{3+}	Total U
$LiF-BeF_2$ (69-31 mole %)	600	0.82*	0.89
$NaF-BeF_2$ (57-43 mole %)	600	0.58	0.63
	800	0.10	0.85

*Sample contained metal, result probably high.

---

[6] Private communication, J. F. Eichelberger to W. R. Grimes, April 19, 1955.

[7] M. S. Grim, *ANP Quar. Prog. Rep. Sept. 10, 1954*, ORNL-1771, p 56.

be utilized as an aid in phase equilibrium studies. The zone-melting method consists in alternately melting and freezing the salt mixture at very slow rates to allow use of the principle of fractional recrystallization on a multistage basis. Some preliminary trials with mixtures of LiF and UF_4 indicated that, while some equipment modifications may be required, the method holds promise of being a useful supplement to present phase-study procedures.

CHEMICAL REACTIONS IN MOLTEN SALTS

F. F. Blankenship L. G. Overholser
Materials Chemistry Division

Equilibrium Reduction of FeF_2 by H_2 in $NaZrF_5$

C. M. Blood
Materials Chemistry Division

Previous measurements[8] of the partial pressure of HF at equilibrium during reduction of FeF_2 by hydrogen showed higher values than would be predicted from thermochemical data and ideal solution behavior. These high values were tentatively ascribed to a lowered activity of the metallic iron because of alloying of this element with the nickel apparatus. The postulated alloying has been confirmed by low values for final FeF_2 content of the melt and by chemical analyses of portions of the nickel apparatus.

Attempts have been made to repeat these experiments with a mild-steel liner in the nickel apparatus, a steel gas entrance tube, and steel screen baffles. Preliminary data have shown that the presence of a stainless steel thermocouple well extending into the melt has been causing a steady increase in chromium content of the melt with consequent loss of FeF_2 from the solution. This unintended side reaction was taken into account in the calculations and will be avoided in the future.

The results again showed somewhat higher HF values than those predicted. The apparent equilibrium constant (mole fraction of dissolved species used as activity) was 5.7 for this experiment; this is significantly lower than the value of 8 obtained in the nickel equipment and is much higher than the calculated value of 1.6 for ideal behavior.

Reduction of UF_4 by Structural Metals

J. D. Redman C. F. Weaver
Materials Chemistry Division

The reduction of UF_4 by metallic chromium and iron has been studied by methods previously described in ANP quarterly progress reports, and equilibrium data, obtained by using either NaF-ZrF_4 (50-50 mole %) or the NaF-KF-LiF eutectic (11.5-42-46.5 mole %) as the reaction medium, have been reported. More recently, the reduction of UF_4 has been investigated with NaF-ZrF_4 (53-47 mole %) used as the solvent. Also, the reaction of UF_4 with chromium metal and Inconel has been studied by using mixtures of UF_4 and UF_3 dissolved in NaF-KF-LiF.

The results of some studies on the reduction of UF_4 by chromium metal in NaF-ZrF_4 (53-47 mole %) at 600 and 800°C are given in Table 4.4. In these experiments, 2 g of hydrogen-fired chromium was reacted with UF_4 (11.4 wt %) in 40 g of the NaF-ZrF_4 mixture contained in nickel. The values given for K_x were calculated for the reaction

$$2UF_4 + Cr^0 \rightleftharpoons 2UF_3 + CrF_2$$

by using concentrations expressed in mole fractions.

Previous studies with NaF-ZrF_4 (50-50 mole %) as the solvent and 4.1 mole % UF_4 gave a chromium concentration of 2250 ppm and $K_x = 4 \times 10^{-4}$ at 600°C, and 2550 ppm of chromium and $K_x = 5 \times 10^{-4}$ at 800°C. Thus, an increase from 0.48 to 0.51 in the final mole fraction of NaF in the melt containing uranium causes a significant decrease in the equilibrium CrF_2 concentration.

Data for the reaction of UF_4 with metallic iron in NaF-ZrF_4 (53-47 mole %) are given in Table 4.5. In these runs, 2 g of hydrogen-fired iron wire and 11.4 wt % UF_4 were used.

The iron concentrations given in Table 4.5 are very nearly equal to those found for this reaction when NaF-ZrF_4 (50-50 mole %) was used as the solvent. They also agree very closely with those obtained when NaF-KF-LiF (11.5-42-46.5 mole %) was used as the solvent. The iron values were somewhat higher at 600 than at 800°C in all three systems studied.

Data are presented in Table 4.6 for the reaction of chromium metal with 13.3 wt % UF_4 plus 1.5 wt % UF_3 at 600 and at 800°C when NaF-KF-LiF

---

[8] C. M. Blood, *ANP Quar. Prog. Rep. Mar. 10, 1955*, ORNL-1864, p 57.

TABLE 4.4. EQUILIBRIUM DATA FOR THE REACTION OF UF_4 WITH CHROMIUM METAL IN MOLTEN NaF-ZrF_4 (53-47 mole %) AT 600 AND 800°C

Conditions of Equilibration		Found in Filtrate			
Temperature (°C)	Time (hr)	Total Uranium (wt %)	Total Chromium* (ppm)	Total Nickel (ppm)	K_x
600	3	8.4	1710	30	1×10^{-4}
	3	8.6	1740	20	
	5	8.3	1710	35	
	5	8.5	1770	30	
800	3	8.5	2160	50	3×10^{-4}
	3	8.6	2130	40	
	5	8.3	2180	80	
	5	8.6	2170	25	

*Blank of 250 ppm of chromium at 800°C.

TABLE 4.5. EQUILIBRIUM DATA FOR THE REACTION OF UF_4 WITH METALLIC IRON IN MOLTEN NaF-ZrF_4 (53-47 mole %) AT 600 AND 800°C

Conditions of Equilibration		Found in Filtrate			
Temperature (°C)	Time (hr)	Total Uranium (wt %)	Total Iron* (ppm)	Total Nickel (ppm)	K_x
600	3	8.4	435	50	2×10^{-6}
	3	8.5	535	80	
	5	8.6	630	50	
	5	8.6	445	35	
	5	8.4	440	130	
	5	8.7	460	55	
800	3	8.6	455	45	7×10^{-7}
	3	8.4	385	30	
	5	8.6	350	40	
	5	8.4	445	50	
	5	8.5	295	55	

*Blank of 100 ppm of iron at 800°C.

(11.5-42-46.5 mole %) is used as solvent. The runs were carried out in nickel containers, and 2 g of hydrogen-fired chromium metal and 21 g of the NaF-KF-LiF mixture were used.

Results given previously[9] for a mixture containing 15 wt % UF_4 showed equilibrium chromium concentrations of 1100 and 2700 ppm at 600 and 800°C, respectively. A comparison of these values with those given in Table 4.6 shows the effect of a relatively small amount of UF_3 on the equilibrium chromium concentration. It must be recognized that the UF_3 may disproportionate under the conditions studied and that the final UF_3 concentration may be different from that calculated.

Similar studies were made with Inconel in place of the chromium metal. The results given in Table 4.7 were obtained with hydrogen-fired Inconel and 13.3 wt % UF_4 plus 1.5 wt % UF_3 in the NaF-KF-LiF eutectic.

---

[9] J. D. Redman and C. F. Weaver, *ANP Quar. Prog. Rep. Mar. 10, 1955*, ORNL-1864, p 58.

TABLE 4.6. EQUILIBRIUM DATA FOR THE REACTION OF UF_4 PLUS UF_3 WITH CHROMIUM METAL IN MOLTEN NaF-KF-LiF (11.5-42-46.5 mole %) AT 600 AND 800°C

Conditions of Equilibration		Found in Filtrate		
Temperature (°C)	Time (hr)	Total Uranium (wt %)	Total Chromium (ppm)	Total Nickel (ppm)
600	5	10.8	255	110
	5	10.6	195	40
	5	11.7	165	75
	12	11.0	195	25
	12	11.0	350	105
	12	12.4	330	<1
800	5	10.7	1780	60
	5	10.7	1740	270
	5	10.9	2070	10
	5	11.9	1870	35
	5	11.1	1730	20
	5	11.2	2030	55
	5	11.0	1850	65
	12	10.8	1920	10
	12	10.8	1580	3
	12	10.6	1740	<1

TABLE 4.7. DATA FOR THE REACTION OF INCONEL WITH UF_4 PLUS UF_3 IN MOLTEN NaF-KF-LiF (11.5-42-46.5 mole %) AT 600 AND 800°C

Conditions of Equilibration		Found in Filtrate			
Temperature (°C)	Time (hr)	Total Uranium (wt %)	Total Chromium (ppm)	Total Nickel (ppm)	Total Iron (ppm)
600	5	10.6	25	130	105
	5	10.6	30	260	115
	12	10.8	35	110	80
	12	10.7	25	200	50
800	5	10.7	420	95	90
	5	10.5	525	295	110
	5	10.8	485	85	75
	5	10.7	470	60	55
	12	11.1	675	30	60
	12	11.4	725	15	80

The values given in Table 4.7 for 600°C are much lower than the 360 ppm of chromium reported earlier[9] for a mixture containing 15 wt % UF_4 with no UF_3 originally present. At 800°C, a value of 800 ppm for chromium with no UF_3 originally present is to be compared with the somewhat lower values given in Table 4.7. Since the chromium concentration increased when the heating period at 800°C was extended from 5 to 12 hr, it may be that equilibrium had not been attained.

Stability of Chromium and Iron Fluorides in Molten Fluorides

J. D. Redman C. F. Weaver
Materials Chemistry Division

A number of experiments were run to determine, if possible, the extent to which some of the structural metal fluorides are reduced by metallic iron or chromium. In one experiment, 10.9 wt % Fe^{3+} was added as FeF_3 to the NaF-KF-LiF mixture contained in an iron charge bottle and reacted at 800°C. The filtrate was found to contain 14.7 wt % total Fe and 13.8 wt % Fe^{++}. Another run, at 600°C, gave 3.9 wt % Fe^{++} and 4.4 wt % total Fe, which indicated that the Fe^{3+} was almost completely reduced by the metallic iron. Some results obtained for several other combinations are given in Table 4.8. The results given in Table 4.8 show that NiF_2 is quantitatively reduced by metallic chromium and iron at 600 and 800°C in the NaF-KF-LiF mixture and that FeF_2 is reduced by chromium under similar conditions.

Since previous studies[10] had indicated that FeF_2 was relatively stable in the NaF-KF-LiF eutectic at 600 and 800°C, some additional runs were made for which a longer heating period was used. The results of these runs are given in Table 4.9. The data showed that some 90% or more of the iron was divalent after 12 hr of heating. This finding is in agreement with findings of the earlier studies for which the heating period was 3 to 5 hr.

The previous reports[9,10] also presented data which indicated that CrF_2 is not stable in the NaF-KF-LiF eutectic but probably disproportionates according to the reaction

$$3CrF_2 \rightleftharpoons 2CrF_3 + Cr^0$$

The data obtained at 600°C gave a chromium balance approximating that expected for the reaction, but the values obtained at 800°C did

TABLE 4.8. DATA FOR THE REDUCTION OF STRUCTURAL METAL FLUORIDES BY METALLIC IRON OR CHROMIUM IN MOLTEN NaF-KF-LiF (11.5-42-46.5 mole %) AT 600 AND 800°C

Equilibration Time: 5 hr

Equilibration Temperature (°C)	Fluoride Added* (wt %)	Metallic Reducing Agent	Found in Filtrate				
			Cr^{++} (wt %)	Total Cr (wt %)	Fe^{++} (wt %)	Total Fe (wt %)	Total Ni (ppm)
600	1.5 Ni^{++}	Fe			1.29	1.40	130
	1.5 Ni^{++}	Fe			1.21	1.10	110
800	1.5 Ni^{++}	Fe			1.14	1.24	45
	1.5 Ni^{++}	Fe			1.23	1.03	25
600	1.5 Ni^{++}	Cr	0.55	0.41			105
	1.5 Ni^{++}	Cr	0.59	0.77			45
800	1.5 Ni^{++}	Cr	0.84	1.23			245
	1.5 Ni^{++}	Cr	0.52	1.26			85
600	2.5 Fe^{++}	Cr	0.13	0.32		0.009	25
	2.5 Fe^{++}	Cr	0.10	0.43		0.012	105
	2.5 Fe^{++}	Cr	0.13	0.54		0.009	80
800	2.5 Fe^{++}	Cr	0.28	1.22		0.007	115
	2.5 Fe^{++}	Cr	0.34	1.31		0.007	45

*Nickel added as NiF_2; iron added as FeF_2.

---

[10] J. D. Redman and C. F. Weaver, *ANP Quar. Prog. Rep. Dec. 10, 1954*, ORNL-1816, p 63.

not. Additional runs were therefore made at 800°C, and the results are given in Table 4.10.

The values given in Table 4.10 are, in general, in agreement with the previous data. Most of the Cr^{++} changes valence state, but the total chromium content found is too high to account for removal of Cr^{++} by disproportionation. The similarity of total chromium in the filtrates and in the residues suggests that finely divided chromium passes the filter, but, if the case were this simple, the values reported for Cr^{++} should include this metal and therefore be higher than those found. No satisfactory explanation for the behavior of CrF_2 under these conditions can be given at present.

The Disproportionation Pressure of UF_3

S. Langer
Materials Chemistry Division

Previous studies[11] of the disproportionation of UF_3 gave evidence that UF_3 was more stable at elevated temperatures than free energy estimates[12] had indicated. This evidence has been substantiated by vapor pressure measurements on

TABLE 4.9. STABILITY OF FeF_2 IN MOLTEN NaF-KF-LiF (11.5-42-46.5 mole %) AT 600 AND 800°C

Equilibration Time: 12 hr

Equilibration Temperature (°C)	FeF_2 Added (wt % Fe)	Found in Filtrate		
		Fe^{++} (wt %)	Total Fe (wt %)	Total Ni (ppm)
600	13.7	4.8	5.3	185
	13.7	5.6	5.6	255
	5.9	4.5	4.6	210
	5.9	5.3	5.4	235
800	13.7	12.1	13.2	90
	13.7	12.0	13.1	60
	13.7	12.0	12.6	465
	13.7	12.5	12.7	1240
	5.9	5.2	5.7	25
	5.9	5.4	5.7	135
	5.9	5.2	5.4	120

TABLE 4.10. INSTABILITY OF CrF_2 IN MOLTEN NaF-KF-LiF (11.5-42-46.5 mole %) AT 800°C

Time of Heating (hr)	CrF_2 Added (wt % Cr)	Chromium Found (wt %)			
		In Filtrate		In Residue	
		Cr^{++}	Total Cr	Cr^{++}	Total Cr
5	5.8	0.65	6.1	0.20	7.5
	5.8	0.48	5.3	0.44	5.2
	5.8	0.71	5.2	0.43	5.8
	5.8	0.57	5.2		
12	5.0	0.36	4.3	0.42	4.4
	5.0	0.66	4.1	0.44	4.3
	5.0	0.89	4.6	0.50	5.4

---

[11] W. C. Whitley and R. J. Sheil, *ANP Quar. Prog. Rep. Dec. 10, 1954*, ORNL-1816, p 60.

[12] L. Brewer *et al.*, *Thermodynamic Properties and Equilibria at High Temperatures of Uranium Halides, Oxides, Nitrides, and Carbides*, MDDC-1543 (Sept. 10, 1954, rev. Apr. 1, 1947).

UF_3 in the temperature range from 1270 to 1390°C. At these temperatures, the vapor pressure of UF_3 is negligible, while the vapor pressure of UF_4 ranges from 61 to 152 mm Hg, as shown in Fig. 4.5. Hence, the vapor pressure developed above a system initially containing only UF_3 is due to the UF_4 resulting from the disproportionation of UF_3 according to the equation

$$4UF_3 \rightleftharpoons 3UF_4 + U^\circ$$

The condensed phases in the system were presumed to be solid UF_3 (mp, 1400°C), liquid UF_4 (mp, 1035°C) saturated with UF_3, and uranium metal or an alloy of uranium metal with the type 316 stainless steel container material.

The vapor pressures were measured by the method of Rodebush and Dixon.[13] The apparatus was essentially that described by Moore,[14] except that the charge was contained in a tantalum liner in order to minimize alloying of the uranium metal resulting from the disproportionation of UF_3. The low vapor pressure of the system limited the measurements to temperatures above 1270°C, and the failure of the container material (type 316 stainless steel) was the limiting factor at temperatures near 1400°C.

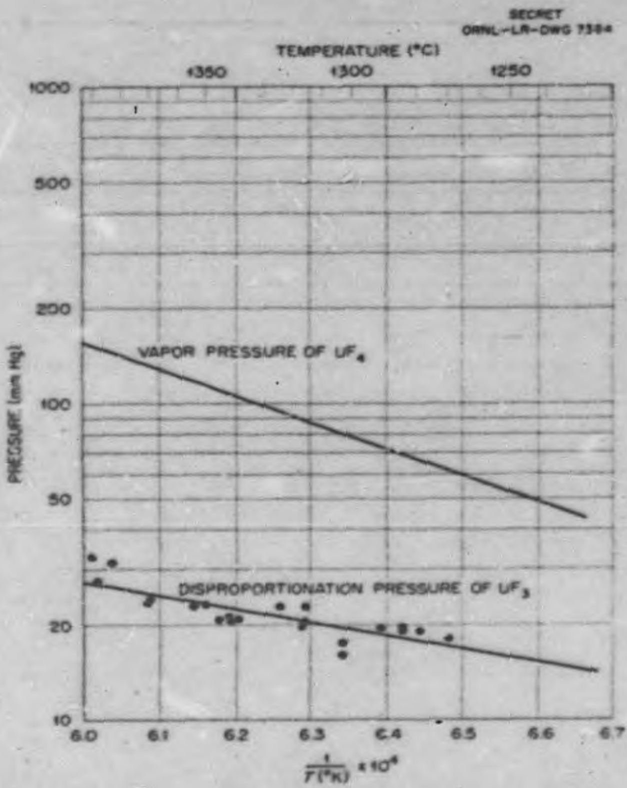

Fig. 4.5. The Vapor Pressure of UF_4 and the Disproportionation Pressure of UF_3.

In all cases, UF_3 of at least 95% purity was used as the starting material. Analysis of the condensate of the vapor phase, collected from the tubes of the vapor pressure cell, showed that the vapor phase was pure UF_4. The disproportionation pressures obtained are given in Table 4.11 and are plotted on Fig. 4.5. The reproducibility of the measurements was not noticeably influenced by ascending or descending temperatures. By using the method of least squares, it was found that a straight line through the points was represented by the equation

$$\log P\ (\text{mm Hg}) = (-4187/T) + 3.945$$

or

$$-RT \ln P\ (\text{mm Hg}) = 19{,}160 - 18.05T\ .$$

The ΔH obtained from the slope of this line is 19,160 cal/mole. This ΔH, however, is a combination of the heat of vaporization of UF_4, the heat of the disproportionation reaction, and the heats involved in the formation of any solutions existing in the condensed phases. Several attempts were made to sample the equilibrium liquid in order to determine its composition, but this proved to be unfeasible because of the limitations of materials at the temperatures involved.

The vapor pressure curve for UF_4 (Fig. 4.5) was obtained from the data of Ryon and Twichell[15] (five points at low pressure were excluded as obviously in error), data of R. E. Moore,[16] and points obtained during the course of this experiment, which extended the temperature range from 1200 to 1300°C. The equation of the line is

$$\log P = (-8428/T) + 7.250$$

---

[13] W. H. Rodebush and A. L. Dixon, *Phys. Rev.* 26, 851 (1925).

[14] R. E. Moore, C. J. Barton, and R. E. Traber, *Vapor Pressures of Zirconium Tetrafluoride and Fused Mixtures with Sodium Fluoride* (to be published).

[15] A. D. Ryon and L. P. Twichell, *Vapor Pressure and Related Physical Constants of Uranium Tetrafluoride*, H-5.385.2 (July 25, 1947).

[16] R. E. Moore, *ANP Quar. Prog. Rep. Mar. 10, 1952*, ORNL-1227, p 155.

TABLE 4.11. DISPROPORTIONATION PRESSURES OF UF_3

Temperature (°C)	Temperature (°K)	$\frac{1}{T(^\circ K)} \times 10^4$	Pressure (mm Hg)
1269.2	1543.0	6.481	18.00
1278.6	1551.8	6.444	18.95
1286.9	1560.1	6.410	19.10
1287.1	1560.3	6.409	19.50
1290.3	1563.5	6.396	19.30
1304.0	1577.0	6.341	17.50
1304.0	1577.0	6.341	16.00
1316.0	1589.0	6.293	22.70
1316.3	1589.5	6.291	20.35
1317.5	1590.7	6.287	19.60
1325.0	1598.0	6.258	22.70
1339.1	1612.3	6.202	20.95
1342.0	1615.0	6.192	20.45
1342.3	1615.5	6.190	21.15
1345.8	1619.0	6.177	20.70
1351.0	1624.0	6.158	23.05
1354.7	1627.9	6.143	22.85
1370.0	1643.0	6.086	23.95
1370.7	1643.9	6.083	23.40
1383.6	1656.8	6.036	31.60
1389.0	1662.0	6.017	27.65
1391.0	1664.0	6.010	32.80

or

$$-RT \ln P = 38{,}600 - 33.18T \ .$$

The heat of vaporization of pure UF_4, as obtained from the slope of the line, is 38,600 cal/mole. This value is in fair agreement with the value of 42,000 cal/mole obtained by R. E. Moore.

It was not surprising to find that the vapor pressure from UF_3 was only a small fraction of that from pure UF_4, but it had not been anticipated that the fraction would rapidly become increasingly smaller with increasing temperatures. Indeed, at sufficiently elevated temperatures, this would not be the case. The effect of dissolved UF_3 is undoubtedly important; it appears that the solubility of UF_3 increases markedly with temperature and also that the UF_4 is complexed to the extent that pronounced negative deviations from Raoult's law are observed. There was no definite evidence of alloying of uranium metal with the tantalum liner; no x-ray diffraction data on uranium-tantalum alloys are available.

An extrapolation of the vapor pressure curves in Fig. 4.5 to the point of intersection might be expected to provide a rough estimate of the eutectic temperature of the UF_3-UF_4 system. The intersection occurs at about 1010°C, whereas cooling curves have shown thermal arrests, which were presumed to correspond to the UF_3-UF_4 eutectic, at 870°C. This discrepancy is probably due not only to the difficulty of obtaining the vapor pressure measurements but also to the long range through which the extrapolation must be made and the change in ΔH with temperature through this range.

The small slope found for the disproportionation pressure curve means that the disproportionation of UF_3 is far from complete under the conditions prevailing in the vapor pressure cell and that UF_3 is thermodynamically stable with respect to pure UF_4 and uranium metal at temperatures below 1400°C.

Reduction of UF_4 with Uranium in Alkali Fluorides

C. J. Barton B. H. Clampitt
Materials Chemistry Division

The investigation of the variables affecting the reduction with metallic uranium of UF_4 dissolved in alkali fluorides was continued during the past quarter. The technique used in these experiments, which are carried out in a small, nickel, filtration apparatus, was described previously.[17] It has become apparent that alloying of nickel and uranium can occur at temperatures far below the minimum nickel-uranium liquidus temperature (732°C) and, consequently, that disproportionation of UF_3 can be expected to occur at the temperatures of interest at nickel surfaces or at any metallic surface with which uranium can alloy. Some effort was therefore devoted to finding container materials that will alloy less readily with uranium. Copper, which has a minimum liquidus temperature of 950°C with uranium, showed some promise in this regard. Although the results obtained in nickel apparatus, and possibly also those obtained in copper containers, are not to be regarded as equilibrium data, these experiments did give some indication of the effect of some of the variables that are involved in the reaction and thus are of value. In some experiments, pure UF_3 was introduced directly for comparison with results obtained in reduction experiments. The results are reported below under the headings of the variables investigated.

Effect of Nickel Surface Area. It was previously reported that the amount of nickel surface area exposed to alkali fluoride–UF_3 melts had a marked effect on the degree of reduction obtained.[17] This observation is substantiated by the data shown in Table 4.12.

In these experiments, the normal surface-to-volume ratio of 2.55 (square centimeters of surface exposed to melt divided by volume of melt in cubic centimeters) was decreased by using a larger charge (40 g) and increased by adding ¼-in. nickel balls or nickel powder. The nickel filter medium surface area, to which the melts were exposed for a short time, was neglected in making these calculations, but it was the same in all experiments. The nickel surfaces were exposed to hydrogen at 750°C before the charge materials were added, and partial sintering of the nickel powder undoubtedly reduced the surface area to a smaller value than that calculated. The marked effect of nickel surface area upon the degree of reduction of uranium, as shown by the data in Table 4.12, was probably due to the previously mentioned effect of alloying of uranium with the nickel.

Effect of Copper Surface Area. In view of the results obtained with nickel, it seemed desirable to determine the effect of another metal on the reduction of UF_4 with uranium. Finely divided copper powder that was hydrogen-fired at 750°C was added to an LiF-NaF-UF_4-U^0 mixture (57.6-38.4-4.0 mole % + 20 wt % excess U^0) in sufficient amount to give a surface-to-volume ratio of about 1000 if the surface area of the nickel container

TABLE 4.12. EFFECT OF SURFACE-TO-VOLUME RATIO ON REACTION OF UF_4 WITH URANIUM METAL IN ALKALI FLUORIDES IN NICKEL CONTAINERS

Solvent	Number of Experiments	Temperature (°C)	Ratio of Surface to Volume (cm^{-1})	Ratio of U^{3+} to Total Uranium
NaF-LiF (40-60 mole %)	2	750	1.89	0.79 to 0.82
	4	750	2.55	0.65 to 0.70
	2	750	4.74	0.43 to 0.51
	3	750	~1000	0.05 to 0.06
NaF-KF-LiF eutectic (11.5-42-46.5 mole %)	5	550	2.55	0.55 to 0.65
	2	550	~1000	0.04 to 0.05
	4	650	2.55	0.55 to 0.65
	2	650	~1000	0.04 to 0.05

---

[17] R. J. Sheil and B. H. Clampitt, *ANP Quar. Prog. Rep. Mar. 10, 1955*, ORNL-1864, p 53.

was neglected. The filtrate obtained after the mixture was heated for 2 hr at 750°C contained 19.2 wt % U^{3+} and 26.0 wt % total uranium. These results compared favorably with those obtained in the absence of the copper and encouraged an investigation of copper as a container material for UF_3-containing melts.

Effect of Excess Uranium. It was reported earlier[17] that there was little difference in the degree of reduction of NaF-KF-LiF-UF_4 with uranium metal whether the theoretical amount of uranium required by the equation

$$\tfrac{1}{4}U^0 + \tfrac{3}{4}UF_4 \rightleftharpoons UF_3$$

was used or whether 1.2 times the theoretical amount was employed. It therefore seemed desirable to investigate this variable with NaF-LiF (40-60 mole %) as the solvent instead of NaF-KF-LiF. This investigation was carried out in nickel apparatus, including nickel filters, and in copper apparatus equipped with a bronze filter medium. The results are given in Tables 4.13 and 4.14. The theoretical total uranium in the filtrate in all these experiments, assuming complete reaction of the UF_4 with the uranium metal according to the above equation, was 27.1 wt %.

The data in Tables 4.13 and 4.14 are somewhat erratic, but it appears that little is to be gained by using more than 100% excess uranium (two times the theoretical amount) under the conditions of these experiments. Comparison of the results in the two tables indicates that UF_3 dissolved in NaF-LiF is more stable in copper than in nickel.

Stability of Binary Alkali Fluoride–UF_3 Mixtures. The preparation of filtered LiF-UF_3 samples containing 91 to 96% of the uranium in the trivalent form was reported earlier,[18] but no data on filtered NaF-UF_3 samples have been reported. Therefore a few experiments were performed to determine the

---

[18] C. M. Blood *et al.*, *ANP Quar. Prog. Rep. Sept. 10, 1954*, ORNL-1771, p 77.

TABLE 4.13. EFFECT OF EXCESS URANIUM ON REDUCTION OF NaF-LiF-UF_4 MIXTURES IN NICKEL APPARATUS

Amount of Excess Uranium (%)	Found in Filtrate (wt %)		Ratio of U^{3+} to Total U
	U^{3+}	Total U	
Theoretical	18.6	28.4	0.65
17	18.5	27.2	0.69
80	20.3	25.2	0.79
140	19.7	26.4	0.75
200	21.0	26.3	0.80
500	20.3	26.3	0.77

TABLE 4.14. EFFECT OF EXCESS URANIUM ON REDUCTION OF NaF-LiF-UF_4 MIXTURES IN COPPER APPARATUS

Amount of Excess Uranium (%)	Found in Filtrate (wt %)		Ratio of U^{3+} to Total U
	U^{3+}	Total U	
20	19.1	27.2	0.71
100	24.1	27.1	0.89
100	23.8	27.8	0.86
200	25.2	27.3	0.92

stability of UF_3 in these systems under the same conditions as those used for more complex systems except that higher temperatures were necessitated by the higher liquidus temperatures. The data are given in Table 4.15. Since the data do not show any significant differences between the two systems in degree of reduction and since UF_3 is known to form a stable complex with NaF in the solid state but not with LiF, it appears that complex formation has little influence on the stability of fused alkali–UF_3 mixtures.

Effect of Filter Medium on Stability of UF_3

M. B. Panish
Materials Chemistry Division

Previous studies[19] on the stability of UF_3 in the NaF-KF-LiF eutectic suggested that the sintered nickel filters used for the filtrations probably had an effect on the degree of reduction found in the filtrates. Since it appeared likely that the UF_3 concentration found in the filtrate did not correspond to that present during the equilibration because the UF_3 was reduced by rapid removal of uranium from the melt through alloying with the nickel filter during filtration, some experiments were performed to confirm or disprove this possibility. These experiments included runs in which a sintered nickel filter was used and others in which a perforated nickel stick was used in place of the filter. The use of container materials other than nickel has been investigated, as well as filtration through graphite.

The runs were made by using NaF-KF-LiF (11.5-42-46.5 mole %) as the solvent and 7 to 14% uranium present as fluoride. The uranium metal added was 500 to 1000% in excess of that required to reduce all the uranium fluoride to UF_3 if it were assumed that all the uranium was present as UF_4. This large excess was used to ensure that some uranium metal was present at unit activity even though a large amount of the uranium present probably alloyed with the walls of the nickel container. Data were obtained only from the runs in which unchanged uranium metal was visible in the heel.

The reaction-filtration apparatus was modified to permit rapid interchange of containers of different types and materials. Sintered nickel of 0.0015-in. pore size was used as the filter in all cases except where otherwise indicated. A nickel stick with four $\frac{1}{32}$-in. holes near the bottom was used to draw up portions of the melts that were not filtered. The results given in Table 4.16 were obtained by using an equilibration period of 2 to 4 hr, except as otherwise indicated.

If it is assumed that there is very little or no uranium metal present in the samples obtained in the perforated nickel stick, it may be deduced from the results in Table 4.16 that the disproportionation of the UF_3 occurs, at least in a major part, because of depletion of the uranium from the melt by the sintered nickel filter. It should be noted that the total uranium found was lower by 1 to 1.5 wt % (absolute) in those cases in which the sintered nickel filters were used, whereas the total uranium was, in general, the same (within experimental error) as that expected in the cases in which the perforated nickel sticks were used. This loss of 1 to 1.5% of the uranium accounts for the difference in the degree of reduction observed in the melts. Analyses of several sintered nickel filters gave results which showed that there was more uranium in the filters than would be expected if they were simply

TABLE 4.15. STABILITY OF UF_3 IN LiF-UF_3 AND NaF-UF_3 MIXTURES

Nominal Composition	Number of Experiments	Temperature (°C)	Ratio of U^{3+} to Total Uranium	Uranium Added as
LiF-UF_3 (73-27 mole %)	1	850	0.75	UF_3
	5	850	0.79 to 0.82	UF_4 + U^0 (20% excess)
NaF-UF_3 (71-29 mole %)	2	820	0.61 to 0.67	UF_3
	4	820	0.72 to 0.82	UF_4 + U^0 (20% excess)

---

[19] R. J. Sheil and B. H. Clampitt, *ANP Quar. Prog. Rep. Mar. 10, 1955*, ORNL-1864, p 53.

TABLE 4.16. EFFECT OF SINTERED NICKEL FILTERS ON THE DISPROPORTIONATION OF UF_3 IN NaF-KF-LiF EUTECTIC

Equilibration Time: 2 to 4 hr, except as indicated
Filter Pore Size: 0.0015 in., except as indicated

Temperature (°C)	Uranium Added as	Calculated Total Uranium in Charge Material (wt %)[a]	Total Analyzed Uranium After Equilibration (wt %)	Ratio of U^{3+} to Total Analyzed Uranium
		Filtered Samples		
600	UF_3		9.2	0.68
	UF_4	13.4	11.4	0.66
	UF_4	13.4	11.8	0.70
700	UF_3		7.6	0.49[b]
	UF_3		9.9	0.73
	UF_3		10.1	0.67
	UF_4	13.4	12.1	0.70
	UF_4	13.4	12.6	0.74
	UF_4	13.4	11.9	0.75[c]
800	UF_3		8.8	0.61
	UF_3		10.2	0.60
	UF_4	13.4	12.2	0.74
	UF_4	13.4	12.4	0.62
		Unfiltered Samples		
550	UF_3		8.3	0.96
600	UF_3		7.6	0.99
	UF_3		9.1	0.98
	UF_4	13.4	13.0	1.08[c]
700	UF_3		9.0	0.98
	UF_4	13.4	13.2	1.01
	UF_4	13.4	12.8	0.99[d]
	UF_4	13.4	13.2	1.03[e]
	UF_4	13.4	12.1	1.08[f]
800	UF_3		7.1	0.97
	UF_3		8.8	1.10[c]

[a] The value given for the calculated total uranium is that expected for total reduction of all UF_4 added. No calculated values are given for runs starting with UF_3, because erratic results were obtained in analyses of the charge materials.

[b] Filter used had a pore size of 0.0004 in.

[c] Small amounts of metallic nickel were observed.

[d] Equilibration time 15 min.

[e] Equilibration time 30 min.

[f] Equilibration time 60 min.

saturated with the melt and that this could account for 25 to 50% of the uranium lost.

Several runs were made with the NaF-KF-LiF eutectic plus UF_3 in gold, platinum, and molybdenum containers. No uranium metal was added, and perforated nickel sticks were used for obtaining samples. The ratio of U^{3+} to total uranium found at 650°C varied from 0.42 to 0.67, and evidence of alloying of uranium with gold and platinum was observed.

Three runs in which the NaF-KF-LiF mixture, UF_4, excess uranium metal, and a graphite filter were used were made in the temperature range 600 to 800°C. The degree of reduction varied from 0.41 to 0.63, and indicated that graphite is not a suitable medium for filtering melts containing U^{3+}. Analyses of the graphite filters gave uranium values that accounted for 3% of the missing uranium at 600°C and 75% at 800°C. Approximately four times as much potassium was found in the filters as existed in the NaF-KF-LiF mixture, and thus it is thought that the potassium may have reacted with the graphite under these conditions to give a carbide.

Stability of PbF_2-BeF_2 Melts in Inconel

C. J. Barton R. J. Sheil
Materials Chemistry Division

The desirability of determining the stability of PbF_2-BeF_2 melts in Inconel was pointed out in the previous progress report.[20] To determine the stability, mixtures containing 50 and 75 mole % BeF_2 were sealed in Inconel capsules and heated for about 10 hr at 800°C in a helium atmosphere. When the capsules were opened and the contents melted out in a helium atmosphere, bright globules, presumed to be metallic lead, were observed on the capsule walls. It was concluded that Pb^{++} ions are not complexed in these mixtures strongly enough to prevent reaction with Inconel at 800°C, and no further testing was performed with mixtures in this system.

Solubility of Metals in Molten Salts

R. E. Cleary
Pratt & Whitney Aircraft

Experiments are under way for determining the solubility of chromium, nickel, and iron in molten salts. The systems being investigated consist of two phases that are thoroughly mixed to ensure intimate contact. The metals to be studied (Cr, Ni, Fe) can be alloyed with uranium to form eutectics with melting points below 900°C, and therefore at experimental temperatures over 900°C the alloy may be used as one phase of a two-phase system. The salt phase of the system must consist of material not reduced by uranium metal, and, consequently, for the initial experiments, the salt phase is limited to alkali-metal halides or combinations of alkali-metal halides.

It was expected from engineering data obtained from thermal-convection loops that the uranium alloys could be formed by heating the metals and the salts in a graphite container under an inert atmosphere or under vacuum. Consequently, an apparatus was constructed with readily available material to carry out the primary part of the experiment. Contrary to expectations, when the experiment was carried out under vacuum with chromium as the added metal, there was catastrophic decomposition of the graphite container and distillation of alkali metals through the vacuum system to the glass-wool trap. A more thorough search for information concerning the reactions of graphite and alkali metals then indicated that potassium reacts with graphite and causes decomposition of the crystal structure. The salt used, NaF-KF-LiF, became green and seeped through the graphite crucible. There was no evidence of alloy formation between the uranium and the chromium. The metal fragments present had retained their initial shape and size, even though the reaction vessel was heated to 1000°C.

In subsequent experiments, a helium atmosphere was also found to be unsatisfactory for this reaction. Additional attempts to make a uranium-chromium alloy in graphite liners in a nickel pot, under helium or vacuum (50 to 75 μ) at a temperature of 1150°C, have proved unsuccessful. Consequently, it is now planned to use molybdenum and/or tantalum crucible liners in a much smaller stainless steel reactor. It is hoped, based on previous work with molybdenum, that these liners will be inert to the reactants. The smaller volumes and mass will make it possible to heat the apparatus to temperatures of over 1200°C in available equipment.

---

[20] L. M. Bratcher *et al.*, *ANP Quar. Prog. Rep. Mar. 10, 1955*, ORNL-1864, p 52.

PRODUCTION OF PURIFIED FLUORIDES

G. J. Nessle F. F. Blankenship
L. G. Overholser
Materials Chemistry Division

Fuel Purification and Preparation Research

C. M. Blood F. L. Daley
F. P. Boody F. W. Miles
Materials Chemistry Division

Investigations of methods for rapid purification of fuel mixtures have included attempts to use electrolysis under a hydrogen atmosphere to remove oxides in order to avoid the container corrosion that results when HF is used and to use metallic zirconium to replace most of the hydrogen in the stripping operation. In addition, attempts have been made to prepare mixtures containing very high UF_3/UF_4 ratios.

Use of Zirconium Metal in Fuel Purification. The time-consuming step in fuel purification processes is the reduction of such materials as FeF_2 and NiF_2 with hydrogen. Reduction of these materials by the addition of an active metal should afford a more rapid process, but it is not possible to add an excess of active metal to a UF_4-bearing mixture without the formation of large and variable quantities of UF_3. A process has been demonstrated on a 5- and 50-lb test scale, however, that is quite rapid and effective if small UF_3 concentrations are tolerable or desirable.

To prepare $NaF\text{-}ZrF_4\text{-}UF_4$, the NaF and ZrF_4, in proper quantity, are charged to the standard apparatus and are hydrofluorinated in the usual manner. At this stage, a considerable excess of metallic zirconium chips in a nickel basket is introduced into the reaction vessel. After 3 hr of stirring with hydrogen, the basket and excess zirconium metal are removed. The proper quantity of UF_4 is then added to the melt, and another nickel basket containing a small, known quantity of zirconium metal is introduced. Stirring for 2 hr suffices for the melt to react with all the zirconium introduced.

In a 50-lb test preparation of $NaF\text{-}ZrF_4\text{-}UF_4$ (50-46-4 mole %), the final mixture contained 15% of the uranium as UF_3, with the Fe, Cr, and Ni contents being 50, 35, and 25 ppm, respectively. It appears that utilization of some variant of this procedure might cut the processing time on the 250-lb production unit to below the 24 hr required, at present, for each batch.

Electrolytic Purification of Fluoride Mixtures. Experiments for determining the rate of oxide removal by hydrofluorination were made during the preparation of some $LiF\text{-}ZrF_4$ mixtures. It was found that hydrofluorination of a mixture for 1 hr at 700°C would not lower the oxide concentration below the limit of petrographic detection; similar treatment at 800°C for 2 hr, however, was sufficient. Since the dissolution of NiF_2 by the melt and the length of the subsequent stripping time are directly dependent on the hydrofluorination time and the temperature, attempts were made to remove oxides completely by electrolysis between graphite anodes and nickel cathodes under a hydrogen atmosphere. Previous experiments[21] had shown that oxides could be removed by electrolysis and that the anode products were CO and CO_2 when a graphite anode was used. When hydrogen was used in conjunction with electrolysis in recent experiments, the predominant anode product was HF. The purpose of the experiment was to test the combined effect of oxide removal as a primary anode product and hydrofluorination by the electrolytically produced HF.

After 0.4 equivalent of HF had been produced by electrolysis at a current efficiency of 37%, the HF was stripped from the melt with hydrogen. No oxide was detected by petrographic examination of the transferred product. Chemical analyses showed 1.1 wt % oxide in the sample before electrolysis as compared with 0.4 wt % in the finished product. The structural metal contamination was simultaneously reduced to the following values: Fe, 55 ppm; Cr, 15 ppm; Ni, 30 ppm.

The earlier experiments with electrolysis[21] had been carried out either in the NaF-KF-LiF eutectic or in mixtures containing NaF and 40 to 50% ZrF_4. The alkali fluoride eutectic was very prone to an anode effect, while the ZrF_4-bearing mixtures could be electrolyzed smoothly. Batches of NaF-LiF eutectic proved to be variable in this respect, and, in one case that gave a bad anode effect, the addition of 0.1 mole % ZrF_4 gave no significant improvement. On the other hand, an $NaF\text{-}ZrF_4$ (81-19 mole %) batch could be electrolyzed smoothly; the transition range must lie below 19 mole % ZrF_4.

Mixtures with High UF_3/UF_4 Ratios. Attempts have been made to prepare fuel mixtures con-

---

[21] C. M. Blood *et al.*, *ANP Quar. Prog. Rep. Dec. 10, 1954*, ORNL-1816, p 66.

taining UF_3 and no UF_4 for experimental work. Earlier attempts[22] indicated that such mixtures could be prepared with $NaF-ZrF_4$ mixtures as the base, but not with the NaF-LiF-KF eutectic. In order to obtain solubilities of the order of 3 mole % uranium at 600°C, it was found that compositions containing more than 50 mole % ZrF_4 would be necessary. There was a possibility that UF_3 was capable of furnishing fluoride ions to complex the ZrF_4 so that the physical properties, particularly vapor pressure, might be far different from those of fuels in current use. Accordingly, a trial was made with a composition that could be considered, from a stoichiometric point of view, to be composed of $NaZrF_5$ and $U(ZrF_5)_3$. The composition was $NaF-ZrF_4-UF_3$ (44-53-3 mole %). After a thorough purification of the $NaF-ZrF_4$ base, the UF_3 was added, along with uranium metal (1 wt % of the amount of UF_3) and zirconium metal (0.2 wt % of the amount of ZrF_4), and equilibrated under hydrogen for 2 hr at 700°C. The uranium and zirconium were included in an effort to suppress the formation of UF_4. After cooling to 600°C, the 4-kg melt was filtered; 75% of the uranium had remained as U^{3+}. There was no insoluble heel.

The preparation was then repeated on a 50-lb batch; only 65% of the uranium was U^{3+}. This was thought to be a consequence of the previous history of the preparation vessels for the two batches. The walls of the 4-kg reaction vessel had been subjected to melts which deposited uranium in the form of a nickel alloy, while no preparations involving UF_3 had ever been made in the 50-lb apparatus.

Another trial was made in the small apparatus by using essentially the same procedure, except that a large excess of zirconium in the form of ½-in. bars was allowed to remain in the melt during the equilibration under hydrogen following the addition of UF_3. This time, 85% of the uranium was U^{3+}. These preparations illustrated the effect of variations in the activity of uranium metal and zirconium metal on the stability of UF_3 during processing of a UF_3 fuel, and raised the question of what fraction of UF_3 would normally "survive" in a reaction vessel which had no previous history of exposure to UF_3 or uranium metal and to which no uranium or zirconium had been added.

An experiment to answer this question showed that 70% of the uranium remained as U^{3+} in 3 kg of $NaF-ZrF_4-UF_3$ (52-46-2 mole %) after 3 hr of equilibration with hydrogen bubbling at 700°C. In the 50-lb apparatus, an attempt to prepare a composition containing 1.2 mole % UF_3 and 0.8 mole % UF_4 in $NaZrF_5$ by starting with 1.7 mole % UF_3 and 0.3 mole % UF_4 was unsuccessful, since the resulting product analyzed only 0.5 mole % UF_3. Resampling and reanalysis confirmed the validity of the initial analysis.

Pilot-Scale Purification Operations

J. P. Blakely F. A. Doss
C. R. Croft J. Truitt
Materials Chemistry Division

Fifty-six preparations totaling 630 lb of material were produced during the quarter. These preparations were of various compositions and were consigned to various requesters for small-scale corrosion studies, for physical property determinations, or, in many cases, for use as purified intermediates for phase-equilibrium investigations.

Uranium trifluoride was a component of nearly 25% of the materials prepared. These batches were prepared, in every case, by complete purification of the solvent fluorides with the desired quantity of UF_4 followed by addition and dissolution of the desired quantity of pure UF_3.

The study of optimum conditions for the preparation of BeF_2-bearing melts was continued without complete success being attained. Hydrogen reduction of the nickel and iron compounds to acceptable concentration levels appears to be more difficult in the BeF_2-bearing melts than in the ZrF_4-bearing mixtures. When the HF concentration in the hydrogen from a ZrF_4-bearing fuel reaches 1×10^{-4} mole per liter, the $Fe^{++} + Ni^{++}$ concentration is less than 150 ppm (by analysis of the filtrate). As the data shown in Table 4.17 indicate, this is not the case for the BeF_2-bearing fuels even at HF levels of 10^{-5} mole per liter. Further study of this system will be attempted as time permits.

Production-Scale Operations

J. P. Blakely J. E. Eorgan
Materials Chemistry Division

Production operations were resumed on March 1, 1955, on a three-shift, five-day-week basis to

---

[22] G. M. Watson and C. M. Blood, *ANP Quar. Prog. Rep. June 10, 1954*, ORNL-1729, p 51–52.

TABLE 4.17. IMPURITIES IN $NaF-BeF_2-UF_4$ MIXTURES AS A FUNCTION OF HF CONCENTRATION OF EXIT HYDROGEN

Concentration of HF in H_2 (mole/liter)	Concentration of Impurities (ppm)			
	Fe	Cr	Ni	S
1×10^{-4}	235	12	1	19
	235	50	120	55
	155	55	150	45
	140	15	65	59
	180	40	90	300
	140	25	200	115
	125	10	85	77
1×10^{-5}	55	17	100	57
	65	14	85	77
	125	30	10	7
	195	37	95	6
	130	25	70	44
	140	15	50	315
	90	17	80	
	75	25	125	
	60	20	15	<5

provide test material for the greatly accelerated ANP engineering program. A total of 4800 lb of purified material was prepared during the quarter.

Several small, but significant, changes in operating techniques have contributed to better operation, shorter processing times, and, consequently, higher yields of material per man hour. The three most important changes were the institution of rigid specifications on the purity of the raw materials, the use of a 30% larger flow rate of hydrogen during the final stripping cycle, and the use of parallel rather than series flow of the hydrogen through the receiver and reaction vessel. It appears that these changes have reduced the processing time by nearly 50%. With new or recently cleaned equipment, 250-lb batches can be processed to meet specifications in 24 hr.

It has definitely been established that, by using two men per shift, 1000 lb can be produced per five-day week; it is believed that this production figure can be improved slightly in the near future. Present estimates of ORNL and Pratt & Whitney requirements during the next several months call for production of 1500 lb per week. It is believed that two men per shift on a six-day work week could meet this production level. Such an expansion of effort will necessitate an increase in processing and storage containers, and, since little excess capacity will be available for emergencies, an increase in spare furnaces and other maintenance items will be required to minimize downtime for repair.

The life of the processing equipment has already considerably exceeded expectations. A number of the reactors have prepared more than 25 charges, and only one reactor has ever failed. Tests are now under way to determine how many runs can be made with the "specification" raw materials before excessive stripping times require cleaning of the reactor.

In spite of the shorter processing times described above, product purity is being rigorously maintained. Analyses of ten typical 250-lb batches of $NaF-ZrF_4-UF_4$ mixtures are shown in Table 4.18.

The present supply of ZrF_4 is not adequate to meet the accelerated demand for the molten salts. Commercially available $(NaF)_xZrF_4$, containing about 30 mole % ZrF_4, is being used at present, but, since this must be blended with 40% ZrF_4 to produce ART fuel compositions, nearly 600 lb of ZrF_4 is still required per week for the 1500-lb-per-week demand. Also, in making the hafnium-free fuel for the high-temperature critical experi-

TABLE 4.18. ANALYSES OF TYPICAL NaF-ZrF_4-UF_4 MIXTURES FROM PRODUCTION PLANT

Batch No.	Uranium Content (wt %)	Impurities (ppm)		
		Ni	Cr	Fe
514	8.66	25	85	15
515	8.42	10	50	35
516	8.69	13	28	35
517	8.75	10	43	10
518	8.69	10	48	20
519	8.64	15	34	<1
520	8.51	7	40	35
521	8.83	5	40	105
522	8.28	10	55	45
523	8.70	10	75	50

ment, the use of the commercial $(NaF)_xZrF_4$ will not be permissible.

Since 250 lb per week appears to be the limit of the present capacity of the Y-12 Plant for the production of ZrF_4, alternative sources are being urgently sought. A commercial source which claims to be able to supply the required quantity has been located, and specification tests of their material are in progress. It appears, at present, that this material may solve the problem; if so, the Y-12 ZrF_4-production facility will be used only part time as needed to provide hafnium-free material.

If the commercial source does not materialize, it will be necessary to expand the Y-12 ZrF_4-production facilities immediately. Accordingly, S. H. Smiley at K-25 is using some available pilot-scale equipment to study conversion of $ZrCl_4$ to ZrF_4. It is anticipated that, should additional construction prove necessary, a more efficient conversion plant than the present one could be built.

In order to economize on the use of ZrF_4, about 1750 lb of previously prepared NaF-ZrF_4 and NaF-ZrF_4-UF_4 mixtures has been converted to ART fuel compositions by returning the material to the processing equipment and adding ZrF_4 and UF_4, as required, to adjust the composition. These materials have also been repurified. From the experience gained to date, it appears that, if the material must be melted for delivery to the processing reactor, about 750 lb per week would be the plant's maximum output of reclaimed material.

Batching and Dispensing Operation

J. P. Blakely F. A. Doss
Materials Chemistry Division

Since production of the purified fluorides is done in 250-lb batches and since a large fraction of the tests call for smaller quantities, it is necessary to batch a considerable fraction of the material produced into 5-, 10-, or 50-lb containers. In the recently accelerated program it has been necessary to operate this equipment virtually full time on a one-shift, five-day-week basis. During the quarter a total of 6680 lb of material was batched and dispensed by this unit.

During recent weeks, equipment has been installed to permit hydrogen firing of all 50-lb transfer cans before re-use. Another unit capable of handling the smaller containers is to be installed in the near future. This equipment should minimize contamination of clean fuel by poorly handled and corroded containers.

For the first time since production began in March 1954, usage during a quarter has kept pace with production. Present estimates of anticipated needs indicate that the demand for processed materials will necessitate a six-day production week after July of this year. The balance sheet for the quarter is shown below:

Material on hand February 1, 1955	4,987 lb
Production during quarter	5,430
Total	10,417
Material dispensed during quarter	6,682
Material on hand at end of quarter	3,818 lb

Pratt & Whitney Aircraft received 2000 lb of this material, and the rest was dispensed to various requesters in the ORNL-ANP program.

Loading and Draining Operations

N. V. Smith
Materials Chemistry Division

Responsibility has been assumed by Materials Chemistry Division personnel for loading and draining all test equipment other than the thermal-convection loops in Building 9201-3. This responsibility includes the loading of liquid metals, as well as molten fluorides, and includes the obtaining of reliable samples of the molten material while the equipment is being filled or drained. Investigations are presently under way to ascertain the best procedure for the delivery of oxygen-free sodium or NaK to test equipment and to determine the most reliable method of sampling this material for analysis.

Special Services

J. P. Blakely F. A. Doss
J. E. Eorgan
Materials Chemistry Division

Enriched Fuels for In-Pile Loops. Two batches of fuel containing enriched uranium were processed for use in an in-pile loop. Since the size and nature of the in-pile loop equipment require that the finished fuel batch contain 600 ± 50 g, it has been agreed that in the future the material will be prepared in larger portions and batched into containers of proper size. An adequate mechanism for analytical quality and accountability control has been established to ensure proper handling and dispensing of the finished material.

As a consequence of increased demands for fuels containing enriched uranium, the processing facility has been established in a permanent and properly equipped location. A new, smaller unit that is better adapted to meet the demands of the in-pile loops is being installed, and the larger unit is being remodeled to accommodate requirements for the ART high-temperature critical experiment. Present known demands for material will require operation of the facility for one week per month during the balance of the calendar year.

ART High-Temperature Critical Experiment. Preparations are being made for the production of the necessary materials for the high-temperature critical experiment, for loading the experimental equipment with the NaF-ZrF_4 (fuel carrier) and most of the Na_2UF_6 (fuel concentrate), and for obtaining reliable samples of the mixture as the experiment proceeds.

Production of the fuel carrier is presently under way, and production of the fuel concentrate will proceed when the UF_4 allocation is received. The processing time for this material should not exceed two weeks, but a somewhat longer time will be required to obtain analyses and to comply with accountability procedures.

Fabrication and overhauling of equipment to be used are in progress. It is anticipated that all preparations can be completed by July 1 of this year. Since all operations will be similar to those performed in the ARE startup, there would seem to be no doubt of the validity of the procedures to be used.

Reprocessing Pilot Plant. Plans are under way to provide charge material and to fill the equipment required to test operation of the uranium recovery process developed by personnel of the Chemical Technology Division (cf. Sec. 10). Operations that each require about 800 lb of material are scheduled for July and December of this year. The material, equipment, and procedure seem to present no unfamiliar problems.

Experimental Preparation of Simple Fluorides

E. E. Ketchen B. J. Sturm
Materials Chemistry Division

Variables Affecting UF_3 Preparation. The preparation of UF_3 by heating a stoichiometric mixture of UF_4 and finely divided uranium metal in a sealed ball mill of stainless steel was described in previous reports.[23,24] The requirements for UF_3-bearing fuels appear to be most easily met by the addition of this compound to carefully purified solvent compositions. A study of variables in UF_3 preparation has been made, accordingly, to determine the optimum conditions for production of kilogram quantities of the material.

The variables studied have included number and size of the steel balls used as milling mediums, amount of material charged, and the reaction time and temperature. In order to facilitate loading and unloading of the 4-kg 15-in. reaction vessel, the loading tube diameter was increased to 1 in., and one end plate was welded at 45 deg rather than at 90 deg to the cylinder axis.

In twenty preparations for which various reaction conditions were used, essentially pure UF_3 was obtained when the normal reaction time-temperature program was used. This consisted of heating the rotating mill and contents at 900°C for three 16-hr periods. The mill was cooled to room temperature between heats and pounded with a hammer to remove caked material from the walls.

Over the range studied (0.75 to 2.25 kg), charge size does not appear to affect completeness of conversion. Quantity and size of the milling

---

[23] W. C. Whitley and C. J. Barton, *ANP Quar. Prog. Rep. Sept. 10, 1951*, ORNL-1154, p 159.

[24] B. J. Sturm and E. E. Ketchen, *ANP Quar. Prog. Rep. Mar. 10, 1955*, ORNL-1864, p 66.

medium appeared to have no measurable effect on the purity of the resulting UF_3. All tests in which 1-in. balls and the standard heating program were used were successful. However, when ½-in. balls were used, the product, in every case, appeared to be sintered. This effect is serious because the fine powder is, in general, desired and because the sintered material adheres tenaciously to the mill and the balls. Additional runs with other ball sizes have been made, and the results will be reported when available.

Some 30 kg of satisfactory UF_3 was prepared during the quarter. Should the need arise, the present equipment could produce 15 to 20 lb of this material per week.

Other Preparations. Approximately 5 lb of $(NH_4)_3CrF_6$ was prepared by heating an excess of NH_4HF_2 with $CrF_3 \cdot 3.33H_2O$ at 200°C. This intermediate product was converted to CrF_3 by heating under helium at 500 to 600°C. The lower temperature yields a material containing small amounts of nitrogen, whereas heating at 600°C gives a product that is contaminated by divalent chromium, apparently because of interaction with the nickel container. Chromic fluoride was also prepared by hydrofluorination of anhydrous $CrCl_3$. At 400°C the conversion is incomplete but material prepared at 550°C is quite pure CrF_3.

One batch of AgF was prepared by hydrofluorination of Ag_2CO_3 at 150 to 200°C. Some CeF_3 was synthesized by the addition of HF to an aqueous solution of $Ce(NO_3)_3$ followed by filtration, washing, and drying at 200°C.

An attempt to prepare $(NH_4)_2SnF_4$ by crystallization from an aqueous solution containing $SnCl_2$ and NH_4HF_2 gave a product containing considerable chloride. Stannous hydroxide that is free of chloride has been prepared and is to be reacted with aqueous NH_4HF_2 in another attempt to prepare $(NH_4)_2SnF_4$. The hydrofluorination of $SnCl_2 \cdot 2H_2O$ at 200°C gave a mixture of chloride and fluoride.

About 8 kg of UF_4 was purified by hydrofluorination at 600°C for use as charge material in the preparation of UF_3.

FUNDAMENTAL CHEMISTRY OF FUSED SALTS

EMF Measurements

L. E. Topol
Materials Chemistry Division

Potential measurements were made during the past quarter with combinations of several half cells consisting of metal electrodes bathed in solutions of the corresponding metal ion in the molten salts. The temperature range studied was, in general, 550 to 700°C, with the system maintained under an inert atmosphere. The half cells were contained in crucibles of Morganite, nickel, or platinum; electrical contact between them was achieved by a "salt bridge" consisting of a porous ZrO_2 rod impregnated with the molten salt solvent.

ZrF_4 Concentration Cells. Cells consisting of zirconium rods immersed in various $NaF-ZrF_4$ melts yielded constant and reproducible potentials. The values obtained at various temperatures for a series of cells of the type

$$\mathrm{Zr} \Big/ \mathrm{ZrF}_{4(a_1)},\ \mathrm{NaF}_{(a_2)} \Big/ \frac{\mathrm{ZrO_2}}{\mathrm{NaF\text{-}ZrF_4}} \Big/ \mathrm{NaF}_{(a_2')},\ \mathrm{ZrF}_{4(a_1')} \Big/ \mathrm{Zr}\ ,$$

where (a) denotes the activity of the species, are shown in Table 4.19. In these experiments, three $NaF-ZrF_4$ mixtures were used as the half-cell electrolytes; the concentrations (c) in mole % ZrF_4 were 50.0, 41.8, and 36.0.

In a cell of the type used the anode reaction is:

$$\mathrm{Zr}^0 + 4\mathrm{F}^-_{(a_2)} \longrightarrow \mathrm{ZrF}_{4(a_1)} + 4e^-\ ,$$

while at the cathode the reaction is

$$\mathrm{ZrF}_{4(a_1')} + 4e^- \longrightarrow \mathrm{Zr}^0 + 4\mathrm{F}^-_{(a_2')}\ .$$

The net electrode reaction is, accordingly,

$$\mathrm{ZrF}_{4(a_1')} + 4\mathrm{F}^-_{(a_2)} \longrightarrow \mathrm{ZrF}_{4(a_1)} + 4\mathrm{F}^-_{(a_2')}\ .$$

However, migration through the bridge proceeds according to

$$4t\ \mathrm{Na}^+_{(a_2)} \longrightarrow 4t\ \mathrm{Na}^+_{(a_2')}$$

and

$$4(1 - t)\,\mathrm{F}^-_{(a_2')} \longrightarrow 4(1 - t)\,\mathrm{F}^-_{(a_2)}\ ,$$

where t is the transference number of the sodium

TABLE 4.19. MEASURED POTENTIALS FOR ZrF_4 CONCENTRATION CELLS

Temperature (°C)	EMF (v)			
	Cell No. 1*	Cell No. 2*	Cell No. 3*	$E_1 + E_2$
700	0.141	0.120	0.264	0.261
650	0.129	0.113	0.252	0.247
600	0.114	0.113	0.229	0.227
550	0.092	0.108	0.201	0.200

*Cell No. 1: c_1 = 41.8 mole % ZrF_4; c_1^1 = 50.0 mole % ZrF_4

Cell No. 2: c_1 = 36.0 mole % ZrF_4; c_1^1 = 41.8 mole % ZrF_4

Cell No. 3: c_1 = 36.0 mole % ZrF_4; c_1^1 = 50.0 mole % ZrF_4

ion. The total cell reaction is

$$ZrF_{4(a_1^1)} + 4t\ NaF_{(a_2)} \longrightarrow ZrF_{4(a_1)} + 4t\ NaF_{(a_2^1)} .$$

The electromotive force of the cell may, therefore, be expressed as

$$E = -\frac{RT}{4F} \ln \frac{ZrF_{4(a_1)}}{ZrF_{4(a_1^1)}} \left(\frac{NaF_{(a_2^1)}}{NaF_{(a_2)}} \right)^{4t} .$$

It is reasonable to assume that the fluoride ion in such a system is rather completely complexed by the ZrF_4 to form complex ions of the type ZrF_5^-, ZrF_6^{--}, etc. Since current transported by such large ions should be very small compared with that carried by small simple ions, it seems likely that the transport number of Na^+ is near unity.

The vapor pressure of ZrF_4 over NaF-ZrF_4 melts has been measured with considerable precision. If the ratios of vapor pressures for ZrF_4 at the concentrations shown above are assumed to represent the activity ratios of ZrF_4 and if t is assumed to be unity, the activity ratios for NaF in the various combinations can be obtained directly from the emf equation. The results of such calculations are shown in Table 4.20.

From the calculations, it appears that the rapid and uniform addition of ZrF_4 to molten Na_2ZrF_6 reduces the activity of the NaF until the 50-50 mole % composition is reached; further additions of ZrF_4 do not alter the $NaZrF_5$ complex.

TABLE 4.20. ACTIVITY RATIOS FOR NaF IN NaF-ZrF_4 MIXTURES AT 650°C

	$\frac{NaF_{(c_2)}}{NaF_{(c_2^1)}}$	$\frac{NaF_{(a_2)}}{NaF_{(a_2^1)}}$	$\frac{\gamma NaF_{(a_2)}}{\gamma NaF_{(a_2^1)}}$
Cell No. 2	64.0/58.2	2.4	2.1
Cell No. 1	58.2/50	3.4	3.0
Cell No. 4*	50/44.8	1.1	1.0

*Cell No. 4: c_1 = 50.0 mole % ZrF_4; c_1^1 = 55.2 mole % ZrF_4; $E_{650°C}$ = 0.010 v.

Cells with Structural Metal Fluorides. Cells consisting of metallic nickel electrodes immersed in solutions of NiF_2 in molten NaF-ZrF_4 mixtures showed potentials of 1 to 3 mv when the NiF_2 concentrations in the half cells were varied; the NiF_2 concentrations were, in all cases, sufficiently high to afford a saturated solution. Similar Fe/FeF_2 cells in which the half cells contained equal concentrations of FeF_2 showed potentials of 1 to 10 mv. When the half cells contained differing FeF_2 concentrations but more FeF_2 than that required for saturation, potentials were obtained which varied from about 40 mv at 550°C to 10 mv at 700°C. Exact voltages varied from cell to cell, but the decrease in emf with temperature seemed quite reproducible.

A cell of the type

$$\mathrm{Fe}\Big/\begin{matrix}\mathrm{FeF_3}(c_1)\\ \mathrm{FeF_2}(c_2)\end{matrix},\ \mathrm{NaF\text{-}ZrF_4}\Big/\begin{matrix}\mathrm{ZrO_2}\\ \mathrm{NaF\text{-}ZrF_4}\end{matrix}\Big/\mathrm{NaF\text{-}ZrF_4},\ \begin{matrix}\mathrm{FeF_3}(c_1^1)\\ \mathrm{FeF_2}(c_2^1)\end{matrix}\Big/\mathrm{Fe}\ ,$$

where

$$c_1 = c_1^1 \text{ and } c_2 = c_2^1\ ,$$

resulted in emf's of 1 mv. It was believed that all the FeF_3 would be reduced to FeF_2 by the iron electrodes and that as a result a pure Fe/FeF_2 cell with etched Fe electrodes would be obtained. However, analysis of the final melt proved that most of the FeF_3 was still present; it is not likely that equilibrium was established.

Cells of the type

$$\mathrm{Zr}\Big/\mathrm{ZrF}_{4(c_1)},\ \mathrm{NaF}\Big/\begin{matrix}\mathrm{ZrO_2}\\ \mathrm{NaF\text{-}ZrF_4}\end{matrix}\Big/\mathrm{NaF\text{-}ZrF_4},\ \mathrm{NiF}_{2\left(\begin{smallmatrix}c_2\\ \text{sat'd}\end{smallmatrix}\right)}\Big/\mathrm{Ni}$$

have yielded moderately reproducible potentials at various temperatures. In these cells, $c_1 = 47$ mole % and $c_2 = 5.0$ to 5.6 wt %. From the data obtained, E° is estimated to be 1.41 to 1.42 v by assuming that the saturating phase is the pure fluoride and that the activity of the ZrF_4 can be established, as before, from vapor pressure data. From this E° value, it appears that $\Delta F^\circ = -131$ kcal for the reaction

$$\mathrm{Zr^\circ + 2NiF_2 \longrightarrow ZrF_4 + 2Ni^\circ}$$

This is in excellent agreement with $\Delta F^\circ = -127$ kcal based on the thermochemical estimates of Brewer.[23]

There is some evidence, however, from petrographic and x-ray examination of the cooled melts which indicates that the saturating phase is not NiF_2 but is some, as yet unidentified, complex fluoride. The data presented would seem to indicate that this complex fluoride is quite unstable.

Experimental measurements of cells of the type

$$\mathrm{Fe}\Big/\mathrm{FeF}_{2\left(\begin{smallmatrix}c_1\\ \text{sat'd}\end{smallmatrix}\right)},\ \mathrm{NaF\text{-}ZrF_4}\Big/\begin{matrix}\mathrm{ZrO_2}\\ \mathrm{NaF\text{-}ZrF_4}\end{matrix}\Big/\mathrm{NaF\text{-}ZrF_4},\ \mathrm{NiF}_{2\left(\begin{smallmatrix}c_2\\ \text{sat'd}\end{smallmatrix}\right)}\Big/\mathrm{Ni}\ ,$$

where

$c_1 = 7.0$ to 7.3 wt % ,

$c_2 = 5.1$ to 5.4 wt % ,

have yielded the data shown in Table 4.21.

The thermochemical estimates of Brewer suggest that E° for this cell should have a nearly constant value of 0.25 v over the 550 to 700°C temperature interval. Again, examination of the solidified melts showed that isomorphous complex compounds of NiF_2 and FeF_2 with the solvent occurred. If the junction potential of this cell can be assumed to be negligible, then at 650°C,

$$0.42\ \mathrm{v} = 0.25\ \mathrm{v} - \frac{RT}{2F}\ln\frac{a_{\mathrm{FeF_2}}}{a_{\mathrm{NiF_2}}}$$

and

$$\frac{a_{\mathrm{FeF_2}}}{a_{\mathrm{NiF_2}}} = \sim 10^{-2}\ .$$

Since the saturation solubility of FeF_2 is nearly twice that of NiF_2 at this temperature and since the fluoride ion activity should be similar in the two solutions, it appears that the activity coefficient for Ni^{++} is higher by 200-fold than that for

---

[23] L. Brewer *et al.*, p 107 and 110 in *Chemistry and Metallurgy of Miscellaneous Materials: Thermodynamics* (ed. by L. L. Quill), McGraw-Hill, New York, 1950.

Fe^{++}. It appears also that the solvent-Fe^{++} complex is much more stable (about 8 kcal/mole) than is the complex involving Ni^{++}.

TABLE 4.21. POTENTIALS OF CELLS $Fe/FeF_2/NiF_2/Ni$ IN NaF-ZrF_4 SOLVENT

Temperature (°C)	EMF (v)	
	Trial No. 1	Trial No. 2
700	0.425	0.423
650	0.421	0.424
600	0.414	0.416
550	0.407	0.409

Vapor Pressures of LiF-ZrF_4 Mixtures

R. E. Moore

Materials Chemistry Division

The determination of the vapor pressures of a series of LiF-ZrF_4 mixtures by the method of Rodebush and Dixon[26] and Fiock and Rodebush[27] was started during the past quarter because the NaF-LiF-ZrF_4 system is being considered as a possible fuel carrier. The vapor pressure work on mixtures containing 33.3 mole % ZrF_4 (Li_2ZrF_6) and 50 mole % ZrF_4 was completed. The data for these two mixtures are given in Table 4.22. The vapor pressure equations, which were obtained from the best straight lines on a log pressure vs reciprocal temperature plot, are, for the 33.3 mole % ZrF_4 mixture,

$$\log P \text{ (mm Hg)} = -(8333/T) + 7.967 \ ,$$

and, for the 50 mole % ZrF_4 mixture,

$$\log P \text{ (mm Hg)} = -(8848/T) + 9.397 \ ,$$

where T is in °K. The heats of vaporization are 38 kcal/mole for the 33.3 mole % ZrF_4 mixture and 41 kcal/mole for the 50 mole % ZrF_4 mixture.

The vapor pressures of the LiF-ZrF_4 mixtures are considerably higher than those of the corresponding NaF-ZrF_4 mixtures. For example, the vapor pressures of the 50% LiF mixture are 50 to 100% higher than those of the 50% NaF mixture. It might have been expected that the small lithium ion would produce compounds in the fused state which were more stable than the sodium compounds. One possible explanation for the higher vapor pressures is that LiF_2^- ions may exist in the melt. If the lithium ion has a marked tendency

TABLE 4.22. THE VAPOR PRESSURE OF TWO LiF-ZrF_4 MIXTURES

Temperature (°C)	Observed Pressure (mm Hg)	Calculated Pressure (mm Hg)
	LiF-ZrF_4 (66.7-33.3 mole %)	
944	13	13
992	22	24
1014	30	31
1059	54	52
1112	89	89
1178	166	168
	LiF-ZrF_4 (50-50 mole %)	
809	16	16
812	17	17
830	23	24
849	33	32
897	67	62
941	125	120
977	209	208

---

[26] W. H. Rodebush and A. L. Dixon, *Phys. Rev.* 26, 851 (1925).

[27] E. F. Fiock and W. H. Rodebush, *J. Am. Chem. Soc.* 48, 2522 (1926).

to attract fluoride ions to produce such complexes, fewer fluoride ions would be available for the formation of complex ions with ZrF_4.

Solubility of Xenon in Fused Salts

R. F. Newton
Research Director's Department

The previously described procedures[28] for determining the solubility of xenon in fused salts were modified so that the source of the spread of values obtained could be ascertained. Long exposure without stirring gave essentially the same results and thus indicated that the supposition of the production of fine gas bubbles by stirring, which bubbles were then transferred to the stripper along with the liquid, was unfounded. However, long continued cycling of helium through the melt, without recent exposure to xenon, gave material which was caught in the liquid nitrogen trap and was read on the McLeod gage as xenon. This material may have been SiF_4 from the reaction of the glass with the HF liberated from the NaF-KF-LiF (11.5-42-46.5 mole %). Means for eliminating this material or correcting for it are now under study.

X-Ray Diffraction Study of Liquids

P. C. Sharrah
H. A. Levy
R. D. Ellison
M. D. Danford
P. Agron
M. A. Bredig
Chemistry Division

The construction of an x-ray diffractometer designed specifically for studies on the structure of liquids was completed recently. The diffraction pattern from the horizontal surface of the liquid sample is obtained with a divergent beam technique similar to the Bragg-Brentano flat-sample system frequently used on powder samples. The instrument provides for simultaneous angular motion of the x-ray tube and the detector on arms moving about a horizontal axis lying in the liquid surface. This makes it possible to work with liquids with a free surface where sample holder absorption and scattering are eliminated. A small furnace for work with molten materials is included in the design. Monochromatic x radiation, essential to good work with liquids, is obtained through the use of a bent-crystal monochromator mounted on the arm with the detector. A scintillation detector and a molybdenum target x-ray tube are in use in the system now undergoing final testing.

High-Temperature X-Ray Spectrometer Studies

G. D. White
Metallurgy Division
T. N. McVay, Consultant

A high-temperature attachment for an x-ray spectrometer is being used to help clarify some of the phase relationships in fuel systems of interest. The apparatus consists of a water-cooled aluminum cylinder with a vacuum-tight lid which fits the open end of the cylinder and a projecting rod on the closed end by which the attachment is fitted into the goniometer. The sample holder, tantalum heating element, reflector, and thermocouple leads are all mounted on the lid, which also contains an aperture for pumping a vacuum. Inserted around the center of the cylinder is a beryllium window through which the x rays pass. When assembled, the attachment can be pumped down to a vacuum of less than 1 μ by using a Welch pump and a small diffusion pump.

Initially, the attachment was aligned by using a ThO_2 sample. The bracket which holds the sample can be rotated and can be shifted vertically or horizontally. It is held in position by three radial set screws. By manipulating these set screws, the ThO_2 sample was put in a position where one of its stronger x-ray peaks was at the proper angle and had maximum intensity. Thus far the alignment has remained true, although samples have been x-rayed almost daily for the past three months.

In order for the attachment to be used most effectively, the sample to be studied must give an x-ray diffraction pattern with fairly intense peaks, the diffraction patterns of the polymorphs must be considerably different, and the inversions or phase changes must be fairly rapid, especially if the sample being studied oxidizes readily.

The sample to be x-rayed is ground to a powder and loaded into a nickel sample holder with space left for expansion. After the sample holder has been mounted in the bracket and the thermocouple bead has been placed on the surface of the powder, the lid is fastened to the cylinder. The system is pumped down overnight, and the x-ray diffraction patterns are obtained the next day.

---

[28] R. F. Newton, *ANP Quar. Prog. Rep. Dec. 10, 1954*, ORNL-1816, p 72.

Room-temperature patterns are always obtained before and after heating to check on the alignment and flatness of the surface of the sample.

To date, work has been done on compositions in the systems: NaF-ZrF_4, LiF-ZrF_4, and NaF-BeF_2. Only the study of the composition 2NaF·BeF_2 is discussed here. Two samples of Na_2BeF_4 were found to be different optically. One of the samples contained twinned monoclinic crystals, whereas the parallel extinction of crystals in the other indicated an orthorhombic structure. Room-temperature x-ray diffraction patterns of the samples were very similar, the only difference being in the intensities of the peaks.

High-temperature x-ray diffraction patterns were also obtained on the samples. When heated, both samples showed inversions at 236 and 336°C, and when cooled, showed inversions at 310 and below 185°C. The temperature could not be maintained below 185°C, and therefore the lower inversion temperature could not be obtained.

The intensity and *d* values at room temperature, 300, and 340°C are

At Room Temperature		At 300°C		At 340°C	
d	*I*	*d*	*I*	*d*	*I*
				Sample 1	
4.18	14	2.71	35	2.78	7
3.90	6	2.65	33	2.65	27
3.67	10	2.34	30	2.18	27
2.92	35	2.25	7	2.11	8
2.68	10	2.21	22	Sample 2	
2.62	20	2.17	22	2.96	12
2.43	26	2.11	13	2.78	7
2.37	32	2.02	15	2.73	9
2.23	9			2.65	27
2.11	17			2.18	27
1.84	18			2.11	8

These data suggest that the samples are actually a mixture of two phases: a room-temperature phase and the 300°C form. There are several *d* values at room temperature which are present at 300°C if allowance is made for expansion of *d* values as the temperature is increased. Therefore, the difference in intensity values of the two samples at room temperature could be due to a difference in ratios of the two phases in the samples.

5. CORROSION RESEARCH

W. D. Manly G. M. Adamson
Metallurgy Division

W. R. Grimes F. Kertesz
Materials Chemistry Division

Several Inconel forced-circulation loops that were operated with fluoride mixtures and with sodium as the circulated fluids were examined. Results of corrosion and mass transfer under dynamic conditions were obtained. Data were obtained on an alkali-metal base fluoride mixture containing UF_4 and on ZrF_4-base mixtures with UF_4 and with combinations of UF_4 and UF_3 circulated at low (1,000) and high (15,000) Reynolds numbers at a maximum fluoride mixture temperature of 1500°F.

Further thermal-convection loop studies were made of alkali-metal base fluoride mixtures with UF_3 and UF_4 and ZrF_4-base mixtures with UF_3 and UF_4 in Inconel. The effects of temperature on mass transfer and of the size and shape of the loop on corrosion were investigated, and an evaluation of the erratic results recently obtained with control loops was made. Several brazing alloys on type 310 stainless steel and "A" nickel were tested in sodium and in a ZrF_4-base fuel mixture in an attempt to find a brazing alloy that has good corrosion resistance to both mediums. Cermets that do not form solid-phase bonds were screened for suitability for use in valves, bearings, and seals exposed to liquid metals and fused fluorides.

Mass transfer of sodium in an Inconel thermal-convection loop and of lithium in a type 347 stainless steel loop was studied, as well as the cleaning of beryllium-Inconel systems with Versene.

In the fundamental corrosion research, further work was done on the investigation of film formation on metals, including tests of oxidation theories, and additional experiments were conducted in the investigation of corrosion and mass transfer of metals by fused sodium hydroxide.

The chemical studies of corrosion include investigations of the corrosion of Inconel by $LiF\text{-}BeF_2$ and by $LiF\text{-}BeF_2\text{-}UF_4$, the effect of $UF_3\text{-}UF_4$ mixtures on corrosion of Inconel by various solvents, and studies of the sodium hydroxide–nickel reaction.

FORCED-CIRCULATION STUDIES

G. M. Adamson R. S. Crouse
Metallurgy Division

Fluoride Mixtures in Inconel

Several forced-circulation loops that were operated by the Experimental Engineering Department at the request of the Metallurgy Division were disassembled and examined. The conditions of operation of these Inconel loops in which fluoride mixtures were circulated are summarized in Table 5.1.

Two of the loops examined (4695-1 and -2) had circulated $NaF\text{-}ZrF_4\text{-}(UF_4 + UF_3)$ (50-46-4 mole %) in which about 2 wt % of the uranium had been converted to U^{3+}. The design of loop 4695-1 was similar to that used previously.[1] Operation of this loop was terminated after 385 hr because of a leak at a heating terminal. Examination showed the maximum attack, which was found in a bend in the first heating leg, to be 12 mils (Fig. 5.1). In a straight portion of the heated section, the maximum attack was to a depth of 9 mils. The depths of attack were thus only slightly less than those found in loops which circulated a similar mixture containing no trivalent uranium; however, the number of voids was reduced by about one-half.

The second loop examined (4695-2) had been fabricated with two straight heating sections connected with a U bend (Fig. 5.2), and it had operated for 887 hr before being terminated because of a pump bearing failure. The maximum attack was to a depth of 8 mils (Fig. 5.3), and it was found in the first heated section. A temperature study of this loop showed that the maximum wall temperature occurred in the first heated section but that the maximum fluoride mixture temperature occurred in the second heated section. The loop was assembled so that no heating occurred in the bend, and, upon examination, no attack was found in this area. A thin, as yet unidentified, deposit was found in the final portion of the cold leg. For comparative purposes, a portion of this same batch

---

[1] L. A. Mann, W. B. McDonald, and W. C. Tunnell, *ANP Quar. Prog. Rep. Dec. 10, 1954*, ORNL-1816, Fig. 3.4, p 45.

TABLE 5.1. CONDITIONS OF OPERATION OF FORCED-CIRCULATION INCONEL LOOPS

Operating Conditions	Loop Number				
	4930-A	4935-1	4695-1	4695-2	4695-3
Fluoride mixture circulated	NaF-ZrF_4-UF_4 (53.5-40-6.5 mole %)	NaF-ZrF_4-UF_4 (53.5-40-6.5 mole %)	NaF-ZrF_4 – (UF_4 + UF_3) (50-46-4 mole %, 2.2 wt % of U as U^{3+})	NaF-ZrF_4 – (UF_4 + UF_3) (50-46-4 mole %, 1.7 wt % of U as U^{3+})	NaF-KF-LiF + UF_4 (11.5-42-46.5 mole % plus 12.3 wt % UF_4)
Operating time (hr)	1000	1000	385	887	630
Preliminary operating period at isothermal temperature (hr)	24		50	71	43
Maximum fluoride mixture temperature (°F)	1500	1500	1500	1500	1500
Approximate maximum tube wall temperature (°F)	>1710	1680	>1735	>1670	>1640
Temperature gradient of fluoride mixture (°F)	300	300	300	200	300
Reynolds number	1000	1000	10,000	15,000	10,000
Velocity (fps)	0.6	0.7	6.7	10.2	3.3
Length of heated tube (ft)		23.5			
First section	3.5		5	5	5
Second section	3.5		7	7	7
Total length of loop (ft)	14	48	50	50.5	50.5
Method of heating	Electrical resistance	Gas	Electrical resistance	Electrical resistance	Electrical resistance
Shape of heated section	Coiled	Coiled	Coiled	Straight	Straight
Ratio of hot-leg surface to loop volume ($in.^2/in.^3$)	1.6	3.1	1.5	1.5	1.5
Cause of termination	Scheduled	Scheduled	Leak	Pump bearing failure	Leak
Maximum depth of attack (mils)	25	11	12	8	35

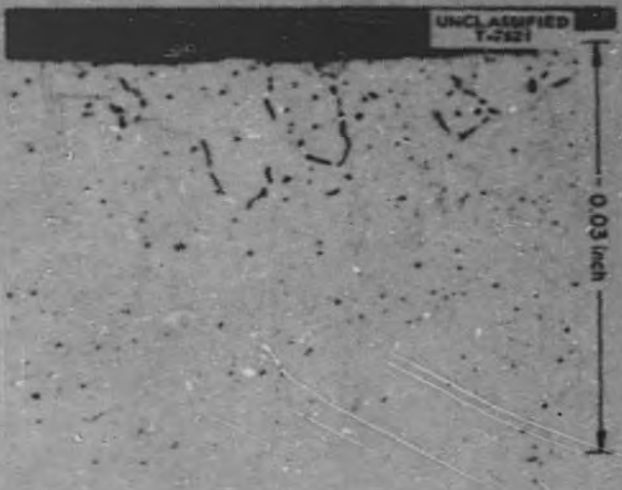

Fig. 5.1. Maximum Attack Found in Inconel Loop 4695-1 After Circulating NaF-ZrF_4-(UF_4 + UF_3) (50-46-4 mole %, 2.2 wt % U as U^{3+}) for 385 hr at a Maximum Fluoride Mixture Temperature of 1500°F and a Reynolds Number of 10,000. 100X. Reduced 16%.

of fluoride mixture was circulated for 1000 hr in an Inconel thermal-convection loop. The hot leg of the thermal-convection loop was attacked to a depth of 10 mils, whereas a depth of 13 to 15 mils was normally found in control thermal-convection loops in which the fluoride mixture contained UF_4 but no trivalent uranium. However, thermal-convection loops operated previously in which trivalent uranium was obtained by adding zirconium hydride were attacked to a depth of only 3 mils.

The deepest attack found in any forced-circulation loop was that found in loop 4695-3. This loop circulated the alkali-metal base mixture NaF-KF-LiF (11.5-42-46.5 mole %) with 12.3 wt % uranium added as UF_4. The maximum attack in this loop (designed as shown in Fig. 5.2) occurred in the second heated section as a very heavy intergranular concentration of subsurface voids to a depth of 35 mils (Fig. 5.4). The temperature pattern of this loop showed that, because of the better heat transfer properties of the alkali-metal base mixtures, both the maximum wall and fluoride mixture temperatures occurred in the second heated section. A deposit that was up to 65 mils thick was found on the lower inside surface of one area in the cold portion of the loop. In other areas, similar deposits that were up to 5 mils thick were found. A spectrographic analysis of the deposit showed the following: >5 wt % Cr, 0.5 wt % Fe, >10 wt % K, 3 wt % Li, 2 wt % Na, 0.5 wt % Ni, >10 wt % U (balance unidentified). Another portion of this batch of fluoride mixture was circulated for 500 hr in an Inconel thermal-convection loop. The maximum attack was to a depth of 42 mils, and was unusual in that it was found only around one third of the circumference of a sample of the hot leg. In the remainder of the hot leg the attack was to a depth of 5 mils. A cold-leg deposit that was 0.3 mil thick was found.

Two other forced-circulation loops that had completed the scheduled 1000 hr of operation were also examined. These loops had circulated NaF-ZrF_4-UF_4 (53.5-40-6.5 mole %). One of these loops (4930-A) was heated by the electrical resistance of a coil,[1] and the other (4935-1) was heated in a gas furnace. These loops were similar except that the gas-fired loop had a heated length of 23.5 ft, and the heated length of the other loop was only 7 ft. To transfer the same amount of power, it was obviously necessary to use a much higher wall temperature for the short loop. The maximum attack in the short loop (4930-A) appeared as a heavy intergranular concentration of subsurface voids to a depth of 25 mils and was found in a bend in the second leg of the heated coil. The maximum attack in a straight section was 21 mils. The attack was both deeper and heavier than that found in loops operated previously with this fluoride mixture, even when much higher velocities and Reynolds numbers were used. Examination of loop 4935-1 showed the maximum attack to be to a depth of 11 mils; however, this attack was moderate in intensity and was found for only a short length at the hottest end of the coil. In this loop no differences were found on opposite sides of the bends. The original purpose of these loops was to compare gas and electric heating; however, because of the differences in heater length, it will be necessary to repeat the tests with identical loops operated under similar conditions.

From the results obtained with these loops and from those reported previously,[2] it is apparent that corrosion and mass transfer in these systems are not so serious as had been feared. It also appears

---

[2] G. M. Adamson and R. S. Crouse, *ANP Quar. Prog. Rep. Mar. 10, 1955*, ORNL-1864, p 75.

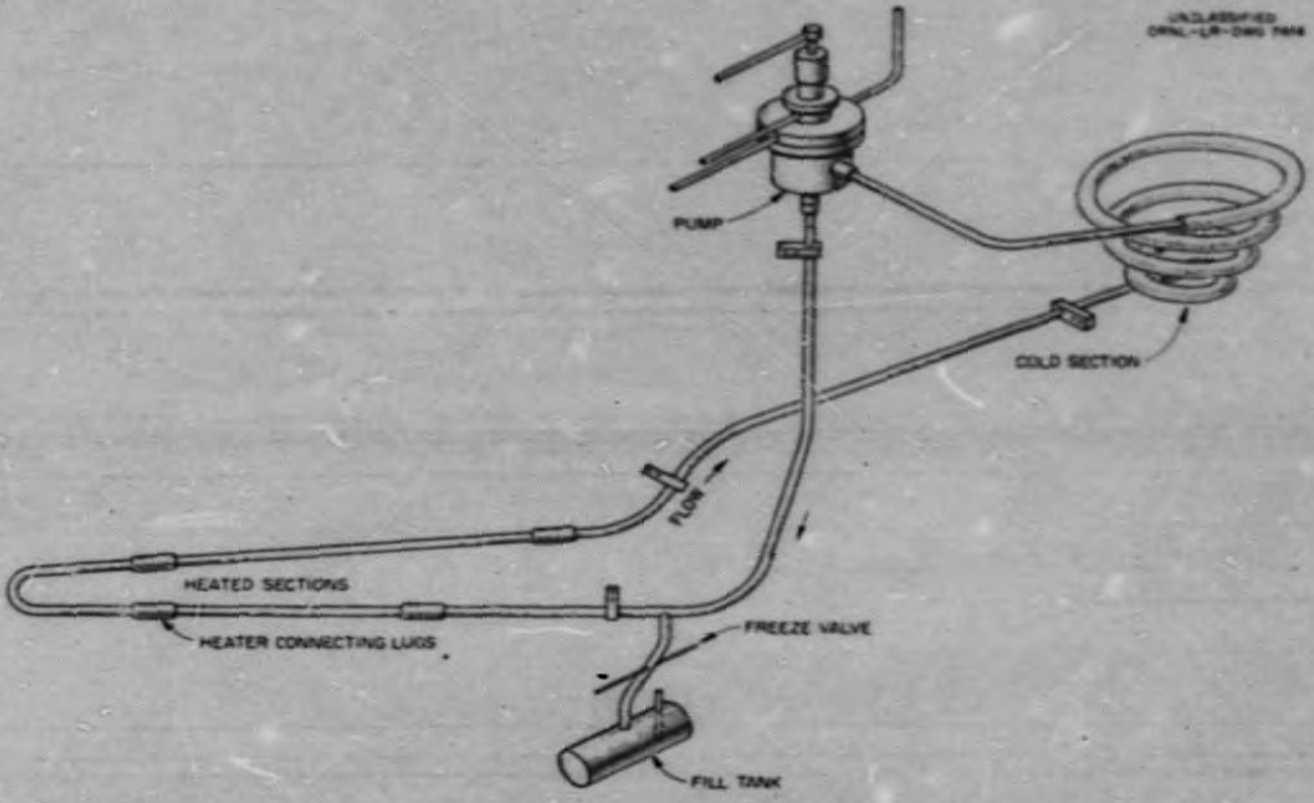

Fig. 5.2. Schematic Diagram of Forced-Circulation Loop with Straight Heated Sections.

that reducing the tube wall temperature in these experiments would result in a reduction in depth of attack. The cold-leg layer found in loop 4695-2 must be investigated further.

The depths of attack found in the forced-circulation loops are not much, if any, greater than those found in the low-velocity thermal-convection loops. Thus velocity and Reynolds number appear to be only minor variables. This conclusion is confirmed by the deep attack found in the low-velocity forced-circulation loop 4930-A. The data obtained from the thermal-convection loops should therefore be applicable to forced-circulation systems.

The most important variable is the maximum tube wall temperature, or, more exactly, the temperature of the reaction interface. This is shown by the deepest attack occurring in areas of maximum wall temperature rather than where the maximum bulk fluoride mixture temperature occurred. Additional evidence is afforded by the deepest attack in a loop having occurred in the hot spots on the inside of bends.[2]

The addition of UF_3 to the ZrF_4-base mixtures reduces the attack, and even though the low UF_3 concentrations used in these forced-circulation loops did not reduce the attack as much as had been hoped, it appears that higher concentrations would result in a greater decrease in attack. Unless the addition of UF_3 can also reduce the attack and mass transfer found with alkali-metal base mixtures without disproportionation of the UF_3 and the formation of deposits, it appears that such mixtures will not be useful in large, Inconel dynamic systems.

Sodium in Inconel

An Inconel forced-circulation loop (4689-4) was examined in which sodium was circulated at a maximum temperature of 1500°F for 1000 hr, with

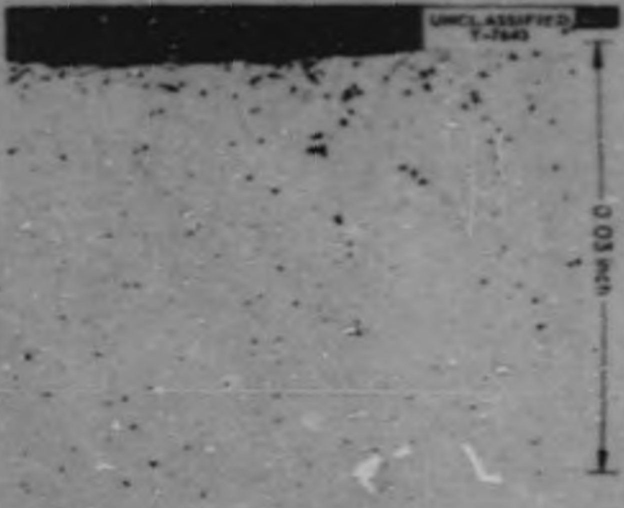

Fig. 5.3. Maximum Attack Found in Inconel Loop 4695-2 After Circulating NaF-ZrF$_4$-(UF$_4$ + UF$_3$) (50-46-4 mole %, 1.7 wt % U as U^{3+}) for 887 hr at a Maximum Fluoride Mixture Temperature of 1500°F and a Reynolds Number of 15,000. 100X. Reduced 11%.

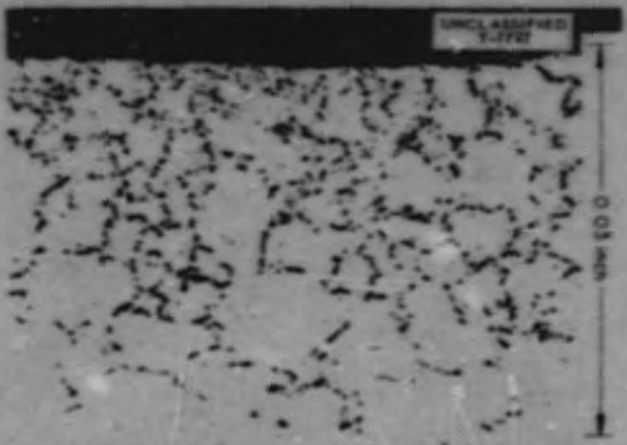

Fig. 5.4. Maximum Attack Found in Inconel Loop 4695-3 After Circulating NaF-KF-LiF + UF$_4$ (11.5-42-46.5 mole % plus 12.3 wt % UF$_4$) for 630 hr at a Maximum Fluoride Mixture Temperature of 1500°F and a Reynolds Number of 10,000. 100X. Reduced 20%.

a 300°F temperature drop and a Reynolds number of greater than 50,000. The loop had the configuration shown in Fig. 5.5. A heavy layer of dendritic metal crystals was found in all sections of the economizer and to a lesser extent in the cold loop, as shown in Fig. 5.6. The crystals were shown by chemical analysis to be 89.6% Ni and 8.6% Cr and to contain 50 ppm Fe. The layer found in the cold end of the economizer was shown by metallographic examination to be 26 mils thick. The hot leg showed intergranular attack to a depth of 2.5 mils. Efforts were made to obtain oxygen analyses on both the original and the drained sodium, but both values are questionable. From other work, it appears that the original sodium contained about 50 ppm oxygen.

A second, similar loop (4951-1) was operated for 480 hr with a 200°F temperature drop, and the results confirmed those reported above. The mass transfer found in this loop is shown in Fig. 5.7. The maximum thickness of the deposit found metallographically was 11 mils. The hot leg in this loop also showed intergranular attack to a depth of 2.5 mils.

Two additional loops were operated with portions of the cold legs constructed from type 316 stainless steel. Loop 4689-6 had a type 316 stainless steel economizer and cold leg, while loop 4689-5 had only a type 316 stainless steel cold leg. Both these loops also showed mass transfer, but not so much as was found in loop 4689-4. The maximum deposit thickness in loop 4689-5 was 15 mils and in loop 4689-6 it was 12 mils. The hot legs showed similar intergranular attack to a depth of 2.5 mils in loop 4689-5 and 1.5 mils in loop 4689-6. These data indicate that a type 316 stainless steel cold leg reduces the mass transfer slightly, but further study of the variables in the process is necessary. Additional loops are being operated under controlled conditions in which the effects of oxygen concentration of the sodium, the use of a cold trap, the use of a lower maximum sodium temperature, and the use of an all-stainless-steel system are being investigated.

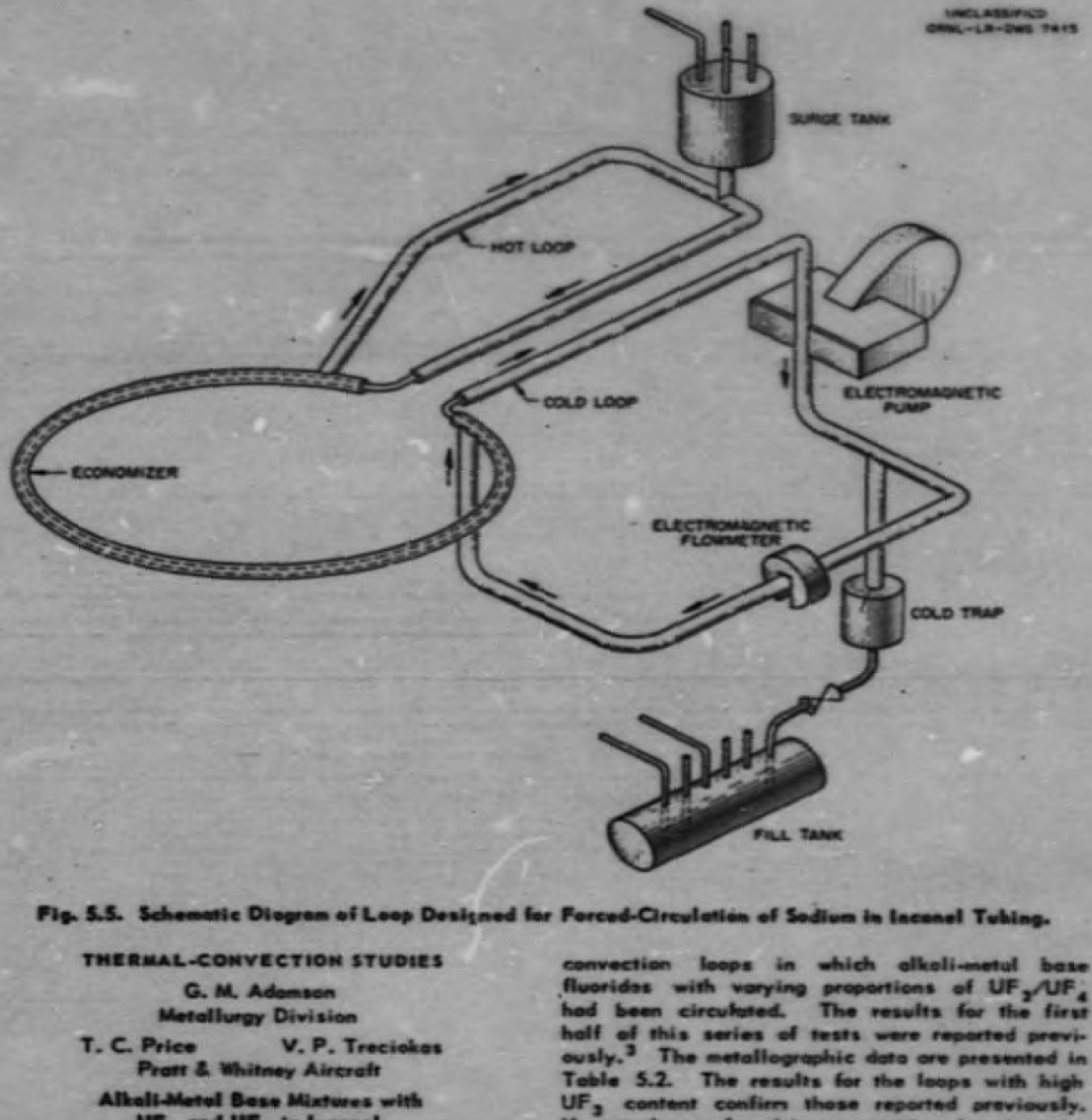

Fig. 5.5. Schematic Diagram of Loop Designed for Forced-Circulation of Sodium in Inconel Tubing.

THERMAL-CONVECTION STUDIES

G. M. Adamson
Metallurgy Division

T. C. Price V. P. Treciokas
Pratt & Whitney Aircraft

Alkali-Metal Base Mixtures with UF_3 and UF_4 in Inconel

The results of metallographic examinations have been received for the remaining Inconel thermal-convection loops in which alkali-metal base fluorides with varying proportions of UF_3/UF_4 had been circulated. The results for the first half of this series of tests were reported previously.[3] The metallographic data are presented in Table 5.2. The results for the loops with high UF_3 content confirm those reported previously. No attack was found in any section, but deposits

---

[3] G. M. Adamson and V. P. Treciokas, *ANP Quar. Prog. Rep. Mar. 10, 1955*, ORNL-1864, p 70.

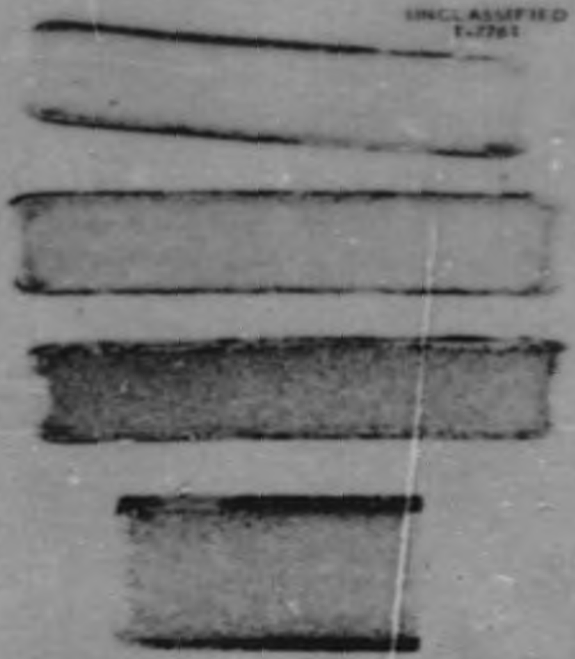

Fig. 5.6. Sections from Cold Leg and Economizer of Forced-Circulation Inconel Loop 4629-4 After Circulating Sodium for 1000 hr at a Maximum Sodium Temperature of 1500°F and a Temperature Drop of 300°F.

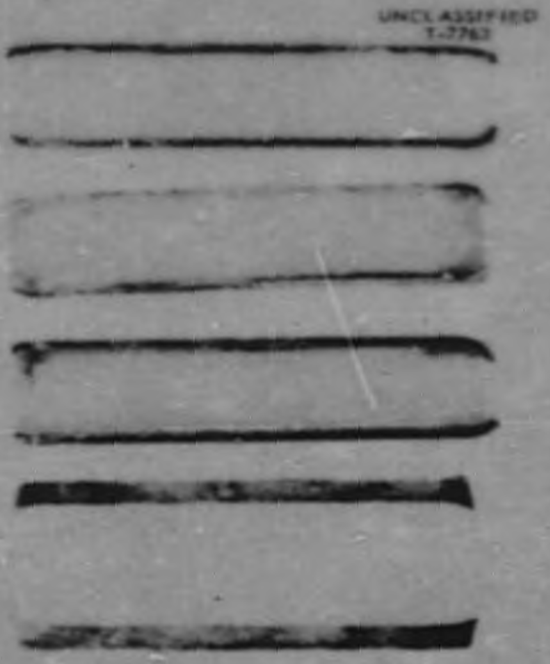

Fig. 5.7. Sections from Cold Portions of Forced-Circulation Inconel Loop 4951-1 After Circulating Sodium for 480 hr at a Maximum Sodium Temperature of 1500°F and a Temperature Drop of 200°F.

TABLE 5.2. RESULTS OF METALLOGRAPHIC EXAMINATION OF INCONEL THERMAL-CONVECTION LOOPS AFTER CIRCULATING NaF-KF-LiF (11.5-42-46.5 mole %) CONTAINING UF_3 AND UF_4

Loop No.	Time of Operation (hr)	Initial Uranium Content (wt %)	U^{3+} Content (wt %)		Maximum Attack (mils)	Metallographic Notes
			Fill	Final		
591	500	11.5	1.7	0.65	2	Thin cold-leg deposit
626	500	11.2	1.5	0.8	1.5	Cold-leg deposit 0.3 mil thick
594	1000	12.6	2.0	0.6 to 0.7	2	Cold-leg deposit 0.5 mil thick
625	546	13.2	3.0	0.9	0	Layer to 1 mil thick in all sections
593	1000	13.8	5.6	0.9	0	Layer to 1 mil thick in all sections
592	1000	10.9	5.2	0.9	0	Layer to 1 mil thick in all sections

were visible in both the hot and cold legs. The trivalent uranium content had been almost completely lost by disproportionation in all loops.

The results for the three loops with low UF_3 contents are encouraging. In loop 594, after 1000 hr, the hot-leg attack was only to a depth of 2 mils, and there was no evidence of a hot-leg layer (Fig. 5.8). The cold legs of these loops showed thin, as yet unidentified, layers. Even in these loops it seems likely that some disproportionation occurred, because one-half the original U^{3+} content was lost.

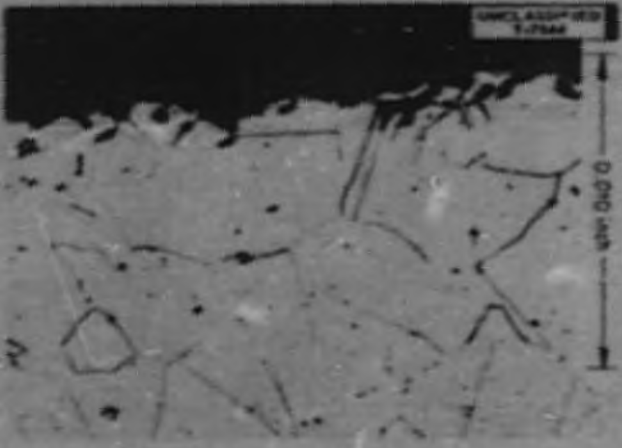

Fig. 5.8. Hot-Leg Attack of Inconel Thermal-Convection Loop After Circulating NaF-KF-LiF (11.5-42-46.5 mole %) Containing UF_3 and UF_4 for 1000 hr at a Hot-Leg Temperature of 1500°F. 250X. Reduced 21%.

Chemical analyses of the fluoride mixtures before and after operation of the loops are presented in Table 5.3. The data show that the impurities react differently in the alkali-metal base mixtures than they do in the ZrF_4-base mixtures. The chromium content appears to decrease slightly, whereas the nickel content shows a small increase.

Zirconium Fluoride Base Mixtures with UF_3 and UF_4 in Inconel

A group of Inconel thermal-convection loops was operated at a hot-leg temperature of 1500°F with the ZrF_4-base mixture NaF-ZrF_4-UF_4 (50-46-4 mole %) containing varying amounts of the UF_4 converted to UF_3. Metallographic results have been received on only the first half of this series of tests and are reported in Table 5.4. The chemical results for these tests are given in Table 5.5. While the depths of attack found were slightly lower than the 11 mils now being found after 500 hr in control loops, the results are disappointing in that, in previous thermal-convection loops operated with a mixture containing UF_3 obtained by the reduction of UF_4 with ZrH_2, attacks as low as 3 mils were found. As in the forced-circulation loops, the presence of UF_3 reduces the amount and intensity of the attack more than it does the depth. In the loops operated previously, the UF_3 content was not known and may have been slightly higher. It should be noted that the chromium content was

TABLE 5.3. RESULTS OF CHEMICAL ANALYSES OF ALKALI-METAL BASE MIXTURES BEFORE AND AFTER CIRCULATION IN INCONEL LOOPS

Loop No.	Uranium (wt %)		Nickel (ppm)		Chromium (ppm)		Iron (ppm)	
	Before	After	Before	After	Before	After	Before	After
591	11.5	11.5	65	100	40	30	140	75
626	11.2	11.2	10	110	40	15 to 50	120	65
594	12.6	10.7	60	110	115	15 to ?	70	75
625	13.2	12.5	60		40	40	140	
593	13.8	10.0	45	85	75	15	80	80
592	10.9	10.5	110	95	55	20 to 80	165	70

TABLE 5.4. RESULTS OF METALLOGRAPHIC EXAMINATION OF INCONEL THERMAL-CONVECTION LOOPS AFTER CIRCULATING ZrF_4-BASE MIXTURES CONTAINING UF_3 AND UF_4

Loop No.	Operating Time (hr)	Maximum Attack (mils)	Metallographic Notes	
			Hot-Leg Appearance	Cold-Leg Appearance
633	500	10	Moderate to heavy general attack and intergranular voids	No attack or deposit
634	500	8	Moderate to heavy intergranular voids	Few voids to a depth of 1 mil with deposit covering voids
683	500	7	Moderate intergranular voids	Few voids to a depth of 1 mil
635	1000	7	Moderate general attack and intergranular voids	Few voids to a depth of 0.5 mil and some thin deposit

TABLE 5.5. RESULTS OF CHEMICAL ANALYSES OF ZrF_4-BASE MIXTURES CONTAINING UF_3 AND UF_4 BEFORE AND AFTER CIRCULATING IN INCONEL THERMAL-CONVECTION LOOPS

Loop No.	U^{3+} (wt %)		Total U (wt %)		Nickel (ppm)		Chromium (ppm)		Iron (ppm)	
	Before	After*	Before	After	Before	After	Before	After	Before	After
633	1.37	0.7	11.8	11.4	25	15	100	570	65	50
634	1.28	0.9	8.8	8.9	35	20	65	300	40	70
683	1.43	0.8	9.0	8.5	25	25	140	230	25	30
635	1.98	0.7	8.9	9.7	60	10	100	225	80	40

*These values showed considerable variation and it was difficult to estimate an average; the hot-leg value was consistently lower than the cold-leg value.

lower than normal in three of these loops after circulation. Additional loops in this series are still in operation.

Effect of Temperature on Mass Transfer

A group of Inconel loops was operated with NaF-ZrF_4-UF_4 (53.5-40-6.5 mole %) for 1500 hr at various hot-leg temperatures in order to determine the effect of temperature on mass transfer. The data obtained in these experiments are tabulated in Table 5.6. It is not completely understood why attack is deeper at 1200°F than at 1350°F, but this effect has been noted in previous tests and appears to be real. The remaining loops show a definite increase in depth of attack with increasing hot-leg temperature. In loops operated previously under similar conditions for 500 hr, no effect of temperature on the depth of attack was found. Since the mass transfer effect is masked by the effect of impurities and nonequilibrium conditions during the first 500 hr of operation, it may be considered that the increased depths of attack with increased temperatures, in the loops operated for 1500 hr, were caused by mass transfer.

Effect of Loop Size and Shape on Corrosion

A series of Inconel loops was operated with NaF-ZrF_4-UF_4 (50-46-4 mole %) to determine the effect on depth of attack of varying the loop size and shape. These loops all operated for 1000 hr with hot-leg temperatures of 1500°F. The data obtained from these experiments are presented in Table 5.7.

Within the accuracy of the data, it does not appear that varying the length of the horizontal leg is any more effective than varying the vertical leg. For special materials in limited supply, it appears from the data that the loop size may be

TABLE 5.6. EFFECT OF HOT-LEG TEMPERATURE ON MASS TRANSFER IN INCONEL THERMAL-CONVECTION LOOPS CIRCULATING $NaF-ZrF_4-UF_4$ (53.5-40-6.5 mole %)

Operating time: 1500 hr

Loop No.	Hot-Leg Temperature (°F)	ΔT (°F)	Final Chromium Concentration (ppm)	Maximum Attack (mils)	Metallographic Notes	
					Hot-Leg Attack	Cold-Leg Appearance
578	1200	165	610 to 640	8	Heavy with small voids	No visible deposit
579	1350	190	690 to 815	5	Moderate to heavy intergranular voids	No visible deposit
583	1350	195	675 to 775	5	Moderate to heavy intergranular voids	No visible deposit
580	1500	~210	615 to 830	12	Heavy intergranular voids	No visible deposit
584	1500	210	955 to 980	15	Heavy intergranular voids	Very light deposit
585	1600	240	540 to 810	18	Heavy intergranular voids	Metal in cold trap

TABLE 5.7. EFFECT ON CORROSION DEPTH OF VARYING THE SIZE AND SHAPE OF INCONEL THERMAL-CONVECTION LOOPS

Circulated fluid: $NaF-ZrF_4-UF_4$ (50-46-4 mole %)
Operating time: 1000 hr
Hot-leg temperature: 1500°F

Loop No.	Length of Vertical Leg (in.)	Length of Horizontal Leg (in.)	ΔT (°F)	Maximum Depth of Attack (mils)	Final Chromium Content (ppm)	Hot-Leg Attack
601	8	8	143	10	620 to 680	Heavy
606	8	8	145	10	530 to 675	Heavy
598	15	2	172	11	1030 to 1075	Moderate to heavy
603	15	8	188	10*	740 to 965	Heavy
600	26	8	220	16.5	980 to 1040	Heavy
605	26	8	218	16	890 to 915	Heavy
597	15	15	208	10	895 to 1040	Moderate to heavy
602	15	15	195	13	890 to 960	Heavy
599	15	26	195	15	710 to 1030	Moderate to heavy
614**	26	17	245	15	835 to 890	Heavy

*In this loop, a very few boundaries were attacked to a depth of 14 mils.

**Control; standard size, shape, and temperature differential.

reduced to 15 by 15 in., at least for screening experiments. A series of loops of this size will be operated to get a better statistical picture for determining whether all the loops *should* be reduced to this size.

Evaluation of Control Loop Results

A gradual increase in depth of attack of the standard Inconel thermal-convection loops operated with ZrF_4-base mixtures has been noted recently, and difficulty has been experienced in reproducing results. As part of a study of this difficulty, three Inconel loops were filled the same day from the same batch of fluoride mixture and operated for 500 hr in as nearly an identical manner as possible. The data obtained from these experiments are given in Table 5.8. The attack was again deeper than in previously operated standard loops, and the data show no reproducibility. It should also be noted that in each loop some cold-leg attack was found, whereas previously the cold legs appeared to be attack-free.

To determine whether the increase in attack could be caused by a leak during operation or by air blown into the fluoride mixture during filling, an additional series of three loops was operated. In one experiment, 1 liter of air was slowly bubbled through the fluoride mixture in the fill pot before transfer to the loop. In the second experiment, the loop was airtight, but it was operated with the helium atmosphere at atmospheric pressure. In the third, the helium atmosphere was again at atmospheric pressure, and, in addition, a Swagelok connection above the loop was loosened slightly so that there was a slight air leak. The data from these loops are presented in Table 5.9. A fourth, standard loop was operated as a control with the normal helium atmosphere at a pressure of 7 psi.

The data indicate that to get increased attack from contamination during operation would require

TABLE 5.8. RESULTS OF OPERATION OF IDENTICAL INCONEL CONTROL LOOPS

Loop No.	Filling Order	Maximum Attack (mils)	Metallographic Notes		Average Final Chromium Content (ppm)
			Hot-Leg Attack	Cold-Leg Attack	
684	3	11	Moderate to heavy intergranular voids	Light, general, to a depth of 1 mil	850
685	2	14	Moderate to heavy intergranular voids	Very light, general, to a depth of 1 mil	750
686	1	9	Moderate to heavy intergranular voids	Very light, general, to a depth of 1 mil	770

TABLE 5.9. ATTACK IN INCONEL LOOPS AFTER CIRCULATING CONTAMINATED $NaF\text{-}ZrF_4\text{-}UF_4$ (50-46-4 mole %)

Operating time: 500 hr
Hot-leg temperature: 1500°F

Loop No.	Variable	Maximum Attack (mils)	Average Final Chromium Content (ppm)
687	Static helium atmosphere (atmospheric pressure)	10	800
688	Small air leak in riser pipe	21	2000
689	Air bubbled through original fluoride mixture before transfer to loop	9	950
690	Control (7 psi helium pressure)	10	775

both an air leak and a loss of helium pressure, a combination which does not seem likely to occur. It also appears that the small amount of air that could be trapped in a transfer line would be enough to cause difficulty. One other possible source of the increased attack may be the cleaning cycle. Therefore, a group of loops cleaned by various procedures have been operated, but the results are not yet available.

GENERAL CORROSION STUDIES

E. E. Hoffman
W. H. Cook C. F. Leitten, Jr.
Metallurgy Division

Brazing Alloys on Type 310 Stainless Steel and "A" Nickel in Sodium and in Fuel Mixtures

Brazing alloys submitted by the Wall Colmonoy Corporation have been tested in both static sodium and in static NaF-ZrF$_4$-UF$_4$ (53.5-40-6.5 mole %). These tests were conducted in an effort to find a brazing alloy that has good corrosion resistance to both mediums.

The tests were conducted on type 310 stainless steel T-joints brazed with the brazing alloys listed in Table 5.10, which also presents the results of exposure to static sodium at 1500°F for 100 hr. The brazing alloys are listed in order of decreasing corrosion resistance. The results for tests of these alloys in static NaF-ZrF$_4$-UF$_4$ (53.5-40-6.5 mole %) are given in Table 5.11, where, as in Table 5.10, the brazing alloys are listed in order of decreasing corrosion resistance.

A comparison of the results in Tables 5.10 and 5.11 indicates that brazing alloy B-13 (9% Si–2.5% P–88.5% Ni) has the best corrosion resistance to both test mediums. Metallographic examination showed no attack along the surface of the braze fillet when tested in sodium (Fig. 5.9a). The cracks shown in Fig. 5.9a are not the results of corrosion, but rather were caused by the brittleness of the alloy. Similar cracking was observed in many of the brazed T-joints listed in Tables 5.10 and 5.11. Brazing alloy B-13 is shown in Fig. 5.9b after being tested in NaF-ZrF$_4$-UF$_4$ (53.5-40-6.5 mole %) for 100 hr at 1500°F. Surface attack to a depth of 1 mil can be seen along the entire brazed fillet. No cracks can be observed in this joint.

Several conclusions can be drawn from a study of the metallographic notes in Tables 5.10 and 5.11. Brazing alloys containing relatively high percentages of phosphorus appear to be inferior in sodium. However, additions of silicon tend to improve the corrosion resistance. On the other hand, brazing alloys having high percentages of

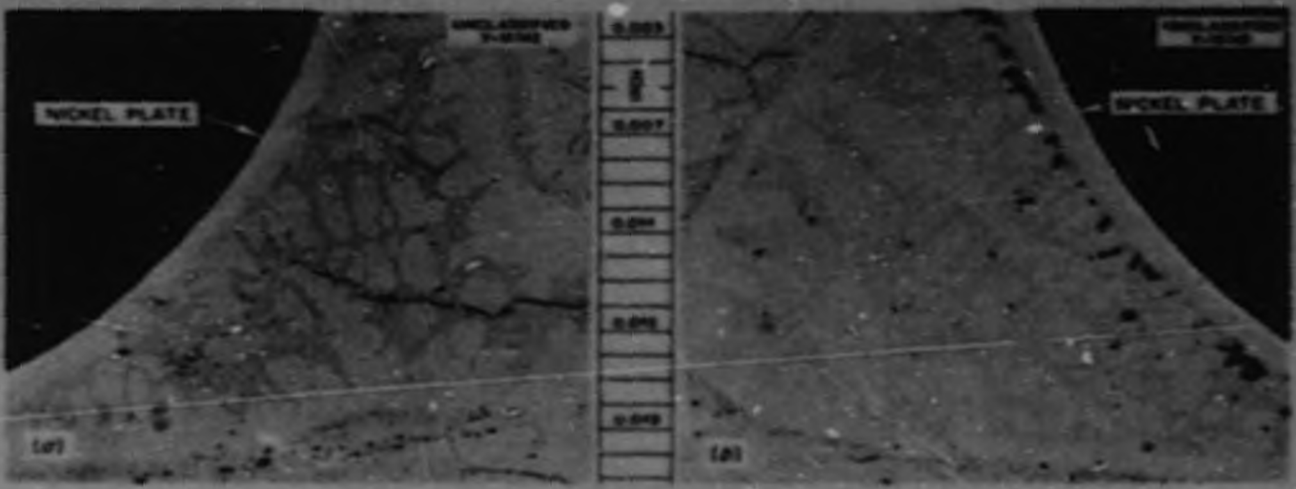

Fig. 5.9. Type 310 Stainless Steel T-Joints Brazed with Brazing Alloy B-13 (9 wt % Si, 2.5 wt % P, 88.5 wt % Ni) After Exposure for 100 hr at 1500°F to (a) Static Sodium and (b) Static NaF-ZrF$_4$-UF$_4$ (53.5-40-6.5 mole %). Etched with aqua regia. 200X. Reduced 26%.

TABLE 5.10. BRAZING ALLOYS ON TYPE 310 STAINLESS STEEL TESTED IN STATIC SODIUM AT 1500°F FOR 100 hr

Alloy Designation*	Alloy Composition (wt %)	Weight Change (g)	Weight Change (%)	Metallographic Notes
B-13	9 Si–2.5 P–88.5 Ni	0	0	No attack along surface of fillet; several cracks in fillet
P-11	10.5 Si–7.5 Mn–82 Ni	−0.0002	−0.018	No attack along surface of fillet; several cracks in fillet
P-12	9 Si–15 Mn–76 Ni	−0.0003	−0.033	No attack along surface of fillet; several cracks in fillet
P-10	16.27 Si–5.9 Mn–77.83 Ni	+0.0004	+0.043	No evidence of attack; several large cracks throughout fillet
P-13	7.5 Si–22.5 Mn–70 Ni	−0.0008	−0.085	Erratic surface attack to a depth of 0.5 mil; several cracks in fillet
B-12	10.5 Si–1.25 P–88.25 Ni	0	0	Erratic surface attack along fillet to a depth of 1 mil
B-14	7.5 Si–3.75 P–88.75 Ni	−0.0001	−0.01	Uniform surface attack along fillet to a depth of 1 mil
P-14	6 Si–30 Mn–64 Ni	−0.0002	−0.022	Erratic surface attack to a depth of 1 mil; large cracks throughout fillet
G-20	9 P–11.49 W–79.51 Ni	−0.0012	−0.14	Maximum attack of 4 mils along surface of fillet
S-10	14.31 Cr–9.34 Si–2.66 Mn–19.32 Fe–54.37 Ni	0	0	Subsurface voids to a depth of 3 mils along fillet surface
B-15	6 Si–5 P–89 Ni	0	0	Maximum attack of 4 mils along surface of fillet
B-16	4.5 Si–6.25 P–89.25 Ni	−0.0001	−0.01	Small subsurface voids to a depth of 4 mils
G-21	10.98 P–6.16 W–82.86 Ni	−0.0001	−0.011	Uniform surface attack along entire fillet to a depth of 4 mils
B-17	3 Si–7.5 P–89.5 Ni	−0.0012	−0.14	Maximum attack of 4 mils along surface of fillet
L-20	38 Ni–5 Cr–57 Mn	−0.0004	−0.043	Attack in the form of stringers to a maximum depth of 5 mils; not uniform

*Brazing alloys listed in order of decreasing corrosion resistance to sodium.

silicon in the absence of phosphorus tend to be attacked in the fluoride mixture.

Static tests have also been completed on a series of commercial and experimental brazing alloys used to braze "A" nickel T-joints in a dry hydrogen atmosphere. These tests were also conducted in sodium and in NaF-ZrF$_4$-UF$_4$ (53.5-40-6.5 mole %) for 100 hr at 1500°F. The results of the tests in the fluoride mixture are presented in Table 5.12; the results of the tests in sodium are shown in Table 5.13. The brazing alloys which appear to have fair corrosion resistance to both media are the 90 wt % Ni–10 wt % P alloy, the 80 wt % Ni–10 wt % Cr–10 wt % P alloy, and Nicrobraz. A 1.5-mil layer of small subsurface voids can be seen in Fig. 5.10a along the surface of the "A" nickel T-joint brazed with Nicrobraz and tested in sodium; the same brazing alloy after being tested in NaF-ZrF$_4$-UF$_4$ (53.5-40-6.5 mole %) is shown in Fig. 5.10b. No attack can be seen along the surface of the braze fillet.

Several of the brazing alloys which showed good static corrosion resistance have also been tested in seesaw apparatus, and the results are given in Table 5.14. These tests were conducted on brazed Inconel T-joints exposed for 100 hr at a hot-zone temperature of 1500°F. A temperature differential of about 400°F was maintained in all the seesaw tests.

All the brazing alloys listed in Table 5.14 had

TABLE 5.11. BRAZING ALLOYS ON TYPE 310 STAINLESS STEEL TESTED IN STATIC NaF-ZrF$_4$-UF$_4$ (53.5-40-6.5 mole %) AT 1500°F FOR 100 hr

Alloy Designation*	Alloy Composition (wt %)	Weight Change (g)	Weight Change (%)	Metallographic Notes
G-20	9 P–11.49 W–79.51 Ni	−0.0017	−0.152	No attack on surface of fillet; several cracks in fillet
B-15	6 Si–5 P–89 Ni	−0.0046	−0.510	Uniform surface attack along fillet to a depth of 0.5 mil
B-16	4.5 Si–6.25 P–89.25 Ni	−0.0057	−0.562	Surface attack along fillet to a depth of 0.5 mil
G-21	10.98 P–6.16 W–82.86 Ni	−0.0061	−0.674	Erratic surface attack to a depth of 0.5 mil along fillet
B-17	3 Si–7.5 P–89.5 Ni	−0.0053	−0.516	Surface attack along fillet to a depth of 0.5 mil; several cracks in fillet
B-13	9 Si–2.5 P–88.5 Ni	−0.0027	−0.279	Surface attack along entire fillet to a depth of 1 mil
P-12	9 Si–15 Mn–76 Ni	−0.0034	−0.331	Surface attack in form of small voids to a depth of 1 mil; several cracks in fillet
B-14	7.5 Si–3.75 P–88.75 Ni	−0.0052	−0.479	Surface attack along entire fillet to a depth of 1 mil
P-11	10.5 Si–7.5 Mn–82 Ni	−0.0042	−0.401	Surface attack to a depth of 1.5 mils; several cracks in fillet
B-12	10.5 Si–1.25 P–88.25 Ni	−0.0018	−0.171	Surface attack to a depth of 2 mils: large cracks throughout fillet
P-10	16.27 Si–5.9 Mn–77.83 Ni	−0.0026	−0.290	Uniform surface attack along fillet to a depth of 3 mils
S-10	14.31 Cr–9.24 Si–2.66 Mo–17.32 Fe–54.37 Ni	−0.0030	−0.344	Surface attack to a maximum depth of 7.5 mils along entire fillet
P-13	7.5 Si–22.5 Mn–70 Ni	−0.0043	−0.455	Complete attack of entire fillet
L-20	38 Ni–5 Cr–57 Mn	−0.0078	−0.74	Complete attack of entire fillet
P-14	6 Si–30 Mn–64 Ni	−0.0099	−1.06	Complete attack of entire fillet

*Brazing alloys listed in order of decreasing corrosion resistance to the fluoride mixture.

fair corrosion resistance to both sodium and the fluoride mixture, with the possible exception of the 65 wt % Ni–25 wt % Ge–10 wt % Cr alloy. The Coast Metals No. 52 alloy had good corrosion resistance to the fluoride mixture in the seesaw test in contrast to its poor resistance in the static test. A large degree of porosity was present in Coast Metals No. 50 alloy that hampered the evaluation of the corrosion data. These two brazing alloys will be retested in order to check the results of these seesaw tests.

Screening Tests of Solid-Phase Bonding

The alloys which have been proposed for use in the fabrication of the ANP reactor fuel and coolant lines have a tendency to form a solid-phase bond at elevated temperatures in liquid metals and in fused fluoride salts. Bonding of this type makes them unsuitable for use in valves, bearings, and seals; thus cermets and ceramics that do not form a solid-phase bond are being investigated. The cermets (metal-bonded ceramics) appear to be the more promising because of their high corrosion resistance and other chemical and physical characteristics.

The test apparatus being used is shown in Fig. 5.11. This apparatus was adapted from that designed for lever-arm stress-rupture tests.[4] The container for the central components, for the test specimens, and for the liquid metal or fused fluoride salt serves as a housing for the compression tube and upper platen. By using this arrangement

---

[4] R. B. Oliver *et al.*, *ANP Quar. Prog. Rep. Mar. 10, 1955*, ORNL-1864, Fig. 7.2, p 105.

TABLE 5.12. BRAZING ALLOYS ON "A" NICKEL T-JOINTS TESTED IN STATIC NaF-ZrF$_4$-UF$_4$ (53.5-40-6.5 mole %) AT 1500°F FOR 100 hr

Alloy* Composition (wt %)	Weight Change (g)	Weight Change (%)	Metallographic Notes
80 Ni–10 Cr–10 P	0	0	No attack on braze fillet
50 Ni–25 Mo–25 Ge	0	0	No attack on braze fillet
Nicrobraz 69 Ni–5 B–15 Cr–5 Si–5 Fe–1 C	−0.0004	−0.016	No attack on braze fillet
Electroless nickel 90 Ni–10 P	−0.0004	−0.013	No attack on braze fillet
65 Ni–25 Ge–10 Cr	0	0	Small subsurface voids to a depth of 0.5 mil along braze fillet
Coast Metals No. 52 90 Ni–4 B–4 Si–2 Fe	−0.0014	−0.05	Nonuniform attack to a depth of 6 mils along braze fillet
General Electric No. 81 66 Ni–10 Si–19 Cr–4 Fe–1 Mn	−0.0003	−0.012	Nonuniform attack to a depth of 12 mils along fillet
35 Ni–55 Mn–10 Cr	−0.0111	−0.48	Complete attack of braze fillet
60 Mn–40 Ni	−0.0159	−0.59	Complete attack of braze fillet
68 Ni–32 Sn	−0.0998	−3.49	Joint partially dissolved at fillet surface

*Brazing alloys listed in order of decreasing corrosion resistance to the fluoride mixture.

TABLE 5.13. BRAZING ALLOYS ON "A" NICKEL T-JOINTS TESTED IN STATIC SODIUM AT 1500°F FOR 100 hr

Brazing Alloy* Composition (wt %)	Weight Change (g)	Weight Change (%)	Metallographic Notes
Electroless nickel 90 Ni–10 P	−0.0004	−0.018	No attack along fillet surface
Coast Metals No. 52 90 Ni–4 B–4 Si–2 Fe	−0.0019	−0.068	Surface attack along fillet to a depth of 0.5 mil
80 Ni–10 Cr–10 P	−0.0017	−0.061	Nonuniform attack along fillet to a depth of 1 mil
General Electric No. 81 66 Ni–10 Si–19 Cr–4 Fe–1 Mn	−0.0018	−0.078	Attack on surface of fillet to a depth of 1 mil
Nicrobraz 69 Ni–5 B–15 Cr–5 Si–5 Fe–1 C	−0.0022	−0.082	1.5 mil layer of small subsurface voids along fillet edge
50 Ni–25 Mo–25 Ge	−0.0009	−0.036	Surface attack along fillet to a depth of 2.5 mils
65 Ni–25 Ge–10 Cr	−0.0024	−0.085	Uniform surface attack along fillet to a depth of 3 mils
60 Mn–40 Ni	−0.0020	−0.079	Uniform attack along entire fillet to a depth of 9 mils
35 Ni–55 Mn–10 Cr	−0.0005	−0.020	Small voids in from surface of fillet to a depth of 13 mils
68 Ni–32 Sn	−0.0171	−0.540	Complete attack of whole fillet

*Brazing alloys listed in order of decreasing corrosion resistance to sodium.

TABLE 5.14. BRAZING ALLOYS ON INCONEL T-JOINTS EXPOSED IN SEESAW APPARATUS TO SODIUM AND TO NaF-ZrF$_4$-UF$_4$ (53.5-40-6.5 mole %) FOR 100 hr AT 1500°F

Brazing Alloy* Composition (wt %)	Bath Material	Weight Change		Metallographic Notes
		(g)	(%)	
Coast Metals No. 52 89 Ni–5 Si–4 B–2 Fe	Fluoride mixture	−0.0008	−0.052	Nonuniform surface attack along fillet to a depth of 0.5 mil
	Sodium	−0.0011	−0.073	No attack along surface of fillet
Low-melting Nicrobraz 80 Ni–5 Cr–6 Fe–3 B–5 Si–1 C	Fluoride mixture	−0.0008	−0.063	Nonuniform surface attack to a depth of 0.5 mil along fillet
	Sodium	−0.0007	−0.051	Subsurface voids to a maximum depth of 1.5 mils along surface of fillet
Coast Metals No. 50 93 Ni–3.5 Si–2.5 B–1 Fe	Fluoride mixture	−0.0014	−0.085	Uniform surface attack along fillet to a depth of 0.5 mil
	Sodium	−0.0012	−0.077	Very erratic surface attack along fillet to a depth of 1.5 mils
70 Ni–11 Cr–6 Si–13 Ge	Fluoride mixture	−0.0011	−0.067	Nonuniform attack to a depth of 1.5 mils along surface of fillet
	Sodium	−0.0023	−0.139	Nonuniform attack along surface of fillet to a depth of 2.5 mils
Nicrobraz 70 Ni–14 Cr–6 Fe–5 B–4 Si–1 C	Fluoride mixture	−0.0005	−0.030	Erratic surface attack along fillet to a depth of 1.5 mils
	Sodium	0	0	Very erratic stringer attack to a maximum depth of 4 mils along surface of fillet
65 Ni–25 Ge–10 Cr	Fluoride mixture	−0.0010	−0.056	Stringer-type attack to a maximum depth of 4 mils in a few localized areas
	Sodium	−0.0019	−0.113	Intermittent surface attack to a maximum depth of 4 mils along fillet

*Brazing alloys listed in order of decreasing corrosion resistance to both test mediums.

the test specimens can be brought into mutual compression between the platens.

Corrosion-resistant cermets and hard-facing alloys have been tested in an apparatus fabricated from Inconel for solid-phase bonding in NaF-ZrF$_4$-UF$_4$ (53.5-40-6.5 mole %) for 100 hr at 1500°F. The test specimens were dimensionally the same (±0.0002 in.) and the contacting surfaces had roughnesses of less than 10 μin. The test was begun by holding the contacting surfaces of the test specimens apart while the apparatus was flushed with NaF-ZrF$_4$-UF$_4$ (53.5-40-6.5 mole %) at 1500°F. This was done to ensure that any surface films on the specimens would be removed prior to the application of the compression load. A fresh charge of NaF-ZrF$_4$-UF$_4$ (53.5-40-6.5 mole %) at 1500°F was then put into the test chamber, and the test specimens were pressed together at the desired contact pressure. At the conclusion of the 100-hr test period, the NaF-ZrF$_4$-UF$_4$ was removed, and the system was cooled to room temperature and disassembled.

The contact surfaces of the test specimens were examined with a low-power microscope for signs of solid-phase bonding. The seating was not perfectly uniform in any of the tests, and therefore the contact pressures between the test specimens were probably in excess of the calculated values in certain areas. Table 5.15 is a summary of the solid-phase-bonding screening tests made at calculated contact pressures of 6,600, 10,000, and 50,000 psi. In the most severe tests, that is, those in which the calculated contact pressure was 50,000 psi, no bonding was observed, except for a slight amount in the tests of K150A vs K152B and K162B vs K162B. Since uniform contact was extremely difficult to obtain, the slight bonding that occurred in these tests may have been caused by contact pressures in excess of 50,000 psi. This explanation seems even more reasonable when it is considered that the quantity and composition of the binder metal of the test specimens,

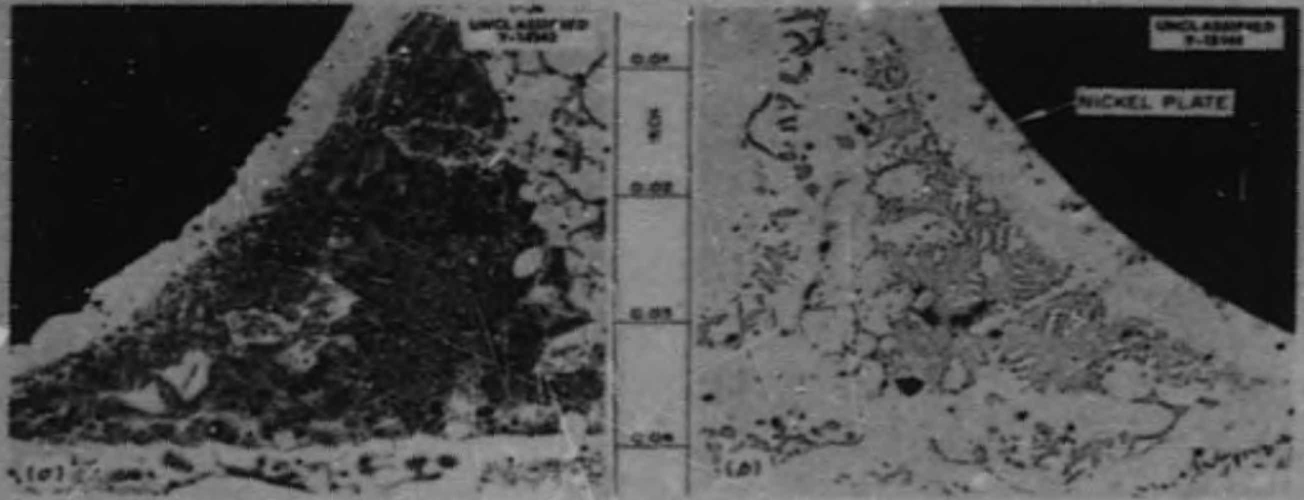

Fig. 5.10. "A" Nickel T-Joints Brazed with Nicrobraz After Exposure for 100 hr at 1500°F to (*a*) Static Sodium and (*b*) Static NaF-ZrF$_4$-UF$_4$ (53.5-40-6.5 mole %). Etched with (*a*) 10% oxalic acid and (*b*) aqua regia. 100X. Reduced 24%.

TABLE 5.15. RESULTS OF SOLID-PHASE-BONDING SCREENING TESTS OF VARIOUS CERMETS AND ALLOYS EXPOSED TO NaF-ZrF$_4$-UF$_4$ (53.5-40-6.5 mole %) AT 1500°F FOR 100 hr AT VARIOUS CONTACT PRESSURES

Compositions: K150A (80 wt % TiC–10 wt % NbTaTiC$_3$–10 wt % Ni)
K151A (70 wt % TiC–10 wt % NbTaTiC$_3$–20 wt % Ni)
K152B (64 wt % TiC–6 wt % NbTaTiC$_3$–30 wt % Ni)
K162B (64 wt % TiC–6 wt % NbTaTiC$_3$–25 wt % Ni–5 wt % Mo)

Contact Pressure (psi)	Contacting Specimens	Results*
6,600	K150A vs Stellite 25	Some bonding
	K162B vs Stellite 25	Some bonding
10,000	K150A vs Stellite 6	Some bonding
	K162B vs Stellite 6	Some bonding
	K152B vs K152B	No bonding
	K152B vs K162B	No bonding
	K162B vs K162B	No bonding
50,000	K150A vs K150A	No bonding
50,000	K150A vs K151A	No bonding
	K150A vs K152B	Some bonding
	K150A vs K162B	No bonding
	K151A vs K151A	No bonding
	K151A vs K152B	No bonding
	K151A vs K162B	No bonding
	K152B vs K152B	No bonding
	K152B vs K162B	No bonding
	K162B vs K162B	Some bonding

*There was inconsistent bonding of test specimens to the supporting Inconel platens in all tests.

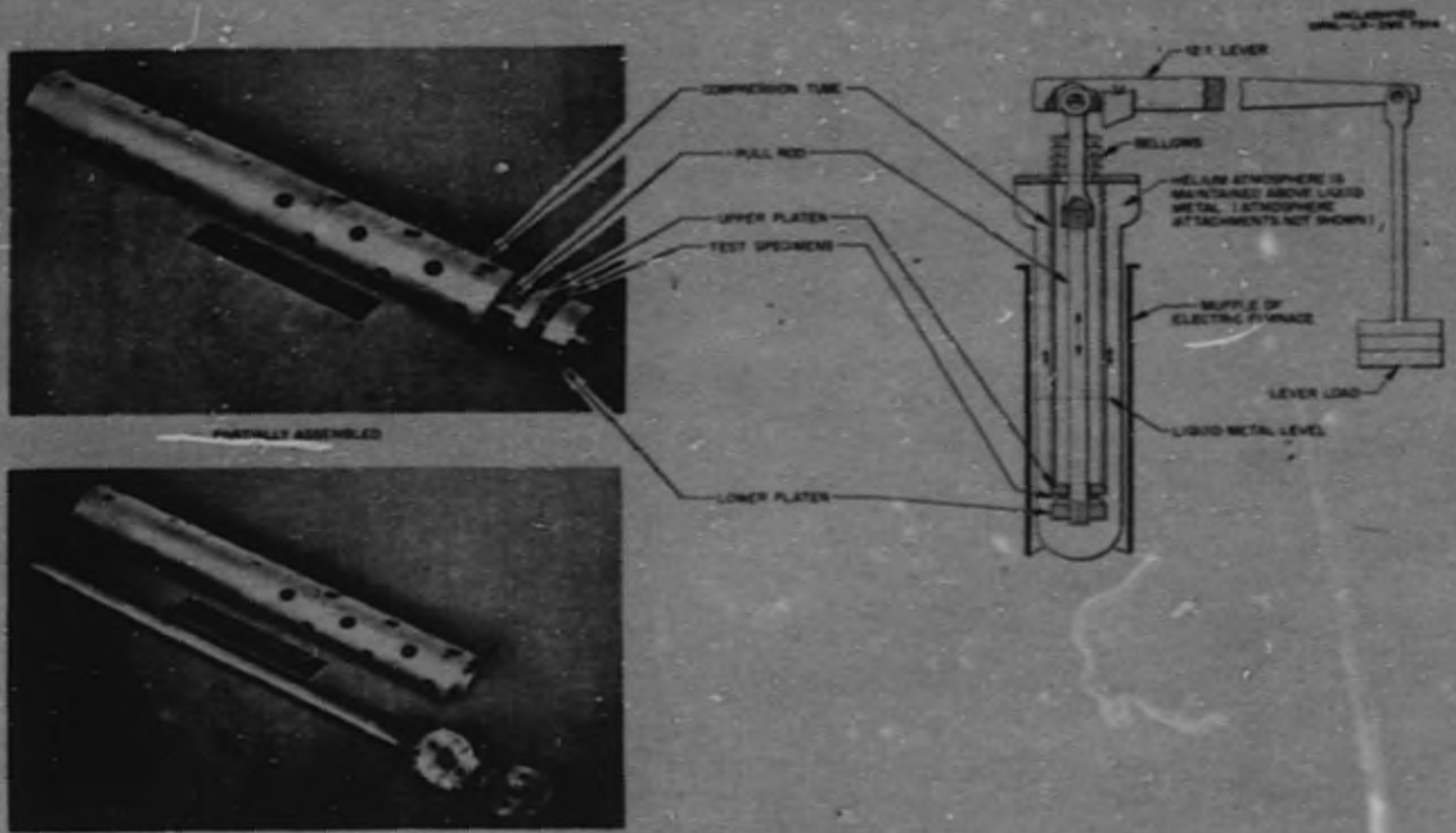

PARTIALLY ASSEMBLED

DISASSEMBLED

Fig. 5.11. Apparatus for Solid-Phase-Bonding Screening Tests.

particularly that for K150A vs K152B, show no apparent relationship to the occurrence of the bonding. On the basis of these data, it is believed that none of these Kentaniums would form solid-phase bonds to each other in NaF-ZrF$_4$-UF$_4$ (53.5-40-6.5 mole %) at 1500°F in 100 hr if the true contact pressure between the cermets did not exceed 50,000 psi. A recheck of the pairs that did bond is planned that will conclude the screen testing of the Kentaniums, K150A, K151A, K152B, and K162B, for solid-phase bonding in all contact combinations with each other in NaF-ZrF$_4$-UF$_4$ (53.5-40-6.5 mole %) at 1500°F for 100 hr.

Sodium in Inconel

A 1000-hr test was recently completed in which sodium was circulated in an Inconel thermal-convection loop. Samples of the sodium used in this test were analyzed and found to contain approximately 0.03% oxygen. The oxygen content was admittedly high and could have been reduced by a factor of 10 by adequate cold trapping; however, this test did show how serious that mass transfer can be even in a thermal-convection loop when the oxygen content is high. The hot leg of the loop was held at a temperature of 1500°F, and the coldest section of the cold leg was held at 1200°F. The mass transfer that occurred was concentrated in an area in the cold leg where an air blast had impinged on the tube wall during the test, as shown in Fig. 5.12. Very little mass transfer was detected in other sections of the cold leg. A similar test will be conducted in which the oxygen content of the sodium will be held below 0.005% to determine the effect the oxygen content has on mass transfer in a sodium-Inconel system.

Lithium in Type 347 Stainless Steel

Lithium was circulated in two stainless steel thermal-convection loops for periods of 1000 and 3000 hr, respectively. The hot- and cold-leg temperatures were 1000 and 550°F, respectively.

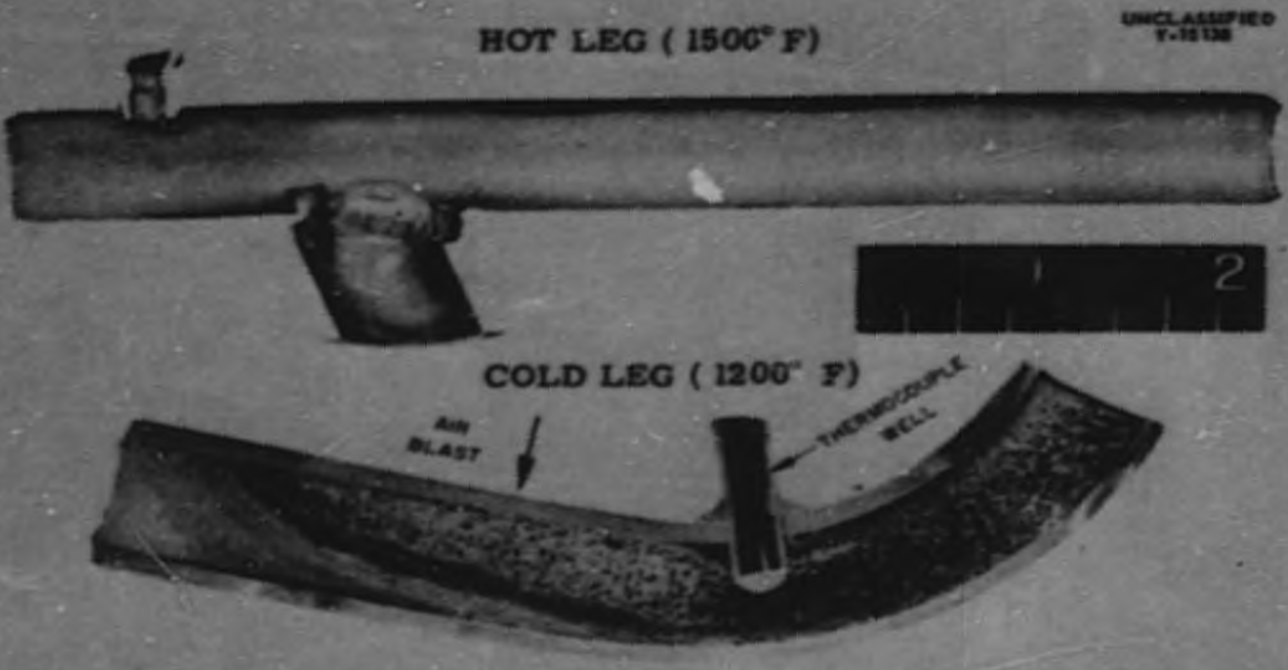

Fig. 5.12. Specimens of Hot and Cold Legs of an Inconel Thermal-Convection Loop After Circulating Sodium for 1000 hr. Crystal deposition resulting from mass transfer may be seen in the cold leg.

The loops operated satisfactorily during the test periods, and macroscopic examination revealed no mass-transferred crystals in the loops or in the lithium drained from the loops.

The hot zone of the loop that operated for 1000 hr had subsurface voids and a ferritic surface layer to a depth of 0.3 to 1.0 mil. Lithium metal had penetrated to this depth. The weld zone of the pipe in this area was attacked to a depth of 3 mils. The cold leg of the loop was unattacked; however, there were a few small (0.2 mil) crystals attached to the surface. Similar crystals were previously identified as carbides.

The attack in the hot leg of the loop that operated for 3000 hr was similar to that found in the 1000-hr test specimen; however, the spongy ferritic surface layer was 1.0 to 1.5 mils thick, as shown in Fig. 5.13. The attack in the weld zone was intergranular and extended to a depth of 4 to 5 mils, as shown in Fig. 5.14. The preferential attack in the weld zone is due to attack of the grain boundary carbides by the molten lithium. A deep groove in the pipe wall may be seen at the weld zone–parent metal interface.

The cold-leg section (Fig. 5.13) of this loop was very similar in appearance to that of the loop operated for 1000 hr. A few small (0.2 mil) carbide particles were attached to the wall of the tube.

It is believed that the corrosion resistance of type 347 stainless steel to lithium in this temperature range would be improved by lowering the carbon content of the steel and by using seamless instead of welded pipe. The austenite-to-ferrite transformation detected in the hot legs of these loops is attributed to leaching of nickel from the type 347 stainless steel by the lithium.

Versene Cleaning of Beryllium-Inconel Systems

Versene has been proposed as the cleaning agent for the ART, and therefore the corrosion resistance

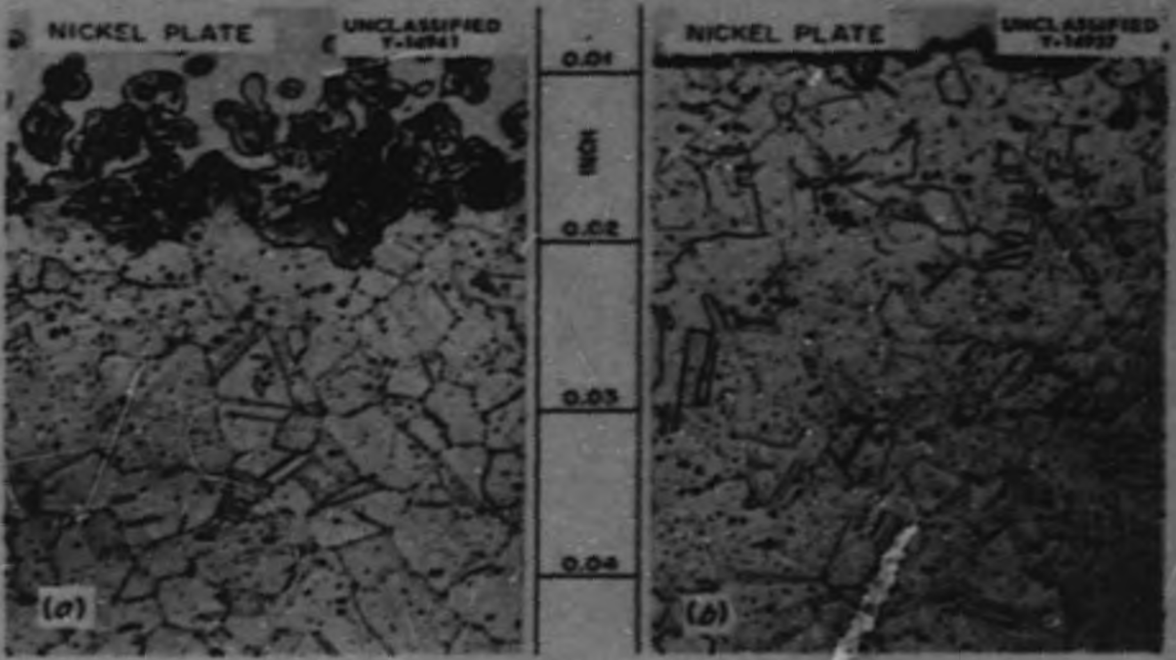

Fig. 5.13. Hot- and Cold-Leg Surfaces of Type 347 Stainless Steel Thermal-Convection Loop After Circulating Lithium for 3000 hr at a Hot-Leg Temperature of 1000°F and a Cold-Leg Temperature of 550°F. Note austenite-to-ferrite phase transformations which occurred on hot-leg surface (*a*) and small crystals deposited on cold-leg surface (*b*). Specimens nickel plated after testing. Etched with aqua regia. 1000X.

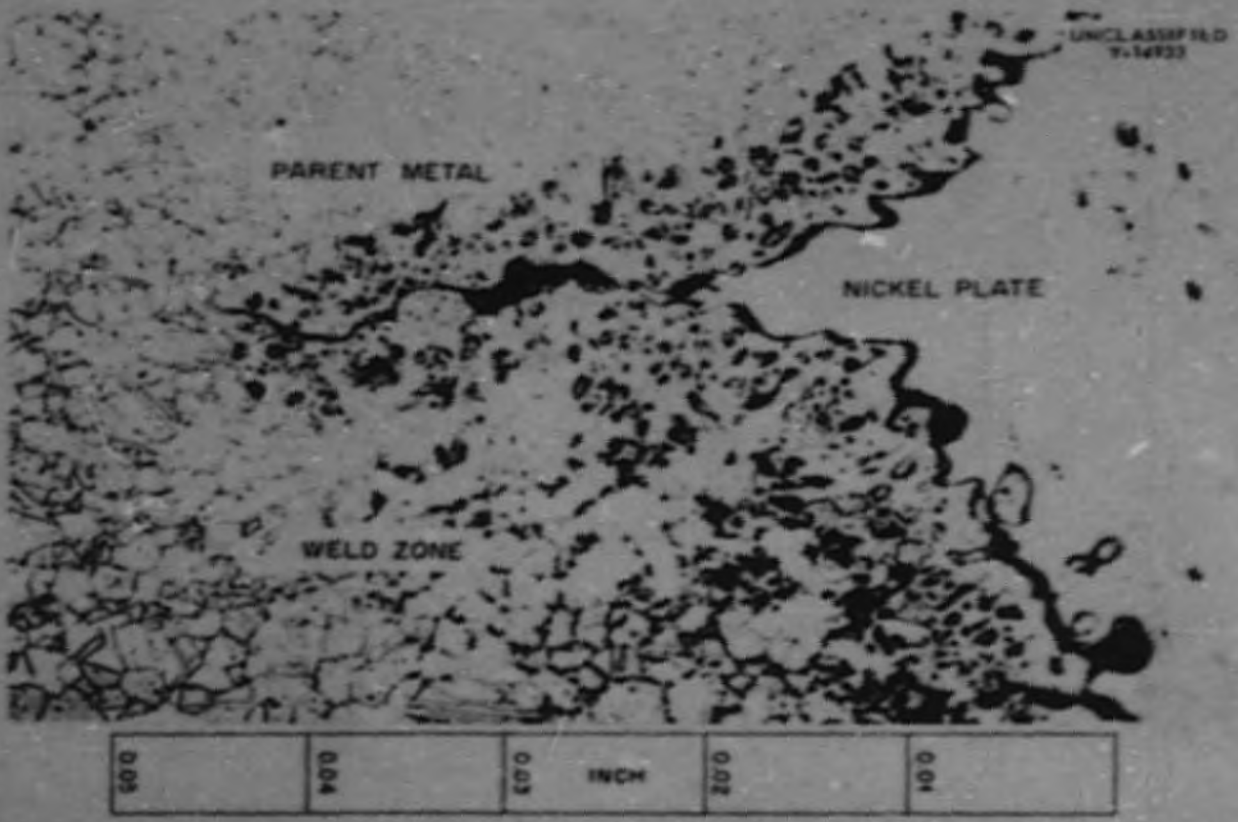

Fig. 5.14. Inside Wall of Hot-Leg Weld from Type 347 Stainless Steel Thermal-Convection Loop After Circulating Lithium for 3000 hr at a Hot-Leg Temperature of 1000°F. Note deep (4 mils) attack in weld zone as compared with 1-mil attack on parent metal. Etched with aqua regia. 1000X.

of beryllium to dynamic Versene was studied. The testing procedure was designed to simulate the cleaning procedure used in the ARE, which was cleaned with a Versene solution.

Tests have been completed with two loops constructed of Inconel with a beryllium insert. The beryllium sample was placed within the loop between two similar Inconel inserts which were held in place by crimping. The tubular beryllium insert was $\frac{3}{4}$ in. OD, $\frac{9}{16}$ in. ID, and 3 in. in length.

A 1% Versene solution was pumped through each loop at a rate of 2 gpm (2.6 fps) by a centrifugal pump. Disodium versonate was used, and the concentration was determined on a weight-volume basis. The testing temperature for both loops was 180°F, and the Versene was circulated in each for a period of 24 hr.

Upon completion of the first test the Versene was drained while the loop was still at test temperature. When the loop was sectioned, a small amount of Versene was found in a static region of the loop located in the annular gap between the beryllium insert and the Inconel sleeve. No trace of retained Versene was found in this section of the second loop, which was flushed with distilled water after the Versene was drained.

Macroscopic examination showed the beryllium inserts in both loops to be quite similar. Each insert had retained its original polished appearance. No effect of the Versene solution was found by macroscopic or metallographic examination of the inner surface of the beryllium insert or the Inconel in either test. The outer surfaces of the beryllium inserts, however, were attacked by the Versene solution. The attack was in the form of erratic pits that varied in depth from 0.5 to 2.5 mils.

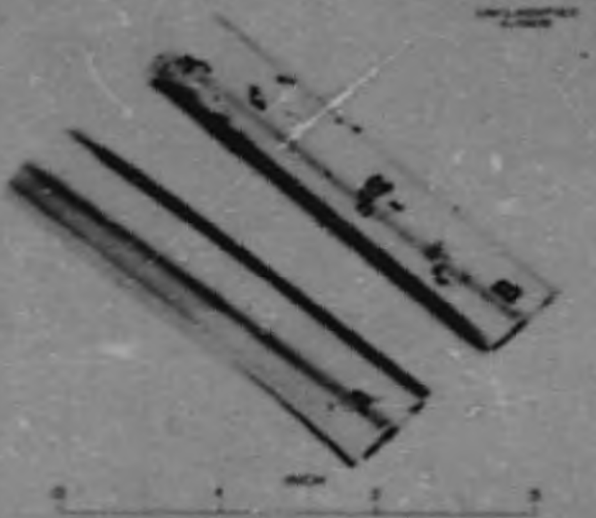

Fig. 5.15. As-received (*a*) and As-tested (*b*) Beryllium Insert from Second Inconel Loop in Which Versene Cleaning Solution Was Circulated at 180°F at a Rate of 2 gpm.

The erratic attack of the Versene on the outer surface of the beryllium insert used in the second test is shown macroscopically in Fig. 5.15. The unattacked inner surface and the erratically attacked outer surface of the beryllium insert used in the first test are shown in Fig. 5.16. The 2.5-mil outer surface attack shown in Fig. 5.16 is representative of that found by metallographic examination of the beryllium inserts used in both tests. In each test the beryllium insert lost weight, as shown in the following tabulation.

	Test No. 1	Test No. 2
Original weight, g	16.8715	16.7970
Final weight, g	16.8680	16.7941
Weight loss		
g	0.0035	0.0029
%	0.021	0.017

A chemical analysis of a portion of the Versene solution used in the second test revealed a beryllium concentration of 0.0024 mg/ml. Since 1.5 liters of 1% Versene solution was used in this test, the total amount of beryllium in the solution was 3.8 mg, which agrees fairly well with the 2.9-mg weight loss of the beryllium insert used in this test.

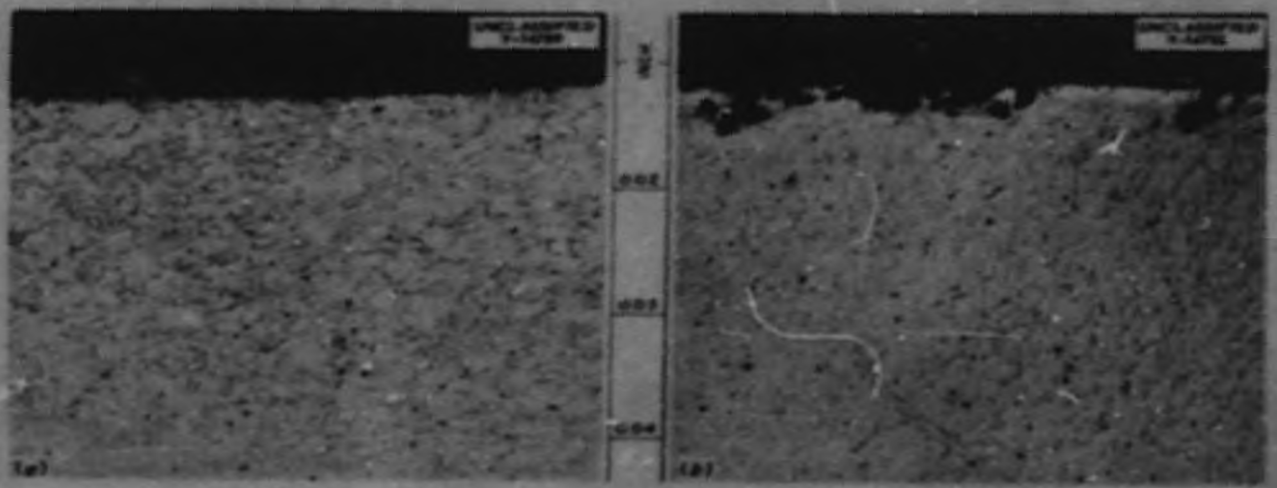

Fig. 5.16. Inner (*a*) and Outer (*b*) Surfaces of Beryllium Insert From First Inconel Loop in Which Versene Cleaning Solution Was Circulated at 180°F at a Rate of 2 gpm. Etched with oxalic acid. 100X. Reduced 24%.

FUNDAMENTAL CORROSION RESEARCH

G. P. Smith
Metallurgy Division

Film Formation on Metals

J. V. Cathcart
Metallurgy Division

Most of the work done in the past on the oxidation of metals has been devoted to a study of the oxidation characteristics of the "heavy" metals and alloys such as copper, nickel, iron, aluminum, the stainless steels, etc. These materials either were structurally important or their physical properties were such as to make them particularly amenable to oxidation studies. Comparable investigations of the alkali and alkaline-earth metals are almost entirely lacking.

Rather elaborate oxidation theories have been devised for the heavier metals, but it has been assumed, in general, that the alkali and alkaline-earth metals exhibit a linear oxidation rate, in accordance with the old crack theory of Pilling and Bedworth.[5] Their theory was that a metal, for which the ratio of the density of the oxide to that of the parent metal is greater than unity, should obey a linear oxidation law. It was reasoned that the oxide film formed would be highly subject to cracking and that, consequently, there would be a constant re-exposure of fresh metal surface to oxygen. Thus the rate of oxidation should be independent of the thickness of the oxide film, the quantity of oxide formed being directly proportional to the time of exposure to oxygen.

In order to test the crack theory of oxidation directly, as well as to obtain experimental data on the oxidation of the alkali metals, an investigation of the oxidation characteristics of sodium was undertaken. Sodium fulfills completely the Pilling and Bedworth criterion for a metal that exhibits a linear oxidation rate. This study was initiated because preliminary experiments indicated that sodium, contrary to the theory, actually forms a highly protective oxide film in dry oxygen. Subsequent work verified these early findings. The research has been continued in an effort to clarify the oxidation mechanism operative for sodium and to relate it to the more thoroughly investigated oxidation mechanisms of copper, aluminum, and other structural metals.

On the basis of the results obtained with sodium, it was concluded that a fundamental error existed in the currently accepted oxidation concepts for metals that obey a linear oxidation rate law and that it was therefore desirable to investigate carefully the oxidation of some metal that does exhibit a linear oxidation rate. Columbium was especially suitable for this study. Below approximately 400°C, it obeys a parabolic oxidation rate law, while above this temperature its oxidation rate is linear. At 400°C the initial stages of oxidation also appear to follow a parabolic rate, but after several hours of oxidation the rate increases and becomes almost linear.[6] Thus a careful investigation of the structure and composition of the oxide films formed at or near 400°C should provide valuable information as to the conditions which lead to a linear oxidation rate.

An added incentive for the study of the oxidation properties of columbium was that this metal possesses very desirable high-temperature structural properties. Its use has been limited largely by its excessive oxidation at high temperatures. It was believed that further information concerning its oxidation mechanism would be helpful in overcoming this defect.

The experimental procedures used and the results of the studies of sodium and columbium oxidation are presented below.

Sodium Oxidation. The oxidation rate of sodium was followed by measuring the change in pressure in a closed reaction chamber as the reaction proceeded. A sensitive, differential manometer in which Octoil-S diffusion pump oil was used as the manometric fluid served as the pressure-sensing device.

The apparatus used is shown in Fig. 5.17. The sodium reservoir consisted of a glass bulb closed at one end with a thin-walled break-off tip. The reservoir was filled, under vacuum, through a side arm, with sodium that had been purified by repeated vacuum distillations at a pressure of 10^{-6} to 10^{-7} mm Hg. After the side arm was removed, the reservoir was attached to a tube below the oxidation bulb, as shown in Fig. 5.17. A small furnace was built which could be placed around the entire apparatus, with the sodium reservoir and the

---

[5] N. B. Pilling and R. E. Bedworth, *J. Inst. Metals* 29, 529 (1923); see also, U. R. Evans, *Metallic Corrosion, Passivity, and Protection*, Longmans, Green and Co., 1948, New York, p 102.

[6] H. Inouye, *Scaling of Columbium in Air*, ORNL-1565 (Sept. 1, 1953).

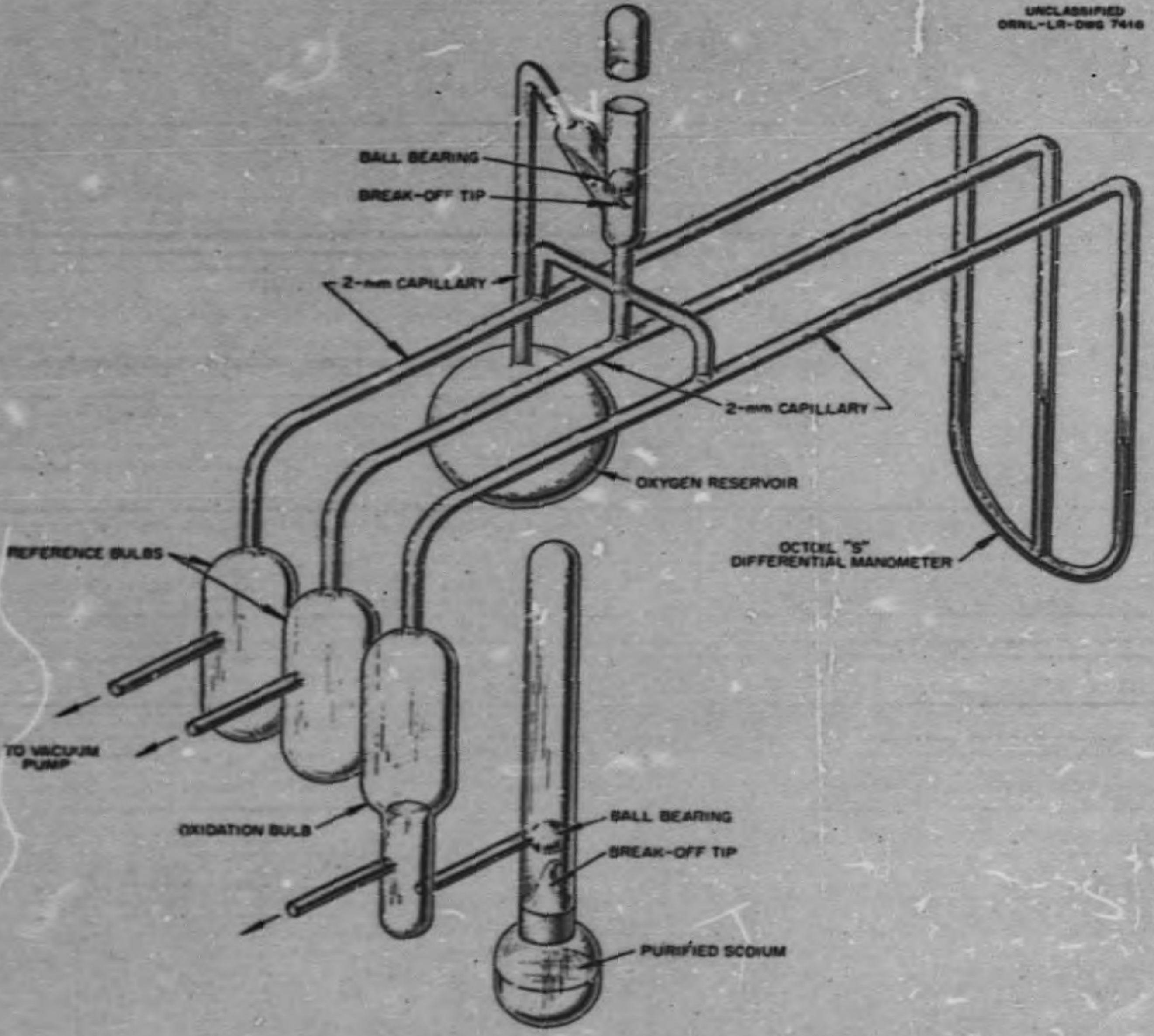

Fig. 5.17. Sodium Oxidation Testing Apparatus.

manometer protruding from suitable holes. The entire apparatus could thus be baked-out under vacuum before any sodium was admitted to the system. Care was taken to load the manometer by the vacuum distillation of Octoil-S from a separate bulb into the manometer arms. This procedure assured that the manometric fluid would not act as a source of appreciable gas.

After a bake-out period of 16 to 20 hr the system was allowed to cool to room temperature, and the break-off tip above the sodium reservoir was crushed. The sodium was then distilled into the tube below the oxidation bulb, and the sodium reservoir was removed. Finally, the sodium was distilled into the oxidation bulb and allowed to condense on the walls. Both these final distillations were made under a pressure of approximately 2×10^{-7} mm Hg. As the last step before the admission of oxygen, the tube below the oxidation bulb was sealed off, as were the vacuum leads to the two reference bulbs.

A 50-cc flask served as an oxygen reservoir. Prior to being attached to the oxidation apparatus, it was filled with carefully purified oxygen to a pressure such that when the gas was allowed to expand into the reference and oxidation bulbs the resultant pressure was 200 mm Hg. The purification of the oxygen was accomplished by passing it over hot copper oxide (to remove hydrogen) and Ascarite (to remove carbon dioxide) and finally drying it over magnesium perchlorate and in a liquid-nitrogen trap.

The tube leading from the oxygen reservoir to the break-off tip was made of 2-mm capillary tubing. By thus minimizing the volume above the reservoir, it was possible in the low-temperature runs to immerse the reservoir in a cold bath to precool the oxygen to the desired reaction temperature.

When the break-off tip above the oxygen reservoir was smashed, the oxygen passed through the T connection above the manometer and simultaneously filled the reference and oxidation bulbs to identical pressures. The intersection of the tubes of the T was then collapsed as quickly as possible with a hand torch. The three arms of the manometer were thus separated and any change in pressure in the oxidation bulb resulting from the reaction of sodium and oxygen was reflected in a change in the relative heights of the oil columns of the manometer.

The use of the above-described T connection instead of a stopcock had two advantages. First, it avoided all possibility of a leak occurring in the system, but, more importantly, by dispensing altogether with stopcocks, this arrangement eliminated the danger of contamination of the sodium surface by stopcock-grease vapor and permitted the bakeout of the entire system during the initial stages of evacuation. It was felt that these considerations were sufficiently important to forego the greater conveniences of a stopcock.

Oxidation rate measurements have been made at five temperatures: −79, −20, 25, 35, and 48°C. At 25, 35, and 48°C, an apparatus identical to that shown in Fig. 5.17 was used, except that only one reference bulb was found to be necessary. For reasons described below, the second reference bulb proved very helpful, however, for experiments [illegible] the two lower temperatures.

For all experiments the oxidation and reference bulbs were immersed in a constant-temperature bath contained in a 4-liter Dewar flask. Mineral oil served as the bath liquid for the three higher temperatures. At −20°C a saturated sodium chloride–ice bath proved to be satisfactory, and at −79°C a slurry consisting of powdered dry ice and a 50-50 vol % solution of carbon tetrachloride and chloroform was used to attain the desired temperature. The densities of the liquid phase and the dry ice in the latter bath were approximately equal, and thus a slurry was produced in which there was little tendency for the segregation of the dry-ice particles.

At −79°C the sodium oxidized at a very slow rate. The maximum pressure change which occurred in the system as a result of the oxidation was 0.2 to 0.3 mm Hg. Therefore it was necessary to pay particularly careful attention to factors which could cause spurious pressure readings. One obvious source of error was a temperature difference between the reference and oxidation bulbs. This difficulty was overcome by utilizing a relatively thin slurry in the cold bath and stirring it very vigorously. A less easily corrected source of trouble was that, of necessity, the reference and oxidation bulbs were maintained at dry-ice temperature, whereas the manometer and connecting tubes were at room temperature. A simple gas law calculation shows that, in such a system, any change in the temperature of either the cold bath or the manometer will produce, in general, a difference in pressure between the oxidation bulb and the reference bulb. A special case that is an exception to this rule occurs when the volumes of gas at the two temperatures are identical on both sides of the manometer. The magnitude of the pressure difference is dependent both on the ratio of the volume of gas held at the two temperature extremes and on the difference in temperature. Thus, this effect was of no great importance for experiments close to room temperature, but it became significant at −79°C.

It was impossible to maintain exactly equal volumes on both sides of the manometer, and the attainment of precise temperature control in the cold bath at −79°C was almost as difficult. The equilibrium temperature of any dry-ice bath is determined by the sublimation point of carbon dioxide; however, the constancy of the sublimation temperature is dependent upon the constancy of the partial pressure of carbon dioxide above the bath. Thus, unless the bath is contained in a closed vessel, variations in temperature will occur in the bath because of changes in the partial pressure of carbon dioxide above it. In addition, the negative heat of solution of carbon dioxide in carbon tetrachloride and chloroform caused the temperature of the bath to fall below the equilibrium sublimation temperature when the cold mixture was first prepared. Since the bath was contained in a Dewar flask, the lowered temperature tended to persist for long periods of time unless a heater was immersed in the bath.

It was decided therefore that precise temperature control of the apparatus at −79°C was impractical. However, it was essential that some reference point be established for the bath so that the apparatus could be brought back to the initial conditions of the experiment after, for example, each renewal of the dry-ice charge in the bath. The addition of a second reference bulb proved satisfactory for this purpose. The two reference bulbs represented a "differential gas thermometer." It was observed that within about 10 min after the start of an experiment a small difference in the heights of the oil in the reference arms of the manometer was usually established. This difference remained constant as long as the temperature of the bath and the room temperature were unchanged. When deviations in this difference were observed, it was possible to make slight alterations in the bath temperature (for example, by removing part of the cover of the Dewar flask and thus decreasing the partial pressure of carbon dioxide above the bath) and thus re-establish the desired pressure difference in the reference bulbs.

It was recognized that the constancy of the pressure difference between the two reference bulbs did not necessarily indicate a corresponding constancy in the cold-bath temperature. Frequently, the adjustments in the bath temperature that were necessary to maintain the pressure difference represented a counterbalance to changes in room temperature. The resultant small changes in the bath temperature meant, of course, a change in the temperature at which oxidation occurred; but, since the oxidation rate of sodium is not a sensitive function of temperature at −79°C, this alteration of the experimental conditions was not considered to be significant. In any event, as may be seen in Fig. 5.18, the use of the technique described above produced excellent agreement of the data for three separate experiments at −79°C.

The experimental data obtained at the five temperatures investigated are shown in Fig. 5.18. The change in pressure in the system, which is obviously a function of the thickness of the oxide film formed, is plotted against the time of oxidation on a log-log scale. Each curve represents the composite of data taken from three or more experiments.

Perhaps the most striking feature of the experiments was the slowness with which oxidation occurred. Very roughly, one unit on the ordinate scale in Fig. 5.18 is equal to a film thickness of 10 Å. Thus at −79°C after 1000 min of oxidation, the thickness of the oxide film was only about 30 Å, while at 48°C, it was 500 Å.

Since the curves, as plotted, were not linear, there was an indication that the data did not fit any of the conventional oxidation rate equations of the form

$$x^n = kt \ , \qquad n = 1, 2, 3,$$

where x is the thickness of the oxide film after time t, and k is the rate constant. The data were also tested against the logarithmic rate equation

$$x = k \log t \ ,$$

but no fit was obtained.

As may be seen from the curves in Fig. 5.18, the oxidation rates of sodium at −79 and −20°C decrease very sharply after the first 150 to 200 min of oxidation. This behavior is qualitatively similar to that predicted by Cabrera and Mott[7] for oxidation processes leading to the formation of very thin films. The oxide thickness (30 to 40 Å) observed at −79°C is very close to the thickness range required by this theory. The data were checked against the appropriate rate equation

$$\frac{1}{x} = A - B \ln t \ ,$$

where x and t are oxide thickness and time, respectively, and A and B are constants, but no

---

[7] N. Cabrera and N. F. Mott, *Repts. Progr. in Phys.* 12, 163 (1949).

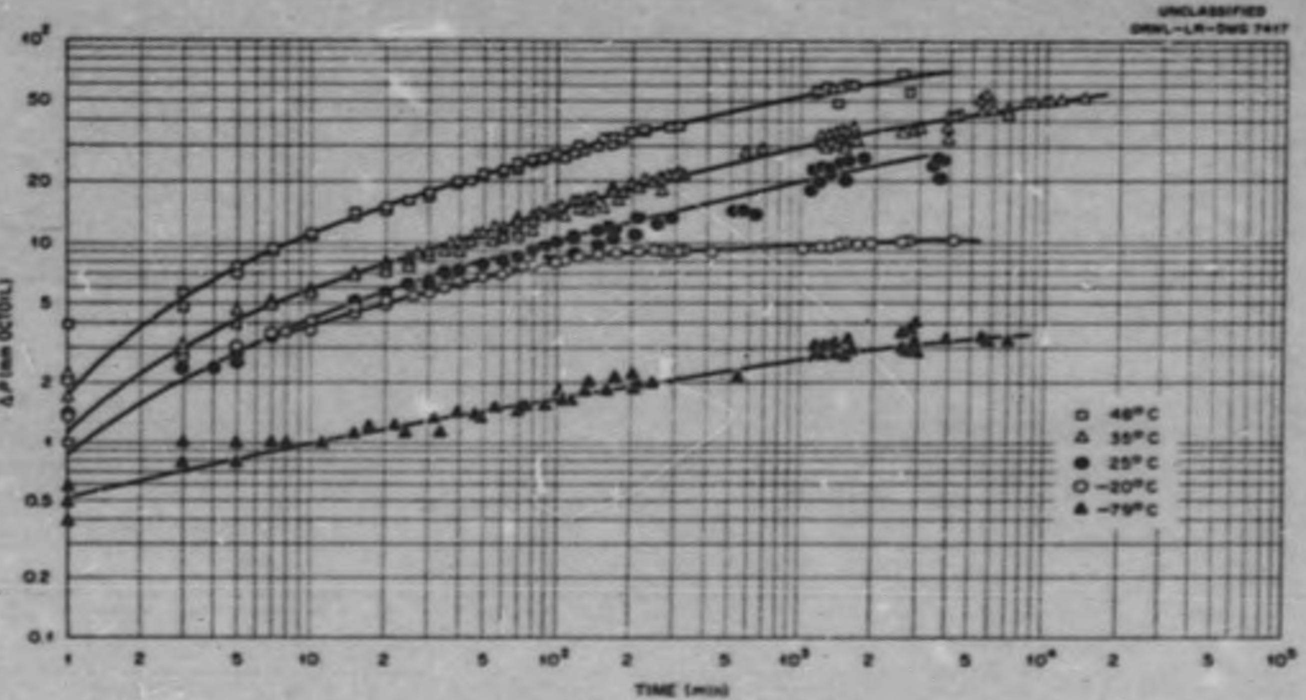

Fig. 5.18. Data on Oxidation of Sodium as a Function of Time and Temperature. In apparatus used, a change in system pressure is a function of the thickness of the oxide film formed.

agreement was found. However, the qualitative similarity between the observed rate curves and those predicted by the theory suggests that the results obtained at −79 and −20°C represent an oxidation process in which the mechanism proposed by Cabrera and Mott is competing with some second mechanism. It is hoped to test this idea by making oxidation measurements at temperatures below −79°C.

The very small amount of oxide which was formed at all temperatures investigated emphasized the highly protective character of sodium oxide films in carefully dried oxygen. The frequently accepted idea that sodium obeys a linear oxidation rate must be discarded. The results also suggest that the oxidation mechanism for sodium (and possibly also that for the other alkali and alkaline-earth metals) need not be regarded as being of a specialized nature but may be very similar to the oxidation mechanism for the heavier metals, such as copper and aluminum. As further details of the oxidation characteristics of sodium and other "ultra-light" metals become available, it may prove possible to devise a theory of oxidation which is applicable to at least the low-temperature oxidation of all metals.

At the present time the oxidation data obtained at 25°C are being rechecked, and the time of oxidation is being extended. It is felt that these additional data are required in order to obtain a meaningful analytical expression for the rate curves. The measurements at 48°C will also be extended in a similar manner.

The completion of these rate studies will mark the end of what might be termed the "classical" phase of the investigation of the oxidation of sodium. It is planned that the future work with sodium will include a study of the surface topography and structure of the sodium oxide films. Electron microscopy and diffraction techniques will be required for this work. The investigations of Harris, Gulbransen, and others have demonstrated that, contrary to all existing oxidation theory, oxide films formed on copper, nickel, and iron are not of uniform thickness and that the major portion of the oxide is contained in nuclei scattered over the metal surfaces. These findings emphasize the necessity of combining rate measurements with a detailed examination of the oxide films formed in any complete oxidation study.

Columbium Oxidation. The work on columbium is in the preliminary stage. It is planned to measure the rate of oxidation of columbium at several temperatures in the neighborhood of 400°C and then to correlate the oxidation rate and oxide layer thickness with the structure and porosity of the oxide. In this manner it should be possible to establish the conditions which exist in the film, both when a parabolic law is obeyed and when the rate becomes linear.

A check has been made on the oxidation rate of columbium at 400°C in highly purified oxygen. Qualitative verification was obtained of the phenomenon, reported by Inouye,[8] of the transition of the oxidation rate from a parabolic to a linear relationship. The initial stages of oxidation produced oxide films which exhibited interferences (colors). As the reaction proceeded, however, the specimens became coated with a white, opaque oxide film whose surface was rough. The appearance of the white oxide seemed to coincide approximately with the transition from the initial parabolic oxidation rate to a linear rate.

Mass Transfer and Corrosion in Fused Hydroxides

M. E. Steidlitz
Metallurgy Division

The study of corrosion and mass transfer of metal by fused sodium hydroxide is under way. Over 60

TABLE 5.16. MASS TRANSFER OF NICKEL IN SODIUM HYDROXIDE UNDER A HYDROGEN ATMOSPHERE FOR 100 hr

Bucket Temperature (°C)	Temperature Differential of System* (°C)	Number of Tests	Amount of Mass Transfer (Visual Observation)
450**	100	1	Little
430	100	1	None -
575	100	1	Very little
600	100	2	Very little to little
600	200	1	Very little
625	50	1	None
625	100	2	Very little
650	50	1	Barely observable
650	100	2	Moderate
650	200	1	Moderate
675	50	1	Little
675	100	1	Moderate
700	50	1	Moderate
700	100	7	Moderate to heavy
800	50	1	Heavy
800	100	1	Very heavy

*Bucket temperature less the cold-finger temperature.

**This test was made under a helium atmosphere.

---

[8] H. Inouye, *Scaling of Columbium in Air*, ORNL-1565 (Sept. 1, 1953).

600°C, as well as an acceleration in the rate of transfer with increasing temperature in the range 600 to 700°C. The mass-transferred deposit at the liquid line, as shown in Fig. 5.20, indicates the type of metal crystal growth which occurs. This specimen is a duplicate of No. 21, for which the bucket temperature was 700°C and the cold-finger temperature was 600°C.

Several compounds that were chosen for their strong reducing properties have been added to the hydroxide melt. It was hoped that these materials, together with the hydrogen atmosphere, will lower the mass transfer rate in nickel. Results of tests with sodium or sodium hydride added to the sodium hydroxide are shown in Fig. 5.21. All the nickel cold fingers shown were held at 600°C, and the bucket temperatures were 700°C. No addition was made to the sodium hydroxide to which No. 37 was exposed, and Nos. 38 through 41, respectively, were exposed to sodium hydroxide containing 5% Na, 10% Na, 5% NaH, and 10% NaH, respectively. In no case did the addition decrease the mass transfer. The same was true for the third and last additive tried, sodium hydrogen phosphite.

In all the tests with additives, there was evidence that some, if not most, of the added material distilled out of the bucket. These same compounds might be found to be effective in a more confined system such as a closed loop. No tests have yet been run at the temperature at which mass transfer is first noticed, and it is possible that these additives might increase the maximum temperature that can be attained without mass transfer occurring.

The results of tests on Inconel in sodium hydroxide are shown in Table 5.17. The mass transfer of Inconel was significantly less than that of

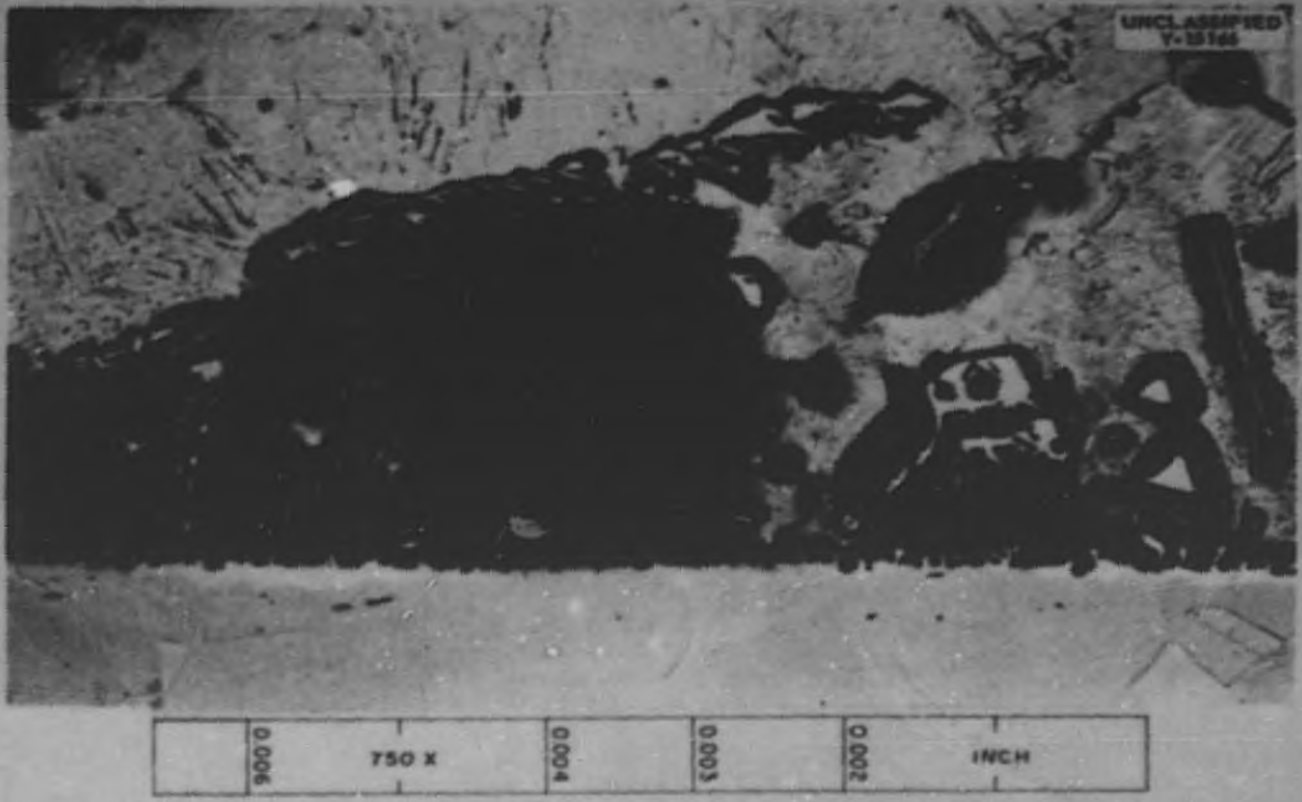

Fig. 5.20. Mass-Transferred Deposit on Cold Finger Exposed to Sodium Hydroxide at a Bucket Temperature of 700°C with a Temperature Differential of 100°C for 100 hr. 250X.

individual tests have been conducted in the "cold-finger" apparatus. Although some analyses of these tests are not complete, certain patterns of hydroxide are being observed.

The cold-finger apparatus, which was described previously,[9,10] consists of any externally heated bucket of hydroxide into which dips an air-cooled cold finger. Both the cold finger and the bucket are constructed of the metal being tested. Thermal gradients are observed between the outside of the bucket and the inside of the cold finger so that there is never thermocouple metal in the hydroxide bath. All tests have been run for 100 hr, except as otherwise noted, at the indicated maximum temperatures and temperature gradients under a flowing hydrogen atmosphere.

The sodium hydroxide used in this study is reagent grade. It is dehydrated in place under vacuum at 300°C for at least 8 hr followed by a minimum of 16 hr at 400°C. In some instances, previously dehydrated hydroxide is used, in which case, a rapid pumping at 400°C is deemed sufficient.

The metals studied to date have been nickel, Inconel, and Hastelloy B. Of these, nickel and Inconel show some promise of being suitable for use with the hydroxide at temperatures of the order of 600°C. Hastelloy B is by far the least resistant of the three to attack by the hydroxide, being badly corroded at 600°C.

The conditions and visual observations of the tests on nickel are presented in Table 5.14. In no case was oxidation corrosion observed. Mass transfer does occur at 600°C, as shown in Fig. 5.19. The cold fingers seen in Fig. 5.19 are nickel, with the exception of No. 19, which is Inconel. Bucket temperatures were 600, 630, 670, and 700°C for Nos. 17, 18, 20, and 21, respectively. The cold fingers were kept 100°C cooler than the corresponding buckets. The sequence shows clearly the very small amount of mass transfer at

UNCLASSIFIED
Y-14550

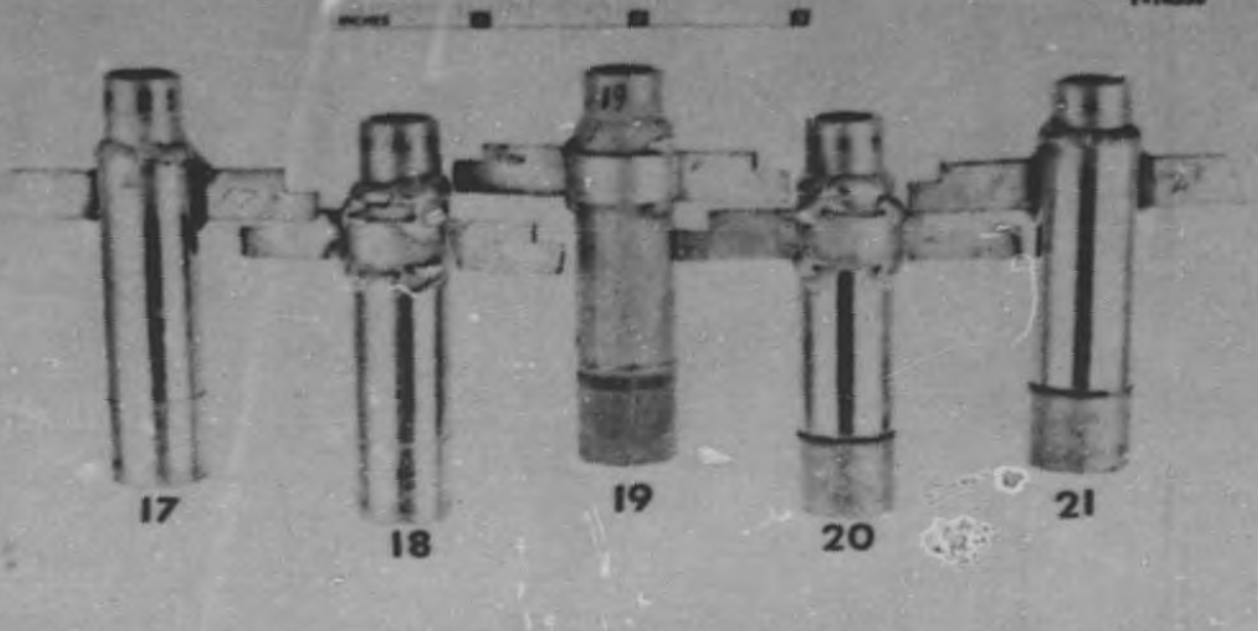

Fig. 5.19. Mass-Transferred Deposits on Nickel and Inconel Cold Fingers Exposed for 100 hr to Sodium Hydroxide. Numbers 17, 18, 20, and 21 are nickel and were exposed at bucket temperatures of 600, 630, 670, and 700°C, respectively, with a temperature differential of 100°C. Number 19 is Inconel and was exposed at a bucket temperature of 700°C with a temperature differential of 100°C.

---

[9] M. E. Steidlitz and W. H. Bridges, *ANP Quar. Prog. Rep. Mar. 10, 1953*, ORNL-1864, p 91.

[10] W. H. Bridges, *Met. Semiann. Prog. Rep. Apr. 10, 1954*, ORNL-1727, p 52.

UNCLASSIFIED
Y-14868

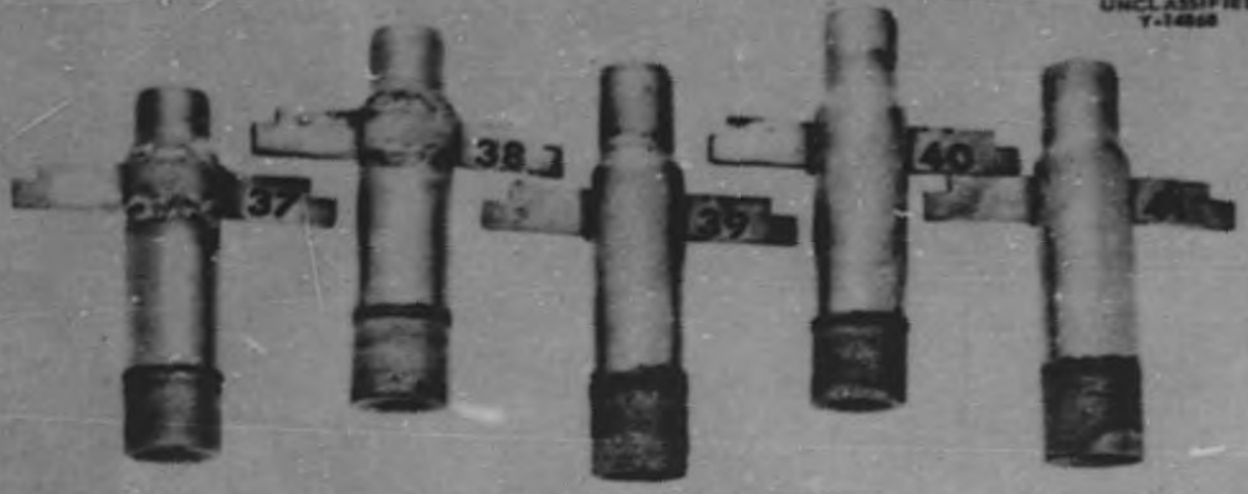

[redacted]

Fig. 5.21. Mass-Transferred Deposits on Nickel Cold Fingers Exposed for 100 hr to Sodium Hydroxide With and Without Various Additives. Cold finger maintained at 600°C; bucket maintained at 700°C; No. 37 exposed to sodium hydroxide with no additives; Nos. 38 through 41 exposed to sodium hydroxide containing 5% Na, 10% Na, 5% NaH, and 10% NaH, respectively.

TABLE 5.17. CORROSION AND MASS TRANSFER OF INCONEL IN SODIUM HYDROXIDE UNDER A HYDROGEN ATMOSPHERE FOR 100 hr

Bucket Temperature (°C)	Temperature Differential of System* (°C)	Number of Tests	Comments
450**	100	1	Brown deposit; no mass transfer
450	100	1	Clean; no mass transfer
550	200	3	Brown stain; no mass transfer
600	100	1	Brown stain; no mass transfer
600	200	1	Brown stain; no mass transfer
650	100	1	Brown stain; barely observable mass transfer
700	100	1	Brown stain; very little mass transfer
800	100	1	Rust color on bucket; medium mass transfer

*Bucket temperature less the cold-finger temperature.
**This test was made under a helium atmosphere.

nickel, but the Inconel corroded to some extent. Specimen No. 19 of Fig. 5.19 is an Inconel cold finger tested under the same conditions as was the nickel specimen No. 21. The metal deposit on No. 19 is less than that on No. 21, but the tarnish on No. 19 indicates that there was some corrosion. Therefore, in the remaining Inconel tests, the Inconel bucket (that is, the hot zone) was examined for corrosion. Inconel buckets that were exposed to sodium hydroxide at bucket temperatures from 450 to 800°C are shown in Figs. 5.22 through 5.26. It is most interesting to note the change in type and extent of attack that occurs between 600 and 650°C. At 600°C and below, 1 to 2 mils of grain-boundary attack may be seen both on the inside and outside wall of the bucket. The attack on the outside wall was caused by hydroxide that crept out over the bucket lip. Above 600°C, an oxidized layer formed that was 3 to 15 mils in depth. This temperature sensitivity is, as yet, unexplained.

Other metals are to be studied in an attempt to raise the temperature limit at which no mass transfer occurs. It is hoped that questions such as what causes the change in rate and type of attack in the 600 to 700°C range will also be resolved.

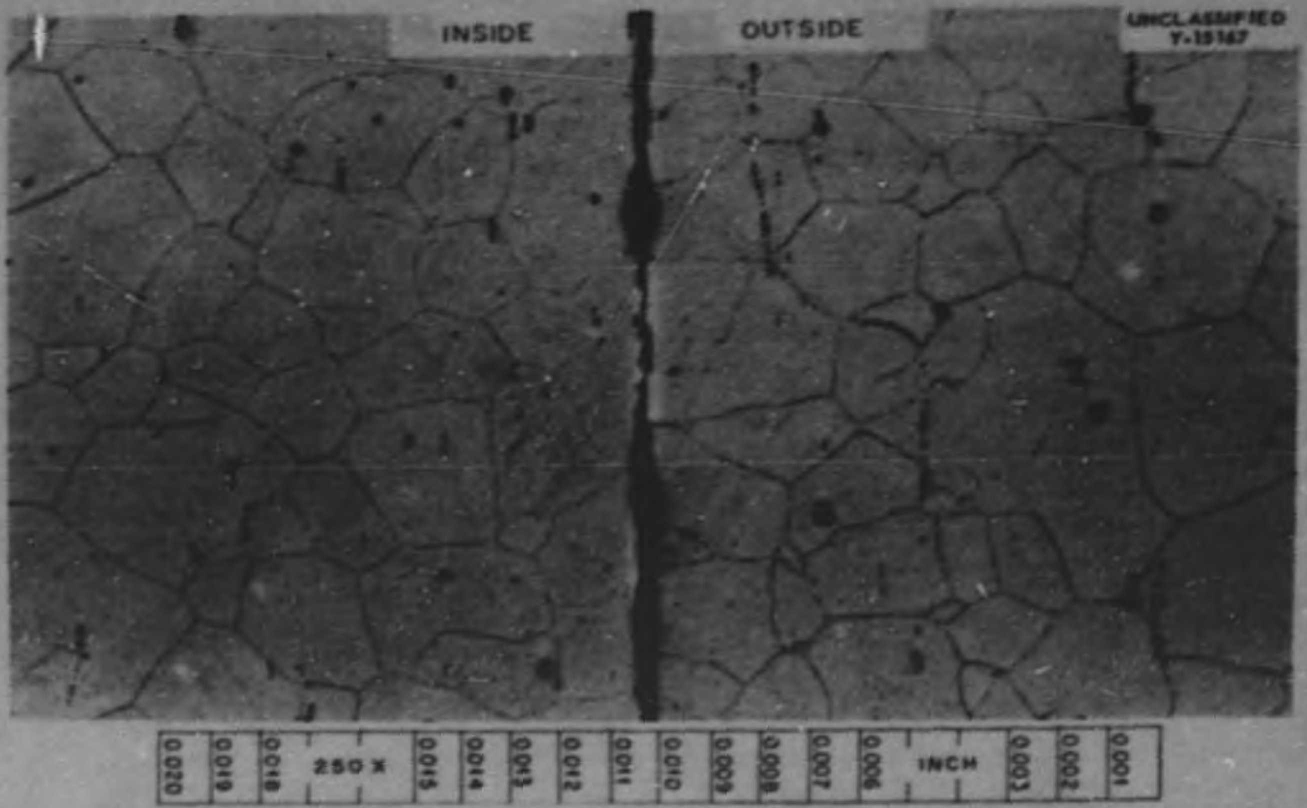

Fig. 5.22. Inconel Bucket Exposed to Sodium Hydroxide for 100 hr. Bucket temperature, 450°C; cold-finger temperature, 350°C. 250X.

CHEMICAL STUDIES OF CORROSION

F. Kertesz
Materials Chemistry Division

Corrosion of Inconel by LiF-BeF$_2$ and by LiF-BeF$_2$-UF$_4$

H. J. Buttram R. E. Meadows
Materials Chemistry Division

Inconel capsules containing the BeF$_2$-bearing mixtures LiF-BeF$_2$ (69-31 mole %) and LiF-BeF$_2$-UF$_4$ (67.3-30.2-2.5 mole %) were tested for corrosion in tilting-furnace tests. After 100-hr exposures, metallographic observations of the capsule walls revealed no attack; chemical analyses confirmed these findings. The chromium concentration was found to be about 250 ppm in the LiF-BeF$_2$ mixture and 400+ ppm in the UF$_4$-containing analog. These results are of the same order of magnitude as those obtained for the ZrF-base mixtures.

Effect of UF$_3$-UF$_4$ Mixtures on Corrosion of Inconel by Various Solvents

H. J. Buttram R. E. Meadows
Materials Chemistry Division

Incidental to attempts to study the disproportionation of UF$_3$, confirmation of the beneficial effect of UF$_3$ on corrosion of Inconel by NaF-ZrF$_4$ (53-47 mole %) and NaF-KF-LiF (11.5-42-46.5 mole %) was obtained. A series of UF$_3$-UF$_4$ mixtures in these solvents was heated in Inconel capsules. The contents were analyzed for total uranium and trivalent uranium after testing in the tilting furnace or under static conditions. Considerable dispro-

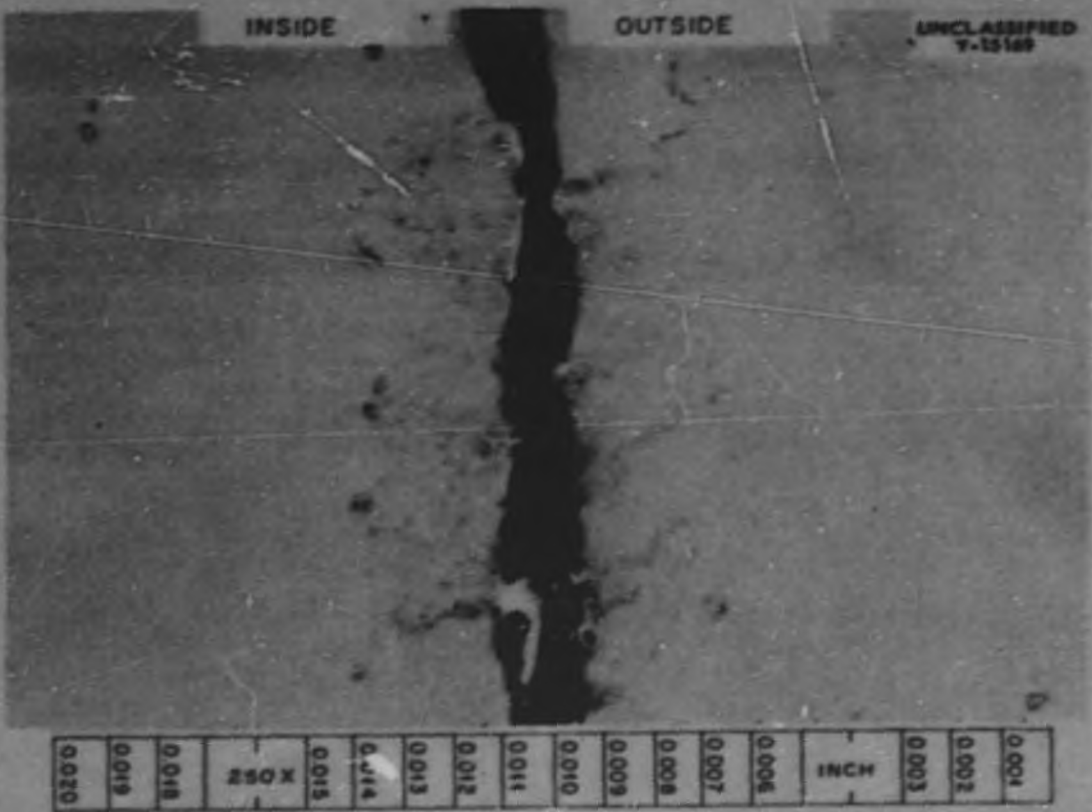

Fig. 5.23. Inconel Bucket Exposed to Sodium Hydroxide for 100 hr. Bucket temperature, 600°C; cold-finger temperature, 500°C. 750X.

portionation of the added UF_3 was observed in both solvents, especially when the UF_4/UF_3 ratio was low; the NaF-KF-LiF mixtures showed, in each case, more disporportionation than did the NaF-ZrF_4 solutions.

Analyses of the melts for chromium revealed that the beneficial effect of UF_3 on corrosion of Inconel was again demonstrated. If a plot is made of chromium concentration after testing as a function of the starting UF_3/UF_4 ratio, it is seen that a small percentage of UF_3 (UF_3/UF_4 − 0.2) causes a sharp decrease in the amount of chromium removed from the Inconel walls. Increasing the UF_3 content up to a 50-50 mixture with UF_4 was found to be beneficial, but any further increase in the UF_3/UF_4 ratio apparently had little effect.

Studies of the Sodium Hydroxide–Nickel Reaction

F. Kertesz F. A. Knox
Materials Chemistry Division

During previous work on the equilibrium hydrogen pressure of the sodium hydroxide–nickel reaction, it was found that the reproducibility was somewhat poor. Similar difficulties were observed during determinations of the equilibrium solubility of the metal in molten hydroxide. In studying the possible reaction

$$2NaOH + Ni \longrightarrow Na_2O\text{-}NiO + H_2$$

the hydrogen pressure or the nickel concentration was determined as a function of time and temperature. The hydrogen pressure was measured with

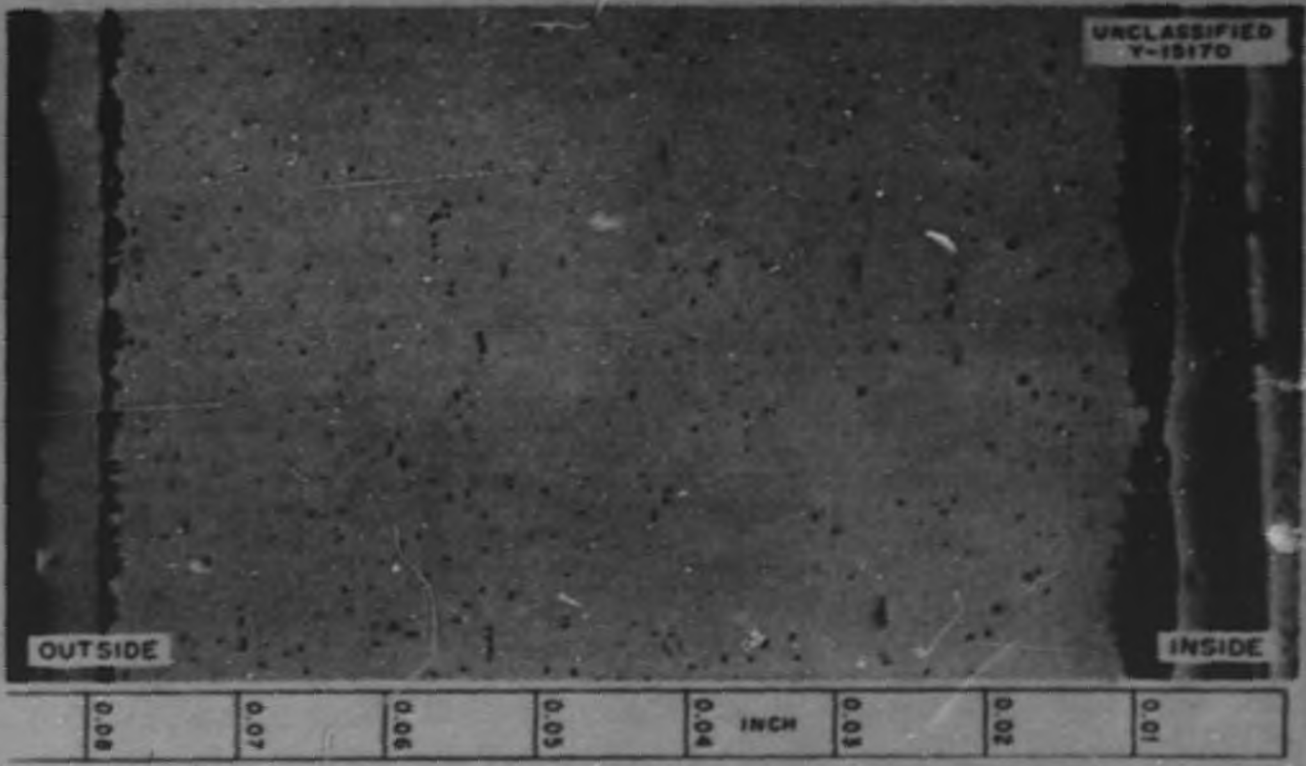

Fig. 5.24. Inconel Bucket Exposed to Sodium Hydroxide for 100 hr. Bucket temperature, 650°C; cold-finger temperature, 550°C. 75X.

the reaction chamber connected to a manometer, and the nickel concentration was determined by analyzing the contents of a quartz-jacketed metal capsule after the desired exposure time. Since the two sets of data were necessarily determined on separate systems, there was the possibility of unknown variables being present, even though every effort was made to keep the variables identical.

This experimental difficulty has recently been counteracted by constructing an apparatus that makes possible simultaneous determinations of the hydrogen equilibrium pressures and the equilibrium nickel solubility. A charge of purified sodium hydroxide is loaded into a hydrogen-fired nickel capsule which is sealed under helium and then placed in a quartz tube that is evacuated and sealed. The jacketed capsule is heated to the test temperature for the desired time period. If the exposure is sufficiently long, the hydrogen pressure developed should be in equilibrium with the melt, since it should not diffuse through the quartz. The pressure should be nearly equal inside and outside the nickel capsule, because hydrogen diffuses easily through this metal at the temperatures used. Upon completion of the high-temperature exposure, the capsule is placed in a flanged metallic cylinder which, after evacuation, is connected to a mercury manometer. A small metal pin held near the quartz capsule by a metallic bellows extending through a lateral hole in the cylinder can then be tapped to break the quartz jacket. The pressure established in the system can be read on the manometer, and a simple calculation will give the pressure inside the quartz capsule before it was broken.

Calibration tests with capsules containing hydrogen at a known pressure showed that the

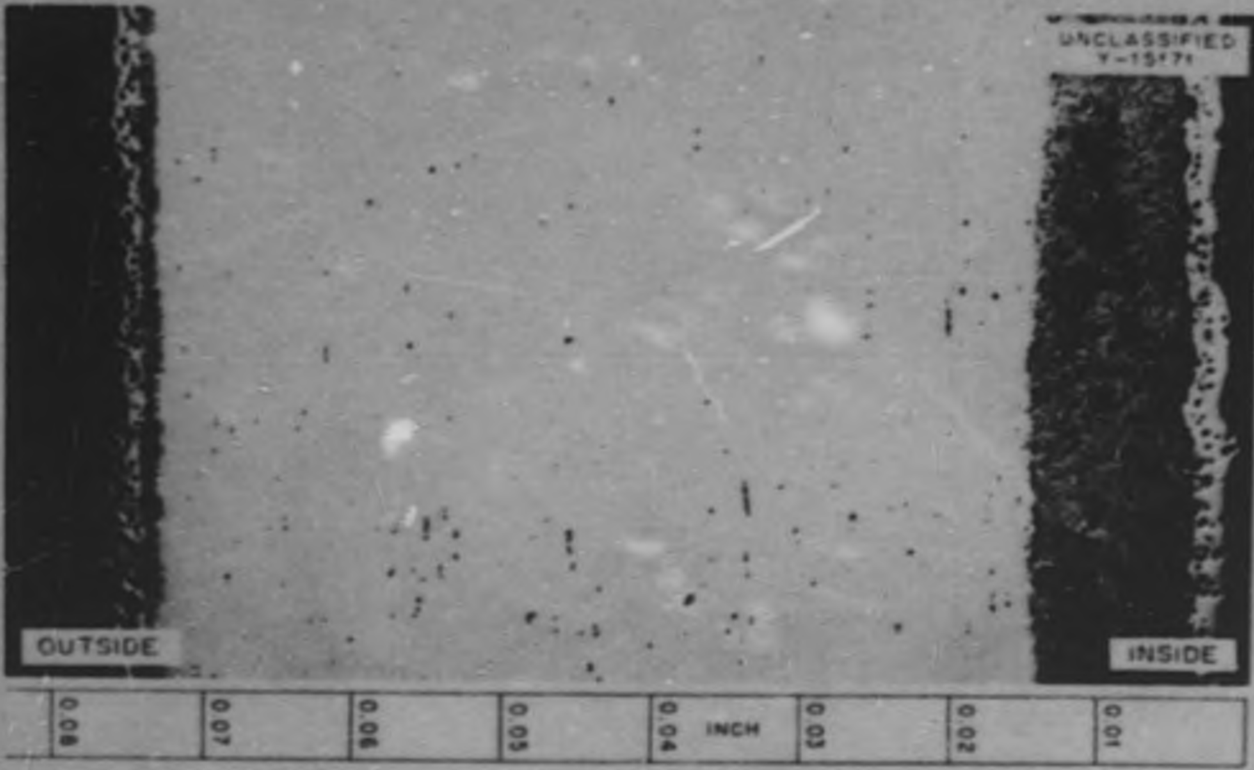

Fig. 5.25. Inconel Bucket Exposed to Sodium Hydroxide for 100 hr. Bucket temperature, 700°C; cold-finger temperature, 600°C. 75X.

method allowed pressures to be determined to within 1%. After the pressure measurement the nickel capsule was opened and the hydroxide was leached out, with the total alkalinity and the dissolved nickel being determined on the same sample.

Some of the quartz-jacketed nickel capsules containing sodium hydroxide were kept at 800°C for various lengths of time in order to ascertain the time necessary to reach equilibrium. Runs for long periods of time were unsuccessful because of failure of the nickel capsules. It was found that the nickel content of the hydroxide remained nearly constant when the time of exposure was varied considerably, which would indicate that equilibrium was reached after a short exposure time. The hydrogen pressures determined by this method did not level off as expected, and the resulting pressure was found to be greatly in excess of that to be expected from consideration of the reaction postulated.

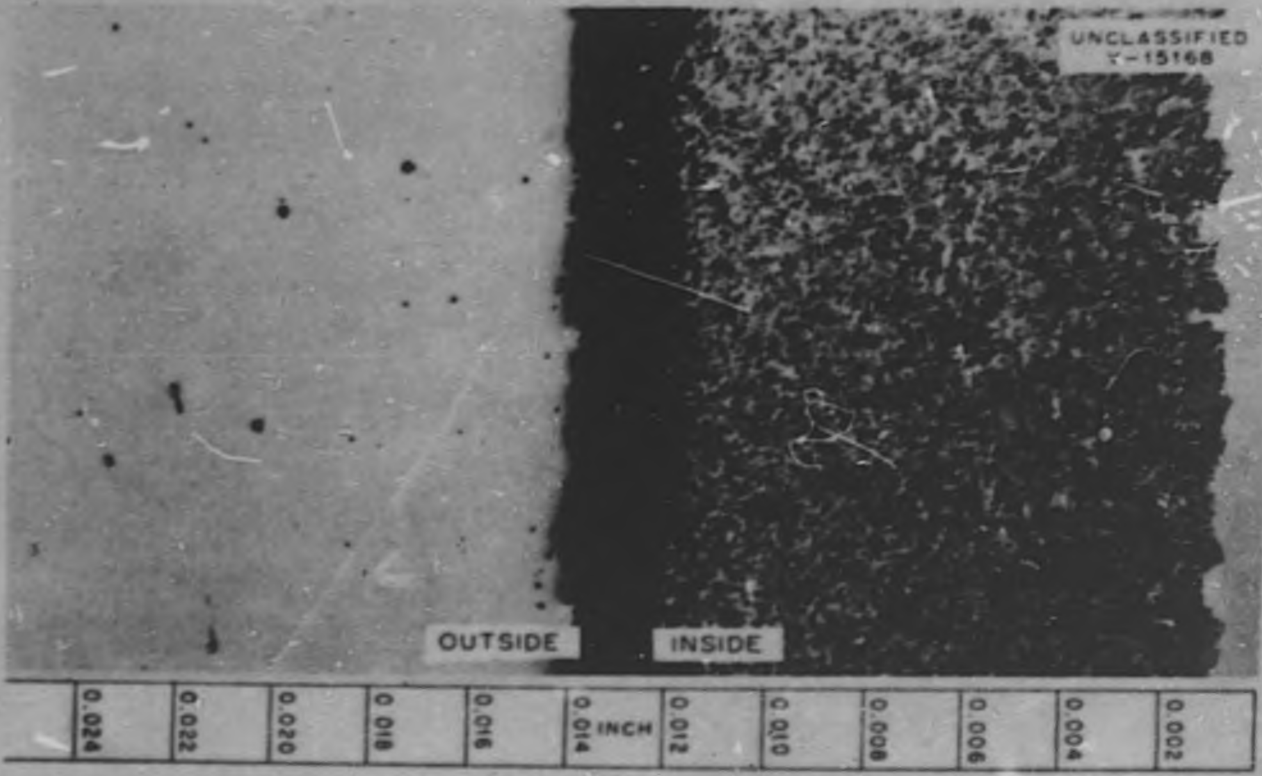

Fig. 5.26. Inconel Bucket Exposed to Sodium Hydroxide for 100 hr. Bucket temperature, 800°C; cold-finger temperature, 700°C. 250X.

6. METALLURGY AND CERAMICS

W. D. Manly J. M. Warde
Metallurgy Division

Additional fabrication studies of Hastelloy B have increased the evidence that the poor high-temperature fabricability is related to the impurity content from which the strength may be derived. Several nickel-molybdenum binary and ternary alloys were studied in oxidation tests and in room- and elevated-temperature tensile tests. The ternary alloys all included 20% molybdenum plus nickel and a third heavy element. The results of additional stress-rupture and tensile property studies of the nickel-molybdenum alloys are presented. For comparison with previously obtained data on the static oxidation of several brazing alloys, cyclic tests were run; the static and cyclic data were similar for tests at 1500°F. Cyclic tests at 1700°F are under way.

Fabrication was completed of a 20-tube Inconel fuel-to-NaK heat exchanger, the fuel-to-NaK intermediate heat exchanger No. 2, two 500-kw NaK-to-air radiators, and a liquid metal-to-air radiator designed by the Cornell Aeronautical Laboratory.

Special extrusions were made of three billets of vanadium and four high-purity molybdenum billets containing 0.7% titanium, and studies of flow patterns of duplex and three-ply materials during impact extrusion were continued. The fabrication of clad columbium was investigated, and diffusion barrier studies were made. Additional information was obtained on the properties of B_4C-Cu mixtures and a magnesium-lithium alloy that are being considered as possible shielding materials.

Several type 310 stainless-steel-clad columbium thermal-convection loops were fabricated for corrosion testing, and the brazing of cermets to Inconel was investigated. An Inconel spun core of the configuration proposed for the ART core was found to be dimensionally stable after thermal cycling.

Rare-earth ceramics for use in control rods were formed into the proper shapes for testing in critical assemblies.

DEVELOPMENT OF NICKEL-MOLYBDENUM ALLOYS

J. H. Coobs H. Inouye
Metallurgy Division

M. R. D'Amore
Pratt & Whitney Aircraft

Fabrication Studies

Hastelloy B. Two impact extrusions of Hastelloy B rod were made at 2000°F with good recovery of sound material. The billets were prepared from a vacuum-melted ingot of commercial Hastelloy B and were extruded in the as-cast condition. During subsequent hot reduction of the extruded rod to sheet, the material cracked severely, and no usable material was obtained.

Two extruded tube blanks that had been shipped to the Superior Tube Co. for reduction to small-diameter tubing were processed; one blank was made from wrought material and the other from cast material. The tube blank made from a vacuum-melted cast billet fractured during the first reduction operation, but the blank made from a wrought billet was successfully processed from 1.5-in.-OD, 0.250-in.-wall to 0.187-in.-OD, 0.017-in.-wall seamless tubing. It was found that severe reduction schedules were permissible and that intermediate stress-relieving heat treatments were unnecessary.

Previously reported experiments[1] showed that higher extrusion ratios were attainable if the Hastelloy B billet was canned in Inconel. Therefore wrought Hastelloy B billets with and without Inconel cans have been prepared for further tube extrusion experiments.

Attempts to roll extruded Hastelloy B rod at 2000°F were unsuccessful; the material cracked severely after several 5% reduction passes. Since 0.03% cerium additions had previously[2] been found to improve the high-temperature fabricability of Hastelloy B, additional melts were prepared with various quantities of cerium added in the form of an 11% Ce–89% Al master alloy. A small vacuum melt containing 0.3% cerium cracked during hot reduction, and in subsequent experiments it was shown that a maximum of 0.1% cerium was useful in improving the high-temperature fabricability.

---

[1] H. Inouye and J. H. Coobs, *ANP Quar. Prog. Rep. Dec. 10, 1954*, ORNL-1816, p 100.

[2] H. Inouye, J. H. Coobs, and M. R. D'Amore, *ANP Quar. Prog. Rep. Mar. 10, 1955*, ORNL-1864, p 97.

An alloy with the nominal Hastelloy B composition, 4% Fe–28% Mo–68% Ni, but without the tramp elements vanadium, silicon, manganese, cobalt, chromium, tungsten, and aluminum, was prepared for evaluating the effects of impurities on the fabrication properties of Hastelloy B. Three-pound vacuum melted slab ingots 0.500 in. thick were prepared and rolled at 2100°F to 0.150-in.-thick sheet. This material showed no tendency to crack during hot rolling under moderate reduction schedules. The microstructure of the alloy in the as-cast condition showed random distribution of a second phase, which appeared to be an oxide. The source of this phase might be traced to the starting material or the melting practice. It is becoming increasingly evident that the poor high-temperature fabricability of Hastelloy B is related to the impurity content. However, since the superior strength of commercial Hastelloy B in comparison with that of Inconel might be derived from these impurities, mechanical property tests of the pure 4% Fe–28% Mo–68% Ni alloy are under way. The preliminary room-temperature tensile data, presented in Table 6.1, are encouraging in that they show the tensile strength and ductility to be comparable to those of the commercial alloy under these test conditions. Additional mechanical property tests are under way.

TABLE 6.1. ROOM-TEMPERATURE TENSILE STRENGTH OF THE 4% Fe–28% Mo–68% Ni ALLOY

Condition	Tensile Strength (psi)	Elongation (%)
Annealed	130,000	60
Annealed, aged 500 hr at 1300°F	137,000	2.5

Nickel-Molybdenum Binary Alloys. The previously reported[3] work on nickel-molybdenum binary alloys was extended by a study of an 85% Ni–15% Mo alloy. The alloys studied previously were 80% Ni–20% Mo, 76% Ni–24% Mo, and 68% Ni–32% Mo. An oxidation test of the 85% Ni–15% Mo alloy at 1500°F in static air indicated a lower rate of oxidation than that observed for the 80% Ni–20% Mo alloy, but a higher rate than the rates for the 76% Ni–24% Mo and 68% Ni–32% Mo alloys. Therefore additional oxidation tests are planned to supplement the present data. The presently available data appear to indicate that the rate of oxidation of these binary nickel-molybdenum alloys is not a function of the molybdenum content. Two thermal-convection loops for circulating fluoride mixture in the 85% Ni–15% Mo tubing are being fabricated.

Both room- and elevated-temperature (1100 to 1650°F) tensile tests of this alloy have been completed. Erratic results were obtained in the room-temperature tests of specimens aged 284 hr at elevated temperatures (1300 to 1650°F). The tensile strength was low at all test temperatures, and low elongations were observed at test temperatures above 1300°F. The results of these tests are given in Table 6.2.

Nickel-Molybdenum Ternary Alloys. A screening program was initiated in order to observe the effects of additions of alloying elements to nickel-molybdenum alloys. The alloy compositions investigated have all included 20% molybdenum plus nickel and a third element. The ternary systems that have been evaluated are:

2 to 10% Cb–20% Mo–bal Ni
3 to 10% Cr–20% Mo–bal Ni
2% Al–20% Mo–78% Ni
2% V–20% Mo–78% Ni
1% Zr–20% Mo–79% Ni
1% Ti–20% Mo–79% Ni

The physical property data obtained for alloys containing 2 to 10% columbium were reported previously.[4] The aluminum-molybdenum-nickel alloys were investigated because of the exceptional creep properties reported in the literature for this alloy system. Hot-forgeability studies were conducted on 100-g arc melts containing from 2 to 10% aluminum, but only the alloys containing less than 5% aluminum were found to be forgeable at 2100°F. Further studies will be conducted on this alloy system.

Vanadium, zirconium, and titanium additions were investigated in an effort to improve the elevated-temperature ductility of the 20% Mo–80% Ni alloy. No difficulties were experienced in the hot rolling of these alloys.

Preliminary room-temperature tensile strength data for the alloys containing aluminum, vanadium, zirconium, and titanium in both the annealed and aged conditions are presented in Table 6.3. All specimens aged at 1650°F for long periods of time

---

[3] H. Inouye and J. H. Coobs, *ANP Quar. Prog. Rep. Dec. 10, 1954*, ORNL-1816, p 103.

[4] *Ibid.*, p 100.

TABLE 6.2. RESULTS OF TENSILE TESTS OF AN 85% Ni–15% Mo ALLOY

Condition of Test Specimen*	Test Temperature (°F)	Yield Point, 0.2% Offset (psi)	Tensile Strength (psi)	Elongation in 2-in. Gage Lengths (%)
Annealed 1 hr at 2100°F	Room	32,100	60,400	15
Annealed, aged 284 hr at 1300°F	Room	32,700	70,200	17.5
Annealed, aged 284 hr at 1500°F	Room	32,000	99,700	50
Annealed, aged 284 hr at 1650°F	Room	31,500	68,400	21
Annealed 1 hr at 2100°F	1100	18,700	39,900	16.5
	1300	17,850	30,300	7.5
	1500	17,000	26,000	5.0
	1600	16,600	23,200	6.3
	1650	16,000	20,700	9.0

*Sheet, 0.065 in. thick.

TABLE 6.3. ROOM-TEMPERATURE TENSILE STRENGTHS OF SEVERAL NICKEL-MOLYBDENUM BASE TERNARY ALLOYS

Alloy Composition (wt %)	Condition of Test Specimen	Tensile Strength (psi)	Elongation (%)
2 Al–20 Mo–78 Ni	Annealed	150,500	32
	Annealed, aged 500 hr at 1500°F	118,500	59
	Annealed, aged 284 hr at 1650°F	70,500	12
2 V–20 Mo–78 Ni	Annealed	117,000	32
	Annealed, aged 284 hr at 1300°F	127,000	30
1 Zr–20 Mo–79 Ni	Annealed	101,000	33
	Annealed, aged 284 hr at 1300°F	115,000	58
1 Ti–20 Mo–79 Ni	Annealed	115,000	60
	Aged 284 hr at 1650°F	73,700	15.5

show lower strengths and ductilities than those unaged or aged at lower temperatures. The specimens aged at 1650°F were exposed to a hydrogen atmosphere, while the other specimens were treated under a helium atmosphere or in evacuated quartz capsules. The possibility of hydrogen embrittlement of the specimens aged at 1650°F is being investigated.

The alloys containing 3 to 10% chromium have been evaluated in oxidation, stress-rupture, and tensile tests. The quantity of seamless tubing made for corrosion testing has been limited, however, because of shattering during extrusion. Although sound rod and tube blanks have been made at an extrusion temperature of 2200°F, consistent results could not be obtained. A study of these alloys has led to the supposition that the shrink cavities within the ingot are the cause of the fracturing. The billets are currently being inspected, by x-ray and gamma-radiation techniques, prior to extrusion, in an effort to correlate the soundness of the starting material with the extrusion result.

The hot rolling of extruded rods of chromium-molybdenum-nickel alloys in the 1950 to 2200°F temperature range was unsuccessful because of severe cracking. Subsequent studies showed that the hot shortness was probably caused by oxygen contamination of the electrolytic chromium used. It was found that additions of 0.1% cerium for each 3% chromium in the melt would render these alloys hot forgeable. Further experiments have been conducted with 100-g arc melts containing up to 2% titanium and 2% aluminum as deoxidants. The aluminum additions were found to be ineffective, but the titanium additions served to reduce the hot shortness. It was determined that approximately 2% titanium would render a 5% Cr–20% Mo–75% Ni alloy completely hot forgeable. The extruded rods of the hot-short alloys could readily be rolled to sheet at room temperature. Work-hardening data for a 3% Cr–20% Mo–77% Ni alloy are presented in Table 6.4. The alloys containing between 3 and 10% chromium work-hardened at the same rate.

TABLE 6.4. WORK-HARDENING OF A 3% Cr–20% Mo–77% Ni ALLOY

Reduction (%)	Hardness (VPN)
0	168
10.4	260
21.1	312
30.9	337
45.5	409
52.4	441
63.1	480

Room-temperature tensile strength data for chromium-molybdenum-nickel specimens subjected to various heat treatments are listed in Table 6.5. The data reported are the average of the results of two to three tests of each alloy. Included in the tests were alloys that contained additions of 0.5% columbium or up to 0.25% cerium. The minor additions of columbium appeared to increase slightly the tensile strength and ductility of these alloys, and an average decrease of 5% in elongation and a slight increase in tensile strength were noted for the alloys with small amounts of cerium added.

The elevated-temperature tensile strengths of chromium-molybdenum-nickel alloy specimens after various aging treatments are given in Table 6.6. All the specimens were tested at the aging temperatures listed. The results are given for single tests. The elevated-temperature ductilities of these alloys are low compared with the ductilities at room temperature. The minor additions of cerium apparently aided in obtaining higher elevated-temperature strengths in these alloys, but more tests are needed to verify this observation. No relationship between the physical properties and the chromium content is readily apparent in either room- or elevated-temperature tests.

In the temperature range above 1300°F the alloys containing up to 10% chromium appear to be single-

TABLE 6.5. ROOM-TEMPERATURE TENSILE STRENGTH DATA FOR CHROMIUM-MOLYBDENUM-NICKEL ALLOY SHEET SPECIMENS

Aging Time: minimum, 284 hr; maximum, 500 hr

Alloy Composition (wt %)	Condition of Test Specimen	Tensile Strength (psi)	Elongation (%)
3 Cr–20 Mo–77 Ni	Annealed	107,000	61
	Aged at 1300°F	109,500	60
	Aged at 1500°F	111,100	64
	Aged at 1650°F	67,500	19
5 Cr–20 Mo–75 Ni	Annealed	120,000	58
	Aged at 1300°F	119,000	59
	Aged at 1500°F	115,000	62
	Aged at 1650°F	72,500	14
7 Cr–20 Mo–73 Ni	Annealed	116,000	63
	Aged at 1300°F	116,000	63
	Aged at 1500°F	114,000	59
	Aged at 1650°F	69,000	14
10 Cr–20 Mo–70 Ni	Annealed	110,500	71
	Aged at 1300°F	111,600	63

TABLE 6.6. ELEVATED-TEMPERATURE TENSILE STRENGTH DATA FOR CHROMIUM-MOLYBDENUM-NICKEL ALLOY SHEET SPECIMENS

Alloy Composition (wt %)	Aging Treatment		Tensile Strength (psi)	Elongation (%)
	(hr)	(°F)		
3 Cr–20 Mo–77 Ni	500	1300	33,200	6.3
	500	1500	27,300	5.0
	284	1650	26,100	19.0
3 Cr–0.5 Cb–20 Mo–76.5 Ni	362	1300	38,100	6.3
	362	1500	30,000	5.0
5 Cr–0.5 Cb–20 Mo–74.5 Ni	500	1300	39,500	7.5
	500	1500	29,400	5.0
5 Cr–0.25 Ce–20 Mo–74.75 Ni	362	1300	59,700	16.5
	362	1500	43,100	11.0*
7 Cr–20 Mo–73 Ni	362	1300	40,800	9.0
	362	1500	29,800	3.5*
7 Cr–0.5 Cb–20 Mo–72.5 Ni	500	1300	48,800	12.5
	500	1500	38,500	7.5
	284	1650	29,800	3.8
7 Cr–0.1 Ce–20 Mo–72.9 Ni	362	1300	54,500	17.5
	362	1500	40,500	8.8*
10 Cr–0.5 Cb–20 Mo–69.5 Ni	500	1300	38,300	8.8
	500	1500	43,600	9.0
	284	1650	29,900	6.3

*Specimen fractured outside 2-in. gage length.

phase. Additional studies of the microstructures will be conducted on alloys made with high-purity chromium as the starting material. Further evidence of the equilibrium structure is shown in aged specimens. No significant changes in tensile strength or ductility are observed in specimens aged at 1300 and 1500°F. The low strength and ductilities of specimens aged at 1650°F may have been caused by the hydrogen atmosphere used during the aging treatment. Aging treatments at temperatures other than 1650°F were accomplished either in evacuated quartz tubes or under a helium atmosphere.

The results of stress-rupture tests (presented later in this section) have shown low strengths and ductilities for most of these alloys and indicate that vacuum melting alone is not sufficient to obtain optimum properties. The possibility of increasing the strength and the ductility through cerium additions appears to be promising, since the alloys with cerium additions have shown better physical properties during stress-rupture testing. It has become apparent that improved deoxidation practices are necessary in melting these alloys, and efforts are being directed toward the production of sounder ingots.

Oxidation Studies

Oxidation studies were continued on nickel-molybdenum alloys containing from 3 to 10% chromium. The results reported previously[5] for these alloys were based on oxidation tests of small arc-melted specimens that had not been chemically analyzed. The alloys have therefore been retested by using specimens from chemically analyzed heats of material, and the results are presented in Table 6.7. In comparison with the previous results, the oxidation rate for the 3% chromium composition was slightly lower, and increases were noted for the alloys containing 5, 7, and 10%

---

[5] H. Inouye and M. R. D'Amore, *ANP Quar. Prog. Rep. Mar. 10, 1955*, ORNL-1864, p 104.

TABLE 6.7. OXIDATION OF CHROMIUM-MOLYBDENUM-NICKEL ALLOY DURING 168 hr AT 1500°F IN STATIC AIR

Alloy Composition (wt %)	Weight Gain (mg/cm^2)	Remarks
3 Cr–20 Mo–77 Ni	5.17	Oxide spalled completely during cooling to room temperature
5 Cr–20 Mo–75 Ni	5.30	Oxide spalled completely during cooling to room temperature
7 Cr–20 Mo–73 Ni	3.14	Oxide spalled badly during cooling to room temperature
10 Cr–20 Mo–70 Ni	0.45	No spalling occurred

chromium. It appears that about 10% chromium is necessary to form a nonspalling protective oxide on the ternary alloy. However, it has been observed that the oxidation rate under static conditions can be reduced 50% by the addition of 3% chromium.

STRESS-RUPTURE STUDIES OF NICKEL-MOLYBDENUM ALLOYS

D. A. Douglas J. H. DeVan
J. W. Woods
Metallurgy Division

Hastelloy B

A series of creep-rupture tests on Hastelloy B in the solution-annealed condition has been completed in an argon atmosphere at 1500 and 1650°F. The results are summarized in the design curves presented in Figs. 6.1 and 6.2. A similar series of tests in fused salts is nearing completion that provides an interesting comparison with the argon results.

Stress-rupture plots are presented in Fig. 6.3 for Hastelloy B in the two environments at 1300, 1500, and 1650°F, and it may be noted that at each temperature the values obtained in fused salts are actually superior to those obtained in argon. Although no adverse effect on physical properties was expected, in view of the absence of corrosive attack of the fused salts on Hastelloy B under static conditions, the reason for the increase in rupture strength is not entirely clear at present.

The test chamber must be flushed with a cleaning charge before the fluoride mixture to be used for the test is admitted, and therefore the specimens tested in fused salts were at temperature approximately 5 hr longer before stress was applied than were the specimens tested in argon. Consequently, the slightly longer aging of the specimens tested in the fused salt may account for the improvement in strength. There are objections to this theory, however. A specimen aged 70 hr prior to stressing and testing in argon showed inferior properties relative to those of a comparable unaged specimen tested in argon. Also, there is some doubt as to whether aging can account for the improvement at 1650°F, since the phase diagram, if minor elements are neglected, indicates a one-phase region at this temperature. (Photomicrographs, however, have shown evidence that aging at this temperature under stress does occur.) Other tests are being carried out to establish the exact causes for the apparent anomaly in strengths in the two environments.

Tests in hydrogen and air also have been made in order to determine the effects of these environments on the creep-rupture properties of Hastelloy B at 1500°F. The creep curves obtained at 12,000 psi in hydrogen, argon, air, and fused salt are shown in Fig. 6.4. In comparison with the effect of argon, the effect of hydrogen is apparently negligible, and the effect of air follows closely the pattern observed for Inconel and "A" nickel in air, insofar as reduced creep rate and longer rupture life are concerned. However, the final elongations of Hastelloy B in air are equivalent to or lower than those in argon, whereas the elongation of other nickel-base alloys are markedly greater in air than in argon. A test program similar to that carried out on solution-annealed Hastelloy B has been initiated on solution-annealed specimens aged 100 hr at 1300°F to determine

UNCLASSIFIED
ORNL-LR-DWG 7558

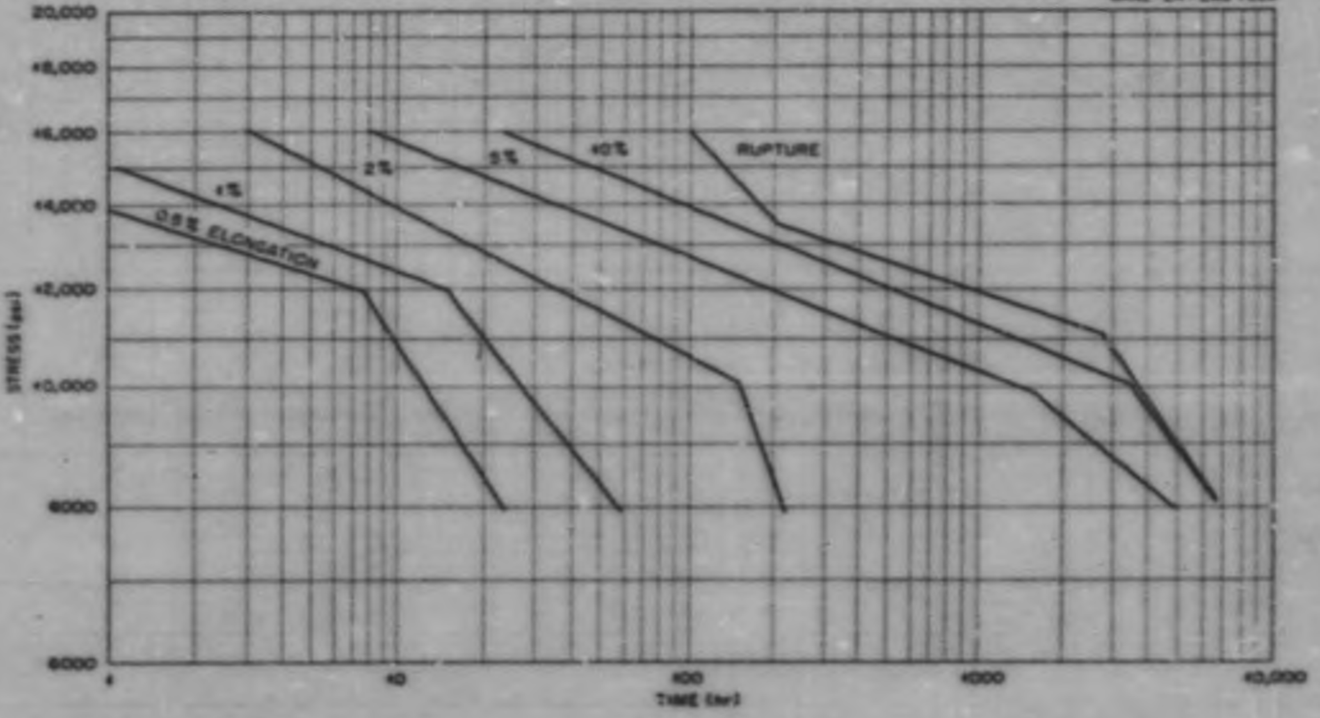

Fig. 6.1. Stress-Rupture Curves for 0.060-in.-Thick Sheet Specimens of Hastelloy B Solution-Annealed at 2100°F and Tested in Argon at 1500°F.

whether aging treatment results in serious embrittlement at service temperatures.

Modified Nickel-Molybdenum Alloys

Creep-rupture tests of modified nickel-molybdenum alloys at 1500°F in argon are under way. The results of tests on these alloys, prepared by vacuum melting, have been somewhat disappointing with respect to ductility attained before rupture. It is currently believed that the low ductility may be attributed to melting practice rather than to the nature of the alloy systems. A heat to which a small amount of deoxidant was added showed a significant improvement in properties compared with those of other single-phase alloys tested to date. The alloy had the composition 74.75% Ni–20% Mo–5% Cr–0.25% Ce and was inferior to Hastelloy B from the standpoint of rupture strength, but, at 8000 psi, it had a final elongation of 28% compared with 16% for Hastelloy B and 7% for a similar alloy to which no deoxidant (cerium) was added. The results of recent creep-rupture tests of several modified nickel-molybdenum alloys are presented in Table 6.8.

TENSILE PROPERTIES OF HASTELLOY B

P. Patriarca R. E. Clausing
Metallurgy Division

It has been shown[6] that the physical properties of wrought Hastelloy B alloy are directly influenced by the precipitation which occurs at temperatures within the intended operational range of ANP reactors and heat exchangers. An extensive program is now under way to obtain short-time tensile strength data for this material after heating at temperatures from 1100 to 1600°F for times from 100 to 1000 hr. Typical microstructures obtained from these heat treatments have been studied and photographed, and a correlation is being made

---

[6] P. Patriarca *et al.*, *ANP Quar. Prog. Rep. Mar. 10, 1955*, ORNL-1864, p 116.

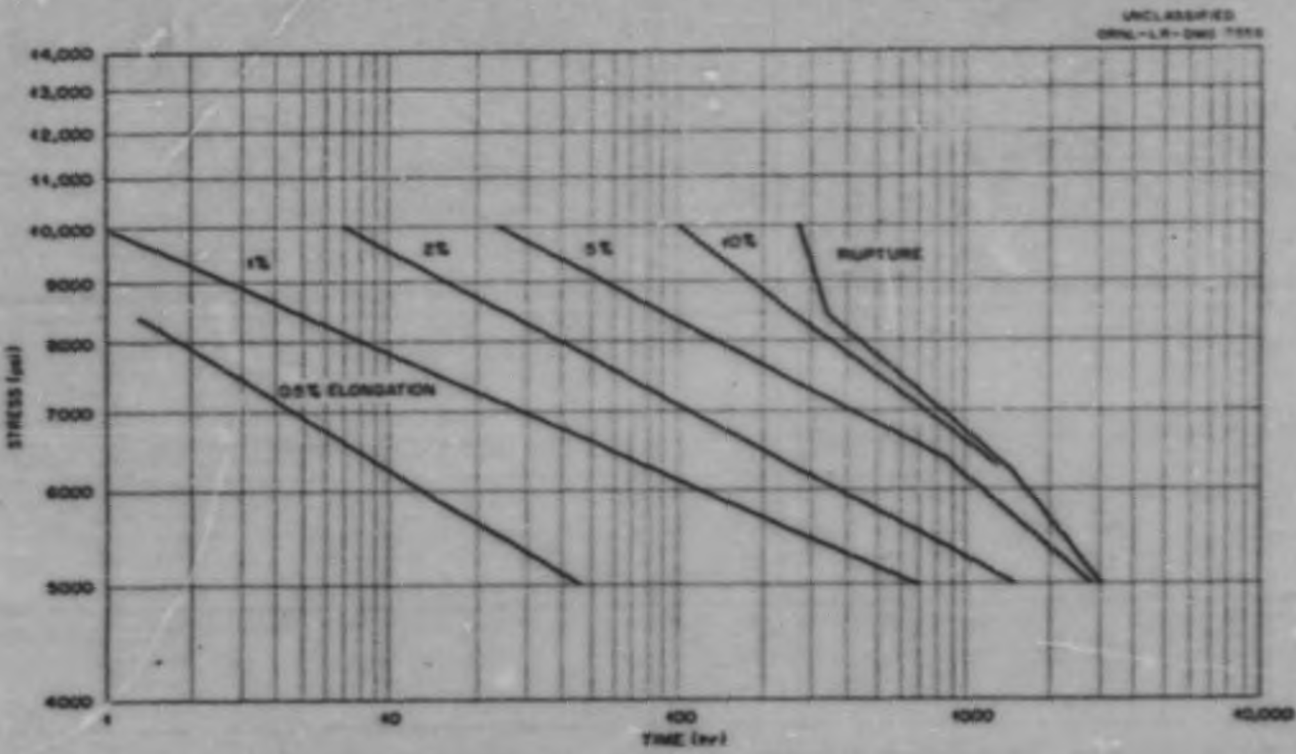

Fig. 6.2. Stress-Rupture Curves for 0.060-in.-Thick Sheet Specimens of Hastelloy B Solution-Annealed at 2100°F and Tested in Argon at 1650°F.

TABLE 6.8. CREEP-RUPTURE TESTS OF MODIFIED NICKEL-MOLYBDENUM ALLOYS

Alloy Composition (wt %)	Stress (psi)	Time to Rupture (hr)	Elongation (%)
77 Ni–20 Mo–3 Cr	8000	90	7
	5000	675	9
75 Ni–20 Mo–5 Cr	8000	80	7
74.75 Ni–20 Mo–5 Cr–0.25 Ce	6000	444	28
73 Ni–20 Mo–7 Cr	8000	380	9

between physical properties and the corresponding microstructures. As a result of this investigation, more comprehensive information on the high-temperature properties of this material is being obtained. The relative merits of various preaging heat treatments of Hastelloy B are also being studied, and it is hoped that, as a result of this work, a procedure can be developed which will stabilize the microstructure sufficiently to reduce the sensitivity to high-temperature aging.

A summary of the short-time tensile data that have been obtained to date is presented in Figs. 6.5, 6.6, and 6.7, and in Table 6.9. It may be noted in Fig. 6.5, which shows the results of the test in which the variable of aging time was investigated, that the tensile-strength and yield-point

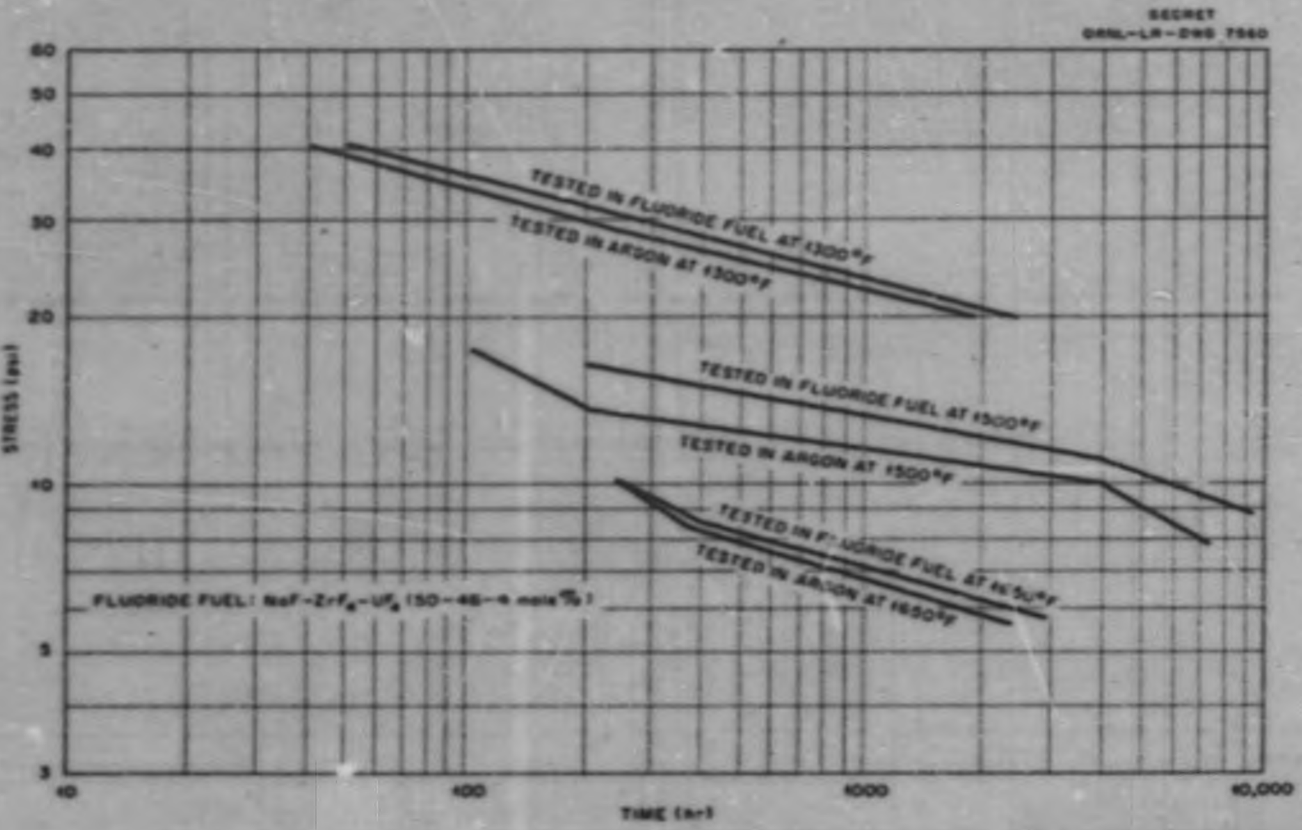

Fig. 6.3. Comparison of Hastelloy B Stress-Rupture Data in Argon and in the Fuel Mixture NaF-ZrF_4-UF_4 (50-46-4 mole %) at 1300, 1500, and 1650°F.

TABLE 6.9. ROOM-TEMPERATURE TENSILE PROPERTIES OF HASTELLOY B IN THE SOLUTION-ANNEALED AND SPHEROIDIZED CONDITIONS

Condition of Specimen	Tensile Strength (psi)	Yield Strength (psi)	Elongation (%)
Spheroidized	175,000 to 185,000	100,000 to 115,000	15 to 20
Solution-annealed 2 hr at 2100°F	125,000 to 130,000	50,000 to 60,000	55 to 65

curves for 500- and 1000-hr aging times reach a maximum at approximately 1300°F, while the ductility curve reaches a minimum at this same temperature. The results of metallographic studies, discussed previously,[6] indicated that this was caused by the extensive precipitation of a second phase – beta or a combination of two phases, beta and gamma – throughout the matrix. The high-temperature tensile properties obtained by a special spheroidization heat treatment[6] are compared in Figs. 6.6 and 6.7 with those of solution-annealed material in the unaged and in the aged conditions. Although the spheroidization treatment was intended to produce a stable microstructure between 1300 and 1600°F, it may be noted that the ductility is lowered considerably in the 1100 to 1300°F

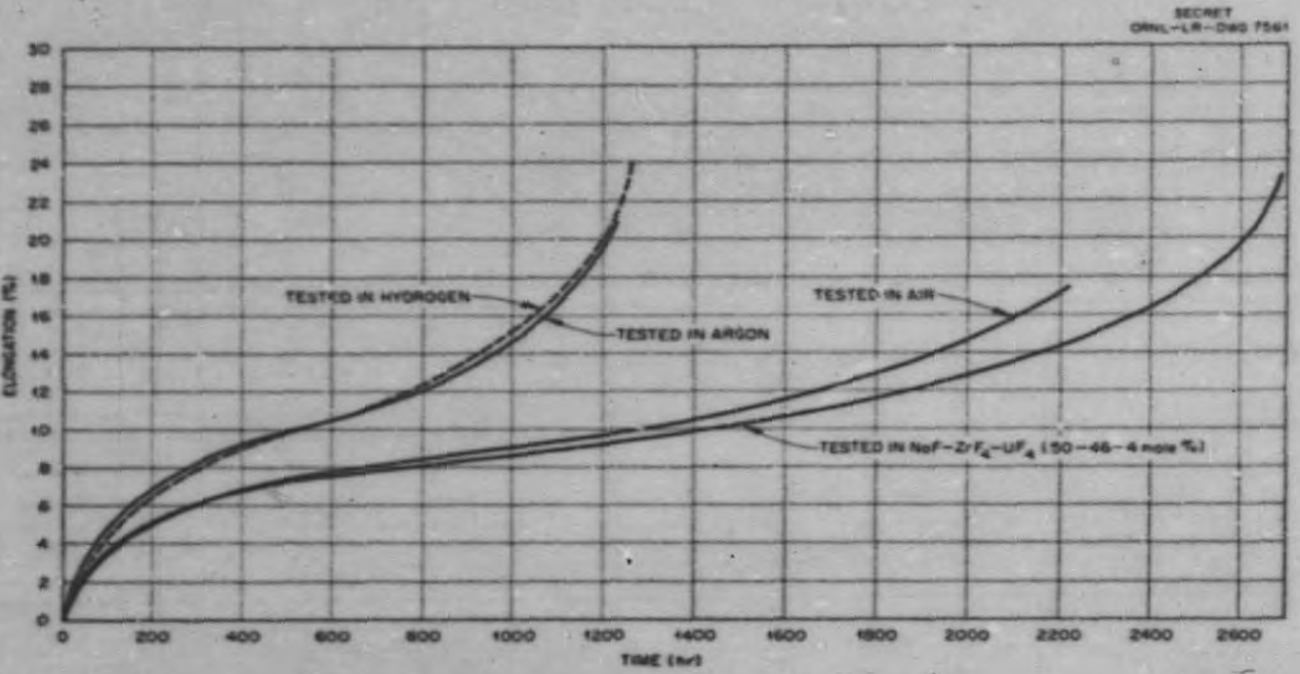

Fig. 6.4. Creep Curves for Hastelloy B Sheet That Was Solution Annealed at 2100°F and Tested at 1500°F and 12,000 psi in Various Environments.

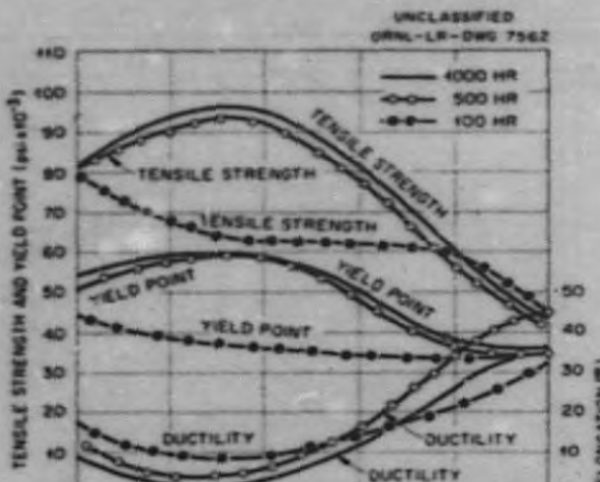

Fig. 6.5. High-Temperature Tensile Properties of Hastelloy B That Was Solution Annealed at 2100°F Prior to Aging at the Testing Temperature for Various Times.

temperature region. Even though very high tensile and yield strengths were obtained with this treatment, the low high-temperature ductility would probably prevent useful application of this material above 1000°F. Investigations of other promising pretreatments are now in progress, as well as investigations of the composition variables which have been shown to be of significance.

DEVELOPMENT OF BRAZING ALLOYS

P. Patriarca G. M. Slaughter
Metallurgy Division

R. L. Heestand
Pratt & Whitney Aircraft

High-Temperature Oxidation Tests

Tests for evaluating the static oxidation resistance of several brazing alloys were conducted previously at 1500 and 1700°F, and cyclic tests have now been initiated. In the 500-hr cyclic tests the samples are subjected to 190 air cools from 1500°F. The results obtained thus far are compared with the results of the static tests in

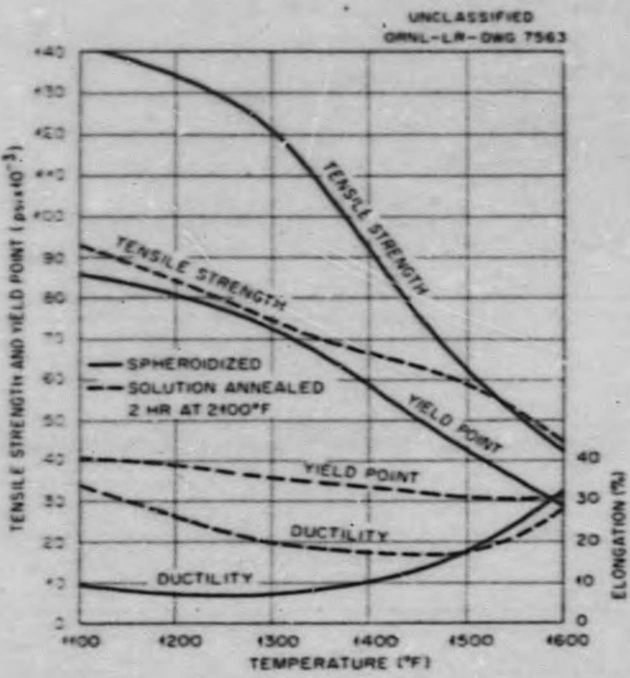

Fig. 6.6. High-Temperature Tensile Properties of Hastelloy B in the Solution Annealed and Spheroidized Conditions.

Table 6.10. It may be seen that many of the alloys tested have good resistance to oxidation under both static and cyclic conditions.

Tests are now under way for evaluating the attack resulting from cycling from 1700°F. An apparatus is also being prepared for testing the oxidation resistance of brazed joints in moving moist air.

Physical Property Tests

An investigation has been conducted of accumulative effects on the physical properties of Inconel tubing as a result of fabrication of tube-to-fin joints by high-temperature brazing with Coast Metals alloy No. 52. Brazed tube-to-fin specimens with at least 1 in. of stacked fins were machine ground to the original tubing dimensions. Threaded end sections were then brazed to these tubes to form short-time tensile test specimens.

Room- and high-temperature tensile tests were then conducted on the as-brazed specimens and on specimens that were subsequently heated in a vacuum for periods up to 500 hr at 1500°F prior to testing. The results indicated that no significant decrease in strength or elongation of the tubing resulted from the brazing and subsequent heat treatments. Tensile strengths of approximately 100,000 psi and elongations in 1 in. of approximately 30% were recorded in the room-temperature tests. At 1500°F, the samples possessed tensile strengths of approximately 27,000 psi, and they retained good ductility.

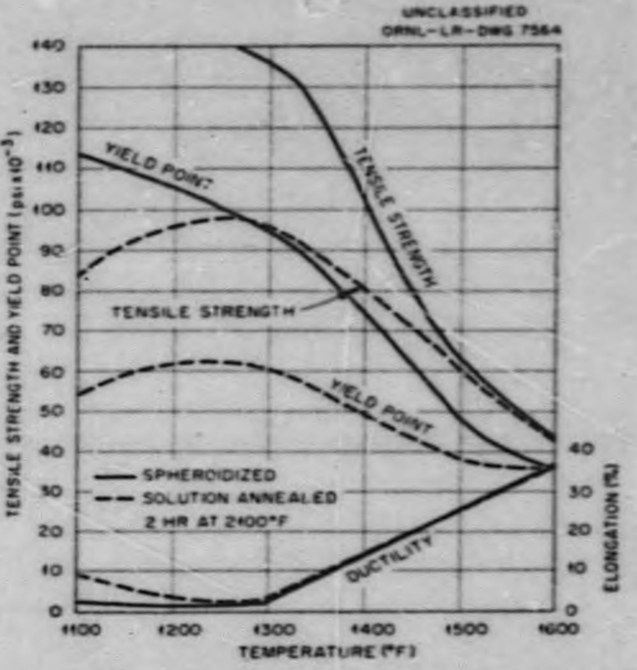

Fig. 6.7. High-Temperature Tensile Properties of Hastelloy B in the Solution Annealed and Spheroidized Conditions After Aging for 100 hr at the Test Temperature.

Test samples are now being prepared to evaluate the effects of other brazing alloys, such as Nicrobraz and the 90% Ni–10% P alloy.

FABRICATION OF TEST COMPONENTS

P. Patriarca
R. E. Clausing G. M. Slaughter
Metallurgy Division
R. L. Heestand
Pratt & Whitney Aircraft

Twenty-Tube Heat Exchanger

A fuel-to-NaK heat exchanger containing 20 Inconel tubes was fabricated for studying the heat transfer characteristics of fluoride fuel mixtures

TABLE 6.10. COMPARISON OF RESULTS OF STATIC AND CYCLIC 500-hr OXIDATION TESTS OF DRY-HYDROGEN-BRAZED INCONEL T-JOINTS AT 1500°F

Brazing Alloy	Composition (wt %)	Oxidation Results*	
		Tested in Static Air for 500 hr	Tested for 500 hr with 190 Air Cools to Room Temperature
	Commercial Alloys		
Nicrobraz	70 Ni–14 Cr–6 Fe–5 B–4 Si–1 C	Slight	Slight
Low-melting Nicrobraz	80 Ni–5 Cr–6 Fe–3 B–5 Si–1 C	Slight	Slight
Coast Metals No. 50	93 Ni–3.5 Si–2.5 B–1 Fe	Slight	Slight
51	92 Ni–4.5 Si–3 B–0.5 Fe	Slight	Moderate
52	89 Ni–5 Si–4 B–2 Fe	Slight	Moderate
53	81 Ni–4 Si–4 B–8 Cr–3 Fe	Slight	Slight
NP	50 Ni–12 Si–28 Fe–4 Mo–4.5 P–1 Mn–0.5 Cr	Slight	Slight
Mond Ni Co. Alloy	64 Ag–33 Pd–3 Mn	Severe	Severe
Copper	100 Cu	Complete	Complete
	Experimental Nickel-Base Alloys		
G-E No. 62	69 Ni–20 Cr–11 Si	Slight	Slight
81	66 Ni–19 Cr–10 Si–4 Fe–1 Mn	Slight	Slight
Ni-Cr-Si	73.5 Ni–16.5 Cr–10 Si	Slight	Slight
Ni-Si	88 Ni–12 Si	Slight	Slight
Ni-Ge	75 Ni–25 Ge	Slight	Slight
Ni-Ge-Cr	65 Ni–25 Ge–10 Cr	Slight	Slight
Electroless Ni-P	88 Ni–12 P	Slight	Moderate
Ni-P-Cr	80 Ni–10 P–10 Cr	Slight	Slight
Ni-Mo-Ge	50 Ni–25 Mo–25 Ge	Slight	Slight
Ni-Sn	68 Ni–32 Sn	Moderate	Severe
Ni-Mn	40 Ni–60 Mn	Complete	Complete
Ni-Mn-Cr	35 Ni–55 Mn–10 Cr	Severe	Severe
	Experimental Precious-Metal Base Alloys		
Pd-Ni	60 Pd–40 Ni	Slight	Slight
Pd-Ni-Si	60 Pd–37 Ni–3 Si	Slight	Slight
Pd-Al	92 Pd–8 Al	Very slight	Moderate
Pd-Ge	90 Pd–10 Ge	Slight	Severe
Au-Ni	82 Au–18 Ni	Very slight	Slight
Au-Co	90 Au–10 Co	Very slight	Slight
Au-Cu	80 Au–20 Cu	Complete	Complete

*Very slight, less than 1 mil of penetration; slight, 1 to 2 mils of penetration; moderate, 2 to 5 mils of penetration; severe, greater than 5 mils of penetration; complete, fillet completely destroyed.

over a wide range of Reynold numbers (cf. Sec. 2, "Experimental Reactor Engineering"). The design of this heat exchanger specified that the $\frac{3}{16}$-in.-OD, 0.017-in.-wall Inconel tubes were to be joined to a dished header at the NaK inlet end and to a radial header at the NaK outlet end. A thick-walled Inconel pressure shell was to be used to confine the molten fuel located outside the tubes.

The fabrication techniques used on this heat exchanger consisted essentially in manual heliarc welding and subsequent back brazing of the tube-to-header joints. All welding was performed by qualified operators[7] using specified procedures,[8] and complete penetration was utilized, except on the tube-to-header joints. Complete protection of the roots of the welds by an inert gas was employed at all times to minimize scaling and oxidation. The tube-to-header joints were back brazed to eliminate the "notch effect" resulting from incomplete weld penetration and to ensure against the development of leaks in the event of corrosion through an area of shallow weld penetration.

An evaluation of the corrosion resistance of brazing alloys had shown that low-melting Nicrobraz[9] was compatible with both sodium and the fused fluoride salts, and therefore this alloy was used in the back-brazing process, which was performed in a dry-hydrogen atmosphere by using the conventional "canning" procedures. Two brazing operations were required because the Globar pit furnace available did not possess a heating zone of sufficient length to heat both ends of the unit to the brazing temperature. A "window" was removed from the pressure shell to permit preplacement of the brazing alloy on the NaK inlet end of the tube bundle, as shown in Fig. 6.8. The window was welded shut after placement of the alloy, and helium leak-testing indicated that all welded and brazed joints were leaktight. The completed heat exchanger is shown in Fig. 6.9.

Intermediate Heat Exchanger No. 2

The semiautomatic heliarc welding of the tube-to-header joints of the two fuel-to-NaK heat exchangers for the intermediate heat exchanger No. 2 test program was discussed previously.[10] The 400 welds were helium leaktight before initiation of the stages of fabrication described here.

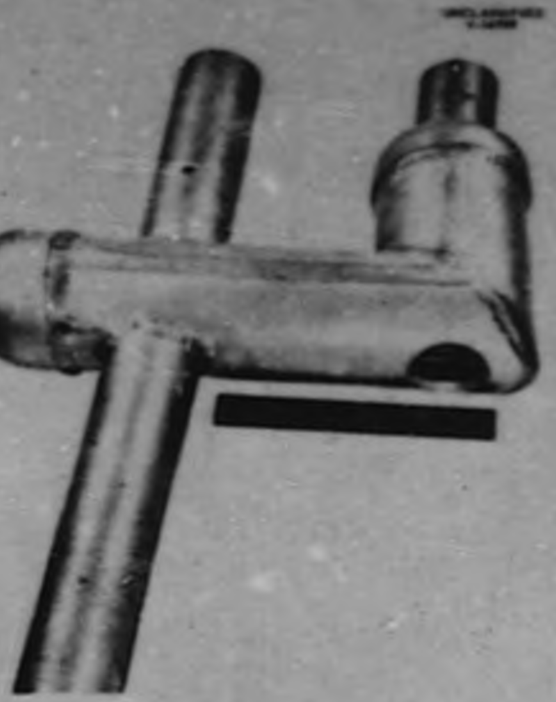

Fig. 6.8. Twenty-Tube Fuel-to-NaF Heat Exchanger Showing "Window" Cut in Pressure Shell to Permit Preplacement of Brazing Alloy on NaK Inlet End of the Tube Bundle.

Header Welding. In order to minimize cracking of the brittle alloy used in back brazing and to avoid contamination of areas to be welded with the boron and silicon of the brazing alloy, the header components were heliarc welded to each tube bundle before back brazing of the tube-to-header joints. However, to permit access to the joints, the components were not attached until after preplacement of the brazing alloy (low-melting Nicrobraz) had been completed.

The welding is shown at an early stage in Fig. 6.10. Strongbacks were used to minimize distortion of the header and consequent tube-to-header

---

[7] T. R. Housley and P. Patriarca, Operator's Qualification Test, QTS-1.

[8] T. R. Housley and P. Patriarca, Procedure Specification, PS-1.

[9] A brazing alloy developed by the Wall-Colmonoy Corp., Detroit, Mich.

[10] P. Patriarca *et al.*, *ANP Quar. Prog. Rep. Mar. 10, 1955*, ORNL-1864, p 131.

Fig. 6.9. Completed 20-Tube Fuel-to-NaK Heat Exchanger.

Fig. 6.10. Welding of a Header of the Intermediate Heat Exchanger No. 2. The strongbacks used to minimize distortion may be seen.

weld fracture. Joint designs were used that permitted complete penetration,[11] and qualified operators and specified procedures were used at all times. A photograph of a completed, leaktight, header section prior to back brazing is shown in Fig. 6.11.

Back Brazing of Tube-to-Header Joints. The low-melting Nicrobraz alloy was preplaced on the headers as a dry powder and then secured firmly in position with a methylacrylate cement. Since the heating zone of the Globar-heated brazing furnace was not long enough for a complete tube bundle, only one end of the tube bundle could be brazed at a time. As a result, it was necessary that the complete welding and brazing of one header on one end of a tube bundle be done prior to the brazing alloy preplacement and header welding of the other end so as to avoid spalling of the preplaced brazing alloy from the underside of the cold header during the brazing of the first header. It was thought that hot hydrogen gas might volatilize the binder on the cold header and leave the brazing alloy insecurely positioned in

---

[11] T. R. Housley and P. Patriarca, *Joint Design of Inert-Arc Welded Pressure Vessels for High-Corrosion Application* (to be issued).

Fig. 6.11. Completed Header of an Intermediate Heat Exchanger No. 2 Tube Bundle.

its overhead locations. This important consideration increased the fabrication time to some degree, since the welding of both heads and the brazing of both heads could not be performed in sequence.

The dry-hydrogen furnace brazing was performed with the tube bundle in a horizontal position in the Globar furnace. The bundle was securely jigged in a long, rectangular, stainless steel retort, and a dry-hydrogen atmosphere was maintained in the retort during brazing. A time-temperature record of every brazing thermal cycle was measured by means of a Chromel-Alumel thermocouple firmly attached to the assembly, and a plot of a typical cycle is shown in Fig. 6.12. A preheated brazing furnace was used to shorten the time required for each operation, since no visible warpage or distortion of the heat exchanger resulted.

Fabrication and Assembly of Comblike Spacers. The use of wire comblike spacers was considered to be the most practical means for holding the tube bundle rigid over its free-span length and for keeping the tubes separated in such a way as to permit the required mode of fluid flow between them. The "combs" were placed at 5-in. intervals along the bundle, with alternate spacers positioned 90 deg to each other. It was required, for the heat transfer evaluation, to place the spacers on one bundle perpendicular to the axis of the tubing, whereas on the second bundle they were placed in a plane at a 30-deg angle to the tubing axis. Both types of spacer arrangement are shown in Fig. 6.13. It may be seen that the fabrication and assembly of these spacers required the use of precision jigs and careful determination and control of the cone-arc plug-welding conditions. Meticulous care also had to be maintained when the holes were punched in the strip headers, because extremely close tolerances were specified.

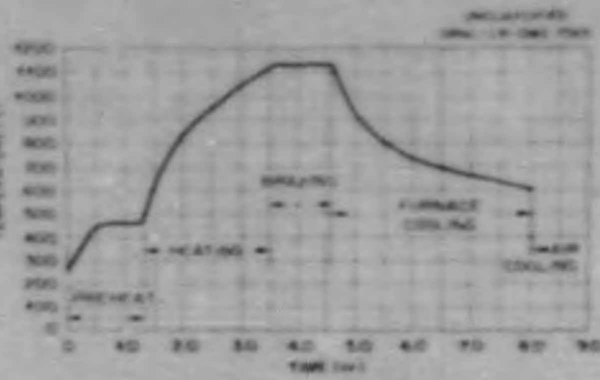

Fig. 6.12. Brazing Cycle Used in the Fabrication of Intermediate Heat Exchanger No. 2.

Installation of Tube Bundle into Pressure Shell. The installation of the tube bundles into their pressure shells required light machining of the shell to permit proper fit-up; that is, each pressure shell had to be precision machined for its corresponding tube bundle to accommodate the very small variations in dimensions. The heavy-walled pressure shell was beveled according to the recommended joint design, and, as prescribed for high-corrosion applications, the root pass was heliarc welded. The remainder of the welding was performed by using the metallic-arc process to minimize the heat input and consequent distortion of the unit. Figure 6.14 shows the heat exchanger after completion of the root pass. The large

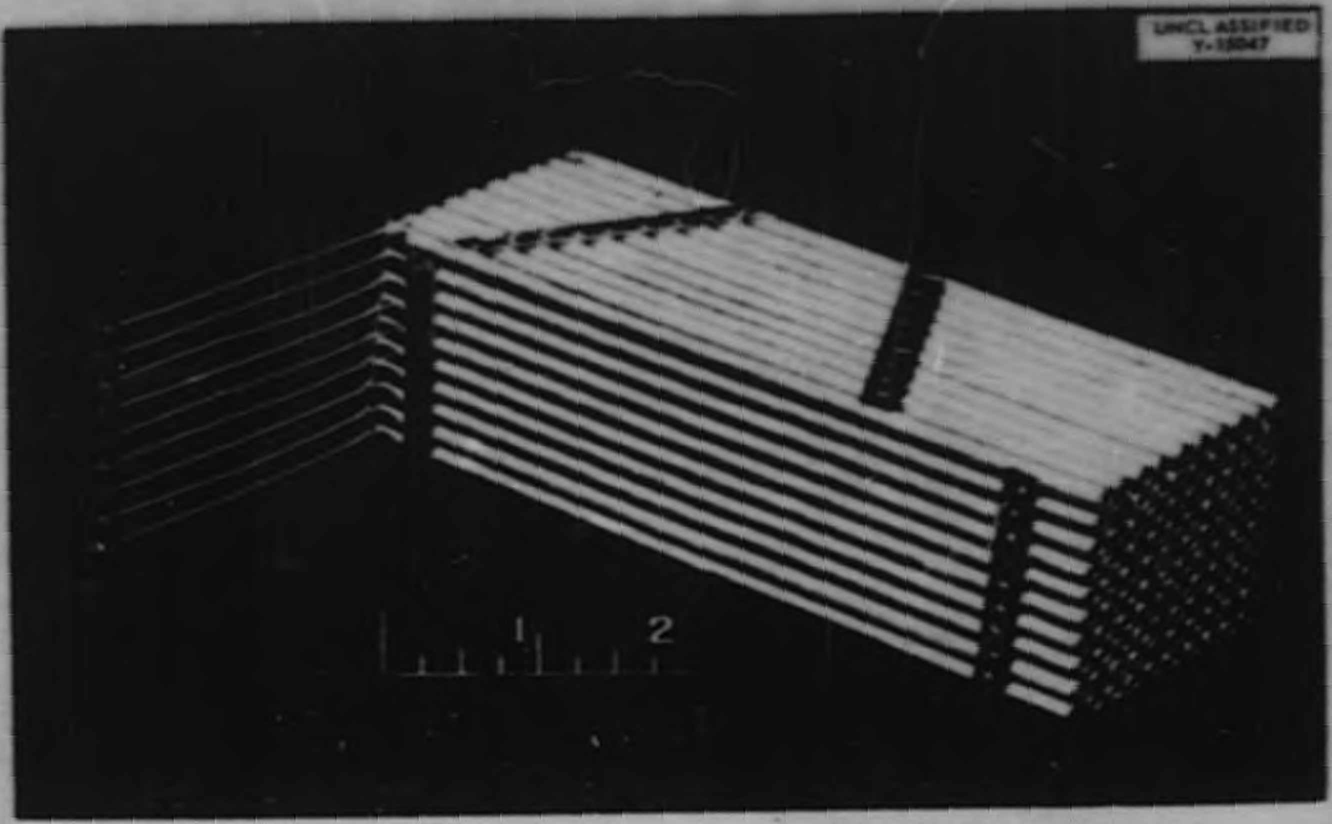

Fig. 6.13. Sample Tube Bundle Showing Two Types of Comblike Spacer Arrangements.

I-beam was used as a strongback for the system to prevent severe distortion.

Joining of Two Tube Bundles. The two tube bundles were joined together after being welded into their respective pressure shells; the completed unit is shown in Fig. 6.15. It may be seen that the joining operation required several manual heliarc welds to connect the NaK circuits and to attach the inlet and exit nozzles. Leak-testing with a helium leak detector indicated no flaws, and the heat exchanger was subsequently delivered for installation into the test rig. A detailed report covering the fabrication of heat exchangers is being prepared.

NaK-to-Air Radiators

It was reported previously[12] that the fabrication of two 500-kw NaK-to-air radiators had been initiated for use in the intermediate heat exchanger No. 2 test program and that the type 310 stainless-steel-clad copper high-conductivity fins had been sheared, degreased, and edge-protected with aluminum bronze. The construction of these units has now been completed, and a brief discussion of the intermediate steps is presented here.

Preplacement of Brazing Alloy. Coast Metals brazing alloy No. 52 was designated for use on this radiator because it possesses good flowability at 1020°C and has good resistance to high-temperature oxidation. Its good compatibility with sodium was also of distinct advantage, since the brazing alloy might come in contact with the NaK during service if used to seal small pin-hole leaks or if sufficient weld metal corrosion occurred to expose a braze metal surface. Also, severe tube-wall

---

[12] P. Patriarca et al., ANP Quar. Prog. Rep. Mar. 10, 1955, ORNL-1864, p 128.

Fig. 6.14. **Intermediate Heat Exchanger No. 2 After Completion of the Root Pass of the Pressure Shell Weld.** Strongback used to minimize distortion.

dilution during brazing or solid-state diffusion in service might produce a high concentration of brazing alloy constituents near the circulating NaK.

The dry-powder method of brazing alloy preplacement was used in the fabrication of these radiators. A stainless steel template containing holes that were precision drilled was utilized to place controlled amounts of brazing alloy on each tube-to-fin joint. The brazing powder was secured to the fin with Nicrobraz cement. A $\frac{1}{16}$-in.-thick template containing holes 0.246 in. in diameter provided the optimum quantity of brazing alloy per joint and was used to preplace alloy on the 2200 fins.

Assembly of Fins. The assembly of the fins on the radiator was conducted with the tube bends down, as is shown in Fig. 6.16. The assembly of the first 4 in. of fins was extremely time-consuming because the tubes were not rigidly in place. A heavy metal template was required to force each individual fin into place. Since some of this difficulty was also derived from the slight curvature of the straight lengths of tubing, it is thought that improvements in the bending techniques might substantially assist assembly of future units.

A set of Lucife "finger" jigs was designed and built that simplified the fin assembly problem. These jigs, which can be seen in Fig. 6.16, aligned the tubes in the positions to fit the punched geometry of the fin. Supporting sheet-metal channels were placed at 4-in. intervals to impart over-all structural stability to the radiator. These channels were heliarc welded together to form sheet-metal side plates. Two thin sheets of Inconel were also placed tightly together against the channels at these 4-in. intervals. The capillary joint be-

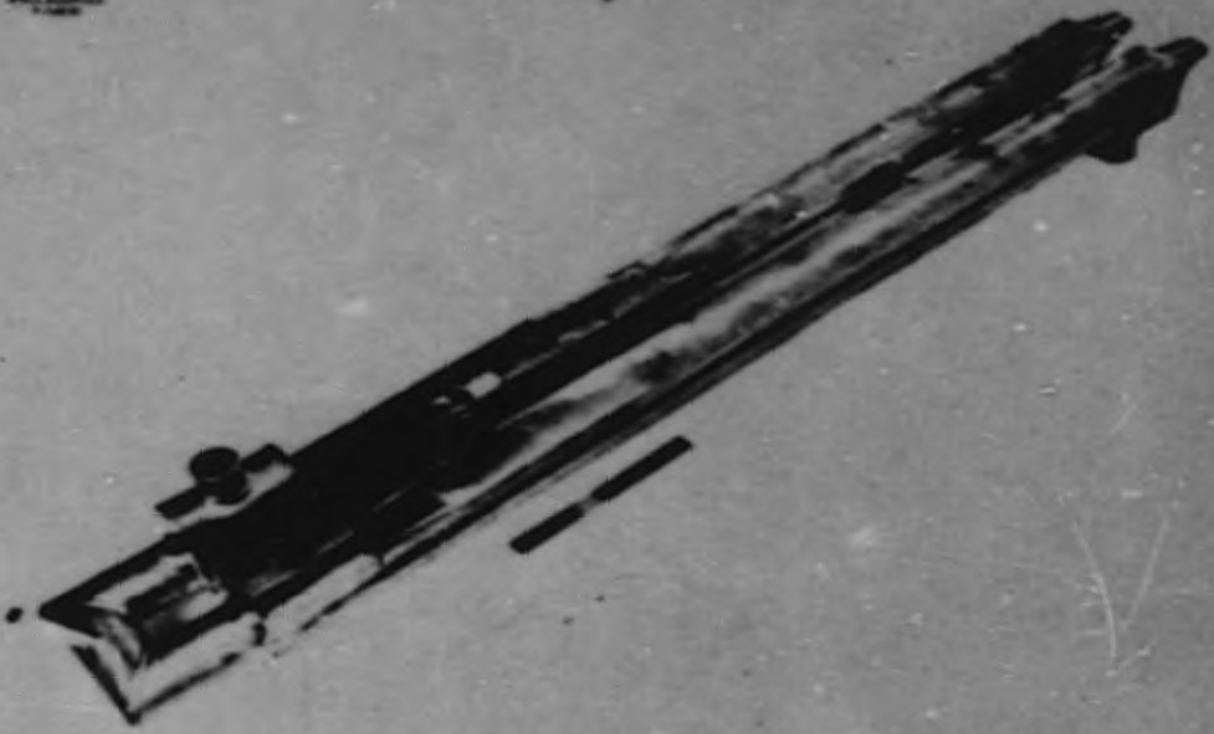

Fig. 6.15. Completed Intermediate Heat Exchanger No. 2.

tween the two Inconel sheets acted as a sump to accommodate any excess brazing alloy.

Assembly of Headers. The original design for the radiators required that all tubes enter the cylindrical headers normal to the curvature at the point of entrance. Sample specimens were prepared to determine the tube-bending and fitting techniques, but the complex tube design caused extreme difficulties in placing the headers on the tubes. Therefore a new design was proposed and accepted that utilized a split header of 3-in. schedule-40 pipe so that all tubes except the two outside rows on each radiator half-section entered the headers without being bent.

Careful hand polishing of each of the tubes was required to permit assembly of the split headers without the use of additional force from a hand press. Precision drilling and deburring of the headers were also employed to prevent bending and distortion of the thin-walled Inconel tubes. After assembly of the headers, the tubes were meticulously hand filed to conform to the exact curvature of the interior surfaces. Abrasive grinding or wet milling was avoided because entrapped abrasive or lubricant would lead to inconsistencies during tube-to-header welding.

Welding. The tube-to-header joints were manually heliarc welded, and a helium backup atmosphere was maintained on the underside of the joint throughout welding. The split headers, nozzles, and end plates were also welded by using manual heliarc welding techniques. Extreme care was taken to ensure complete penetration and good coverage by the backup gas.

After the manifold welds were completed, the integrity of the system was determined by helium leak-testing. Although it was assumed that pinhole leaks could be sealed during the subsequent brazing operation, large leaks were to be avoided. When questionable welds were found, the headers

Fig. 6.16. Early Stages of Assembly of NaK-to-Air Radiator.

were removed by simply cutting off the tubes at the underside of the header plates. New headers were then attached by rebending the tubes and repolishing them. This procedure was employed on the radiators in order to obtain leaktight units before brazing.

Brazing. The back brazing of the tube-to-header welds and the brazing of the tube-to-fin joints were accomplished by using conventional canning techniques. The brazing alloy was preplaced on the fins, as described above, and a medicine dropper was used to place the braze slurry on the tube-to-header joints.

A special baffle design was used for the brazing of these radiators, since it was very important to flush out the copious amounts of methylacrylate binder present in the tube-to-fin matrix. A sheet-metal cover was attached to the front of the radiator, and clean, dry inlet gas was forced between the fins before being exhausted to the outside of the can. The inside of the sheet-metal cover and inlet tube was designed to permit relatively even flow throughout the entire frontal area, and good circulation of hydrogen was obtained around the tube-to-header joints.

The radiator was securely supported on a strongback to prevent sagging or distortion during the high-temperature brazing cycle. The support bars were made from stainless steel which had been previously aluminized at 1500°F. This aluminizing prevented the support bars from being brazed to the radiator, since an aluminum oxide film prevents wetting by Coast Metals alloy No. 52.

The radiator was placed in the brazing can with four thermocouples attached in various positions around the periphery. This temperature measurement around the radiator was desirable from a control standpoint, even though previous experiments had indicated that all parts of a unit of this size could be held to within 25°C at the brazing temperature. In the preliminary experiment, 12 thermocouples were attached at various points over the test specimen. This close control was necessary because the flow temperature of the brazing alloy is 1020°C, and the copper in the fins melts at 1083°C.

The thermal cycle used in brazing these radiators is shown in Fig. 6.17. The unit was placed in the furnace at room temperature to minimize distortion and was gradually raised to the brazing temperature. The two completed radiators are shown in Fig. 6.18; as may be seen, negligible distortion

UNCLASSIFIED
ORNL-LR-DWG [illegible]

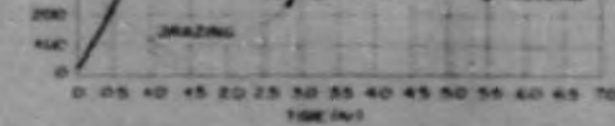

Fig. 6.17. Brazing Cycle Used in the Fabrication of a 500-kw NaK-to-Air Radiator.

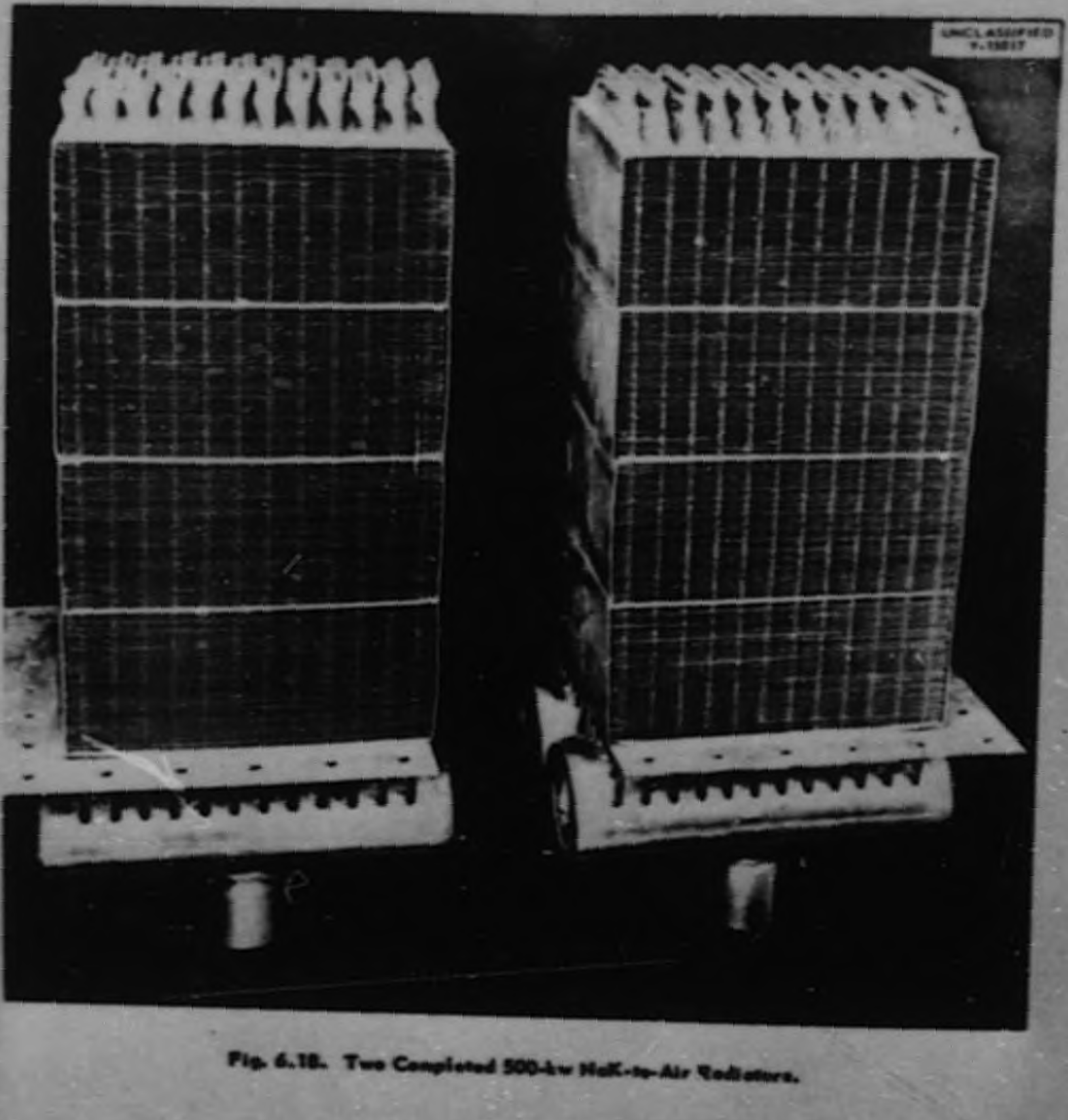

Fig. 6.18. Two Completed 500-kw NaK-to-Air Radiators.

occurred. Since no excess of brazing alloy was found, it appears that the sump technique for the removal of the excess is practical for large assemblies. Good flowability of the brazing alloy was obtained. A cross section of a typical tube-to-fin joint brazed under conditions simulating those used in the fabrication of the radiators is shown in Fig. 6.19. It may be seen that good edge protection of the exposed copper was obtained in these tube-to-fin joints and that good fillets were present in the tube-to-header joints.

Fig. 6.19. Tube-to-Fin Joint Brazed Under Conditions Simulating Those Used in the Fabrication of the NaK-to-Air Radiators.

Leak-testing with a mass-spectrometer helium leak detector indicated no flaws in the integrity of the closed NaK circuits. The two radiators were therefore delivered for installation into the test rig.

Cornell Radiator No. 1

The assembly and partial fabrication of a full-scale liquid metal-to-air radiator designed by the Cornell Aeronautical Laboratory were described previously.[13] Since the header plates on this heat exchanger were $\frac{5}{8}$ in. thick, the brazed tube-to-header joints cracked easily. Severe stresses resulted from the differences in thermal expansion coefficients between the stainless steel base metal and the brazing alloy. However, an investigation of several high-temperature brazing alloys revealed that Coast Metals alloy No. 50 possessed sufficient ductility to overcome this cracking upon furnace cooling from its brazing temperature of 2050°F. Other brazing alloys such as Coast Metals alloy No. 52 and G-E alloy No. 62 cracked to such an extent that they were not considered satisfactory for this application.

Since brazing with Coast Metals alloy No. 50, which is a nickel-silicon-boron-iron alloy, would necessarily result in the diffusion of boron into the type 316 stainless steel base metal, an investigation was conducted to determine the extent of penetration and the effects on the mechanical properties of the base metal. Metallographic examination of typical brazed tube-to-header joints indicated that the diffusion was minor (2 to 3 mils), even though long-time heating and cooling cycles were used. Samples examined after subsequent heating for 24 hr at 1650°F also exhibited diffusion to the same extent. After 100 hr at 1650°F, the diffusion had progressed to 4 to 5 mils. Several brazed tensile-test samples were prepared so that a study could be made of the effects of brazing on the mechanical properties. Tests at room temperature and at 1600°F at the Cornell Aeronautical Laboratory indicated no appreciable reduction in the tensile strength of the base metal.

The back brazing was carried out by placing the radiator in the furnace at room temperature and heating at a rate of 150°C/hr until the brazing temperature was reached. The radiator was held at 2050°F for $\frac{1}{2}$ hr and then furnace cooled at a maximum rate of 150°C/hr. The completed heat exchanger is shown in Fig. 6.20. Testing with a mass-spectrometer helium leak detector indicated that all welded and brazed joints were leaktight.

---

[13] P. Patriarca *et al.*, *ANP Quar. Prog. Rep. Mar. 10, 1955*, ORNL-1864, p 132.

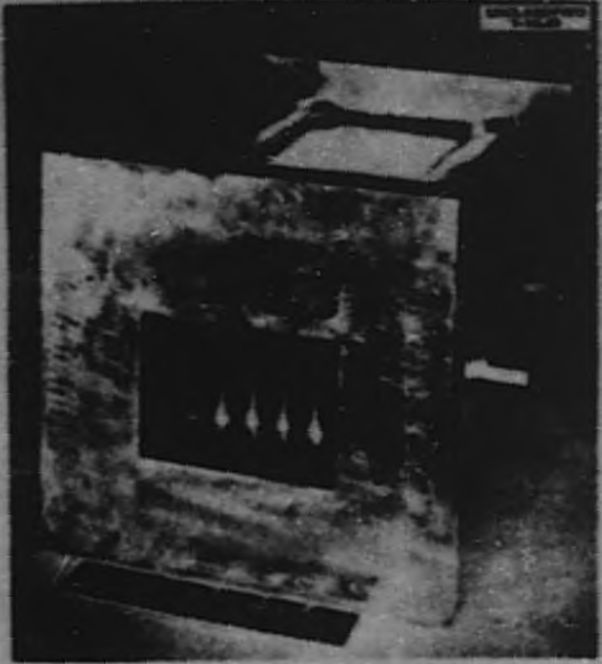

Fig. 6.20. Completed Cornell Aeronautical Laboratory Sodium-to-Air Radiator No. 1.

The radiator has therefore been delivered to the Cornell Aeronautical Laboratory.

SPECIAL MATERIALS STUDIES

Special Alloy Extrusions

J. H. Coobs H. Inouye
Metallurgy Division

M. R. D'Amore, Pratt & Whitney Aircraft

Three billets of vanadium were extruded at 2000°F. The pressure required for an extrusion ratio of 9:1 was approximately 45 tsi. The billets were canned in mild steel to protect the vanadium from oxidation during extrusion. The canning material was removed from the extruded tube blanks by pickling in hot HCl. The tube blanks have been shipped to the Superior Tube Co. for further reduction and cladding on the outside with stainless steel. The clad tubing will be used in corrosion studies.

Four high-purity molybdenum billets containing 0.7% titanium were extruded into rod to be used for welding studies at Battelle Memorial Institute. The extrusions were made at 2600°F, and it was demonstrated that the pressure required could be reduced by using a salt-type lubricant. These billets failed to extrude in the first two attempts when Fiberglas and Necrolene were used as the lubricating materials. Since the salt lubricant thermally decomposes at 2600°F, it was swabbed onto the container walls. The use of salt in the container reduced the pressure required from 700 to 427 tons on a 3-in. ram for an extrusion ratio of 4.5:1. Similarly, at an extrusion ratio of 6.25:1, the pressure required was reduced from 700 to 508 tons.

The studies of flow patterns of duplex and three-ply materials during impact extrusion were continued. The flow pattern studies of three-ply composites have been directed toward the production of stainless steel seamless tubular fuel elements. The experiments on duplex materials are designed for studying the fabrication problems involved in the cladding of tube materials. Six additional extrusions of composite stainless steel–mild steel billets have been completed. The results of the extrusions have not been completely evaluated, but it appears that material recovery may be improved by tapering the billet nose to conform with the cone of the die.

Dimensional Stability Test on an Inconel Spun Core

P. Patriarca
Metallurgy Division

A proposed design for the core shell of the ART calls for the use of a spun Inconel configuration, and therefore an investigation was conducted to determine the dimensional stability of a small-scale specimen (Fig. 6.25) obtained from Pratt & Whitney Aircraft. The stability of this configuration was tested by measuring the distances between several reference points both before and after thermally cycling from 1500°F to ambient

Fig. 6.25. Inconel Spun Core Shell.

TABLE 6.13. CONDITIONS OF THERMAL CYCLING OF INCONEL SPUN CORE

Cycle No.	Heating Time (hr)	Time at 1500°F (hr)	Cooling Time (hr)
1	4	½	4
2	4	½	4
3	1	½	4
4	1	½	¾

under the conditions listed in Table 6.13. The cycling process was performed in a protective helium atmosphere. At the completion of the experiment, no recordable diametrical, axial, or thickness instability was observed.

Brazing of Cermets to Inconel

P. Patriarca R. E. Clausing
Metallurgy Division

The use of cermet valve seats has been proposed for certain high-temperature fused fluoride fuel applications. Cermets composed of titanium carbide with a nickel binder (Kentanium type) are among those most likely to be used (cf. Sec. 5, "Corrosion Research"). If these valve seats are to be brazed to an Inconel valve body, the brazed joint must be sufficiently ductile to withstand the stresses created by unequal thermal expansion coefficients (10.2×10^{-6} in./in./°F for Inconel and 4.0×10^{-6} to 5.7×10^{-6} in./in./°F for the cermets). In addition the brazed joint must possess adequate strength and corrosion resistance at temperatures to 1500°F.

Good wetting of the cermet has been obtained by using Electroless-plated nickel-phosphorus brazing alloy.[16] Satisfactory joints have been obtained with a 0.0001-in. layer of nickel-phosphorus followed with a 0.003- to 0.004-in. layer of electroplated copper. The addition of a nickel shim between the plated cermet and the Inconel is desirable, since it serves as a cushion to dissipate the thermally induced stresses in the joint. During the brazing operation, the nickel-phosphorus melts at approximately 1740°F and wets the Kentanium surface; continually increasing the temperature then melts the copper, which alloys with the nickel-phosphorus to form a ductile joint.

A test sample was prepared that satisfactorily withstood two air cools from 1700°F. It was composed of a ¼ × ¼ × 2 in. Kentanium 150A cermet (90% TiC–10% Ni) brazed to a ½-in. Inconel plate along a ¼ × 2 in. face. A 3/16-in. nickel shim was incorporated in the joint. The specimen was severely cracked, but, as can be seen in Fig. 6.26, the joint remained sound. Sample joints are now being prepared for tensile tests.

CERAMIC RESEARCH

J. A. Griffin J. R. Johnson
C. E. Curtis A. J. Taylor
Metallurgy Division

Rare-Earth Ceramics

Ceramics composed of rare-earth oxides should combine the property of high absorption cross section (for thermal neutrons) and the usual ceramic properties of high density, strength, corrosion resistance, and high melting temperature. Since these properties are those required for a control rod for the ART, enough Sm_2O_3 and Gd_2O_3 was obtained for testing. These oxides, in the form of bars 3 × ½ × 1/16 in. thick (pressed from the powdered

---

[16] P. Patriarca *et al., ANP Quar. Prog. Rep. Mar. 10, 1954,* ORNL-1692, p 90.

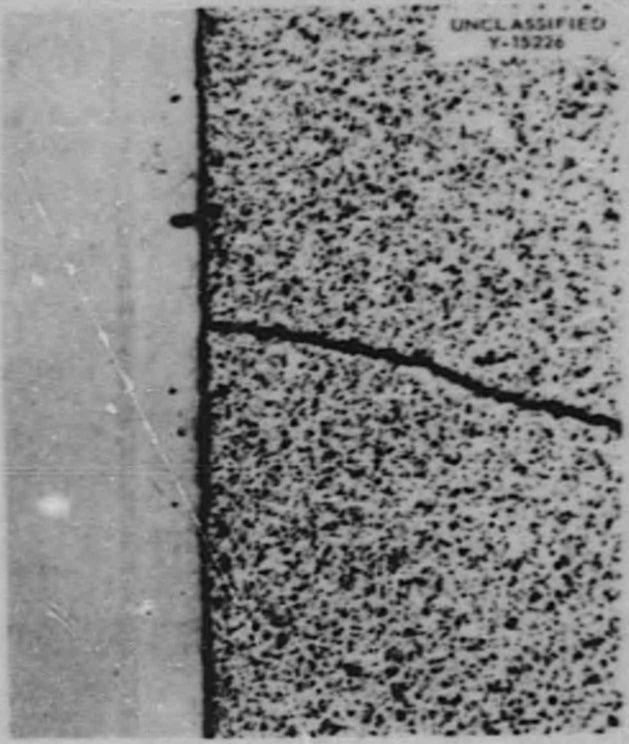

Fig. 6.26. Brazed Joint of Kentanium 150A Cermet to Nickel. Note sound appearance of joint despite severe crack in the cermet.

oxides), were fired at 1300 and 1500°C in air. The results of physical property measurements on these specimens are presented in Table 6.14.

Both Sm_2O_3 and Gd_2O_3 sintered at 1500°C to form ceramics of good strength. High resistance to thermal shock would not be expected because the coefficients of thermal expansion are rather high. The oxide Gd_2O_3 sintered at both 1300 and 1500°C was stable in boiling water; however, Sm_2O_3 sintered at 1500°C was not stable.

A mixture of the oxides (available commercially) containing 63.8% Sm_2O_3 and 26.3% Gd_2O_3 (balance, other rare-earth oxides) was fabricated into cylinders, and these specimens have been tested in the critical experiment (cf. Sec. 3 "Critical Experiment"). After heat treatment at 1500°C, the cylinders had a density of 10.94 and a porosity of 8%, and they were stable in boiling water. They were machined to the following dimensions: $\frac{3}{4}$-in.-OD, $\frac{1}{2}$-in.-ID, 0.8-in.-long hollow cylinders, and 0.45-in.-OD, $\frac{3}{4}$-in.-long solid cylinders to fit into hollow cylinders. Similar ceramics of the mixed oxides are being tested for radiation damage and thermal conductivity.

Exploratory tests for possible new compounds of these oxides were made by combining each in equimolecular proportions with each of the following: MgO, CaO, SrO, CdO, BaO, Al_2O_3, Fe_2O_3, SiO_2, SnO_2, ZrO_2, HfO_2, and ThO_2. After a heat treatment at 1500°C for 2 hr, x-ray examination

TABLE 6.14. RESULTS OF PHYSICAL PROPERTY MEASUREMENTS OF RARE-EARTH OXIDES FIRED AT 1300 AND 1500°C IN AIR

Property Measured	Sm_2O_3		Gd_2O_3	
Sintering temperature (°C)	1300	1500	1300	1500
Density (bulk)	6.0	7.4	6.97	7.6
Per cent of theoretical*	81	100	93	102**
Apparent porosity (%)	23	4	10.4	1.2
Modulus of rupture (psi)	1800	2000	2740	2840
Modulus of elasticity (psi)	4.4×10^6	26.5×10^6	14.5×10^6	18.0×10^6
Coefficient of linear thermal expansion (in./in./°C)		9.9×10^{-6}		10.5×10^{-6}
Melting temperature (°C)	2350 ± 20			2350 ± 20

*Theoretical densities: Sm_2O_3, 7.43; Gd_2O_3, 7.407.

**Higher than theoretical density, probably due to 2% terbium present.

showed that both rare-earth oxides formed compounds with Al_2O_3, Fe_2O_3, SiO_2, and SrO. The compounds with Al_2O_3 and Fe_2O_3 have the perovskite structure, and their possible use as dielectrics is being investigated. In each case the Fe_2O_3 compound was magnetic. Both Sm_2O_3 and Gd_2O_3 form solid solutions with CaO, MgO, HfO_2, ZrO_2, and ThO_2. In each case the CdO volatilized out of the mixture at 1500°C.

Several rare earths were available only in very small quantities, and hence they were studied only with respect to their x-ray diffraction patterns. Their structures, as received and after calcination at 1400°C, are given in Table 6.15.

TABLE 6.15. STRUCTURES OF RARE-EARTH OXIDES

	As Received	After Calcination at 1400°C
CeO_2	*fcc*	*fcc*
Pr_2U_3	*U**	*U*
Nd_2O_3	*U*	*U***
Sm_2O_3	*U* + *c*	*U*
Eu_2O_3	*c*	*U*
Gd_2O_3	*c*	*U*
Dy_2O_3	*c*	*c*
Ho_2O_3	*c*	*c****
Er_2O_2	*c*	*c*
Tm_2O_3	*c*	*c*
Yb_2O_3	*c*	*c*

**U* = undetermined; *c* = cubic.

**2 phases present; both anisotropic.

***2 phases present; one cubic, one anisotropic.

The rare-earth oxides Eu_2O_3, Nd_2O_3, Pr_2O_3, and Dy_2O_3 are now on hand in sufficient quantities for determining some of their sintered properties and whether their reaction products with Al_2O_3 and Fe_2O_3 have valuable properties. Specimens of Eu_2O_3 in the form of disks $\frac{3}{4}$ in. in diameter and 0.003 in. thick and bars $3 \times \frac{1}{4} \times \frac{1}{8}$ in. are being prepared for physical property measurements and radiation damage studies.

An $(Sm,Gd)_2O_3$-Fe cermet was prepared by Shevlin at the Ohio State Experiment Station. This cermet consists of 30 wt % rare-earth oxides and 70 wt % iron. Powders of these two materials were milled for 24 hr in 1-qt-capacity steel mills with tungsten carbide slugs and methyl alcohol. The mill charge was dried and granulated, and the batch of material was pressed isostatically at 35,000 psi. The blank thus formed was sintered in hydrogen at 2725°F for $1\frac{1}{2}$ hr. The specimen was machined to a cylinder about 0.8 in. in diameter and 3 in. long by using a conventional lathe and steel tip tools. A porosity of 14% was measured by determining kerosene absorption, and a porosity of 25.9% was calculated on the basis of theoretical density; these values indicate the close pore volume to be 11.9%.

UO_2 Particles Coated with ZrO_2

In anticipation of a possible need for protecting particles of UO_2 from reaction with molten silicon in the development of an SiC-Si fuel element, a technique was developed by Shevlin, at the Ohio State Experiment Station, for coating particles of UO_2 (20 to 50 mesh) with a thin layer of ZrO_2. This was done by heating the particles to about 500°F in an open-topped container on a hot plate. While this container was vibrated mechanically to agitate the particles, they were sprayed with a solution of ammonium zirconyl carbonate. Under these experimental conditions, droplets of the solution were dried, the salt was decomposed, and the oxide (ZrO_2) product was deposited on the UO_2 surface to form a continuous film, which was difficult to remove by rubbing. It appears possible to use this process to form diffusion barriers which would prevent UO_2 from reacting with aluminum and other metals. Attempts will be made to deposit Al_2O_3 and NiO coatings on UO_2 by this process, and it is planned to heat-treat ZrO_2 and Al_2O_3 to explore the possibility of consolidating the coatings. Heat treatment of NiO under reducing conditions will also be investigated to determine the practicability of producing nickel coatings in this manner.

7. HEAT TRANSFER AND PHYSICAL PROPERTIES

H. F. Poppendiek
Reactor Experimental Engineering Division

Fused salt heat transfer studies have included an experimental determination of the friction factor as a function of Reynolds modulus for the case of turbulently flowing NaF-ZrF_4-UF_4 in Inconel tubes. A full-scale ART fuel-to-NaK heat exchanger was studied as a water-to-water heat exchanger. Some velocity profile data were obtained for the 18-in. ART core, and a study was made of the temperatures and corresponding tensile stress fluctuations in the Inconel walls of the ART core for momentary periods of flow stagnation near the wall. The results of a theoretical and experimental study of a free-convection system containing a volume heat source are presented.

The enthalpies, heat capacities, and viscosities of several fluoride mixtures were obtained. Also, some preliminary thermal conductivity data were obtained with a new conductivity cell.

FUSED SALT HEAT TRANSFER

H. W. Hoffman
Reactor Experimental Engineering Division

S. J. Pias
Pratt & Whitney Aircraft

Previously reported heat transfer experiments with the fuel mixture NaF-ZrF_4-UF_4 (53.5-40-6.5 mole %) flowing in an Inconel tube gave results which were 24% below the general heat transfer correlation. Two possible explanations for this discrepancy are that there may have been errors in temperature measurement or that an additional thermal resistance may have been present at the fluid-metal interface. Calibration of the mixing-chamber and tube-wall thermocouples revealed no temperature errors. A study of the effectiveness of the mixing chambers is now in progress to be sure that good mixed mean fluid temperatures were obtained. A visual examination of the tube showed no surface deposits for this system. However, the lack of residual salt adhering to the tube surface suggests a "nonwetting" condition. To check on the general possibility of some type of two-phase flow, a study of the pressure-drop characteristics of NaF-ZrF_4-UF_4 in forced convection through nearly isothermal circular tubes was undertaken. The preliminary data are shown in Fig. 7.1. The results suggest that two-phase flow does not occur in this system, because the friction factor measurements fall near the general single-phase curve. The influence of a nonwetting fluoride on forced-convection heat transfer is not yet known.

The heat transfer characteristics of the mixture NaF-KF-LiF-UF_4 (11.2-41-45.3-2.5 mole %) are currently being investigated. Preliminary results for an Inconel system, shown in Fig. 7.2, lie 40% below the general heat transfer correlation. A fragile green film was found on the inside surface of the tube. X-ray and petrographic examination revealed only the constituents of the salt. Further heat transfer studies are planned, for which a stainless steel test section will be used. Pressure-drop measurements are also to be made.

A small-scale loop that is to include a centrifugal sump pump has been designed and is being fabricated. The proposed system is shown schematically in Fig. 7.3. The fluid flow rate will be obtained by weighing the salt as it empties into a weigh tank suspended within a weigh chamber. The weigh tank will be arranged so that it can be rapidly emptied. The sump well will be used to maintain the liquid level in the pump during the weighing operation.

ART FUEL-TO-NaK HEAT EXCHANGER

J. L. Wantland
Reactor Experimental Engineering Division

A full-scale ART fuel-to-NaK heat exchanger tube bundle (100 Inconel tubes, 6 ft long, $\frac{3}{16}$ in. OD, 0.017-in. wall thickness) was assembled, instrumented, and studied as a water-to-water heat exchange system (Fig. 7.4). Cold water was circulated through the tubes (NaK side) at Reynolds numbers of sufficient magnitude to produce low and calculable thermal resistances; hot water was circulated around the tube bundle in a parallel direction (fuel side). The inlet and outlet temperatures of both streams were measured by two thermocouples located in each of the four mixing chambers. The "fuel" side was instrumented with static pressure taps. Both flow rates were measured

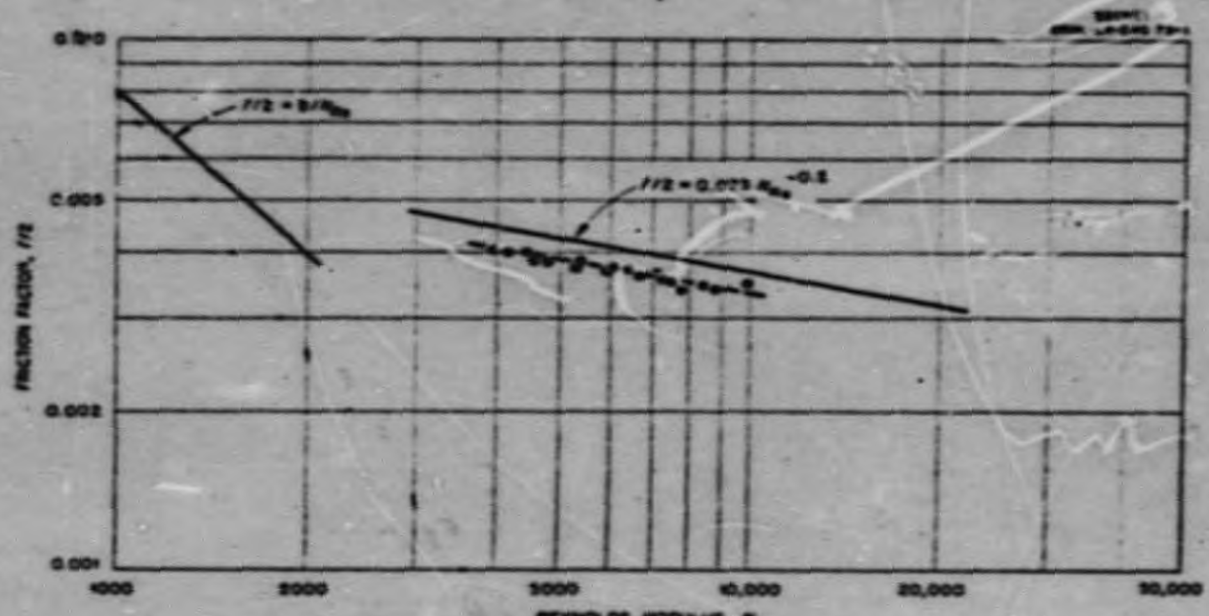

Fig. 7.1. Friction Factor for Isothermal Flow of NaF-ZrF_4-UF_4 (53.5-40-6.5 mole %) in a Smooth Circular Tube.

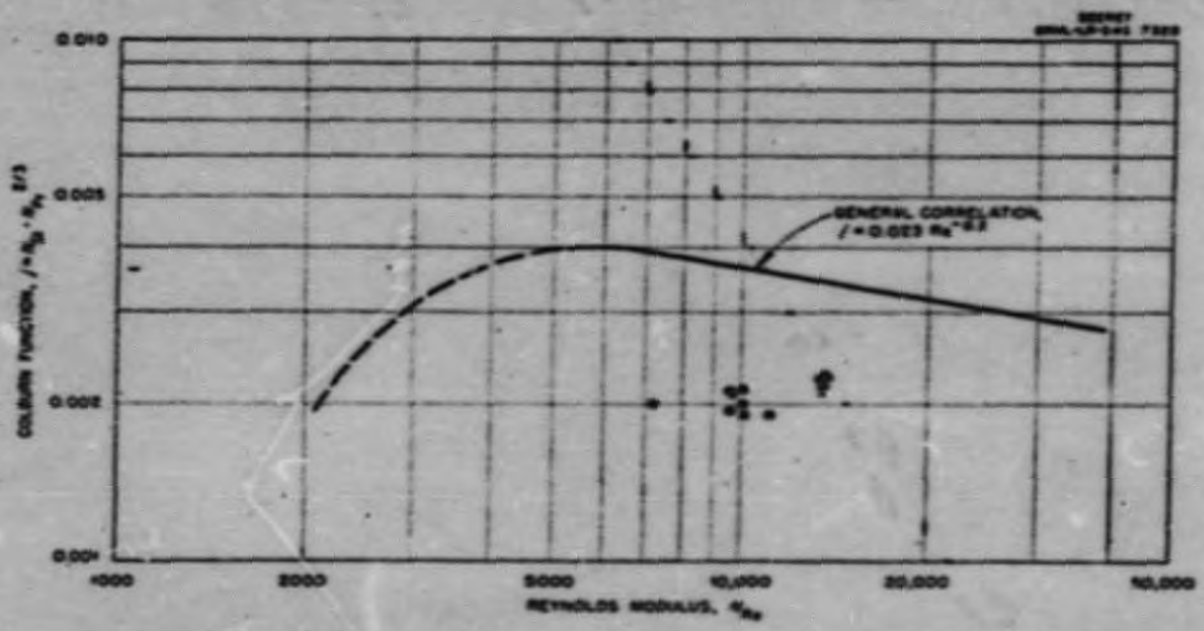

Fig. 7.2. Comparison of Heat Transfer Measurements on NaF-KF-LiF-UF_4 (11.2-41-45.3-2.5 mole %) in Inconel with the General Correlation for Ordinary Fluids.

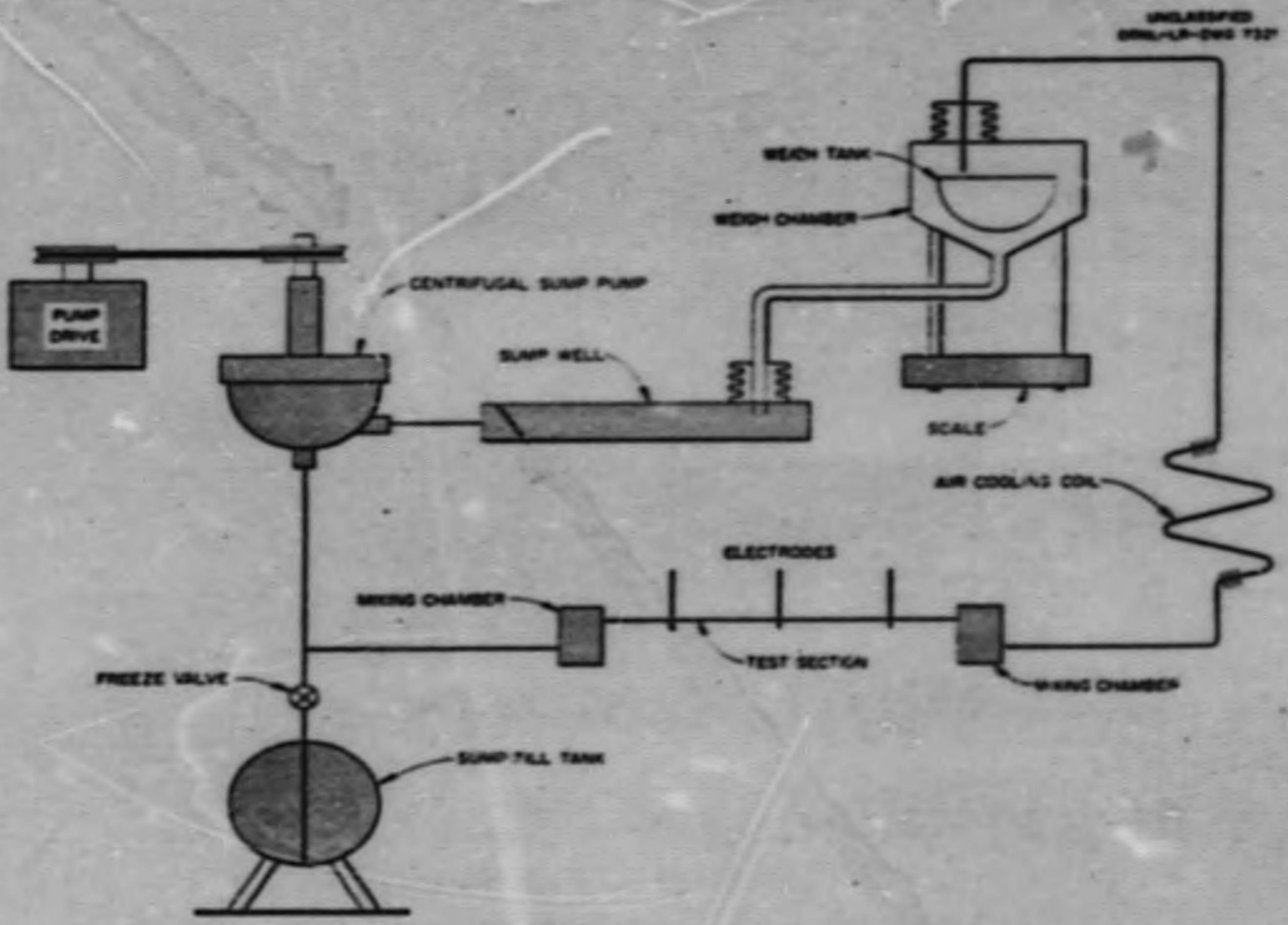

Fig. 7.3. Schematic Diagram of Small-Scale Pumping System for Heat Transfer Studies with Fused Salts.

by utilizing weigh tanks and electric timers.

Preliminary heat transfer and friction characteristic curves for the fuel side of the ART heat exchanger are shown in Figs. 7.5 and 7.6. Figure 7.5 is based on 18 data points that fall within ±10% of the mean curve. Heat balances were within a maximum of 2% of being perfect, and the temperatures measured in a given mixing chamber agreed to within 0.2°C of each other.

This heat exchanger system is being modified so that the fuel-side characteristics can be determined by utilizing the tube bundle as an electrical-resistance heater. Results of the study should further substantiate the curve shown in Fig. 7.5.

ART CORE HYDRODYNAMICS

J. O. Bradfute F. E. Lynch
L. D. Palmer
Reactor Experimental Engineering Division

G. L. Muller
Pratt & Whitney Aircraft

Further flow studies were conducted with the quarter-scale model of the 18-in. ART core. Many photographs of particles inserted in water flowing through the core without rotation have been taken, and quantitative velocity profiles have been obtained.

A vaned section was added at the inlet to the

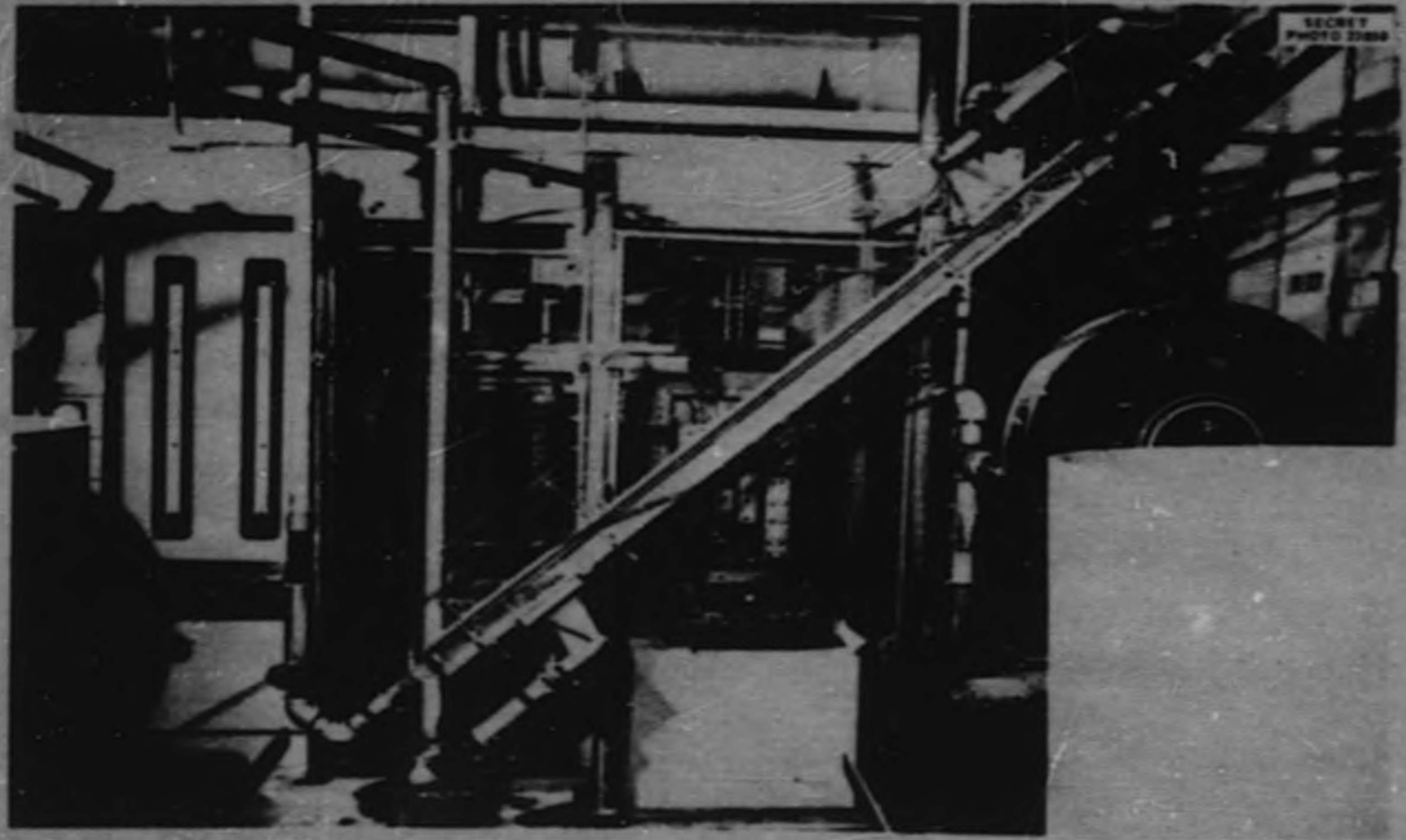

Fig. 7.4. ART Fuel-to-NaK Heat Exchanger Experiment.

core model to give the fluid a rotational component (approximately a 45-deg helical angle at the entrance). The velocity profiles were then observed qualitatively with the flow-visualization technique. Separation was observed next to the island wall rather than the shell wall, which was the case with straight-through flow. The axial component profiles are shown in Fig. 7.7.

In addition, a series of 16-mesh screens was added at the inlet, both with and without the rotation-producing vanes. Little effect attributable to the screens was noted in the straight-through case, except that the separation region appeared to be much less turbulent; indeed, the negative profiles were easy to see. They appeared to be approximately parabolic, and thus they suggested

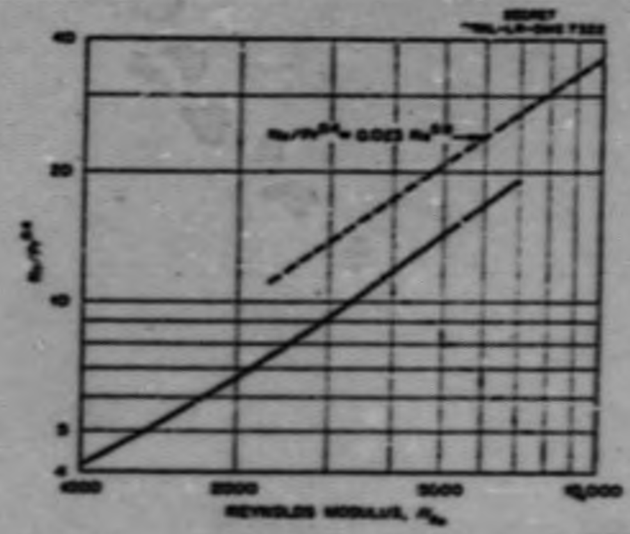

Fig. 7.5. Preliminary Heat Transfer Characteristics of the Fuel Side of the ART Fuel-to-NaK Heat Exchanger as Determined by Water-to-Water Tests.

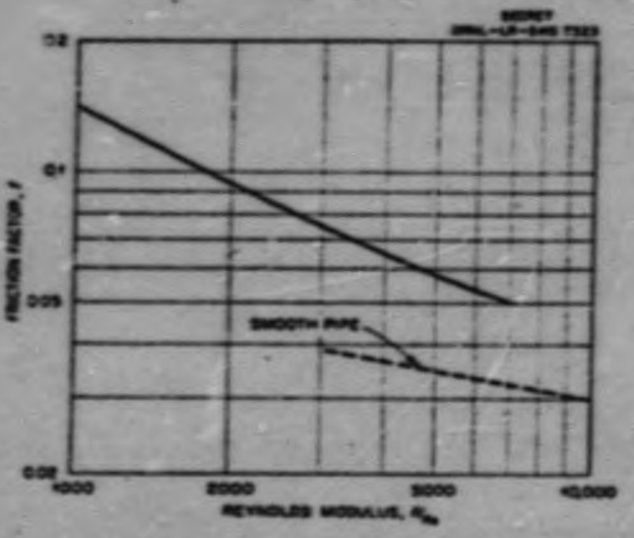

Fig. 7.6. Preliminary Friction Characteristics of the Fuel Side of the ART Fuel-to-NaK Heat Exchanger.

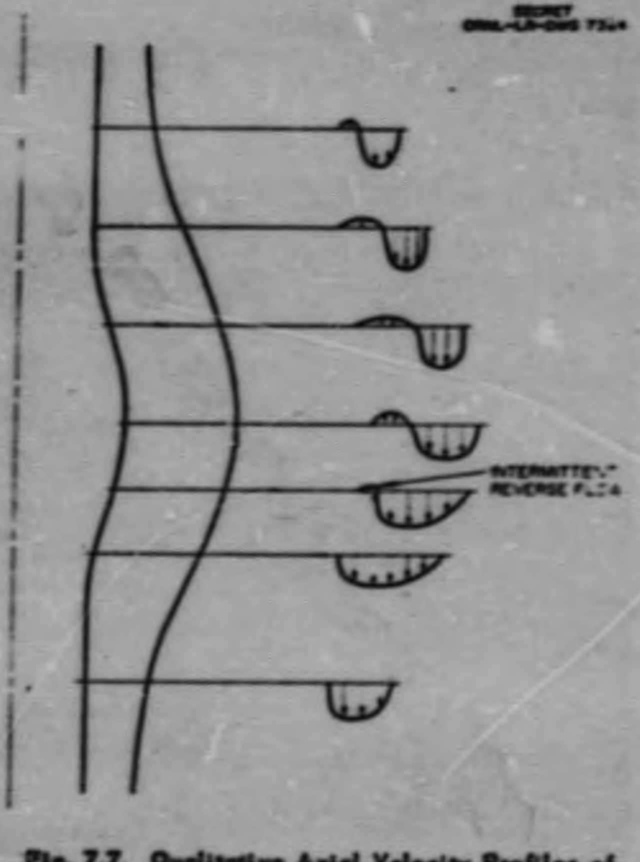

Fig. 7.7. Qualitative Axial Velocity Profiles of Flow Through a Model of the ART Core at a Reynolds Number of 3000 with a Rotational Velocity Component at the Inlet.

a laminar type of flow. No effect of the screens could be observed with rotational flow.

A two-dimensional diffuser has been designed which permits a variation of diffuser geometries and cross-sectional area ratios. The entire diffuser section is to be made of Plexiglas so that the flow can be studied by the flow-visualization system. The assembly is now being fabricated.

A preliminary feasibility study is at present being made on the control of the boundary layer in the core for the purpose of preventing separation of the boundary layer. A boundary layer suction technique is being considered.

A plastic 10/44-scale model of the 21-in. core has been designed and is now being fabricated. The odd scale was chosen to make the model fit the available testing facility.

REACTOR CORE HEAT TRANSFER

H. F. Poppendiek N. D. Greene
L. D. Palmer
Reactor Experimental Engineering Division

The hydrodynamic studies being made for the ART core indicate that when separation regions exist they are often characterized by repetitive, short periods of flow stagnation. A study was made of the temperature and tensile stress fluctuations in the Inconel core wall that result from these periods of flow stagnation. The following idealized system depicting the ART core wall during a short period of flow stagnation was considered. It was postulated that a layer of fuel contiguous to the Inconel wall suddenly stagnated for a period of 0.1 sec under the volume heat flux condition of 5 kw/cm^3. This flux is representative of the conditions in the ART because of the high flux peak at the wall. After a 0.1-sec time interval the fuel and wall temperature would rise about 260°F if no heat transfer were present; transient heat conduction into the Inconel wall, however, would reduce this temperature rise. A numerical composite-slab heat transfer analysis was made for this problem, and the results indicate that the Inconel-fuel interface temperature would rise about 60°F in 0.1 sec. This temperature rise would, of course, be much smaller if the thermal conductivity of Inconel were not so poor. The corresponding elastic thermal stress for this temperature fluctuation was found to be about −15,000 psi. These results suggest that the fluid flow in the core should not be allowed to fluctuate.

All mechanical components, including the power supply, of the volume heat source experiment for reactor cores with nonuniform flow cross section have been constructed and installed. System leak testing and flow calibration are now being carried out. An "infinitely" adjustable power input (that is, 15 to 100 kw) to the test section will be possible by means of several saturable reactors that have been shown to possess excellent voltage regulation characteristics under the desired load. The electrical and power instrumentation is nearing completion. The temperature structure within an insulated, divergent test channel will soon be studied for low power densities.

Several heat transfer analyses that are useful in predicting the thermal structure within a circulating-fuel reactor core have been completed. A report is being prepared which tabulates some of the detailed temperature profiles derived for the forced-convection volume-heat-source systems described previously.[1,2] These temperature data will make it possible to determine rapidly the complicated, radial, fuel-temperature profiles in circulating-fuel reactors whose pipe or channel ducts are being cooled at the walls. Also, a transient temperature solution was derived for the case in which fuel stagnates momentarily next to the Inconel core shell. Another analysis was concerned with a boundary layer temperature solution where a volumetric heat source exists in the fluid; thermal and hydrodynamic boundary layers are not presumed to be equal.

FREE CONVECTION IN FLUIDS HAVING A VOLUME HEAT SOURCE

D. C. Hamilton F. E. Lynch
Reactor Experimental Engineering Division

The objectives of the free-convection research and the progress were previously reported.[3] Both the theoretical and experimental analyses of the three-parallel-plates system have been completed, and a report is to be issued.[4] The three-parallel-

---

[1] H. F. Poppendiek and L. D. Palmer, *Forced Convection Heat Transfer in Pipes with Volume Heat Sources Within the Fluids*, ORNL-1395 (Nov. 5, 1953).

[2] H. F. Poppendiek and L. D. Palmer, *Forced Convection Heat Transfer Between Parallel Plates and in Annuli with Volume Heat Sources Within the Fluids*, ORNL-1701 (May 11, 1954).

[3] D. C. Hamilton and F. E. Lynch, *ANP Quar. Prog. Rep. Dec. 10, 1954*, ORNL-1816, p 113.

[4] D. C. Hamilton and F. E. Lynch, *Free Convection Theory and Experiment in Fluids Having a Volume Heat Source*, ORNL-1888 (to be issued).

plates system is shown schematically in the upper inset of Fig. 7.8; it consists of three parallel and equally spaced vertical copper plates, 8 in. wide and 36 in. high, with a channel width, x_0, of 0.5 in. Plastic bottoms and ends make leakproof containers of the two free-convection channels, which are filled with a dilute electrolyte (HCl in H_2O). With the two outer plates grounded and the center plate maintained at a given a-c voltage, heat is generated uniformly within the electrolyte. The heat thus generated is transferred by free convection to the outer walls and then through the outer walls to the coolant channels in which cooling water flows vertically upward. Thermocouple probe wells were provided so that the temperature within each wall could be measured at various vertical levels in the system. The variables measured were coolant flow rate and temperature rise, power input to the apparatus, and the three wall temperatures at various levels.

A theoretical analysis for laminar flow was made that was based on the postulates that, in the region away from the top or bottom, the velocity profile becomes fully established and unidimensional and that the temperature becomes linear with the vertical coordinate, z, and has the same vertical gradient, A, as the coolant mixed mean temperature. Both velocity and temperature solutions were obtained. The maximum temperature at a given level occurs at the center wall. The equation for the dimensionless center wall temperature, $\Phi(0)$, follows, and $\Phi(0)$, N_I, and N_{III}, are defined on Fig. 7.8:

Semiquantitative visual observations of the paths of suspended droplets indicated that the free-convection circuit existed as one long cell and that the velocity profile became established in the middle region and was similar to that predicted by the theoretical analysis. The onset of turbulence occurred at a Grashof modulus of 5×10^9, the same as that for ordinary free convection.

A curve is given in the lower inset of Fig. 7.8 that shows the typical vertical variation of the experimental $\Phi(0)$. In comparing the laminar regime minimum $\Phi(0)$ data with the theory, it is seen that, for N_{III} less than 1300, the data are about 20% lower than the theory; this is good agreement. For these data, A was uniform and approximately equal to A_c, the coolant mixed mean temperature gradient. For the data (not shown here) for which N_{III} was greater than 1300, A was definitely not uniform; it was as much as ten times greater than A_c; and the $\Phi(0)$ data were 50% lower than the theory.

From the turbulent regime data, it is seen that free convection can reduce the maximum temperature difference in such systems to at least one tenth that which would be present if the heat were transferred by conduction alone.

Variables not defined on Fig. 7.8 are: k, thermal conductivity; g, acceleration due to gravity; β, temperature coefficient of expansion; α, thermal diffusivity; ν, kinematic viscosity; and S, volume heat source term.

$$\Phi(0) = \lambda^{-2}\left[\sin\lambda \sinh\lambda - a(1 - \cos\lambda \cosh\lambda) + c(\cos\lambda \sinh\lambda - \sin\lambda \cosh\lambda)\right] \quad ,$$

where

$$\lambda = \left(\frac{N_I}{64}\right)^{1/4} ,$$

$$a = -1 - 2\left(\frac{\sin^2\lambda + \sin\lambda \sinh\lambda - \lambda \sin\lambda \cosh\lambda - \lambda \cos\lambda \sinh\lambda}{\sinh^2\lambda - \sin^2\lambda}\right) \quad ,$$

$$c = \frac{(\cosh\lambda - \cos\lambda)(\sinh\lambda + \sin\lambda) - 2\lambda \sin\lambda \sinh}{\sinh^2\lambda - \sin^2\lambda} \quad .$$

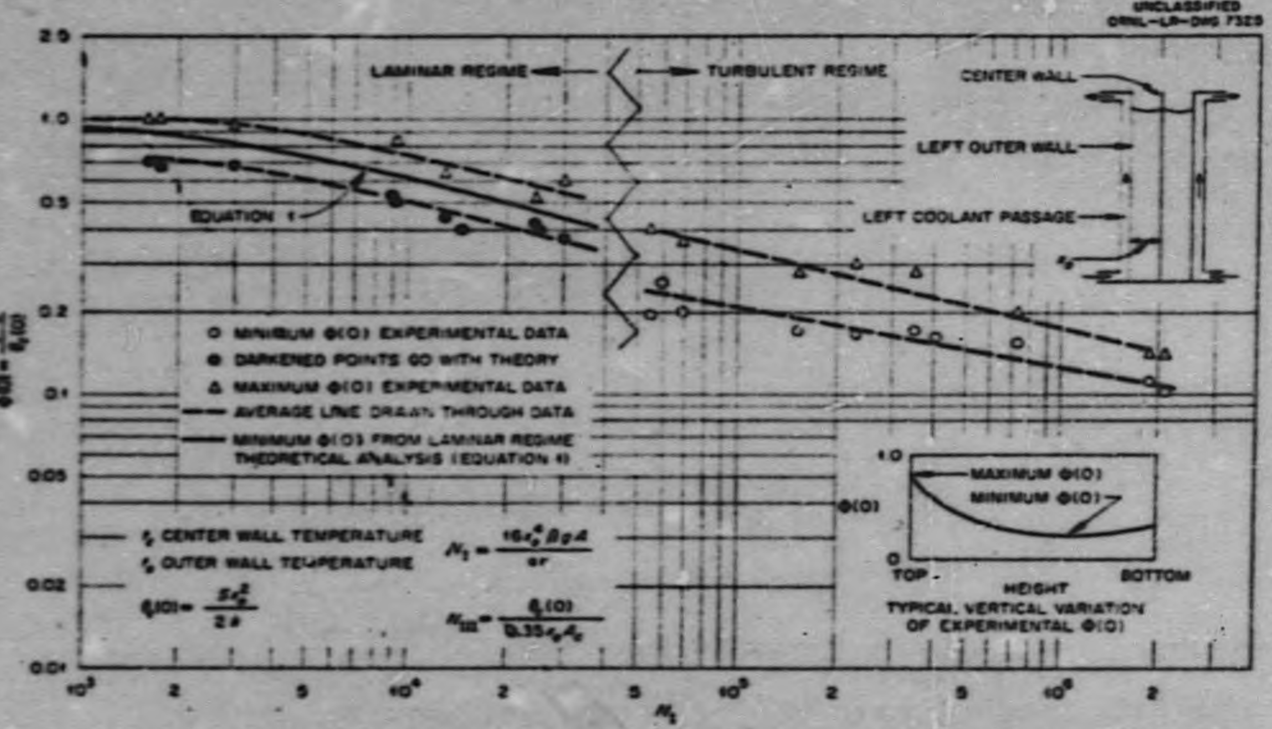

Fig. 7.8. Dimensionless Temperature Function for $N_{III} < 1300$.

HEAT CAPACITY

W. D. Powers

Reactor Experimental Engineering Division

The enthalpies and heat capacities of four fluoride compositions and of lithium hydride have been determined by using the copper-block calorimeter. The results are listed below:

NaF-ZrF_4-UF_4 (50-46-4 mole %)

Liquid (540 to 894°C)

$$H_T - H_{25^\circ C} = -3.3 + 0.3178T - (4.28 \times 10^{-5})T^2$$

$$c_p = 0.3178 - (8.56 \times 10^{-5})T$$

NaF-ZrF_4 (50-50 mole %)

Solid (54 to 488°C)

$$H_T - H_{25^\circ C} = -4.4 + 0.1798T + (2.69 \times 10^{-5})T^2$$

$$c_p = 0.1798 + (5.38 \times 10^{-5})T$$

Liquid (546 to 899°C)

$$H_T - H_{25^\circ C} = -9.8 + 0.3508T - (5.39 \times 10^{-5})T^2$$

$$c_p = 0.3508 - (10.79 \times 10^{-5})T$$

$$\Delta H_{fusion} = 63 \text{ at } 510^\circ C$$

NaF-ZrF_4-UF_4 (56-39-5 mole %)

Solid (137 to 503°C)

$$H_T - H_{35^\circ C} = -4.3 + 0.1596T + (5.15 \times 10^{-5})T^2$$

$$c_p = 0.1596 + (10.29 \times 10^{-5})T$$

Liquid (567 to 892°C)

$$H_T - H_{35^\circ C} = 0.6 + 0.3033T - (3.24 \times 10^{-5})T^2$$

$$c_p = 0.3033 - (6.47 \times 10^{-5})T$$

$$\Delta H_{fusion} = 57 \text{ at } 530^\circ C$$

NaF-LiF-ZrF_4-UF_4 (20-55-21-4 mole %)

Liquid (582 to 900°C)

$$H_T - H_{25^\circ C} = -25.9 + 0.4314T - (7.42 \times 10^{-5})T^2$$

$$c_p = 0.4314 - (14.85 \times 10^{-5})T$$

Lithium Hydride

Solid (100 to 490°C)

$$H_T - H_{35°C} = -38.5 + 0.939T + (6.6 \times 10^{-4})T^2$$

$$c_p = 0.939 + (0.132 \times 10^{-2})T$$

In the above expressions,

H_T = enthalpy in cal/g,

c_p = heat capacity in cal/g·°C,

T = temperature in °C,

ΔH_{fusion} = heat of fusion in cal/g.

The enthalpies and heat capacities of the first two mixtures had been previously determined by using the Bunsen ice calorimeters. In view of the present importance of the zirconium fluoride-base fuels, however, it was felt desirable to determine these properties with the more precise copper-block calorimeters.

The heat capacities of liquid fluoride mixtures may be predicted within about 15% on the basis of their chemical composition. It has been found that the product of the heat capacity (cal/g·°C) and a function $\overline{M}/\overline{N}$ is remarkably constant. This function is defined as:

$\overline{M} = \sum_i x_i M_i$,

$\overline{N} = \sum_i x_i N_i$,

$\overline{M}$ = average molecular weight,

M_i = molecular weight of component,

x_i = mole fraction of component,

$\overline{N}$ = average number of ions,

N_i = number of ions in component.

Figure 7.9 shows a plot of heat capacity vs the function $\overline{M}/\overline{N}$. For the 17 fluoride mixtures being studied at present, the average of the product of c_p and $\overline{M}/\overline{N}$ is 9.0. The corresponding average product for the six fluoride mixtures containing approximately equal molar amounts of NaF and ZrF_4 and from 0 to 7 mole % UF_4 was found to be 8.1.

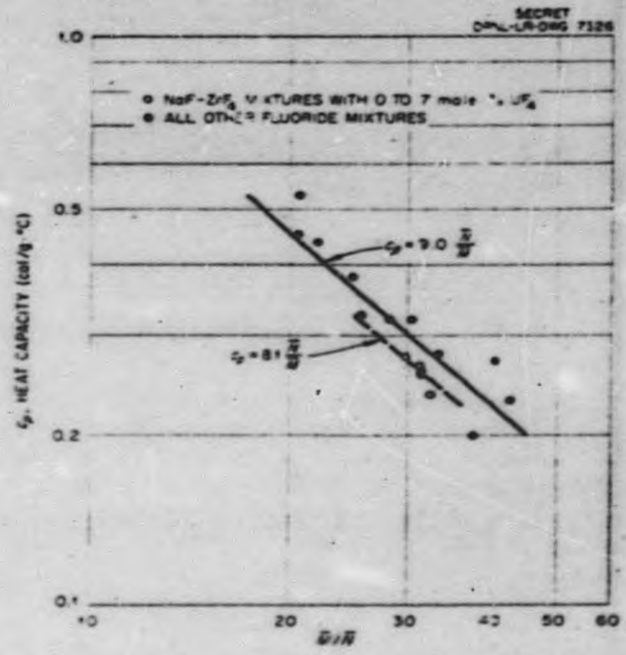

Fig. 7.9. c_p vs $\overline{M}/\overline{N}$ for Molten Fluoride Mixtures.

VISCOSITY

S. I. Cohen

Reactor Experimental Engineering Division

Viscosity measurements were made on seven fluoride mixtures, and the results are tabulated in Table 7.1. The data are expressed in the form

$$\mu = A\,e^{B/T} \quad ,$$

where T is in °K. These viscosity data have been plotted in Fig. 7.10. No equation is listed in Table 7.1 for salt *a* because of the slight curvature in the data, which may be noted in the figure. Salts *b*, *c*, and *d* are mixtures which had been studied prior to the recently completed viscometry refinement program. Salts *a*, *e*, *f*, and *g* are mixtures which have been formulated recently. Measurements were made on all the mixtures (except salt *g*) by using both the Brookfield and capillary viscometers; the results obtained by these two completely different instruments were in satisfactory agreement (deviations from the average line through the data were within ±12%). Measurements on salt *g*, which contained BeF_2, were made in a separate beryllium facility. Data were taken with two capillary viscometers to furnish a check.

Figure 7.11 presents a plot of the viscosities of seven mixtures containing BeF_2. Mixtures *g*, *i*, and *k* were studied at ORNL. Mound Laboratory investigated mixtures *h* and *j*, and mixtures *l* and *m* were studied at KAPL. The formulas of these mixtures in mole percentages, as well as the

TABLE 7.1. SUMMARY OF CURRENT VISCOSITY MEASUREMENTS

Mixture[a]	Composition	Viscosity (cp)	μ	Reference
a	$NaF-LiF-ZrF_4-UF_4-UF_3$ (20.9-38.4-35.7-4-1 mole %)	At 550°C, 13.5 At 800°C, 4.3		(*b*)
b	$NaF-ZrF_4-UF_4$ (50-46-4 mole %)	At 570°C, 11 At 870°C, 3.4	$0.1307\ e^{3730/T}$	(*c*)
c	$NaF-UF_4$ (66.7-33.3 mole %)	At 700°C, 10.25 At 900°C, 5.1	$0.1715\ e^{3984/T}$	(*d*)
d	$NaF-KF-UF_4$ (46.5-26.0-27.5 mole %)	At 600°C, 17 At 900°C, 4.4	$0.0866\ e^{4611/T}$	(*e*)
e	$NaF-LiF-ZrF_4-UF_4-UF_3$ (20-55-21-3.6-0.4 mole %)	At 600°C, 12 At 850°C, 3.7	$0.061\ e^{4611/T}$	(*f*)
f	$NaF-LiF-ZrF_4$ (22-55-23 mole %)	At 600°C, 12 At 900°C, 3.1	$0.061\ e^{4611/T}$	(*f*)
g	$NaF-LiF-BeF_2$ (56-16-28 mole %)	At 575°C, 7 At 800°C, 2.9	$0.105\ e^{3560/T}$	(*g*)

[a] See Fig. 7.10.

[b] S. I. Cohen and T. N. Jones, *Measurement of the Viscosity of Composition 72*, ORNL CF-55-3-61 (Mar. 8, 1955).

[c] S. I. Cohen and T. N. Jones, *Measurement of the Viscosity of Composition 30*, ORNL CF-55-3-62 (Mar. 9,, 1955).

[d] S. I. Cohen and T. N. Jones, *Measurement of the Viscosity of Composition 43*, ORNL CF-55-3-137 (Mar. 16, 1955).

[e] S. I. Cohen and T. N. Jones, *Measurement of the Viscosity of Composition 2*, ORNL CF-55-4-32 (Apr. 1, 1955).

[f] S. I. Cohen and T. N. Jones, *Measurement of the Viscosities of Composition 81 and Composition 82*, ORNL CF-55-5-58 (May 16, 1955).

[g] S. I. Cohen and T. N. Jones, *Measurement of the Viscosity of Composition 78*, ORNL CF-55-5-59 (May 16, 1955).

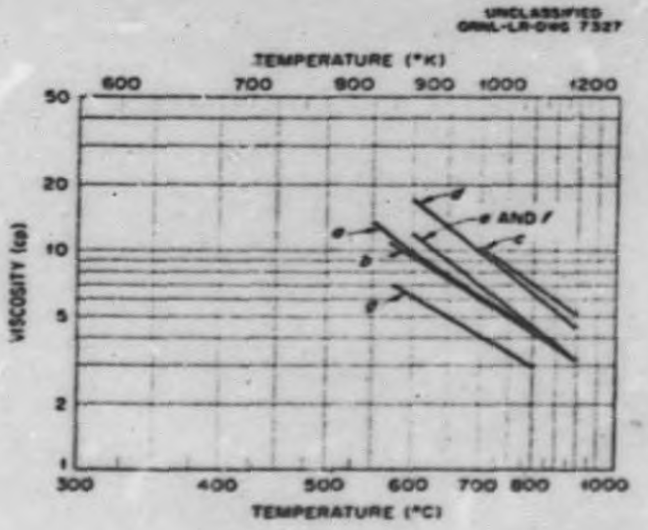

Fig. 7.10. Viscosities of Fluoride Mixtures Currently Being Studied.

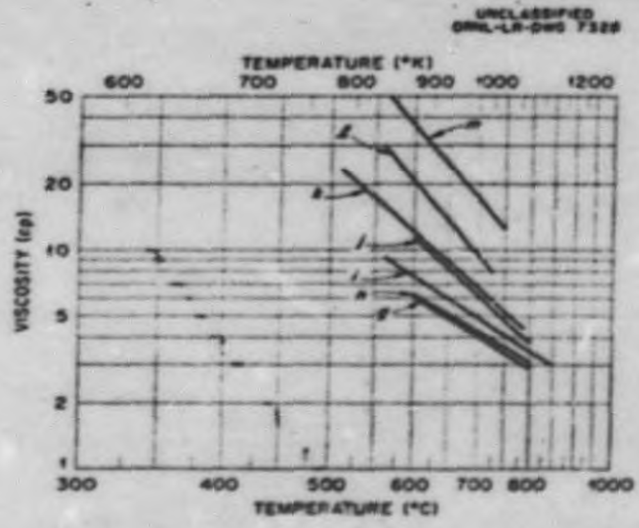

Fig. 7.11. Viscosities of Some Fluoride Mixtures Containing BeF_2.

TABLE 7.2. THE VISCOSITIES AT 700°C OF SEVERAL MIXTURES CONTAINING BeF_2

Mixture[a]	Composition	Viscosity (cp)	BeF_2 Content (wt %)	Reference
g	BeF_2-LiF-NaF (28-16-56 mole %)	4.1	32.2	(*b*)
h	BeF_2-NaF (38.3-61.7 mole %)	4.25	40.0	(*c*)
i	BeF_2-LiF (31-69 mole %)	5.0	44.9	(*d*)
j	BeF_2-NaF (44.4-55.6 mole %)	6.25	47.0	(*c*)
k	BeF_2-NaF (43-57 mole %)	6.75	45.8	(*d*)
l	BeF_2-NaF-UF_4 (51.9-47.9-0.25 mole %)	9.6	53.9	(*e*)
m	BeF_2-LiF-ThF_4-UF_4 (49.43-49.43-1.03-0.12 mole %)	17	58.6	(*f*)

[a] See Figs. 7.11 and 7.12.

[b] S. I. Cohen and T. N. Jones, *Measurement of the Viscosity of Composition 7x*, ORNL CF-55-5-59 (May 16, 1955).

[c] Communication from J. F. Eichelberger, Mound Laboratory

[d] S. I. Cohen, *ANP Quar. Prog. Rep. Mar. 10, 1955*, ORNL-1864, p 143.

[e] J. K. Davidson, R. J. Herbert, and B. T. Morecroft, *Fused Fluoride Homogeneous Reactor System for Submarine Propulsion, (SAR Phase III Study)*, KAPL-992.

[f] Personal communication from J. K. Davidson, Knolls Atomic Power Laboratory.

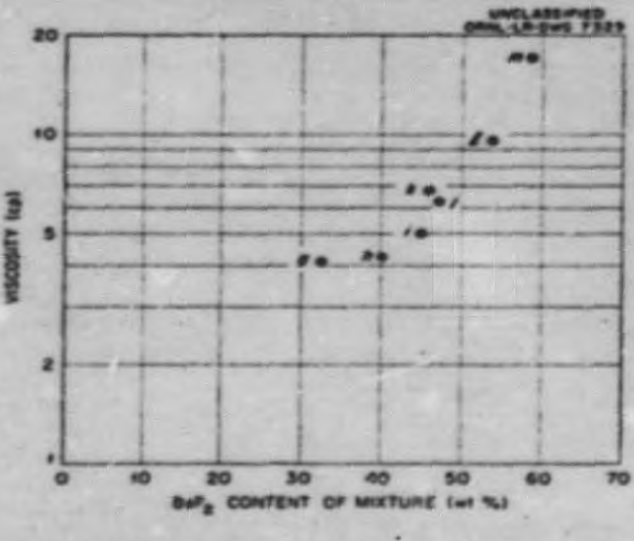

Fig. 7.12. Viscosities at 700°C vs BeF_2 Content of Seven Fluoride Mixtures. Compositions of the mixtures are given in Table 7.2.

BeF_2 contents in weight percentages and the viscosities at 700°C, are listed in Table 7.2.

Figure 7.12 shows a plot of the viscosity of each of these mixtures at 700°C vs the weight percentage of BeF_2 in each of the mixtures; note that the viscosity decreases as the BeF_2 content decreases. Mixture *g* was formulated because it appeared from this trend that the kinematic viscosity might compete with the viscosities of salts in the NaF-ZrF_4-UF_4 system. The kinematic viscosity of mixture *g*, BeF_2-LiF-NaF (28-16-56 mole %), was found to be about 15% higher than that of NaF-ZrF_4-UF_4 (50-46-4 mole %), the salt presently being considered as the fuel for the ART.

THERMAL CONDUCTIVITY

W. D. Powers

Reactor Experimental Engineering Division

Two methods for the determination of thermal conductivities of liquid fluoride mixtures are being investigated. A radial thermal conductivity cell has been redesigned and is being fabricated. The major difficulty in using the apparatus as originally designed was the lack of sufficient guard heating to assure pure radial heat flow.

A flat-plate system is now being investigated. The liquid is contained in cells consisting of two parallel flat plates of metal joined at the edges with 10-mil-thick sheet metal. The conductivity of the liquid in the cell can be calculated by knowing the area of the plates and the distance between them and by measuring the amount of heat passing from one plate to the other and the temperature differences between them. Some preliminary data on a ZrF_4-base fluoride mixture are currently being obtained that are in agreement with previous conductivity data obtained with the variable-gap device.

ELECTRICAL CONDUCTIVITY

N. D. Greene
Reactor Experimental Engineering Division

Conductivity studies of several aqueous electrolytes have indicated the presence of a considerable amount of polarization within the experimental, platinum conductivity cell. Accordingly, a second potential electrode will be installed, which, when used in conjunction with an electrometer having a 10-megohm input, should reduce the effects of polarization. Similar conductivity measurements of some nonaqueous electrolytes (molten salts) will be made to compare the differences in the degree of polarization between the two types of electrolytes.

8. RADIATION DAMAGE

D. S. Billington J. B. Trice
Solid State Division

Preliminary results from a series of MTR irradiations of Inconel capsules designed to compare UF_3- and UF_4-base fuels show no corrosion, no significant uranium segregation, and no changes in concentrations of impurities in the fluoride mixture. The loop in which a fuel mixture was circulated in the LITR has been sectioned, and preliminary examinations have been made. The miniature loop designed for operation in a vertical hole in the LITR is in the final stages of assembly, and charcoal traps to delay fission gases in the event of a rupture have been tested and incorporated in the cooling-air off-gas line.

A tube-burst stress-corrosion apparatus has been assembled for insertion in the LITR, and an LITR-irradiated stress-corrosion rig is ready for examination. The creep apparatus inserted in the MTR has completed six weeks of irradiation and is to be returned to ORNL for measurements. A theoretical study has been completed which indicates that xenon will be sparged from the ART, as presently designed, in sufficient quantity to alleviate the control problem.

MTR STATIC CORROSION TESTS

W. E. Browning G. W. Keilholtz
Solid State Division

H. L. Hemphill
Analytical Chemistry Division

Two more of a series of paired capsules are being irradiated for two weeks each in the MTR. These Inconel capsules are being irradiated in order to compare the effects of UF_3 and UF_4 in NaF-ZrF_4-base fuel mixtures, as described previously.[1] Three additional Inconel capsules that had been irradiated for two weeks were opened and analyzed chemically[2] and metallographically.[3] In two of these capsules the fluoride mixture contained 2 mole % UF_3, and in the other capsule the fluoride mixture contained 2 mole % UF_4. A control capsule for each mixture was also opened and analyzed. No corrosion could be found in any of these five capsules. One irradiated capsule containing UF_4 that was examined earlier had shown slight corrosion. The next series of capsules that will become available for analysis consists of four capsules that will have been irradiated three times as long (six weeks) as those analyzed thus far. The capsules in this series will be more likely to reveal any difference that might exist between the two fuel materials.

The starting fuel mixtures were analyzed[4] for trivalent uranium, total uranium, iron, chromium, nickel, sodium, and zirconium. The UF_3-bearing batch had more than 96% of its uranium in the trivalent condition, whereas no trivalent uranium was found in the UF_4-bearing batch when analyzed by a method which is sensitive to 0.005% U^{3+}. The results of the chemical analyses for uranium, iron, chromium, and nickel in the starting mixture, the control mixtures, and the irradiated mixtures were averaged, and ratios were computed to determine whether there were changes in distribution or composition. The results of these statistical analyses, which are presented in Table 8.1, indicate that there was no significant uranium segregation and that there were no changes in concentration of uranium, iron, chromium, and nickel.

Chemical analyses were also obtained of four additional irradiated Inconel capsules in which the fluoride fuel mixture initially contained 4 mole % UF_4. The uranium analyses of inner cores and outer cores of the samples agreed to within 6%. The iron, chromium, and nickel concentrations were between 0.01 and 0.1%. Additional capsules of this type are being prepared for irradiation in the MTR at 1500°F, for control runs, and for thermal cycling tests.

---

[1] W. E. Browning, G. W. Keilholtz, and H. L. Hemphill, *ANP Quar. Prog. Rep. Dec. 10, 1954*, ORNL-1816, p 120.

[2] Chemical analyses by the General Analysis Laboratory, Analytical Chemistry Division.

[3] Metallographic analyses by the Remote Metallography Group, Solid State Division.

[4] Analyses performed by the Y-12 Analytical Laboratory.

TABLE 8.1. SUMMARY OF ANALYTICAL RESULTS FOR SERIES OF CAPSULES TESTED TO COMPARE EFFECTS OF UF_3 AND UF_4 IN $NaF\text{-}ZrF_4$-BASE FUEL MIXTURES

Capsule Category	Number of Capsules	Uranium Distribution,[a] $U_a(av)/U_b(av)$	Ratio of Final to Initial Uranium Content[b]	Ratio of Final to Initial Impurity Concentration[c]		
				Fe	Cr	Ni
All capsules in series	7	1.003 ± 0.028	1.021 ± 0.022	1.47 ± >1.47	1.08 ± >1.08	(d)
All irradiated capsules	5	1.021 ± 0.033	1.038 ± 0.024	1.45 ± >1.45	0.48 ± 1.5	1.48 ± 0.56
All control capsules	2	0.96 ± 0.0240	0.989 ± 0.02[e]	1.53 ± >1.53	3.0 ± 1.2	(d)
Irradiated capsules containing 2 mole % UF_4	2	1.026 ± 0.044	1.031 ± 0.04[e]	1.67 ± 1.47	0.0 ± 1[e]	3.9 ± 1.1
Control capsule containing 2 mole % UF_4	1	0.947 ± 0.028	0.975 ± 0.024	(d)	(d)	(d)
Irradiated capsules containing 2 mole % UF_3	3	1.001 ± 0.048	1.051 ± 0.05[e]	1.31 ± >1.31	0.54 ± 0.6	0.95 ± 0.05
Control capsule containing 2 mole % UF_3	1	0.972 ± 0.020	0.994 ± 0.02[e]	1.53 ± >1.53	3.0 ± 1.2	(d)

[a] U_a is the uranium content of the inner core of a sample, and U_b is the uranium content of the outer core of a sample.

[b] Corrected for burnup.

[c] Confidence limits are at 95% level.

[d] Values obtained were influenced by a sample which was probably contaminated with Inconel and therefore are not significant.

[e] Estimated.

LITR HORIZONTAL-BEAM-HOLE FLUORIDE-FUEL LOOP

O. Sisman — J. G. Morgan
C. D. Baumann — M. T. Morgan
W. E. Brundage — A. S. Olson
R. M. Carroll — W. W. Parkinson
Solid State Division

The operation of the loop for circulating fluoride-base fuel in the LITR horizontal beam hole to study the effect of reactor irradiation on corrosion and fuel stability was described in the previous report.[5] The fuel mixture was composed of 62.5 mole % NaF, 12.5 mole % ZrF_4, and 25 mole % UF_4. The loop was cleaned by running it at 1500°F for 16 hr with a non-uranium-bearing salt. The actual fuel mixture was circulated in the loop for 645 hr, including 475 hr during which the LITR was at full power (3000 kw). The power generated in the loop was about 2.8 kw, and the linear flow rate of the fuel mixture was 8 to 10 fps, which corresponds to a Reynolds number of 5000 to 6500. The disassembly of the loop to provide specimens for metallurgical examination and chemical analysis and to reduce the loop to pieces of convenient size for fuel recovery has been completed.

After operation of the loop in the LITR, the section between the linear seal flange and the pump was sheared with remotely controlled equipment to permit removal of the pump in its shield. The loop in its water jacket was then transported to the hot cells of the Solid State Division for the remote disassembly operation. The out-of-pile end of the jacket was drawn from the withdrawal shield through a hole in the rear wall of a hot cell equipped with the special disassembly apparatus shown from above in Fig. 8.1.

An electrical impact wrench attached to the manipulator was used to loosen the screws holding the flange to the water jacket to permit partial withdrawal of the loop from the jacket. Electric and thermocouple leads joining the flange and the loop were cut remotely with ordinary sheet metal shears modified to operate hydraulically. Cutting the heat exchanger air tubes and the loop support rods with the band saw then permitted the flange to be pulled off over the sheared ends of the loop tubing (Fig. 8.2). Removal of the flange provided access to the loop for stripping of thermal insulation, heaters, wires, and graphite shield blocks. The loop is shown partially stripped in Fig. 8.3, as photographed through a window of the hot cell.

Tube sections about 2 in. long were cut from the fuel tubes for metallographic specimens. These specimens were taken at about 6-in. intervals from the part outside the jacket seal flange and at 2-ft intervals inside the flange, between the heat exchanger and the irradiated section. Additional specimens were taken from the heat exchanger and the venturi for examination of a longitudinal section. The U bend of the irradiated section was cut into five specimens from $\frac{1}{2}$ to 1 in. long, and additional specimens were cut from the remaining 18 in. of the irradiated section at about 6-in. intervals. The fuel was removed from these specimens by melting in an argon atmosphere. Four 2-in. sections of tube were also taken from the portion of the loop between the jacket flange and the pump, and two more were taken 6 in. back from the irradiated section to furnish samples for chemical analysis of the fuel.

Disassembly of the pump was complicated by its size and by the large stainless steel enclosure around the bowl (Fig. 8.4). A 300-amp, d-c welder equipped with a high-frequency-arc starter was used to cut the enclosure successfully. It was possible to guide the cutting electrode with a manipulator while cutting the sheet metal in a manner that prevented contamination of the fuel system with nonradioactive material. After the pump enclosure was removed, the insulation and the various wires and heaters were taken off to provide access to the pump bowl and the fuel tubes. After the fuel tubes were severed and the ends were clamped, the pump bowl was cut just above the fuel level by using the band saw (Fig. 8.5). There was a small accumulation of fuel (~1 g) visible on the upper parts of the pump baffles, but the activity was high enough to indicate the presence of a considerable quantity of fission products. The remainder of the pump bowl, including the baffles, was cut off immediately below the bowl flange for recovery of any fuel which might have splattered into the baffles. There was no fuel visible on the flanges, shaft, or seal of the upper portion of the pump, but the activity was too high to permit unshielded dismantling and examination. It was assumed that fission products which had vaporized from the fuel were the sources

---

[5] O. Sisman *et al.*, *ANP Quar. Prog. Rep. Mar. 10, 1955*, ORNL-1864, p. 150.

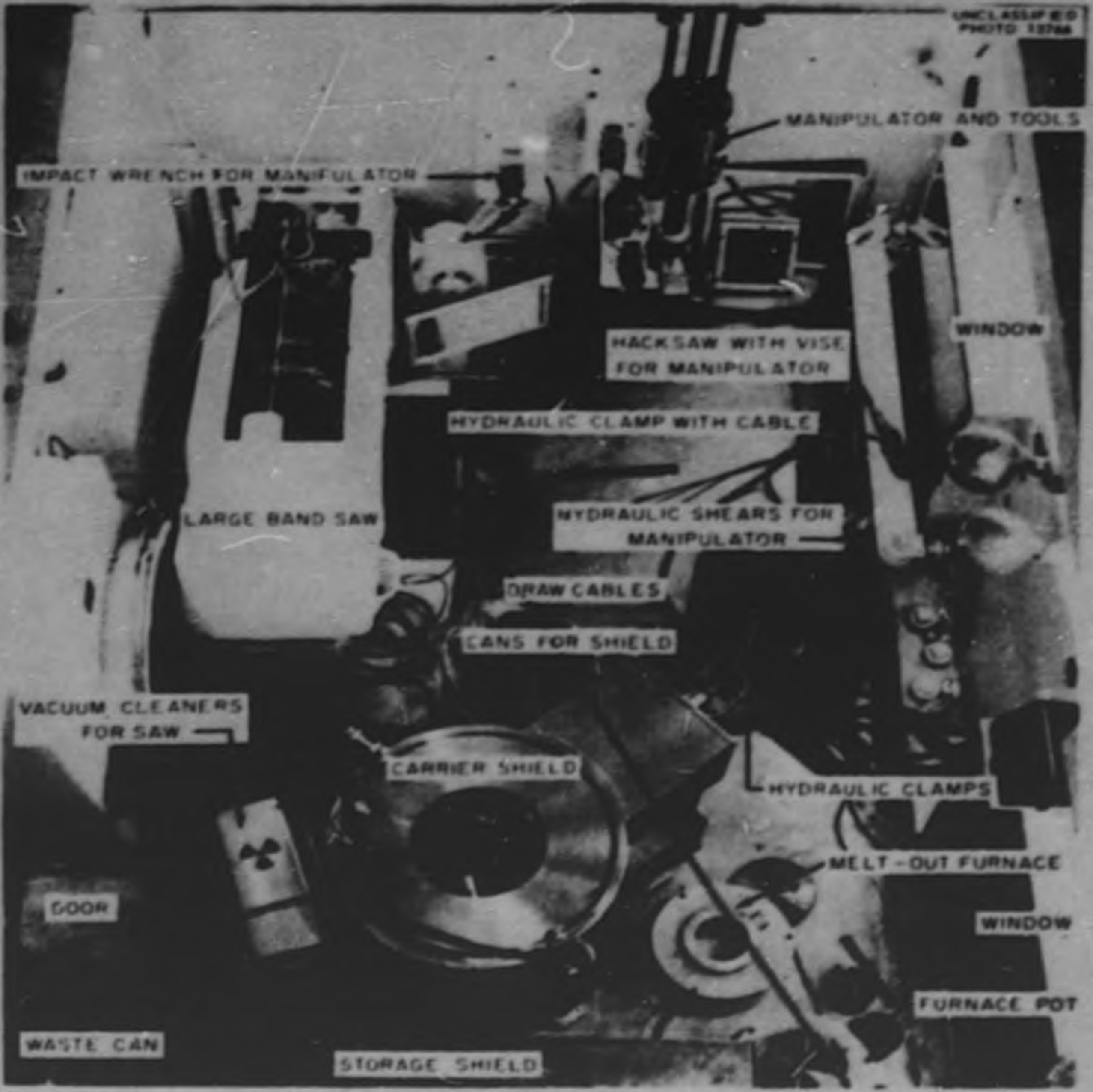

Fig. 8.1. Top View of Hot Cell and Equipment for Disassembly of LITR Fluoride-Fuel Loop.

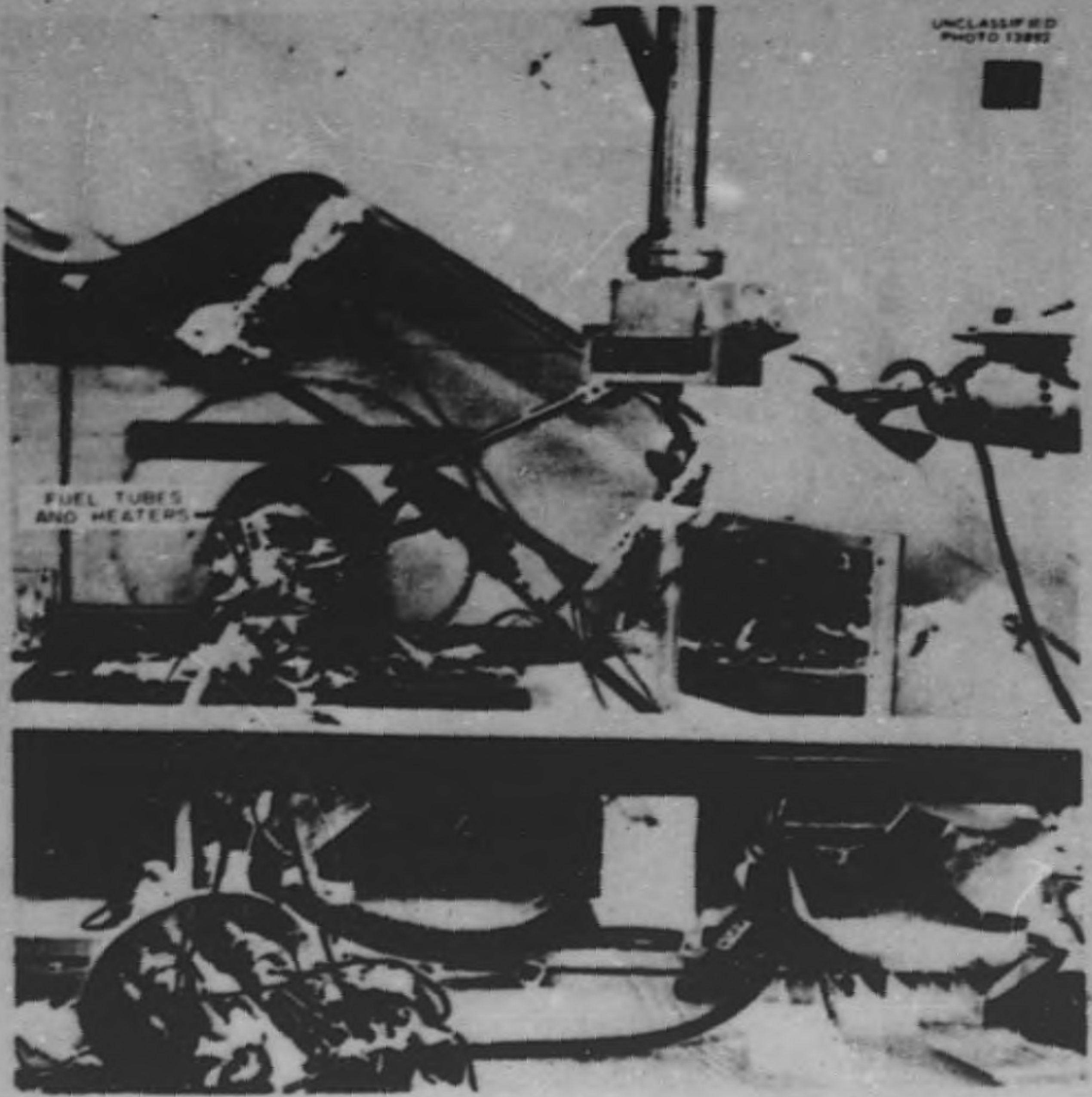

Fig. 8.2. Removal of Flange from Jacket of LITR Fluoride-Fuel Loop.

Fig. 8.3. Partly Disassembled LITR Fluoride-Fuel Loop.

of the activity, and, since an analysis of the condition of bearing and seals was precluded, this portion of the pump was discarded. The fuel-containing parts were stored for uranium recovery.

The metallurgical specimens have been prepared and photomicrographed. A preliminary analysis indicates that subsurface void formation was generally uniform throughout the loop to a depth of 0.8 mil. The uniformity of attack possibly resulted from the lack of a temperature differential in the loop. The temperature record shows that the fuel temperature could not have been more than 20°F lower in the out-of-pile parts of the loop than in the in-pile parts. Some sections showed grain growth, which is an indication that some temperatures were higher than those recorded, but even the areas of grain growth showed no significant change in depth of corrosion.

The fuel in the nose of the loop was in a maximum perturbed flux of approximately 0.8×10^{13} neutrons/cm^2·sec, which corresponds to a fission power density of 0.5 to 0.6 kw/cm^3. The power density gives a measure of the severity of conditions imposed upon at least one section of the loop tubing by radiation effects. No difference in the corrosion could be observed between this region and other, less severely irradiated, regions. Also, about the same depth of attack was found in the venturi section of the loop as was present in the rest of the loop, even though there was a large velocity gradient present. No intergranular attack was noted.

The six sections of tubing taken for chemical analysis were sampled by a drilling method described previously.[6] After the end of a tube section

---

[6] C. C. Webster and J. G. Morgan, *Solid State Semiann. Prog. Rep. Feb. 28, 1954*, ORNL-1677, p 27.

Fig. 8.4. LITR Fluoride-Fuel Loop Pump Prior to Removal of Enclosure for Providing a Helium Atmosphere.

had been cleaned by drilling a $\frac{1}{4}$-in. hole about $\frac{1}{2}$ in. deep in the fuel, each sample was bored out with a $\frac{3}{16}$-in. bit. Tungsten carbide–tipped bits were used to avoid contaminating the fuel with nonradioactive iron, chromium, or nickel. Unirradiated control samples were obtained from the fill line between the charge tank and the loop at the place where this line passed through the pump shield. The chemical analyses of the samples are almost complete, and radiochemical analyses for Cs^{137} and Zr^{95} have been made of two of the samples. The fission power of 2.7 and 2.5 kw indicated for the two samples by the Zr^{95} content compares favorably with the 2.8 kw estimated from electrical measurements made during operation of the loop. The results from the Cs^{137} analysis, 2.1 and 1.5 kw, are considerably lower, and they indicate escape of the Xe^{137} parent from the fuel.

In order to measure the fission power distribution along the irradiated section of the loop, an experiment was conducted in the LITR with a mockup of the loop. The mockup was designed to duplicate both the arrangement of structural materials and the macroscopic cross section of the fuel so that effective thermal-neutron flux values could be measured inside the fuel and then could be used to calculate the power generated by fissioning. The results are being compared with the activation of cobalt monitor foils attached to the loop and with additional data from the activation of borings taken from the metallurgical specimens. The results will be reported when all the data have been assembled and analyzed.

DEPOSITION OF Ru^{103} IN LITR FLUORIDE-FUEL LOOP

M. T. Robinson
Solid State Division

T. H. Handley
Analytical Chemistry Division

The deposition of the fission-product 40-day Ru^{103} on the surfaces of the fuel circuit of the ARE was reported previously.[7] Supporting evidence for this phenomenon has now been obtained from a study of samples taken from the loop described above. Two samples of tubing from the loop were examined by gamma-ray scintillation spectrometry. One sample was taken upstream from the high-flux region of the loop, and the other was taken at an equal distance downstream.

The ratio of Ru^{103} to Zr^{95}-Nb^{95} should have been 0.6 if the Ru^{103} had remained uniformly distributed throughout the loop. However, the ratio for the sample taken upstream was 5.33, and that for the sample taken downstream was 8.07. Within the experimental error, the Zr^{95}-Nb^{95} activity analyzed the same for both samples. The sample taken downstream from the high-flux region contained markedly more Ru^{103} than did the sample taken upstream. This difference is exactly that to be expected from rapid reaction of the ruthenium in the fuel with the container metals. These numbers, combined with operational and dimensional data, yielded a half life of 0.5 min for the rate constant for removal of Ru^{103} from the fuel in the loop. It was assumed for the calculation that the removal rate of Ru^{103} was a first-order function of the concentration.

---

[7] M. T. Robinson, S. A. Reynolds, and H. W. Wright, *ANP Quar. Prog. Rep. Mar. 10, 1955*, ORNL-1864, p 13.

Fig. 8.5. Bottom View of Pump Showing Accumulation of Fuel on Upper Parts of the Baffles.

After a delay of 53 days, the two pipe samples were re-examined to determine the apparent half lives of the two components of the gamma-ray spectrum. For the Ru^{103} peak (0.50 Mev), the half lives of two samples were 42 and 43 days, respectively, and amply confirmed the assignment of that activity. For the Zr^{95}-Nb^{95} peak, however, the results were 40 and 43 days, respectively, instead of the nearly 65 days expected. The contribution to this gamma-ray energy (0.78 Mev) must be largely from 37-day Nb^{95}, the 65-day Zr^{95} being very low in relative amount (a few per cent). It appears very likely that niobium deposits on the Inconel pipes along with ruthenium. The deposition rate for Nb^{95} cannot be estimated, at present, since it is produced very slowly from its Zr^{95} parent, rather than rapidly from fission as is the case with Ru^{103}.

Radiochemical analysis of a fuel sample for Ru^{103} indicated that the amount was below the limit of detection by that technique.[8] This demonstrates that the efficiency of ruthenium removal was comparable to that attained in the ARE.[7] No direct neutron activation of the elements of Inconel was observed.

MINIATURE IN-PILE LOOP

W. R. Willis M. F. Osborne
H. E. Robertson G. W. Keilholtz
Solid State Division

The miniature fluoride-fuel loop for insertion in a vertical hole in the LITR (described previously[9]) was charged with fuel and operated on the bench. It is now in the final stages of assembly for in-pile testing. An exact mockup of the experiment has been inserted in the reactor and has been withdrawn

---

[8] W. W. Parkinson, personal communication.

[9] W. R. Willis *et al.*, *ANP Quar. Prog. Rep. Mar. 10, 1955*, ORNL-1864, p 147.

by using the special withdrawal cask. The operation proceeded smoothly.

DELAY OF FISSION GASES BY CHARCOAL TRAPS

D. E. Guss, United States Air Force
W. R. Willis, Solid State Division

In the event of a leak in the miniature in-pile loop mentioned above, the fission gases released into the cooling-air stream must be contained, and at the same time, the cooling air must continue to flow until the temperature of the system has fallen below the control set point. To accomplish this, two traps, 24 in. long and 10 in. in diameter, filled with 6-14 mesh activated cocoanut charcoal, have been incorporated in the cooling-air off-gas line. These traps, which are connected in series and operate at room temperature, can be expected to hold krypton activity in the system at the design air flow rate of 20 cfm for 30 sec before the release of appreciable activity. If the cooling air then continued to flow at the design rate, the krypton activity, which would be released over a period of about 5 min, would reach a peak in about 2 min. However, since the air flow would stop in less than 1 min after a leak occurred, virtually all the krypton activity would be contained in the traps and would trickle out over a long period of time. Xenon, the other active gas present in quantity, will be held back for a much longer period of time; hence, the trap design was based on the krypton holdup time.

Since the action of the charcoal is to increase the effective volume of the trap space by a factor which depends directly upon the amount of charcoal used, it was possible to estimate the trap size needed for the in-pile experiment simply by scaling up results obtained with each of two small traps. One of the small traps was 2.25 in. long and 1.05 in. in diameter, and the other was 23.5 in. long and 1.05 in. in diameter. A subsequent experiment in which a full-size trap was used to duplicate conditions for the in-pile experiment substantiated the estimates based on performance of the small traps.

The experimental apparatus is shown schematically in Fig. 8.6. Krypton was introduced into a reservoir beneath the trap and, at time zero, was driven through the trap with air. It then passed through a flowmeter and over a counter, where the activity as a function of time was observed. All the runs were made at 23°C.

The two small traps were tested at flow rates in the region of interest, and all the elution curves obtained were similar, the activity rising quite rapidly and almost linearly to a peak and falling off more gradually. A typical elution curve is shown in Fig. 8.7, in which the time coordinate is

UNCLASSIFIED
ORNL-LR-DWG 7330

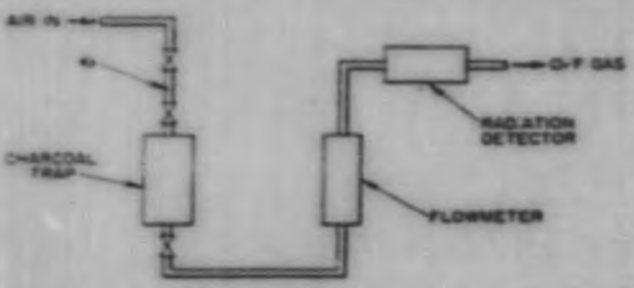

Fig. 8.6. Schematic Diagram of Charcoal-Trap Experiment.

SECRET
ORNL-LR-DWG 7331

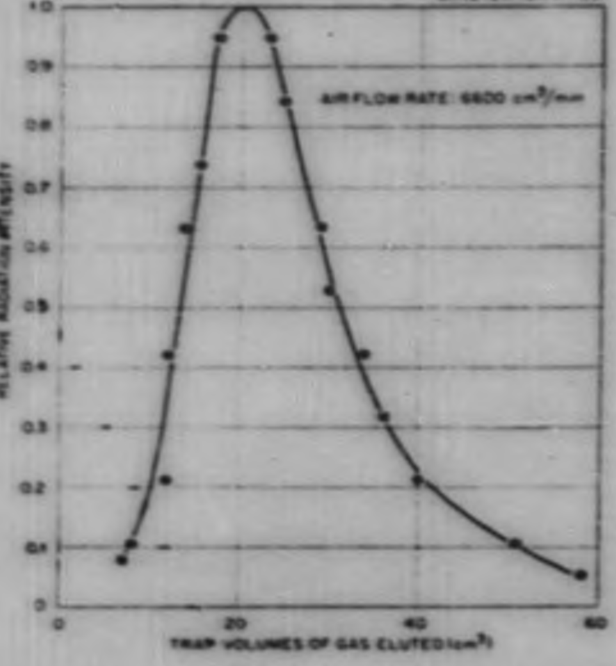

Fig. 8.7. Elution Curve for 334-cm^3 Charcoal Trap Containing Krypton.

expressed in trap volumes of gas eluted. A plot of the inverse of the flow rate vs time to peak activity for the 23.5-in.-long, 1.05-in.-dia trap (shown in Fig. 8.8) indicates a linear relationship. The point on this curve corresponding to the design flow rate is shown.

The elution curve obtained at the in-pile design flow rate is shown in Fig. 8.9. Since the effect of two traps in series is to double the time to peak activity and to broaden the elution curve, it is planned to rely upon two charcoal traps 24 in. long and 10 in. in diameter to delay any burst of fission gases from the in-pile loop for 30 sec before an appreciable amount of activity is released to the stack.

CREEP AND STRESS-CORROSION TESTS

W. E. Davis J. C. Wilson
N. E. Hinkle J. C. Zukas
Solid State Division

Heat transfer experiments have shown that heat dissipation in the longitudinally finned, vertical cylinders in the water-jacketed, helium-filled enclosure of the tube-burst, stress-corrosion apparatus, as presently designed,[10] will limit the fluoride salt power densities to about 500 w/cm^3. Therefore fins have been added between the salt container and a surrounding water jacket, and the heat transfer has been increased sufficiently to permit operation at power densities greater than 1000 w/cm^3. The first complete apparatus has been assembled and awaits filling before irradiation in the LITR. Five more rigs are being fabricated.

Tests are under way to determine the suitability of pressure-regulating valves for supplying gas to stress the tube-burst specimen. Two pressure-volume transformers with 1:1 and 6:1 ratios were designed and are being fabricated. These units are intended to isolate from the remainder of the system the gas used to stress the specimen so that rupture of a specimen will result in a known pres-

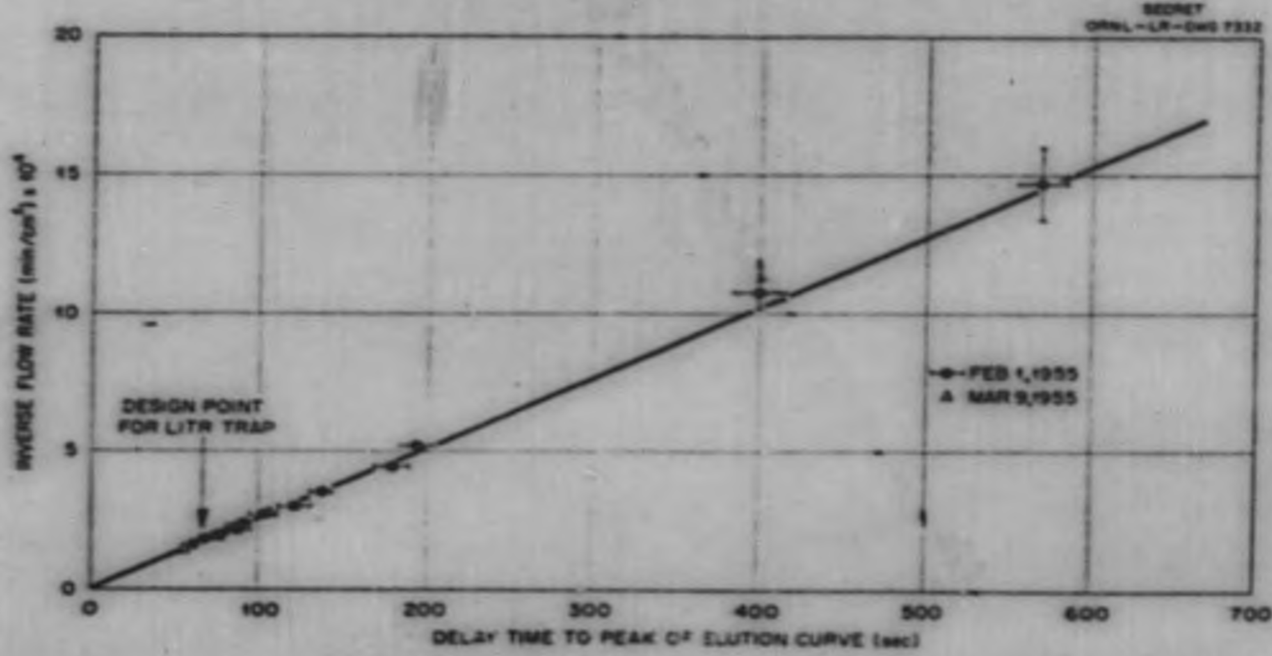

Fig. 8.8. Inverse of the Air Flow Rate vs Time to Peak Activity for a 23.5-in.-Long, 1.05-in.-dia Charcoal Trap Containing Krypton.

---

[10] J. C. Wilson *et al.*, *Solid State Semiann. Prog. Rep. Feb. 28, 1955*, ORNL-1851, p 3.

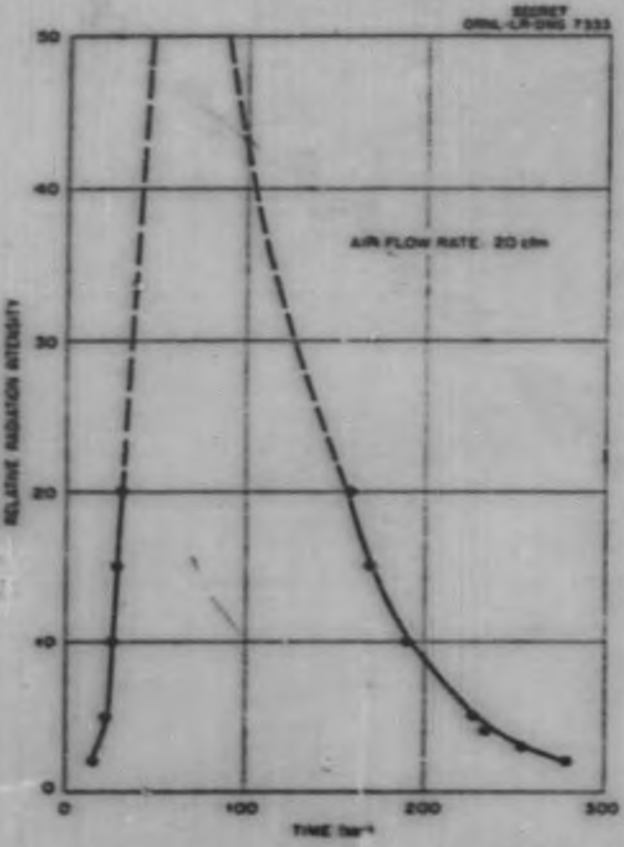

Fig. 8.9. Elution Curve for 30,900-cm^3 Charcoal Trap Containing Krypton.

sure increase in the apparatus. This arrangement will reduce gas consumption and provide a safety feature that will be required for operation in the LITR and the MTR.

Tube-burst test rigs for use in helium and in vacuum were designed and are being fabricated. These rigs will be used for bench tests and to assess the reliability of instrumentation.

A pneumatic gage will be received in June that will measure inside diameters of specimen tubes, before and after irradiation, to 0.00005 in. or strains of 0.00025 in./in. Since measurements of specimen tube-wall thicknesses must be accurate to 0.0001 in. or better, so that the stress may be accurate to 1%, several methods of checking wall thicknesses are being studied.

The stress-corrosion rig irradiated in the LITR previously[11] will be opened when hot-cell arrangements have been completed. A transfer carrier for bringing subsequent rigs from the LITR to the hot cells in Building 3025 was designed and is being fabricated.

The MTR creep apparatus has just completed six weeks of irradiation in the MTR and will be returned to ORNL for measurements.

A THEORETICAL TREATMENT OF Xe^{135} POISONING IN THE ARE AND THE ART

M. T. Robinson
Solid State Division

A theoretical study of xenon poisoning in a circulating-fuel reflector-moderated reactor was made in an attempt to understand the behavior of the ARE and to extrapolate this experience realistically to the ART. The system was assumed to consist of two phases: the liquid fuel and the sparging gas (helium). The theory deals only with *volume-averaged* concentrations and neutron fluxes. Turbulent motion of the two fluids was assumed to assure thorough mixing within each phase. With these assumptions, the differential equations describing the behavior of the poisoning were derived and solved. The various processes are illustrated schematically in Fig. 8.10. The rates of all processes, except the two Xe^{135} production rates, were assumed to be *first order*; that is, the rates are proportional to the Xe^{135} concentration in the starting phase. The rate constants for the two phase-transfer operations are related by application of the law of mass action, and thus the equilibrium solubility of xenon in the fuel is introduced.

The Xe^{135} poisoning of a fluid-fueled reactor under steady-state conditions is given by

$$X_\infty = \frac{(a_0 + a_1 j)\, k_2 \lambda_L}{k_1 k_2 - a_2 \beta \lambda^2_f} \; ,$$

where

X_∞ = steady-state Xe^{135} poisoning (%),
$a_0 = 100 y_{Xe} \sigma_f / \sigma_u$,
$a_1 = 100 y_I \sigma_f / \sigma_u$,

---

[11] W. W. Davis *et al.*, *ANP Quar. Prog. Rep. Mar. 10, 1955*, ORNL-1864, p 155.

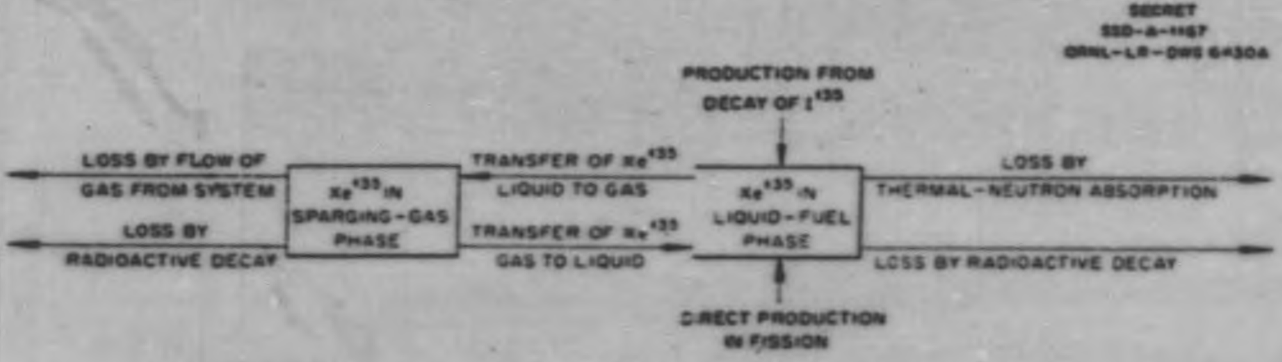

Fig. 8.10. Processes Governing Xe^{135} Poisoning in Liquid-Fueled Reactors.

$k_1 = a_4 + \lambda_f + \lambda_L$,

$k_2 = a_4 + a_2\beta\lambda_f + \lambda_g$,

$a_2 = RTS$,

$\beta = V_L/V_G$,

$\lambda_L = \sigma_{Xe}\phi$,

$\lambda_g = v_G/V_G$,

λ_f = rate constant for transfer of Xe^{135} from liquid to gas,

γ_{Xe}, γ_I = fission yields of Xe^{135}, I^{135},

$\sigma_f, \sigma_u, \sigma_{Xe}$ = thermal-neutron cross sections for U^{235} fission, U^{235} absorption, and Xe^{135} absorption,

a_4 = radioactive decay constant of Xe^{135},

ϕ = volume-averaged thermal-neutron flux,

V_L, V_G = volumes of liquid, gas phases,

v_G = sparging gas volumetric flow rate,

S = solubility of xenon in fuel at 1-atm Xe pressure,

T = absolute temperature,

R = universal gas constant.

The results of the calculations made by the equation and the ART data given in Table 8.2 are presented in Fig. 8.11, which is a design chart for the estimation of the sparging-gas flow rate for conceivable levels of Xe^{135} poisoning. The parameter τ_f (Fig. 8.11) is the phase-transfer mean life from the liquid to the gas:

$$\tau_f = \frac{1}{\lambda_f} .$$

The value of τ_f to be chosen is unknown, but ARE experience indicates a value of about 20 min for that reactor. It is to be expected that the value for the ART will be considerably smaller.

A study of the poisoning behavior of the ART was made for two different types of shutdown. In each case, it was assumed that τ_f = 5 min and that v_G = 1000 STP liters/day. At steady state during full nuclear power operation, the Xe^{135} poisoning would be about 0.40%. If the nuclear power was reduced to zero but sparging was continued, the poisoning would not rise by more than 1 or 2% of the steady-state value before starting to decrease. If sparging was discontinued, the poisoning would rise in about 11 hr to a maximum value of about 12%. If at this point sparging was resumed, about 36 min would be required to reduce the poisoning to below the steady-state value. Intermediate values of 10, 5, 2, and 1% poisoning would be reached in times of about 1, 7, 17, and 25 min, respectively. It appears highly probable that no difficulties will be encountered from Xe^{135} during short shutdowns, since removal of the xenon to acceptable levels by sparging can be made within the time necessary to force the fuel from the dump tanks into the reactor.

A series of calculations has been performed on the Oracle to study the approach of the Xe^{135} poisoning to its steady-state value. In all cases of practical interest, this approach is controlled by the rate of I^{135} production. In fact, except for a change in ordinate, the poisoning is found to follow the iodine growth curve.

It is concluded that the removal of Xe^{135} by sparging with helium (or other inert gas) appears to be a satisfactory means of controlling poisoning in the ART. No difficulties seem to exist in connection with shutdown behavior of the poisoning at the sparging rates selected for ART operation.

TABLE 8.2. DATA USED TO CALCULATE POISONING IN ART

Numerical Data

$a_0 = 0.254\%$

$a_1 = 4.74\%$

$a_2 = 0.0509$

$a_4 = 2.09 \times 10^{-5}\ \text{sec}^{-1}$

$R = 82.0567\ \text{cm}^3\cdot\text{atm/mole}\cdot{}^\circ\text{K}$

$T = 1033^\circ\text{K}\ (1400^\circ\text{F})$

$S = 6 \times 10^{-7}\ \text{moles/cm}^3\cdot\text{atm}$

$\sigma_{Xe} = 1.7 \times 10^6$ barns*

Reactor Data**

	ARE	ART
V_L	5.35 ft^3	5.64 ft^3
V_G	1 ft^3	0.31 ft^3
v_G	0.25 cm^3/sec	1000 STP liters/day
ϕ	8×10^{11} neutrons/cm^2·sec	1×10^{14} neutrons/cm^2·sec
β	5.35	18.2
λ_L	3.4×10^{-6} sec^{-1}	1.7×10^{-4} sec^{-1}

*W. K. Ergen and H. W. Bertini, *ANP Quar. Prog. Rep. Mar. 10, 1955*, ORNL-1864, p 16.

**ARE data from ARE Nuclear Log Book and from J. L. Meem; ART data from J. L. Meem and W. T. Furgerson.

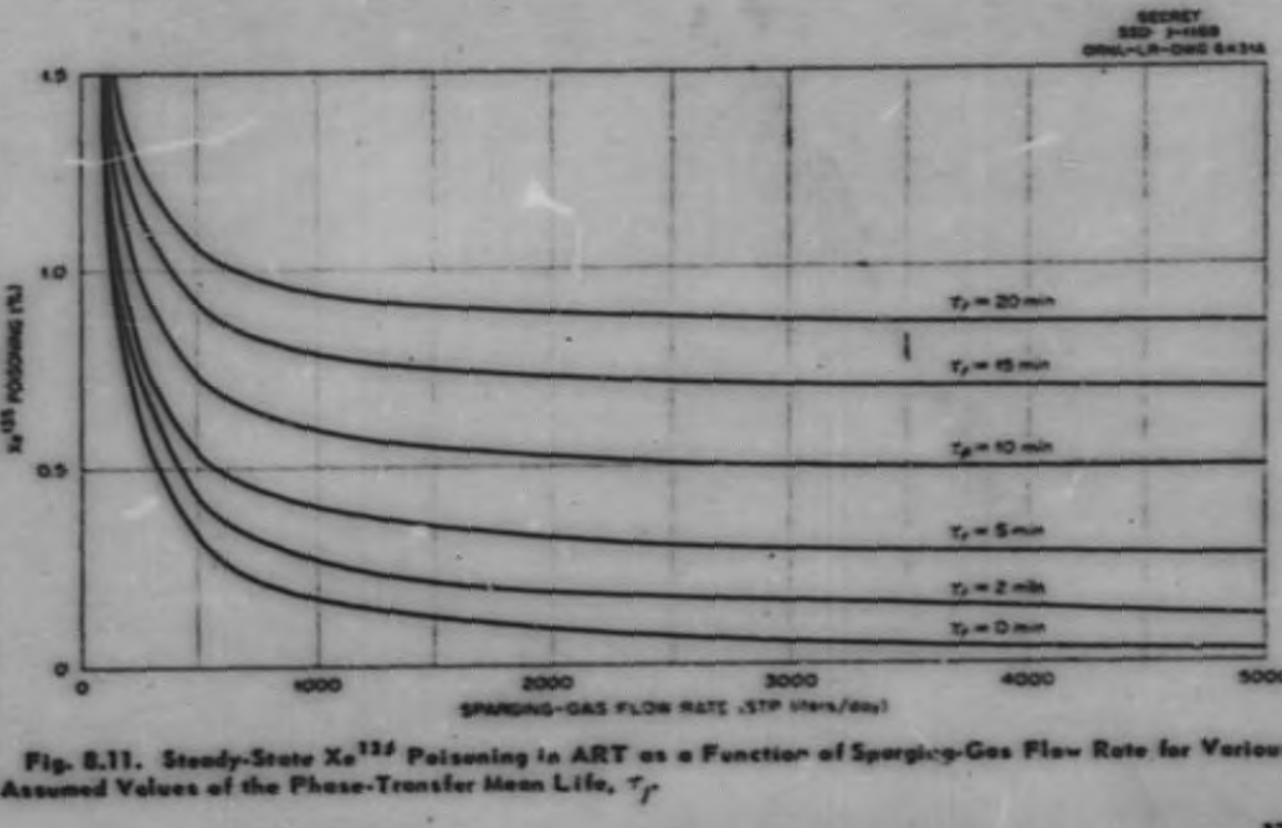

Fig. 8.11. Steady-State Xe^{135} Poisoning in ART as a Function of Sparging-Gas Flow Rate for Various Assumed Values of the Phase-Transfer Mean Life, τ_f.

9. ANALYTICAL CHEMISTRY OF REACTOR MATERIALS

C. D. Susano J. C. White
Analytical Chemistry Division

Modifications of the method for the determination of uranium metal in fluoride-base reactor fuels were completed. Further studies were made on the evaluation of the methylene-blue method for the determination of trivalent uranium in fluoride-base reactor fuels. Investigations were continued on methods for the determination of oxygen as metallic oxides in fluoride salts. An improved separation method involving anion-exchange resins was developed for the determination of alkali metals in fluoride salts. A volumetric method for the determination of zirconium in fluoride-base fuels was proposed.

DETERMINATION OF URANIUM METAL IN FLUORIDE SALT MIXTURES

A. S. Meyer, Jr. B. L. McDowell
Analytical Chemistry Division

The apparatus for the determination of uranium metal in fluoride-base fuels according to a method based on the decomposition of the hydride in an atmosphere of oxygen at reduced pressure[1] is shown in Fig. 9.1. This apparatus has been calibrated and has been applied to the determination of uranium metal in UF_3 and $KF\text{-}UF_3$.

Samples of the uranium metal are placed in a platinum boat in the combustion tube and heated to 250°C for 1 hr in an atmosphere of hydrogen in order to convert any uranium metal present in the sample to the hydride. The excess hydrogen is evacuated from the system after the sample has been cooled to room temperature in an atmosphere of hydrogen. The UH_3 produced from the uranium metal is oxidized by heating at 400°C for 20 min in an atmosphere of oxygen:

$$4UH_3 + 7O_2 \longrightarrow 4UO_2 + 6H_2O$$

The combustion gases are passed through a copper oxide tube at 500°C to ensure complete conversion of the hydrogen to water. The water vapor produced

---

[1] A. S. Meyer, Jr., and B. L. McDowell, *ANP Quar. Prog. Rep. Mar. 10, 1955*, ORNL-1864, p 155.

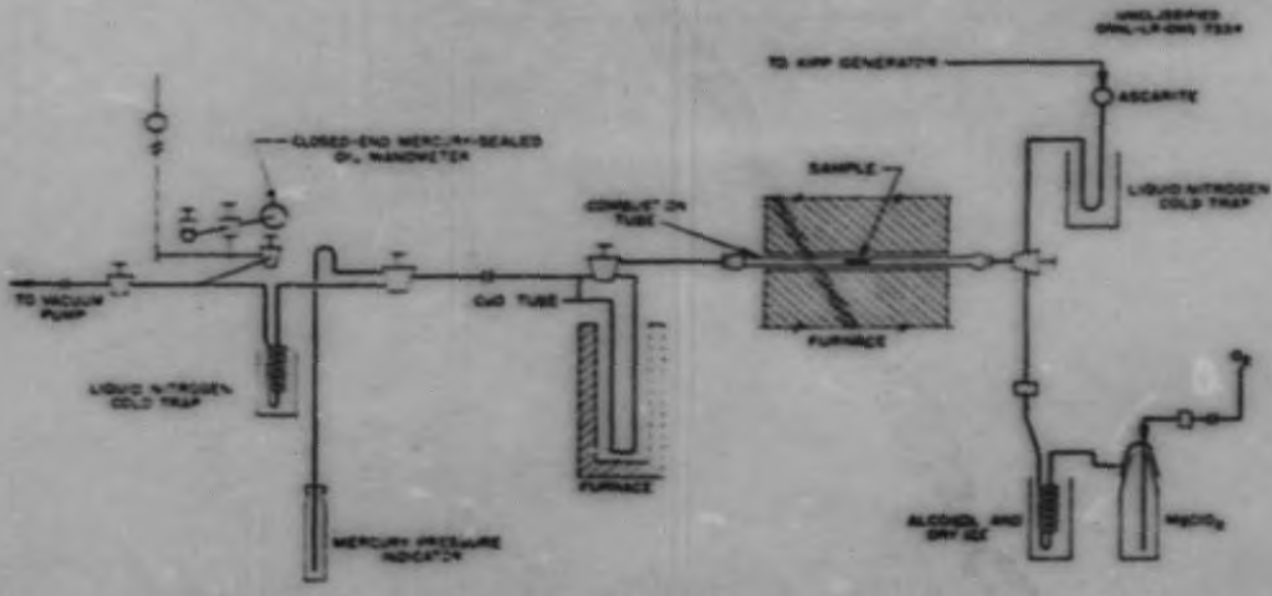

Fig. 9.1. Diagram of Apparatus for the Determination of Uranium Metal.

by the oxidation of the combined hydrogen is collected in the cold trap, and, after the oxygen has been removed by evacuation, the water is allowed to expand into a system of known volume. The pressure of the water vapor is measured on a closed-end mercury-sealed oil manometer similar to that described by Naughton and Frodyma.[2] The pressure registered on the manometer is related to the weight of the uranium present in the sample by empirical calibration of the apparatus.

A preliminary calibration of the apparatus with $BaCl_2 \cdot 2H_2O$ as a standard for hydrogen in the form of water indicated a linear relationship between scale reading and weight of hydrogen for the range 0.18 to 0.8 mg of hydrogen. This linear relationship does not apply to larger amounts of hydrogen because the pressure in the system is approximately equal to the vapor pressure of water. Results which have been obtained for the calibration of the apparatus with samples of pure uranium metal are in agreement with the $BaCl_2 \cdot 2H_2O$ calibration, and they indicate that a scale reading of 1 mm represents 0.36 mg of uranium (Fig. 9.2). The results of the calibration with uranium metal have a coefficient of variation of 7% for the range 6 to 60 mg of uranium.

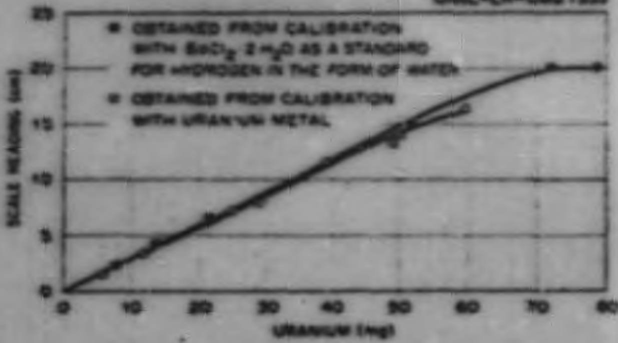

Fig. 9.2. Calibration of Apparatus for Determination of Uranium Metal.

Samples of KF-UF_3 (frozen in a reaction tube) which were analyzed for uranium metal were taken by drilling with increasingly larger bits so that the samples represented portions of the material successively nearer the wall of the reaction tube. Samples of UF_3 and fluoride salt mixtures which were to be analyzed for uranium metal were ground in an atmosphere of hydrogen to prevent oxidation of the uranium metal. The samples, along with the necessary equipment for grinding, were placed in a plastic bag, which could be alternately evacuated and filled with hydrogen. The samples were ground to a particle size that would pass a standard 325-mesh sieve.

Several samples of UF_3 which had been produced by the reduction of UF_4 with uranium metal have been analyzed for uranium metal in the new apparatus. The results for the uranium metal content paralleled those obtained by petrographic analysis of the material. The standard deviation for duplicate determinations on the samples of UF_3 was approximately the same as that obtained for the calibration of the apparatus with uranium metal.

The difficulties encountered earlier in the decomposition of the UH_3 in certain gaseous atmospheres[1,3] have been completely eliminated in the present method. The period of several hours which was required for the decomposition of the hydride in an atmosphere of carbon dioxide was reduced to approximately 20 min when the ignition was carried out in an atmosphere of oxygen. Tests indicate that no interference is introduced by the presence of fluoride salts or trivalent uranium in the samples, and therefore the procedure should be applicable to analyses of all types of fluoride fuels. A topical report on this investigation is being written.

DETERMINATION OF TRIVALENT URANIUM IN FLUORIDE FUELS

A. S. Meyer, Jr. W. J. Ross
Analytical Chemistry Division

Oxidation of Trivalent Uranium by Methylene Blue

A comparison of the methylene-blue[4] and the hydrogen-evolution[5] methods for the determination of trivalent uranium in fluoride-base fuels has been

---

[2] J. J. Naughton and M. M. Frodyma, *Anal. Chem.* **22**, 711 (1950).

[3] A. S. Meyer, Jr., and B. L. McDowell, *ANP Quar. Prog. Rep. Dec. 10, 1954*, ORNL-1816, p 129.

[4] A. S. Meyer, Jr., D. L. Manning, and W. J. Ross, *ANP Quar. Prog. Rep. Mar. 10, 1955*, ORNL-1864, p 157.

[5] D. L. Manning, W. K. Miller, and R. Rowan, Jr., *Methods of Determination of Uranium Trifluoride*, ORNL-1279 (April 25, 1952).

completed. Portions of eutectic mixtures, which had been pulverized and sampled under inert atmospheres, were analyzed simultaneously by both methods in an effort to minimize the effects of the heterogeneity and the instability of such samples. An evaluation of the results showed that satisfactory agreement, comparable to that reported previously[4] for other eutectic mixtures, was achieved in the analytical results for samples of LiF-BeF_2, NaF-LiF, and NaF-BeF_2. The results obtained by the methylene-blue method in the determination of trivalent uranium in KF-UF_4-UF_3 eutectics continue to exhibit negative bias when compared with the results from the hydrogen-evolution method. No further studies were made of NaF-ZrF_4-UF_3 eutectics. All the mixtures studied could be dissolved in methylene-blue solutions that were 1.5 to 6 *M* in HCl and saturated with $AlCl_3$. No hydrogen is evolved during the dissolution of the most reactive trivalent uranium compounds, such as UCl_3, in 1.5 to 3 *M* HCl solutions of methylene blue if efficient agitation is maintained while the solvent is being added to the flask.

Methylene-blue solutions that are 1.5 to 6 *M* in HCl are reduced, during dissolution at room temperature, to methylene white by finely divided metallic chromium, nickel, iron, and uranium-nickel alloy. Zirconium is only very slightly soluble in such solutions over a 2-hr period. The presence of metallic impurities in fluoride-base fuels causes highly erratic results when trivalent uranium is determined by the methylene-blue method, but such impurities have an even greater adverse effect on the hydrogen-evolution method. Dissolution of the metallic impurities in the hot acid solvent results in quantitative evolution of hydrogen. A more comprehensive description of the theoretical and practical aspects of the methylene-blue method for determining trivalent uranium will be issued in the form of a topical report.

Simultaneous Determination of Trivalent Uranium and Total Uranium

The inherent advantage of the methylene-blue method over the hydrogen-evolution method, that is, the possibility of determining trivalent uranium and total uranium in the same sample, is still being investigated. The studies have led to the postulation of an interaction species of pentavalent uranium and methylene white.[4] A detailed study of this postulation has been initiated. The method of Vosburgh and Cooper[6] will be applied to establish the stoichiometry of the complex. Attempts to prepare standard solutions of methylene white through the reduction of methylene blue by zinc amalgam have been unsuccessful because of the ease with which zinc ions react with both the oxidized and reduced forms of methylene blue. An attempt is being made to prepare pure methylene white through electrolytic reduction of methylene blue.

DETERMINATION OF LITHIUM IN LiF-BeF_2 AND LiF-ZrF_4-UF_4

A. S. Meyer, Jr. D. L. Manning
Analytical Chemistry Division

A method for the determination of lithium in LiF-BeF_2 and LiF-ZrF_4-UF_4 has been developed that is based on a separation of lithium by an anion-exchange resin, Dowex-1. In this procedure a sulfate solution of the fluorides that is approximately 1 *N* with respect to H_2SO_4 is passed through a column of Dowex-1 in the hydroxide form. In order to avoid the depletion of the resin in the column by the H_2SO_4, the solution is equilibrated with about 20 ml of a water slurry of the resin in the hydroxide form in a beaker before being placed onto the column. Beryllium, uranium, and zirconium are retained on the column as the beryllate, zirconate, and diuranate anion, respectively, while the lithium passes into the effluent as LiOH. The following equations represent the probable reactions, where ROH is the hydroxide form of the anion-exchange resin:

$$H_2SO_4 + 2ROH \longrightarrow R_2SO_4 + 2H_2O$$
$$Zr(SO_4)_2 + 8ROH \longrightarrow R_4ZrO_4 + 2R_2SO_4 + 4H_2O$$
$$BeSO_4 + 4ROH \longrightarrow R_2BeO_2 + R_2SO_4 + 2H_2O$$
$$2UO_2SO_4 + 6ROH \longrightarrow R_2U_2O_7 + 2R_2SO_4 + 3H_2O$$
$$Li_2SO_4 + 2ROH \longrightarrow R_2SO_4 + 2LiOH$$

It may be seen from the equations that LiOH and water are the only species which are found in the effluent. The lithium is determined by titrating the hydroxide with a solution of standard HCl.

If the fluoride mixtures contain sodium fluoride in addition to lithium fluoride, the sodium will react in the same manner as the lithium and will

---

[6] W. C. Vosburgh and G. R. Cooper, *J. Am. Chem. Soc.* 63, 437 (1941).

be found in the effluent as NaOH. A subsequent titration of the effluent with standard HCl will give the sum of sodium and lithium as the hydroxides. Lithium is then determined by extracting the LiCl, after titration with HCl, with 2-ethyl-1-hexanol and titrating the chloride ion in the nonaqueous medium according to the procedure developed by White and Goldberg.[7]

If a single alkali metal is present in the fluoride mixture, it can be determined directly by titration of the effluent with standard HCl. When more than one alkali metal is present, the sum of the alkali-metal hydroxide concentration in the effluent is obtained by the method just described. Lithium is then determined by the 2-ethyl-1-hexanol procedure;[7] potassium, by the tetraphenyl boron gravimetric method;[8] and sodium, by the difference.

Williams and Vaughan (cf. "ANP Service Laboratory") have utilized a two-stage anion-exchange resin column for the determination of the alkali metal fluorides in the presence of beryllium, zirconium, and uranium fluorides. The first column contains the anion-exchange resin, Dowex-1, in the citrate form, whereas the second column contains the resin in the hydroxide form. Beryllium, zirconium, and uranium remain in the citrate column as the anionic citrate complexes, and the alkali metals pass into the effluent as the alkali metal hydroxides. The alkali metal concentration is then determined by titrating the effluent with standard HCl.

In the method described above, a single column of anion-exchange resin in the hydroxide form is used, and thus the need for the citrate form of the anion-exchange resin is completely eliminated. The method has been tested in the laboratory and found to be satisfactory in every respect. The coefficient of variation of the method is of the order of 1% in the range 10 to 30 mg of lithium. A topical report on the method is being written.

VOLUMETRIC DETERMINATION OF ZIRCONIUM IN FLUORIDE FUELS WITH DISODIUM DIHYDROGEN ETHYLENEDIAMINETETRAACETATE

A. S. Meyer, Jr. D. L. Manning
Analytical Chemistry Division

The volumetric determination of zirconium in the presence of sulfate has been reported by Fritz and Johnson.[9] Excess disodium dihydrogen ethylenediaminetetraacetate (EDTA) forms a very stable complex with zirconium in acidic solutions. The excess EDTA is then back-titrated with bismuth nitrate; thiourea is used as the indicator. The end point is noted by the formation of the yellow bismuth-thiourea complex. An advantage of this method in comparison with previous methods for using EDTA in the determination of zirconium is that anions which form complexes with zirconium, such as fluoride, sulfate, phosphate, thiocyanate, and tartrate, do not interfere.

This volumetric method for the zirconium determination appeared to have several advantages over the gravimetric mandelic acid method now being used, but it was found that the yellow thiourea end point was obscure, especially in the presence of hexavalent uranium, which is also yellow. The precision was consequently poor.

The possibility of modifying the method by back-titrating the excess EDTA with a solution of iron(III), with disodium-1,2-dihydroxybenzene-3,5-disulfonate (Tiron) as the indicator, is now being investigated. This reagent forms an intensely purple complex with iron(III) in an acetate-buffered solution having a pH of about 5.0. Two moles of Tiron combine with 1 mole of iron under these conditions. This complex, which has a pK of about 10, is relatively stable.[10]

The pK of the iron-EDTA complex[9] is about 25, which is approximately the same as that of the zirconium-EDTA complex. It is possible, therefore, to add a solution of iron(III) to a solution of EDTA and Tiron at a pH of 5.0 so that when the EDTA is completely complexed the color of the solution will change from yellow to purple. Qualitative, preliminary tests revealed this change in color at the end point to be well defined. The end point was very sharp when a solution of 0.05 *M* EDTA containing about 50 mg of Tiron was titrated with a solution of 0.05 *M* iron(III). The end point corresponded to the correct stoichiometry of the iron-EDTA reaction in which 1 mole of iron complexes with 1 mole of EDTA. Future work will include

---

[7] J. C. White and G. Goldberg, *Application of the Volhard Titration to the 2-Ethyl-1-Hexanol Separation Method for the Determination of Lithium*, ORNL-1806 (Nov. 4, 1954).

[8] C. R. Williams, *ANP Quar. Prog. Rep. Mar. 10, 1955*, ORNL-1864, p 162.

[9] J. S. Fritz and M. Johnson, *Volumetric Determination of Zirconium and EDTA Method Involving Back-Titration with Bismuth*, ISC-571 (Feb. 1, 1955).

[10] A. E. Harvey, Jr., and D. L. Manning, *J. Am. Chem. Soc.* 72, 4488 (1950).

the determination of zirconium by the modified method of back-titrating the excess EDTA and a study of the possible interferences, particularly fluoride and tetravalent uranium. It is expected that tetravalent uranium would interfere because it would complex with the EDTA in the same manner as the zirconium would.

DETERMINATION OF OXYGEN IN FLUORIDE FUELS

A. S. Meyer, Jr. J. M. Peele
Analytical Chemistry Division

Further tests were carried out on the determination of oxygen as oxide in fluoride fuels[11] by electrolysis of solutions of the samples in fused KHF_2. Quantities of oxygen in excess of 90% of the theoretical value were recovered when known amounts of oxygen were introduced as water by the addition of samples of Na_2CO_3, which react with the fused bifluoride in accordance with the following equation:

$$Na_2CO_3 + 2KHF_2 \longrightarrow 2NaF + 2KF + H_2O + CO_2$$

The yields were not quantitative, because the rate of oxygen evolution decreased as the concentration of water in the electrolyte was reduced. Since traces of hydrogen were detected in the insoluble gases, even though a high concentration of AgF was added to the electrolyte, methods were adapted for the direct determination of oxygen in the effluent gases.

For samples containing large quantities of oxygen the Orsat[12] method for the determination of oxygen in gases was applied by passing the insoluble gas, which was collected over KOH, into a solution of alkaline pyrogallate and measuring the decrease in volume of the gas.

A modification of the Winkler method[13] for the determination of oxygen in water was adapted for samples which contained smaller concentrations of oxygen. The apparatus was modified by converting the sweep gas to purified helium and bubbling the effluent cell gases directly into an alkaline solution which contained KI and a suspension of $Mn(OH)_2$ in which the oxygen was absorbed according to the reaction

$$4Mn(OH)_2 + O_2 + 2H_2O \longrightarrow 4Mn(OH)_3$$

The absorbed oxygen was determined by acidifying the absorber solution and thus liberating an equivalent quantity of iodine, which was then titrated with standard $Na_2S_2O_3$ solution. If only microgram quantities of oxygen are present, the iodine is measured by extracting it into orthoxylene and determining the concentration of iodine in the organic phase spectrophotometrically according to the procedure of Silverman, Bradshaw, and Taylor.[14] Experiments are now being carried out in an attempt to reduce the time required for the quantitative evolution of oxygen. No significant increase in the rate of oxygen generation was obtained by carrying out the electrolysis at a temperature of 250°C rather than at 100°C. The effect of the design and current density of the anode on the efficiency of the generation of oxygen is now being studied. It has been found that the use of a mercury cathode, which is introduced by placing a Teflon cup in the electrolytic cell, simplifies the electrolysis. Fluctuations of the current are decreased, and the evolution of fluorine is greatly reduced. By introducing the sweep gas below the surface of the mercury, the problem of slugging of the entrance line is eliminated. Since AgF is incompatible with mercury under these conditions, it cannot be used to reduce the rate of generation of hydrogen.

DETERMINATION OF OXYGEN IN METALLIC OXIDES BY BROMINATION

J. P. Young G. Goldberg
Analytical Chemistry Division

Extension of the method of Codell and Norwitz[15] for the determination of oxygen in titanium to the determination in fluoride-base fuels was continued during this period. Several modifications of the apparatus described previously[16] were made. New traps of smaller dimensions were designed, and, in addition, an ice-salt trap was placed between the ignition tube and the first dry-ice–alcohol trap to

---

[11] A. S. Meyer, Jr., and J. M. Peele, *ANP Quar. Prog. Rep. Mar. 10, 1955*, ORNL-1864, p 159.

[12] W. W. Scott, *Standard Methods of Chemical Analysis*, 5th ed., II, 2349, Von Nostrand, New York, 1939.

[13] L. W. Winkler, *Ber.* 21, 2843 (1888).

[14] L. Silverman and W. Bradshaw, *Determination of Oxygen in Certain Gases*, NAA-SR-892 (April 15, 1954).

[15] M. Codell and G. Norwitz, *Chem. Eng. News* 32, 4565 (1954).

[16] J. C. White, G. Goldberg, and J. P. Young, *ANP Quar. Prog. Rep. Mar. 10, 1955*, ORNL-1864, p 161.

remove more completely the excess bromine vapor. It was found that if the flow rate of the mixture of helium and bromine vapor were too rapid, the second dry-ice–alcohol trap became plugged with solid bromine during the course of a determination.

In the previous application of the bromination method to the determination of oxygen in BeO, considerable oxide contamination was found in the NaF-FeF$_3$ flux that was used. A small quantity of the impure flux was therefore treated with bromine vapor at 750°C, and then the pretreated flux was used in the determination. Essentially complete recovery of the oxygen in the BeO sample was obtained when this mixture was treated with bromine vapor at 950°C.

Several samples of CrF$_3$ were analyzed for oxide contamination, and reasonable values were found when the samples were treated with bromine vapor at 950°C. The accuracy and optimum conditions for this determination will be investigated with known mixtures of CrF$_3$ and Cr$_2$O$_3$.

Also, several samples of Na$_2$ZrF$_6$ were analyzed for oxide contamination. The bromination was performed at 950°C, and reasonable values of oxygen contamination were found. During the analysis of two samples of Li$_2$ZrF$_6$, a precipitate formed on the surface of the Ba(OH)$_2$ bubbler and caused inefficient flow of gas through the apparatus. It is believed that the occurrence of this precipitate was due to a reaction involving the hydrogen fluoride or fluorine which was present or was formed in the samples being analyzed. A trap of NaF and KBr is being prepared for removal of these gases. The accuracy and optimum conditions for the determination of oxygen contamination in ZrF$_4$ will then be investigated.

DETERMINATION OF OXYGEN IN BERYLLIUM OXIDE BY ACIDIMETRY

J. P. Young
Analytical Chemistry Division

Two alternate possibilities for the determination of oxygen in BeO were investigated:

$$BeO + 2HF \longrightarrow BeF_2 + H_2O$$

$$BeO + 2KF + 2F^- + H_2O \longrightarrow K_2BeF_4 + 2OH^-$$

In several attempts to apply the first reaction as a method for determining oxide present as BeO, it was found that the occurrence of various side reactions made the method impractical.

It was impossible to secure reasonable blanks in the absence of BeO, and furthermore, when BeO was present, no evidence of stoichiometry was found. In these attempts, samples of BeO and BeF$_2$-BeO were placed in contact with solutions of KF, as concentrated as 20% (W/V), at temperatures of 80°C. The concentration of hydroxyl ions presumed to have been formed during the dissolution of the sample was then determined by titration with standard acid. Values from 7.5 to 9.0 pH units were chosen as arbitrary end points for these titrations. Dissolution of either BeO or BeF$_2$ (with oxide contamination) was more rapid in higher concentrations of KF and at pH values of 7.5. A fine crystalline precipitate was formed during the dissolution of all samples containing BeF$_2$. From the results of x-ray diffraction analysis, it was found that this precipitate contained K$_2$BeF$_4$.

DETERMINATION OF TRACE AMOUNTS OF NICKEL IN FLUORIDE FUELS WITH SODIUM DIETHYLDITHIOCARBAMATE

J. P. Young M. A. Marler
Analytical Chemistry Division

The use of sodium diethyldithiocarbamate in the colorimetric determination of nickel in trace amounts was investigated. The work of Chilton[17] served as a basis for these studies.

Sodium diethyldithiocarbamate is a very sensitive colorimetric reagent for nickel; however, this reagent forms colored complexes with a wide variety of cations. Many of the metal complexes of sodium diethyldithiocarbamate are extractible into organic solvents.

The molar absorbancy index for nickel-diethyldithiocarbamate extracted into carbon tetrachloride or 1,2-dichlorobenzene from an aqueous solution whose pH was 9 was found to be about 34,000 at a wavelength of 328 mμ. The molar absorbancy index of nickel dimethylglyoxime is about 11,000 at the wavelength of its maximum absorbancy. Chilton[18] subsequently reported that a more efficient extraction of the nickel complex occurred if the pH of the aqueous phase were first basic to bromcresol green (pH ~5). Without the addition of the complexing agents described by Chilton, it was found that uranium interfered in this method.

---

[17] J. M. Chilton, *Anal. Chem.* 25, 1274 (1953).

[18] J. M. Chilton, *Anal. Chem.* 26, 940 (1954).

as did iron and molybdenum to a very slight degree. With the addition of the complexing agents described by Chilton, it was found that the interference of uranium was still present, although somewhat decreased. Of the other ions present in fluoride-base fuels, chromium and the alkali ions presented no interference, and evidence indicates that zirconium does not interfere. Absorbancy spectra of carbon tetrachloride extracts were determined for aqueous solutions containing sodium diethyldithiocarbamate and all the cations mentioned in this discussion.

AHP SERVICE LABORATORY

W. F. Vaughan C. R. Williams
Analytical Chemistry Division

The number of determinations of the oxygen content of metallic sodium increased sharply during the quarter. Efforts are being made to increase the accuracy of this determination, and two steps have been taken to achieve this goal. More efficient removal of the thin film of adsorbed moisture on the outer surface of the glass bulbs used for the determination is being achieved by immersing the bulbs in acetone and then quickly rinsing them in dry ether before placing them in the hexane–butyl bromide mixture. Also, the reagents, both hexane and butyl bromide, are being desiccated over phosphorus pentoxide so that the water content is less than 5 ppm.

The major portion of the work in the service laboratory continued to be the analysis of fluoride salts, with the emphasis being on the determination of the following components: Na, Zr, Li, K, F, U^{3}, total U, Ni, Cr, Fe, and Mo. A new procedure for the determination of lithium was proposed and tested in which lithium and other alkali metals are first separated from zirconium, beryllium, uranium, and sulfate ions by means of two anion-exchange resin columns in series. The first column is prepared in the citrate form and the second in the hydroxide form. The effluent from the second column is a solution of lithium or alkali metal hydroxides, the concentration of which is determined by titration with standard acid. Work by Manning (cf. "Determination of Lithium in LiF-BeF_2 and LiF-ZrF_4-UF_4") has subsequently shown that only the hydroxide form of the anion resin is required for the separation.

A total of 1673 samples was analyzed, on which 8678 determinations were made. The backlog consists of 151 samples. A breakdown of the work is given in Table 9.1.

TABLE 9.1. SUMMARY OF SERVICE ANALYSES REPORTED

	Number of Samples	Number of Determinations
Reactor Chemistry	1139	6143
Experimental Engineering	525	2515
Miscellaneous	9	20
Total	1673	8678

10. RECOVERY AND REPROCESSING OF REACTOR FUEL

F. R. Bruce
D. E. Ferguson   W. K. Eister   H. E. Goeller
M. R. Bennett   J. T. Long
G. I. Cathers   R. P. Milford
S. H. Stainker
Chemical Technology Division
E. E. Hoffman   C. F. Leitten, Jr.
Metallurgy Division

PILOT PLANT DESIGN

The design of the pilot plant for recovering ANP fuel by a fused salt–fluoride volatility process is expected to be completed by August 15. The engineering flowsheet is 85% complete. Of the 29 pieces of process equipment now contemplated, 10 are completely designed or specified and on order; 2 of the 10 have been received. The scheduled construction completion date is still December 31, 1955.

The plant will be located in cells 1 and 2 of Building 3019. Equipment for highly radioactive materials – the fluorinator, the ARE fuel, dump tank, and the vessel for melting other salts to be processed (for example, salts from the in-pile loops) – will be in cell 1. Equipment for less radioactive materials will be in cell 2. The remainder of the equipment will be in the operating gallery and on the roof above cells 1 and 2.

The present plan of operation is to lower the ARE dump tank into the cell, melt the contents, and pass the molten salt into the fluorinator by means of nitrogen pressure. The process differs from that previously described[1] in the following details: only two cold traps are provided, one at −40°C and one at −62°C; the UF_6 will be recycled, together with fluorine gas, through the absorber and cold traps to effect additional decontamination if necessary to meet product specifications.

The barren molten salt will be removed from the fluorinator with pressure and put into metal cans which will be buried. The sodium fluoride absorber containing the volatile fission-product fluorides will be transported to the burial ground, where it will be dumped and the contents buried. Excess fluorine in the off-gas will be reacted with 5 to 10% aqueous potassium hydroxide in a spray tower.

Two refrigeration units, each consisting of a Freon F-22 and F-13 cascade system, will be used to chill Freon F-11 to −40 and −62°C for recirculation through the cold traps.

PROCESS DEVELOPMENT

In further studies on an absorption bed for removing volatile radioactive material from the UF_6-F_2 gas stream of the fused salt–volatility process, sodium fluoride was found to be much more effective than calcium fluoride. Decontamination was poor in second runs with the same absorbent bed. It is believed that the temperature of the bed is important, but control of the bed temperature was difficult.

The absorbent beds were 1-in.-dia tubes that contained 90 g of either calcium fluoride or sodium fluoride in a 9-in. length or 180 g in an 18-in. length. The CaF_2 used was made by fluorinating $CaSO_4$. Both the CaF_2 and the NaF were 12 to 40 mesh. The gas from a fluorinator was passed directly into the absorbent bed. The fluorination reaction was carried out with 365-g charges of the ARE-type fuel NaF-ZrF_4-UF_4 (53.5-43.0-3.5 mole %) containing 30 g of uranium. Previous work[2] had been done with similar material on a scale of a 67-g charge of fuel.

The NaF was ten times as effective as reported previously. The amount of fluorine used for the fluorination was much less than the ninefold excess used previously. In some of the new runs the fluorine was passed into the molten fuel very rapidly during the induction period and then slowly during the volatilization of the UF_6 to make the residence time of the off-gas in the absorber long.

---

[1] D. E. Ferguson *et al.*, *ANP Quar. Prog. Rep. Mar. 10, 1955*, ORNL-1864, p 164.

[2] D. E. Ferguson *et al.*, *ANP Quar. Prog. Rep. Dec. 10, 1954*, ORNL-1816, p 134.

Calcium fluoride at either 200 or 650°C was about one-third as effective as NaF in removing volatile ruthenium and niobium fluoride from the UF_6-F_2 gas stream. Tests were made with both 9- and 18-in.-long beds (Tables 10.1, 10.2, and 10.3).

Good decontamination was obtained with NaF in either a 9- or an 18-in.-long bed at 650°C when the NaF/U weight ratio was 3/1 (Table 10.1, runs 1, 2, 3) or 6/1 (Table 10.2, runs 5 and 7). When the 9-in.-long bed was re-used (run 4, Table 10.1), so that the over-all NaF/U weight ratio was 1.5/1 for the two runs, decontamination factors for gross beta, gross gamma, and ruthenium beta decreased sharply. With the 18-in.-long bed the same effect was observed, although here the over-all NaF/U weight ratio for the two runs was 3/1 (Table 10.2, runs 6 and 8).

The temperature of the NaF absorbent bed was difficult to maintain at 650°C. The temperature profile over the 18-in.-long bed varied 90°C. The data in Table 10.2 were obtained with the hottest point at 670°C; this temperature may be a little high for efficient operation, but operation at a lower temperature would probably result in too much uranium retention in the cooler section.

CORROSION STUDIES

In 20 laboratory-scale fluorination runs at 650°C, corrosion of nickel test coupons and of the nickel reaction vessel was fairly low. Since conditions changed continually during the runs and since the various components of the vessel were attacked to different degrees, a calculated over-all corrosion rate would have no significance. However, it appears that a large number of ARE fuel fluorination runs can be made in one reaction vessel before corrosion interferes with the process.

TABLE 10.1. DECONTAMINATION IN A 9-in.-LONG NaF ABSORBENT BED

UF_6-F_2 gas stream from fluorination of ARE-type fuel at 630 to 650°C passed through 1-in.-dia bed with temperature of 650°C in hottest portion; same bed used in runs 3 and 4; F_2 flow rate about 300 ml/min initially, then about 150 ml/min during remainder of run

F_2/U mole ratio: run 1 3.7 run 3 8.2
run 2 3.6 run 4 4.8

NaF/U weight ratio in absorber: 3/1 for runs 1, 2, and 3; over-all ratio for runs 3 and 4 = 1.5/1

Activity	Decontamination Factors			
	Run 1	Run 2	Run 3	Run 4
		Over-all		
Gross β	1.3×10^4	5800	1.0×10^4	2900
Gross γ	3.2×10^4	2.1×10^4	2.4×10^4	4500
Ru γ	1700	1600	1.0×10^4	200
Zr-Nb γ	3.2×10^5	7.4×10^4	7.0×10^4	1.0×10^5
TRE*	5.2×10^3	5.0×10^4	4.9×10^4	1.1×10^7
		Across Absorbent**		
Gross β	340	200		35
Gross γ	920	4100		220
Ru γ	940	1400		62
Zr-Nb γ	900	1.2×10^4		2000
TRE β	8	17		8

*Total rare earths.

**Calculated on basis of activity found in absorbent and final product.

TABLE 10.2. DECONTAMINATION IN AN 18-in.-LONG NaF ABSORBENT BED

UF_6-F_2 gas stream from fluorination of ARE-type fuel at 600°C passed through 1-in.-dia bed with hottest point at 670°C; same bed used in runs 5 and 6 and in runs 7 and 8; F_2 flow rate about 200 ml/min

F_2/U mole ratio: run 5 8.1 run 7 8.4
run 6 9.9 run 8 10.2

NaF/U weight ratio in absorber: 6/1 for runs 5 and 7; over-all ratio for runs 5 and 6 and 6 and 7 = 3/1

Activity	Decontamination Factors			
	Run 5	Run 6	Run 7	Run 8
		Over-all		
Gross β	3900	1600	4300	2400
Gross γ	9700	2700	2.0×10^4	4000
Ru γ	1500	140	6700	250
Zr-Nb γ	3.5×10^4	2.9×10^4	9.8×10^4	5.2×10^4
TRE β	3.7×10^4	1.0×10^5		
		Across Absorbent*		
Gross β		2		14
Gross γ		40		82
Ru γ		5		31
Zr-Nb γ		250		700

*Calculated on basis of activity found in absorbent and final product.

The "A" nickel reaction vessel was 2 in. in diameter. The three test coupons were mounted in an upright position at the bottom of the reaction vessel, as shown in Fig. 10.1, in such a way that one-third the surface area of each coupon extended from the liquid into the gas phase. The coupons were 3 in. long, $\frac{3}{4}$ in. wide, and $\frac{1}{4}$ in. thick. Two of the coupons were "A" nickel (nominal composition: 99.4% Ni, 0.05% C), and one of them was cut longitudinally and welded. The third coupon, which was "L" nickel (nominal composition: 99.4% Ni, 0.01% C), was also cut longitudinally and welded.

Each run was made with 200 g of ARE-type fuel NaF-ZrF_4-UF_4 (53.5-43.0-3.5 mole %). The time for an individual run varied from 4.58 to 0.83 hr, the reaction vessel and the coupons being exposed to process conditions for a total of 30 hr. The fluorine flow rate varied from 50 to 300 ml/min and was regulated so that 9.4 moles of fluorine was used per mole of uranium in each run.

Corrosion of the welded coupons (both "A" and "L" nickel) was greater than that of unwelded ones, but in both cases the corrosion was of the solution type (Fig. 10.2), and there was fairly uniform surface removal. Dimensional and weight-change analyses also showed that corrosion was greater in welded than in unwelded coupons (Table 10.4). The most severe attack was on the outer surface of the fluorine gas inlet tube in the vapor zone (Fig. 10.3). The attack on this tube in the liquid zone was more uniform and varied from 4.0 to 7.5 mils in depth. Dimensional analysis of the reaction vessel indicated nonuniform attack of 5 to 9 mils in both the liquid and gas zones. A metallographic examination of the vessel in the region in contact with molten salt showed that the attack there was of a solution nature (Fig. 10.4).

Recovery of uranium was high in all runs (Table 10.5). The uranium loss in the waste salt was consistently lowest in the 50-min runs at the

TABLE 10.3. DECONTAMINATION IN A CaF_2 ABSORBENT BED

UF_6-F_2 gas stream from fluorination of ARE-type fuel at 600°C passed through 1-in.-dia bed;
F_2 flow rate about 200 ml/min
Run 9: 9-in.-long bed at 650°C, F_2/U mole ratio 1.5
Run 10: 18-in.-long bed at 200°C, F_2/U mole ratio 7.5
Run 11: 18-in.-long bed at 200°C, F_2/U mole ratio 8.7

Activity	Decontamination Factors		
	Run 9	Run 10	Run 11
		Overall	
Gross β	1900	960	1700
Gross γ	1800	1200	3600
Ru γ	130	80	200
Zr-Nb γ	5300	6400	4.7×10^4
TRE β		2.3×10^3	
		Across Absorbent*	
Gross β	4	3	5
Gross γ	18	20	65
Ru γ	5	2	8
Zr-Nb γ	40	110	1000
TRE β		13	

*Calculated on basis of activity found in absorbent and final product.

TABLE 10.4. WEIGHT LOSS OF NICKEL CORROSION COUPONS TESTED IN LABORATORY-SCALE FLUORINATION RUNS

Type of Coupon	Original Weight (g)	Final Weight (g)	Weight Change	
			(g)	(%)
Welded "L" nickel	83.9878	80.3760	3.6118	4.3
Welded "A" nickel	86.3445	82.7515	3.5930	4.2
Unwelded "A" nickel	82.6071	80.2160	2.3911	2.9

highest fluorine flow rate. This result was possibly due to a smaller loss of fluorine in corrosion in the short runs than in the long runs. Out of 3935 g of salt, 341 g of uranium was actually recovered as UF_6, which corresponds to an initial uranium content of 8.66%. Analyses of this particular batch of fuel indicated a uranium concentration ranging from 8.30 to 8.75%. Even if the higher value is assumed to be correct, the total recovery was 99.0%.

TABLE 10.5. URANIUM LOSSES IN LABORATORY-SCALE FLUORINATION RUNS

Number of Runs	Duration (hr)	Fluorine Flow Rate (ml/min)	Uranium Loss in Runs (% of total)
1	4.50	55	0.11
4	2.50	100	0.02 to 0.16
5	1.25	200	0.06 to 0.23
9	0.83	300	0.01 to 0.06

[redacted]

Fig. 10.1. Cross Section of Assembled "A" Nickel Reaction Vessel. The pitting type of attack on the fluorine gas inlet tube may be seen at point A.

Fig. 10.2. Cross Section of Welded "L" Nickel Test Coupon Exposed to Molten Salt in a Nickel Reaction Vessel. Note uniformity of attack. Etched with KCN plus $(NH_4)_2S_2O_8$. 12X.

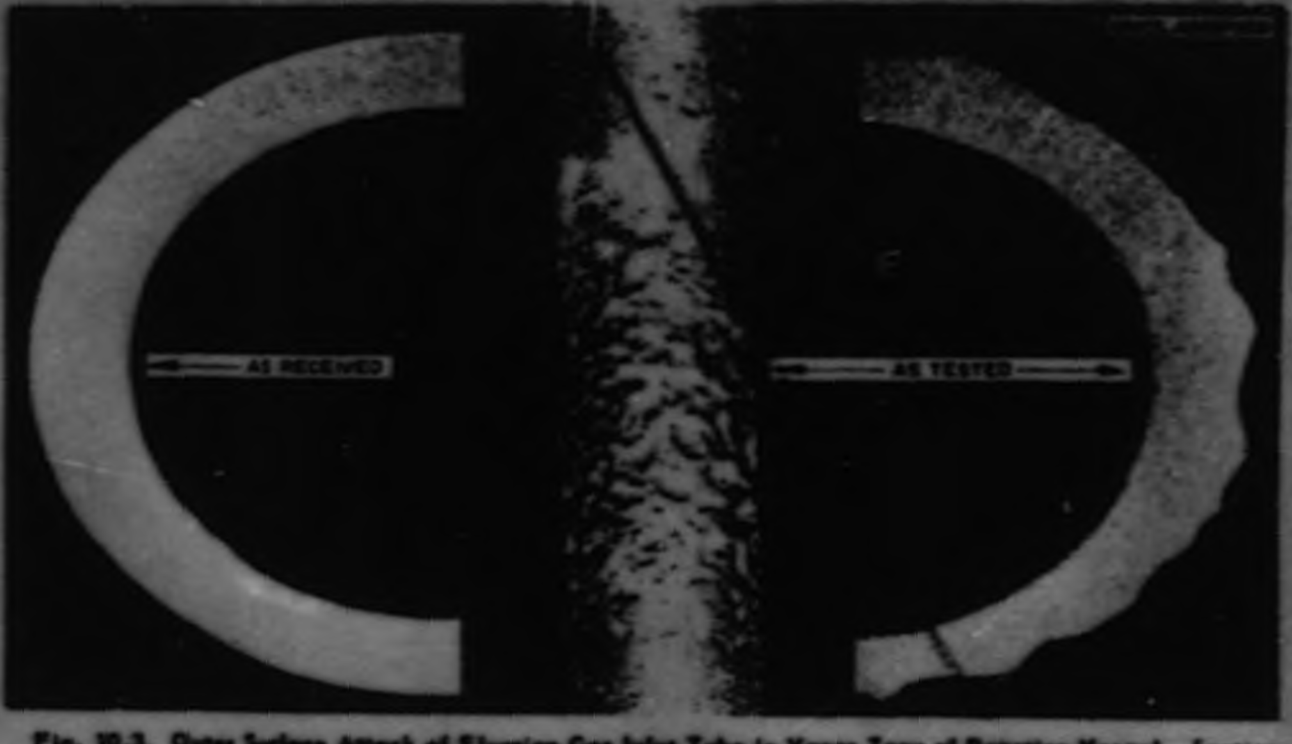

Fig. 10.3. Outer Surface Attack of Fluorine Gas Inlet Tube in Vapor Zone of Reaction Vessel. Section taken at point A of Fig. 10.1. Etched with KCN plus $(NH_4)_2S_2O_8$. 20X.

Fig. 10.6. Inner Surface of Specimen of "A" Nickel Reaction Vessel Taken from Region Exposed to ARE-Type Fuel. Note nonuniform surface attack. Etched with KCN plus $(NH_4)_2S_2O_8$. 250X.

Part IV

APPENDIX

15. LIST OF REPORTS ISSUED FROM FEBRUARY 1955 THROUGH MAY 11, 1955

REPORT NO.	TITLE OF REPORT	AUTHOR(s)	DATE OF DOCUMENT
	I. Reflector-Moderated Reactor		
CF-55-2-142	Vertical Component of Fuel Forces on Reflector and Island	H. C. Hopkins	3-2-55
CF-55-3-161	Gamma and Neutron Heating of the ART Fuel Pump Assembly	L. T. Anderson	3-28-55
CF-55-3-167	Circulating-Fuel-Reactor-Powered Ramjet	W. T. Furgerson, H. C. Hopkins	3-24-55
CF-55-3-191	Fission Product Heating in the Off-Gas System of the ART	C. S. Burtnette	3-28-55
CF-55-4-34	Empirical Correlation for Fatigue Stresses	A. S. Thompson	4-5-55
CF-55-4-44	Allowable Operating Conditions	A. S. Thompson	4-11-55
CF-55-4-83	High Temperature Valve Information Summary	V. J. Kelleghan	4-5-55
CF-55-4-87	ART Design Data	E. S. Bettis	4-18-55
CF-55-4-116	The ART Off-Gas System	W. B. Cottrell	4-21-55
CF-55-4-124	Flexible Mounting Systems	A. S. Thompson	4-11-55
CF-55-4-159	Thermal Stresses in Tube-Header Joints	A. S. Thompson	4-25-55
CF-55-5-76	Calculation of the Beryllium Contribution to the ART Temperature Coefficient of Reactivity	L. T. Anderson	5-11-55
CF-55-5-93	Surface-Volume Ratios for Five Different Fluoride Fuel Systems	T. J. Balles	5-12-55
	II. Experimental Engineering		
CF-55-2-100	ART Reactor Accidents Hazards Tests	L. A. Mann	2-11-55
	III. Critical Experiments		
CF-55-2-93	Three Region Reflector Moderated Critical Assembly with $\frac{1}{8}$ in. Inconel Core Shells	R. M. Spencer	2-14-55
CF-55-4-84	Evaluation of Reactivity Characteristics of Control Rods and Materials Potentially Suitable for Use in the ART. Part II	J. W. Noaks	4-13-55
CF-55-4-137	Evaluation of ART Control Rod Materials. Part III: The Effect of Neutron Irradiation on Some Rare Earth Samples	J. W. Noaks	4-25-55

REPORT NO.	TITLE OF REPORT	AUTHOR(s)	DATE OF DOCUMENT
CF-55-4-178	Evaluation of ART Control Rod Materials. Part IV: The Variation of Reactivity with Control Rod Diameter	J. W. Nooks	4-29-55
	IV. Chemistry		
CF-55-4-18	Solubility of Composition 30 in Water	J. C. White	4-4-55
	V. Corrosion		
CF-55-2-79	Data and Results of ARE Corrosion Capsules	R. Baldock	2-15-55
CF-55-3-157	Examination of First Three Large Fluoride Pump Loops	G. M. Adamson, R. S. Crouse	3-24-55
CF-55-3-179	Examination of Inconel-Fluoride 30-D Pump Loop Number 4695-1	G. M. Adamson, R. S. Crouse, P. G. Smith	3-28-55
CF-55-4-167	Examination of Sodium-Inconel Pump Loop 4689-4	G. M. Adamson, R. S. Crouse	4-21-55
CF-55-4-181	Examination of Fluoride Pump Loops 4930-A and 4935-	G. M. Adamson, R. S. Crouse	4-26-55
	VI. Heat Transfer and Physical Properties		
CF-55-2-89	Measurement of the Viscosities of Composition 35 and Composition 74	S. I. Cohen, T. N. Jones	2-15-55
CF-55-2-148	Electrical Heating and Flow in Tube Bends	H. W. Hoffman, L. D. Palmer, N. D. Greene	2-22-55
CF-55-3-15	Qualitative Velocity Profiles with Rotation in 18 Inch ART Core	G. L. Muller, J. O. Bradfute	3-1-55
CF-55-3-47	Heat Capacity of Lithium Hydride	W. D. Powers, G. C. Blalock	3-7-55
CF-55-3-61	Measurement of the Viscosity of Composition 72	S. I. Cohen, T. N. Jones	3-8-55
CF-55-3-62	Measurement of the Viscosity of Composition 30	S. I. Cohen, T. N. Jones	3-9-55
CF-55-3-137	Measurement of the Viscosity of Composition 43	S. I. Cohen, T. N. Jones	3-16-55
CF-55-3-174	Status Report on Forced Convection Experimental Work in Converging and Diverging Channels with Volume Heat Sources in the Fluids	H. F. Poppendiek, N. D. Greene	3-24-55
CF-55-4-32	Measurement of the Viscosity of Composition 2	S. I. Cohen, T. N. Jones	4-1-55

REPORT NO.	TITLE OF REPORT	AUTHOR(s)	DATE OF DOCUMENT
	VII. Radiation Damage		
CF-55-2-36	The Fate of Certain Fission Products in the ARE	M. T. Robinson, S. A. Reynolds, H. W. Wright	2-7-55
CF-55-4-16	Ru Deposition in In-Pile Loop	M. T. Robinson	4-5-55
CF-55-5-22	A Theoretical Treatment of Xe^{135} Poisoning in the ARE and the ART	M. T. Robinson	5-2-55
	VIII. Shielding		
CF-55-2-111	Calibration of the Revolet, a Remotely Variable Lead-Transmission Gamma-Ray Dosimeter	D. L. Gilliland	
CF-55-4-122	Spectrometer Measurements of Fission Product Gamma Rays for the CFR	E. P. Blizard	4-21-55
	IX. Miscellaneous		
ORNL-1864	Aircraft Nuclear Propulsion Project Quarterly Progress Report for Period Ending March 10, 1955	A. W. Savolainen (ed.)	4-13-55

CONFIDENTIAL

THE AIRCRAFT NUCLEAR PROPULSION PROJECT
AT
THE OAK RIDGE NATIONAL LABORATORY

JUNE 1, 1953

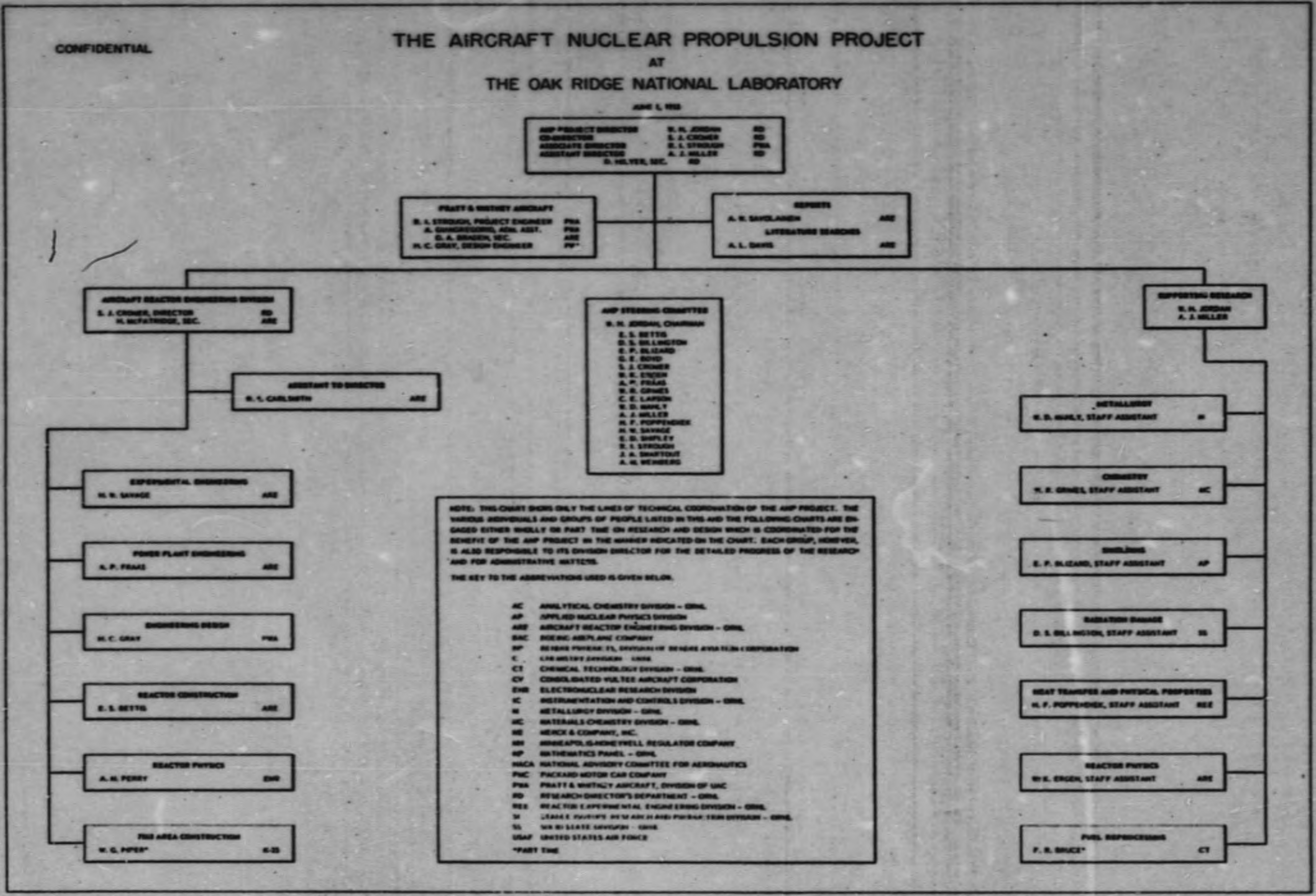

AMP PROJECT DIRECTOR W. H. JORDAN RD
CO-DIRECTOR S. J. CROMER RD
ASSOCIATE DIRECTOR R. I. STROUGH PWA
ASSISTANT DIRECTOR A. J. MILLER RD
D. HELVER, SEC. RD

PRATT & WHITNEY AIRCRAFT
R. I. STROUGH, PROJECT ENGINEER PWA
A. GIANGREGORIO, ADM. ASST. PWA
D. A. BRADEN, SEC. ARE
H. C. GRAY, DESIGN ENGINEER PW*

REPORTS
A. R. SAVOLAINEN ARE
LITERATURE SEARCHES
A. L. DAVIS ARE

AIRCRAFT REACTOR ENGINEERING DIVISION
S. J. CROMER, DIRECTOR RD
H. McFATRIDGE, SEC. ARE

ASSISTANT TO DIRECTOR
R. Y. CARLSMITH ARE

EXPERIMENTAL ENGINEERING
H. W. SAVAGE ARE

POWER PLANT ENGINEERING
A. P. FRAAS ARE

ENGINEERING DESIGN
H. C. GRAY PWA

REACTOR CONSTRUCTION
E. S. BETTIS ARE

REACTOR PHYSICS
A. M. PERRY EHR

7503 AREA CONSTRUCTION
W. G. PIPER* K-25

AMP STEERING COMMITTEE
W. H. JORDAN, CHAIRMAN
E. S. BETTIS
D. S. BILLINGTON
E. P. BLIZARD
G. E. BOYD
S. J. CROMER
W. K. ERGEN
A. P. FRAAS
W. R. GRIMES
C. E. LARSON
W. D. MANLY
A. J. MILLER
H. F. POPPENDIEK
H. W. SAVAGE
E. D. SHIPLEY
R. I. STROUGH
J. A. SWARTOUT
A. M. WEINBERG

SUPPORTING RESEARCH
W. H. JORDAN
A. J. MILLER

METALLURGY
W. D. MANLY, STAFF ASSISTANT M

CHEMISTRY
W. R. GRIMES, STAFF ASSISTANT MC

SHIELDING
E. P. BLIZARD, STAFF ASSISTANT AP

RADIATION DAMAGE
D. S. BILLINGTON, STAFF ASSISTANT SS

HEAT TRANSFER AND PHYSICAL PROPERTIES
H. F. POPPENDIEK, STAFF ASSISTANT REE

REACTOR PHYSICS
W. K. ERGEN, STAFF ASSISTANT ARE

FUEL REPROCESSING
F. R. BRUCE* CT

NOTE: THIS CHART SHOWS ONLY THE LINES OF TECHNICAL COORDINATION OF THE AMP PROJECT. THE VARIOUS INDIVIDUALS AND GROUPS OF PEOPLE LISTED IN THIS AND THE FOLLOWING CHARTS ARE ENGAGED EITHER WHOLLY OR PART TIME ON RESEARCH AND DESIGN WHICH IS COORDINATED FOR THE BENEFIT OF THE AMP PROJECT IN THE MANNER INDICATED ON THE CHART. EACH GROUP, HOWEVER, IS ALSO RESPONSIBLE TO ITS DIVISION DIRECTOR FOR THE DETAILED PROGRESS OF THE RESEARCH AND FOR ADMINISTRATIVE MATTERS.

THE KEY TO THE ABBREVIATIONS USED IS GIVEN BELOW.

AC	ANALYTICAL CHEMISTRY DIVISION – ORNL
AP	APPLIED NUCLEAR PHYSICS DIVISION
ARE	AIRCRAFT REACTOR ENGINEERING DIVISION – ORNL
BAC	BOEING AIRPLANE COMPANY
BP	BENDIX PRODUCTS, DIVISION OF BENDIX AVIATION CORPORATION
C	CHEMISTRY DIVISION – ORNL
CT	CHEMICAL TECHNOLOGY DIVISION – ORNL
CV	CONSOLIDATED VULTEE AIRCRAFT CORPORATION
EHR	ELECTRONUCLEAR RESEARCH DIVISION
IC	INSTRUMENTATION AND CONTROLS DIVISION – ORNL
M	METALLURGY DIVISION – ORNL
MC	MATERIALS CHEMISTRY DIVISION – ORNL
ME	MERCK & COMPANY, INC.
MH	MINNEAPOLIS-HONEYWELL REGULATOR COMPANY
MP	MATHEMATICS PANEL – ORNL
NACA	NATIONAL ADVISORY COMMITTEE FOR AERONAUTICS
PMC	PACKARD MOTOR CAR COMPANY
PWA	PRATT & WHITNEY AIRCRAFT, DIVISION OF UAC
RD	RESEARCH DIRECTOR'S DEPARTMENT – ORNL
REE	REACTOR EXPERIMENTAL ENGINEERING DIVISION – ORNL
SI	STABLE ISOTOPE RESEARCH AND PRODUCTION DIVISION – ORNL
SS	SOLID STATE DIVISION – ORNL
USAF	UNITED STATES AIR FORCE

*PART TIME

CONFIDENTIAL

AIRCRAFT REACTOR ENGINEERING DIVISION
AT
THE OAK RIDGE NATIONAL LABORATORY

JUNE 1, [illegible]

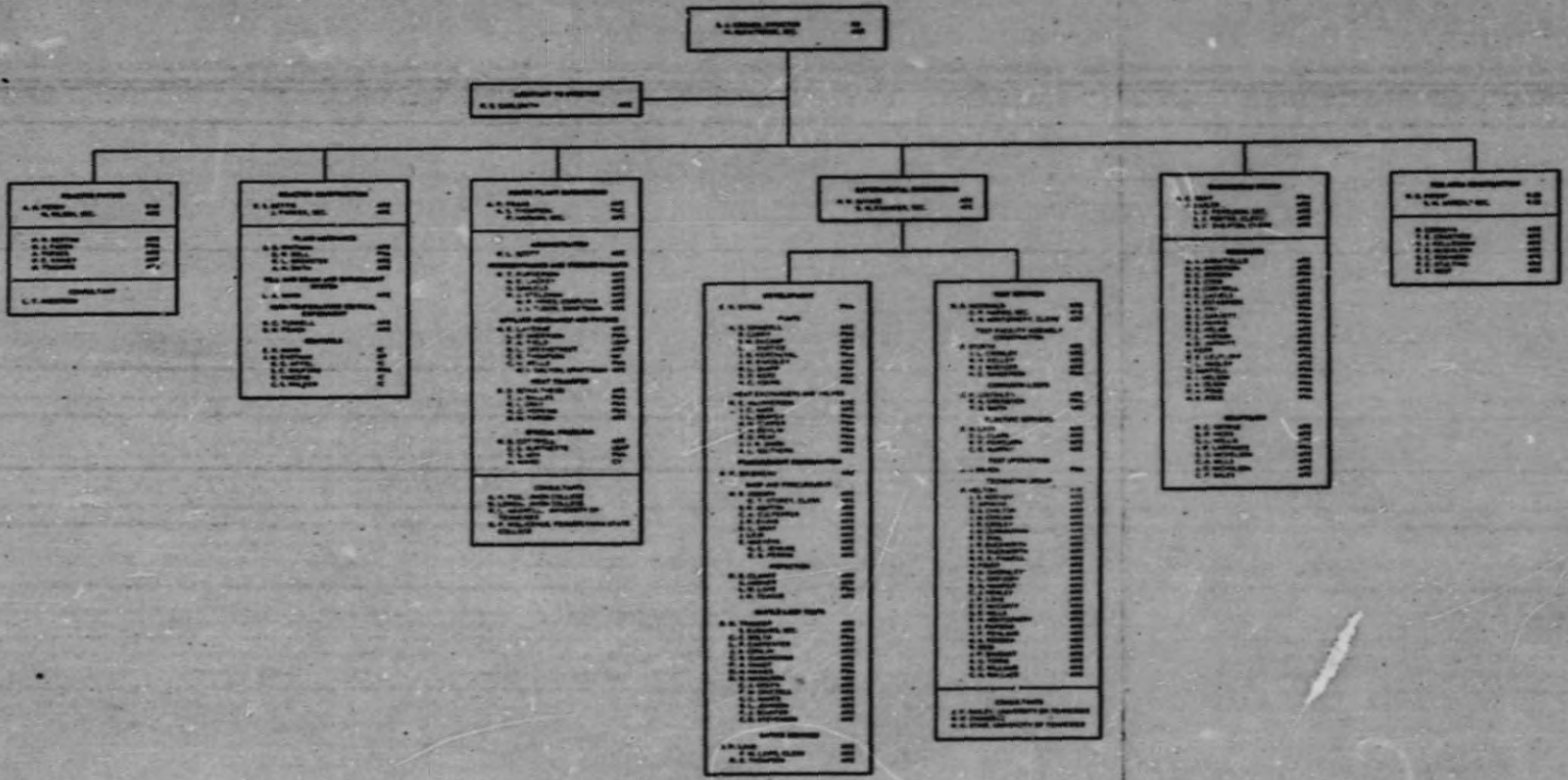

CONFIDENTIAL

THE AIRCRAFT NUCLEAR PROPULSION PROJECT
AT
THE OAK RIDGE NATIONAL LABORATORY